5G AND BEYOND WIRELESS NETWORKS OPTIMIZATION THROUGH UPLINK AND DOWNLINK DECOUPLED ACCESS

A THESIS SUBMITTED TO THE UNIVERSITY OF MANCHESTER
FOR THE DEGREE OF DOCTOR OF PHILOSOPHY
IN THE FACULTY OF SCIENCE AND ENGINEERING

2021

By
Yao Shi
School of Electrical and Electronic Engineering

Contents

List of Tables **7**

List of Figures **8**

List of Abbreviations **11**

Abstract **14**

Declaration **16**

Copyright **17**

Acknowledgements **18**

1 Introduction **19**

1.1 Background 19

1.2 Main Contributions 24

1.3 Thesis Organization 25

1.4 Publication List 26

2 Background and State of the Art **28**

2.1 Heterogeneous Networks 28

2.2 Small Cell 29

2.2.1 The Advantages of SCells 32

2.2.2 The Challenges of SCell 32

2.3 Cell Association Criteria 34

2.3.1 Signal to Interference Plus Noise Power Ratio (SINR) based Cell Association 34

2.3.2 Reference Signal Received Power (RSRP) based Cell Association . . . 34
2.3.3 Reference Signal Received Quality (RSRQ) based Cell Association . . . 35
2.3.4 Cell Range Extension . . . 35
2.4 Downlink and Uplink Decoupling . . . 38
2.5 Millimeter Wave (mmWave) Communications . . . 39
2.6 Multi-Connectivity . . . 41
2.7 Device to Device Communication . . . 42
2.7.1 Short-Range Communication Technologies . . . 42
2.7.2 Advantages of D2D communication . . . 43
2.7.3 D2D Applications . . . 43
2.7.4 Key Technologies and Challenges of D2D . . . 45
2.8 Cellular-Enabled Unmanned Aerial Vehicular Communication . . . 49
2.9 Reinforcement Learning . . . 50
2.10 Mobile Edge Computing . . . 53
2.11 Optimization Problem . . . 55
2.12 Simulation Process . . . 56

3 Capacity Enhancement Decoupled Access 58
3.1 Introduction . . . 58
3.1.1 Main Contributions . . . 60
3.1.2 Organization . . . 60
3.2 System Model . . . 60
3.2.1 Heterogeneous network model . . . 60
3.2.2 Cell Association model . . . 61
3.2.3 Uplink and Downlink Interference Model . . . 62
3.2.4 Resource Allocation . . . 63
3.2.5 Propagation Model . . . 63
3.2.6 Energy Efficiency Model . . . 64
3.3 Capacity-Based Cell Association . . . 64
3.3.1 Coupling/Decoupling Association . . . 65
3.3.2 Single/Multi-BS Association . . . 67
3.3.3 Joint Cell Association and Network Capacity Maximization . . . 70
3.4 Performance Analysis . . . 71
3.4.1 Decoupling Access in Three-Tier HetNet . . . 71

3.4.2 Decoupling Access in Two-Tier HetNet 80
3.4.3 Reduced Density Scenario 83
3.5 Summary 84

4 Interference Management for D2D based on DUDe **86**
4.1 Introduction 86
4.1.1 Main Contributions 90
4.1.2 Organization 92
4.2 System Model 92
4.2.1 Transmission Data Rate 92
4.2.2 Path-loss and Energy-Efficiency Models 94
4.3 Resource Allocation in D2D-Underlay HetNets with DUDe 95
4.3.1 Problem Formulation 95
4.3.2 Cell-Association 96
4.3.3 Resource Block Allocation 97
4.3.4 Power Control 100
4.4 Performance Evaluation 105
4.5 Summary 112

5 DUDe Cellular-Enabled UAV Communications **114**
5.1 Introduction 114
5.1.1 Main Contributions 115
5.1.2 Organization 116
5.2 System Model 116
5.2.1 Network Model 116
5.2.2 Propagation Model 117
5.2.3 Antenna Elements 117
5.2.4 Blockage Model 117
5.2.5 Resource Block Allocation 118
5.2.6 Transmission Data Rate 118
5.3 DUDe Access in Cellular Networks Serving UAVs and GUEs 119
5.4 Energy-Efficiency Maximization 121
5.4.1 GUEs Energy-Efficiency Maximization 122
5.4.2 UAVs Energy-Efficiency Maximization 126
5.4.3 Computational Complexity 128
5.5 Performance Evaluation 129

5.5.1 Proposed DUDe Access Scheme Simulations 129
5.5.2 Energy-Efficiency Maximization 132
5.6 Summary 134

6 Q-Learning and DQL based Power Control for UAVs 136
6.1 Introduction 136
6.1.1 Related Works 137
6.1.2 Main Contributions 138
6.1.3 Organization 138
6.2 RL-Based Optimization of Energy-Efficiency 139
6.2.1 Q-Learning (QL) 139
6.2.2 Deep Q-Learning (DQL) 141
6.3 Implementation of QL and DQL 144
6.4 Performance Evaluation 146
6.5 Summary 152

7 DUDe Access in Mobile Edge Computing 154
7.1 Introduction 154
7.1.1 Main Contributions 156
7.1.2 Organization 157
7.2 System Model 157
7.2.1 Network Model 157
7.2.2 Transmission Model 158
7.2.3 MEC Model 158
7.2.4 Latency Model 159
7.2.5 Communication Model 159
7.2.6 Problem Formulation 161
7.3 JCASA Based on SPA 163
7.3.1 Student-Project Allocation Matching Model 163
7.3.2 Swap Matching 165
7.4 Power Allocation 168
7.5 Performance Evaluation 173
7.6 Summary 182

8 Conclusions and Future Research Directions 183
8.1 Conclusions 183

8.2 Future Work 185

Bibliography **188**

A Proof in Chapter 5 **210**

A.1 Proof of Lemma 1 210

A.2 Proof of Lemma 2 210

Word Count: 40480

List of Tables

2.1 The Parameters of Various Types of Nodes in the LTE-A Network . . 31
2.2 Qualitative Comparison among Existing Cell Association Schemes for Multi-tier Networks 37
2.3 Comparison of Short Range Technologies 42

3.1 Cell Association Schemes 71
3.2 Simulation Parameters 72

4.1 Resource Allocation Schemes 105
4.2 Simulation Parameters 107

5.1 Antenna parameters 117
5.2 Transmission Parameters of the Different Schemes 119
5.3 Complexity of Different Schemes 128
5.4 Simulation Parameters 129

6.1 QL Parameters 146
6.2 DQL Parameters 147
6.3 Simulation Parameters 148

7.1 Summary of MEC Scenarios and Objectives 155
7.2 Resource Allocation Schemes 174
7.3 Simulation Parameters 175

List of Figures

1.1 Evolution of the mobile communication system. 20

2.1 A multi-tier network model. 29
2.2 LTE-A heterogeneous network topology. 30
2.3 The phenomenon of the Uplink and downlink imbalance. 36
2.4 The change of BS coverage after introducing a bias. 37
2.5 A scenario of downlink and uplink decoupling. 38
2.6 Combining DL on C-band with UL on sub-3 GHz band. 39
2.7 Dual connectivity used for DUDe. 41
2.8 D2D application scenarios. 44
2.9 Schematic representation of overlay inband, underlay inband, and outband D2D. 46
2.10 Interference situation in the cell when share the UL and DL resources. 48
2.11 Flappy Bird. 51
2.12 The locations of MEC in end-to-end network. 54
2.13 Typical use cases and requirements of MEC. 54

3.1 Illustration of SMBA association scheme. 67
3.2 Average number of UEs per cell in the UL for different association schemes in single and dual connectivity scenarios ($\beta = 2, \gamma = 0.5$). . . 72
3.3 Ratio of UEs associated with different BSs at different ratios of SCell density to MCell density and association schemes ($\gamma = 0.5$). 73
3.4 Ratio of UEs decoupled in the UL and DL vs. ratio of SCell density to MCell density ($\gamma = 0.5$). 74
3.5 10th, 20th, 50th, 80th, 90th percentile UE UL data rates based on different cell association schemes in single and dual connectivity scenarios ($\beta = 5, \gamma = 0.5$). 75

3.6 Network sum-rate in the UL vs. ratio of SCell density to MCell density in single and dual connectivity scenarios ($\gamma = 0.5$). 77
3.7 Network sum-rate in the UL vs. ratio of UHF SCell density to SCell density in single and dual connectivity scenarios ($\beta = 5$). 78
3.8 Normalized network energy efficiency when the UHF SCells make up different proportions of all the SCells ($\beta = 5$). 79
3.9 Number of handovers in the UL vs. ratio of SCell density to MCell density in single and dual connectivity scenarios ($\gamma = 0.5$). 80
3.10 Ratio of UEs associated with mmWave SCells in the UL vs. ratio of SCell density to MCell density with different ratios of mmWave SCells. 81
3.11 Network data rate in the UL vs. ratio of SCell to MCell density with different ratios of mmWave SCells. 82
3.12 Ratio of UEs associated with different BSs at different ratios of SCell density to MCell density and association schemes (less density scenario, $\gamma = 0.5$). 83
3.13 Network sum-rate in the UL vs. ratio of SCell density to MCell density in single and dual connectivity scenarios (less density scenario, $\gamma = 0.5$). 84

4.1 Interference between MUEs, SUEs and DUEs 93
4.2 Weighted bipartite graph matching. 99
4.3 Network sum-rate vs. ratio of SCell to MCell density. 106
4.4 Network sum-rate vs. ratio of SCell to MCell density. 108
4.5 CUE sum-rate vs. ratio of SCell to MCell density. 109
4.6 10^{th}, 20^{th}, 50^{th}, 80^{th}, and 90^{th} percentile UE data rates based on different schemes. 109
4.7 DUE sum-rate vs. maximum transmission power of DUEs. 110
4.8 Normalized energy-efficiency vs. number of UEs. 111
4.9 Average number of iterations of Algorithms 1 and 2. 112

5.1 Cell Association and Interference map of the proposed scheme. 119
5.2 10^{th}, 20^{th}, 50^{th}, 80^{th}, and 90^{th} percentile data rate per mmWave link and UHF link in the UL and DL. 130
5.3 UL UAV sum-rate and normalized EE vs. UAV altitude. 131
5.4 Network sum-rate in the UL and DL vs. number of UAVs/GUEs. . . . 132
5.5 UL GUE sum-rate and normalized EE vs. ratio of SCell density to MCell density. 133

5.6 UL UAV sum-rate and normalized EE vs. ratio of SCell density to MCell density. 133
5.7 10^{th}, 20^{th}, 50^{th}, 80^{th}, and 90^{th} percentile data rate per UAV and GUE in the UL. 134

6.1 Proposed power control scheme using DQL 144
6.2 DQL Model 145
6.3 10^{th}, 30^{th}, 50^{th}, 70^{th}, and 90^{th} percentile data rate per user in the UL: (a) mmWave band and (b) UHF band - SBS to MBS ratio $= 4$ 148
6.4 UL GUE sum-rate vs. ratio of SBS to MBS. 149
6.5 UL UAV sum-rate vs. ratio of SBS to MBS. 150
6.6 UL mmWave UEs normalized EE vs. ratio of SBS to MBS. 151
6.7 UL UHF UEs normalized EE vs. ratio of SBS to MBS. 151
6.8 Network UL sum-rate vs. ratio of SBS to MBS. 152

7.1 A DUDe MEC model. 156
7.2 Flow-chart of the proposed scheme. 174
7.3 UL sum transmission latency. 176
7.4 UL sum transmission latency. 176
7.5 Sum computation latency of Min-PL-G-FPC, CUDA and SPA-FPC schemes. 177
7.6 Sum-latency. 178
7.7 Sum-latency of Min-PL-G-FPC, SPA-SM-FPC and SPA-SM-OPA. . . 179
7.8 Jain's Fairness Index of UL Transmission Latency vs. number of SBSs. 179
7.9 Jain's Fairness Index of Computation Latency vs. number of SBSs. . . 180
7.10 Normalized UL transmission EE vs. number of SBSs. 181
7.11 10^{th}, 20^{th}, 50^{th}, 80^{th}, and 90^{th} percentile MD data rates based on different schemes. 182

List of Abbreviations

AMC	Adaptive Modulation and Coding
AI	Artificial Intelligence
AWGN	Additive White Gaussian Noise
BER	Bit Error Rate
BS	Base Station
CA	Carrier Aggregation
C&C	Command and Control
CNPC	Control and Non-Payload Communication
CPU	Central Processing Unit
CDA	Coupling/Decoupling Association
CQI	Channel Quality Indicator
CRE	Cell Range Extension
CSI	Channel State Information
CUDA	Coupled Uplink/Downlink Access
CUE	Cellular User Equipment
DC	Dual Connectivity
D.C.	Local Difference of Two Convex Functions
DL	Downlink
DNN	Deep Neural Network
DQL	Deep Q-Learning
DQN	Deep Q-Network
DRL	Deep Reinforcement Learning
DUDe	Downlink and Uplink Decoupling
DUE	Device-to-Device User Equipment
D2D	Device-to-Device
EE	Energy Efficiency
FDD	Frequency Division Duplexing

FPC	Fractional Power Control
GCS	Ground Control Station
GUE	Ground User Equipment
HARQ	Hybrid Automatic Repeat Request
HCP	Hardcore Processes
HD	High-Definition
HetNet	Heterogeneous Network
HPPP	Homogeneous Poisson Point Process
ICIC	Inter-Cell Interference Coordination
LOS	Line-of-Sight
IoT	Internet of Things
LA	Link Adaptation
LAN	Local Area Network
LTE-A	Long Term Evolution Advanced
MAC	Media Access Control
Max-RSS	Maximum Received Signal Strength
MBS	Macro Base Station
MCell	Macro Cell
MCS	Modulation and Coding Schemes
MD	Mobile Device
MDP	Markov Decision Process
MEC	Mobile Edge Computing/Multi-Access Edge Computing
MIMO	Multiple-Input multiple-Output
MINLP	Mixed-Integer Non-Linear Programming
Min-PL	Minimum Path Loss
mmWave	Millimeter Wave
MUE	Macro Cell User Equipment
NLOS	Non-Line-of-Sight
NOMA	Non-Orthogonal Multiple Access
OFDM	Orthogonal Frequency Division Multiplex
OFDMA	Orthogonal Frequency Division Multiple Access
PAN	Personal Area Network
PS	Packet Scheduling
QL	Q-Learning
QoS	Quality of Service

RB	Resource Block
RE	Resource Element
RL	Reinforcement Learning
ReLU	Rectified Linear Unit
RRM	Radio Resource Management
RSSI	Received Signal Strength Indicator
RSRP	Reference Signal Received Power
RSRQ	Reference Signal Received Quality
RUE	Reuse User Equipment
SBS	Small Base Station
SCell	Small Cell
SE	Spectrum Efficiency
SINR	Signal to Interference Plus Noise Power Ratio
SM	Swap Matching
SMBA	Single/Multi-BS Association
SNR	Signal to Noise Ratio
SP	Strauss Process
SPA	Student-Project Allocation
SUE	Small Cell User Equipment
TDD	Time Division Duplexing
UAV	Unmanned Aerial Vehicle
UE	User Equipment
UHF	Ultra High Frequency
UL	Uplink
UPF	User Plane Function
U2G	UAV-to-Ground
3GPP	Third Generation Partnership Project

Abstract

In 3G and 4G eras, many mobile communication services were initially created for users to consume content rather than generate it. Thus, the network traffic in the downlink (DL) tended to be much larger than that in the uplink (UL). As such, traditional networks were designed to mainly maximize DL capacity. However, with the rise of a new trend of user-centric wireless services and applications, the demand for the UL capacity is expected to intensify [1]. A prominent factor that restricts the UL capacity in heterogeneous networks (HetNets) is the UL and DL imbalance problem. As there is a clear disparity between the transmission powers of the macro cells (MCells) and small cells (SCells), the best serving cell per user may be different in the UL and DL directions; hence, if the UL and DL associations are coupled, the UL capacity may be severely limited, and this problem will become even worse when the operating frequency increases. A potential solution to alleviate such a predicament is the DL/UL decoupling (DUDe) technique [2], which allows users to connect to different BSs at different frequency bands in the UL and DL to maximize the link capacity in each direction. DUDe not only shortens the distance between the user equipments (UEs) and serving base stations (BSs), but also makes better use of the spectral resources of SCells.

Most studies of DUDe are based on the minimum path-loss (Min-PL) cell association scheme, which chooses the BS with the minimum path-loss in the UL. However, it does not take the cell loads into consideration and cannot make full use of the network resource. Thus, this thesis first considers decoupling the UL and DL BS from the perspective of maximizing network capacity. Moreover, the increasing desire to incorporate millimeter-wave (mmWave) communications and multi-connectivity in future networks further enriches the possibilities to achieve higher capacities, and they have potential to combine with DUDe to get better performance. MmWave communication is restricted by the high penetration and path loss, but DUDe can shorten the distance between UEs and their serving BSs in the UL, thus enriching the coverage of mmWave cells. As for multi-connectivity, it is highly controversial to adopt dual connectivity in the UL since the transmission power of a UE is much lower than that of a BS. However, DUDe makes it more power-efficient in the UL and brings a solution to this problem. Considering all those things, this thesis investigates the merits of adopting DUDe capacity-based multi-association in the ultra-high frequency (UHF) and mmWave hybrid networks, where mobile users may simultaneously connect to multiple different

UHF SCells, mmWave SCells and/or UHF MCells.

Apart from DUDe, mmWave communications, and multi-connectivity, another way to improve the network capacity is device-to-device (D2D) communication. It is more flexible than traditional cellular communication, and is a potential enabler for the Internet of Things (IoT) networks. However, D2D communication also increases the complexity and heterogeneity of the network structure, and bring challenges for interference management. As such, DUDe facilitates a more benign environment for D2D receivers by lowering the cellular user (CUE) UL transmission power, which results in less interference, and enables more D2D transmissions. To this end, we investigate the application of DUDe in D2D-underlay heterogeneous networks, and propose an efficient joint cell-association, subchannel allocation, and power control scheme for network sum-rate maximization.

This thesis also investigates the potential of DUDe in cellular-enabled unmanned aerial vehicle (UAV) communication networks. Integrating UAVs with cellular networks is considered pivotal to tapping into new business opportunities for cellular operators, especially as the smartphone market is almost saturated. In this thesis, we propose a DUDe scheme for efficiently integrating UAVs within 5G cellular systems, where the UAVs' control and non-payload communication (CNPC) links, as well as the ground user (GUE) uplinks and downlinks, are decoupled from the perspectives of serving BSs and operating frequency bands. Moreover, as battery life is a major constraint for UL transmissions, an optimal power allocation algorithm based on fractional programming and successive convex approximation, and two algorithms based on Q-learning (QL) and deep Q-learning (DQL) are proposed for optimizing the EE of this DUDe scheme.

Lastly, this thesis analyzes the application of DUDe to mobile edge computing (MEC). MEC is a key player in low latency 5G networks, particularly for resolving the conflict between computationally-intensive mobile applications and resource-limited mobile devices (MDs). As such, there has been intense interest in this topic. Generally, computational task offloading is limited by the type of MD-BS association with almost all previous works considering offloading an MD's computational task to the MEC servers attached to its serving BS. In multi-BS association, or DUDe scenarios, however, one MD can have multiple serving BSs, and hence more offloading choices can be exploited. Motivated by this, the thesis considers the communication and computational disparity of small BS (SBS) and macro BS (MBS) cloudlets with the objective to optimize the system performance subject to certain quality-of-service requirements. Specifically, a joint BS association and subchannel allocation algorithm, based on a student-project allocation (SPA) matching model and an optimal power allocation scheme, are proposed to minimize the network sum-latency.

Declaration

No portion of the work referred to in this thesis has been submitted in support of an application for another degree or qualification of this or any other university or other institute of learning.

Copyright

Acknowledgements

First and foremost, I would like to express my sincere gratitude to my supervisor, Prof. Emad Alsusa. He has been supportive and patient throughout my Ph.D., and I have learned a lot of crucial characters of becoming a qualified researcher from him, such as curiosity, passion, and hard-working. He not only offered valuable advice on my research, but also introduced to me knowledgeable peers and professors, in particular Prof. Mohammed W. Baidas to whom I must express my sincere appreciation and gratitude for his expert advice on various optimisation techniques. I also wish to thank Dr. Khairi Hamdi and Dr. Yuanwei Liu for accepting the invitation to be my Ph.D. examiners.

I would also like to thank my collaborators, Mutasem Q Hamdan. He is enthusiastic about my research on UAV communications and was essential in helping me complete the Q-Learning and deep Q-Learning parts in this thesis. I have learned many advanced techniques from him.

I want to extend my thanks to my friends and colleagues who provided help and encouragement. I would like especially to thank Dr. Runze Hu, Dr. Murat Temiz, Ruowei Yin, Han Wu, and other colleagues in the Microwave and Communication Group at the University of Manchester.

My acknowledgment would not be complete without thanking my parents for their relentless support and endless love.

Chapter 1

Introduction

1.1 Background

In just under four decades, mobile telecommunications have evolved from first generation (1G) to the fifth generation (5G). At the same time, the traditional communication network, which mainly focuses on voice services, has been gradually revolutionised into a multi-functional system that provides mobile data, mobile computing and mobile multimedia services. Compared with previous generations of mobile communication technologies, the fourth generation of broadband cellular network technology (4G) has greatly improved the transmission rate, latency and user experience. However, in the face of the rapid development of the Internet of Things (IoT) and the rise of new data-hungry applications such as mobile video, telemedicine and virtual reality, it will be difficult for 4G networks to support the massive data access and ever-increasing data traffic demands of future mobile communications for which 5G comes into being.

5G provides not only better capacity in the downlink (DL), but also higher capacity and lower latency in the uplink (UL). In 3G and 4G eras, most services involved in mobile communications were created for users to consume content rather than generate it. Therefore, compared with the network traffic in the UL, the traffic in the DL is much larger. In such a context, traditional networks are designed to maximize the DL capacity based on the DL performance parameters. However, new services like augmented reality, wireless body area network and vehicular network require higher and faster UL transmission as well. Under these circumstances, a large number of studies have been carried out to improve the UL performance (including those that improve the performances in both UL and DL directions), which can be categorized as network-side and non-network-side.

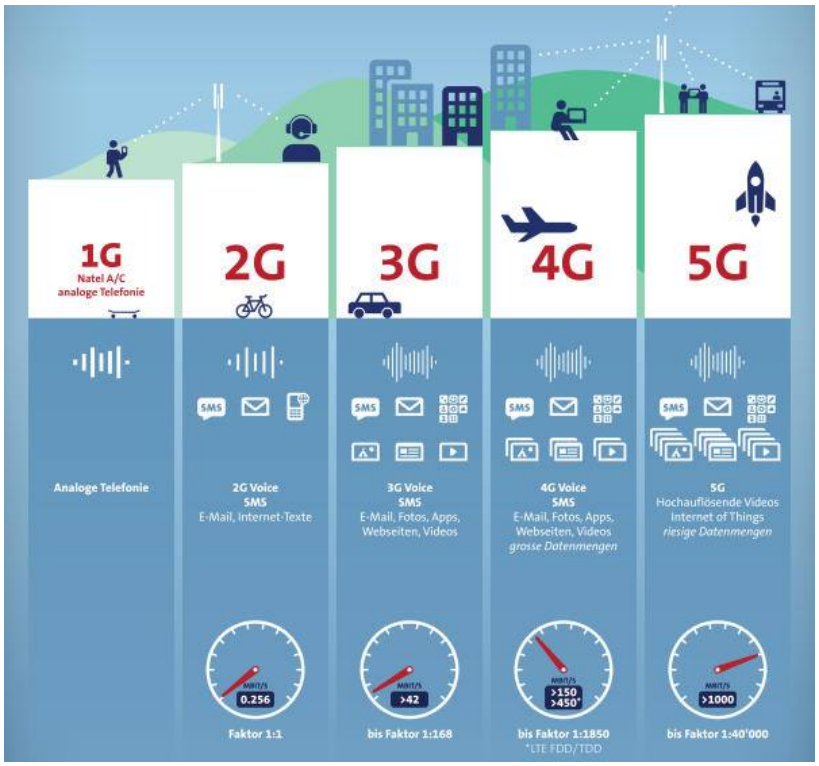

Figure 1.1: Evolution of the mobile communication system.

From the network side, the solution is to deploy low-power nodes such as femtocells and pico cells at the edge of the macro cells (MCells) to increase network capacity and improve network performance. These low power nodes are also known as small cells (SCells). The large deployment of SCells in the network has been considered to be one of the most efficient and cost-effective solutions for meeting the capacity and coverage needs of future mobile communication networks. However, the change in network architecture brings corresponding problems. In conventional wireless cellular networks, a specific user equipment (UE) is connected to the base station (BS) with the maximum DL received signal strength in both the UL and DL [1]. It is called coupled uplink/downlink access (CUDA). In homogeneous networks, this CUDA mode is a nearly optimal access approach, since the best serving BS is the same in the UL and DL. However, with the deployment of more and more small low-cost cells, the traditional homogeneous networks become heterogeneous networks (HetNets). Due to the transmission power disparity of SCells and traditional MCells, the DL coverage of MCells is usually much larger than that of SCells. Consequently, more UEs are associated with MCells in the DL. However, the situation in the UL is completely different. As UEs are battery powered with approximate transmission power, their coverage is

almost the same. If the associated cell in the UL is consistent with that in the DL, the link quality of the MCell edge UEs will be poor. This problem is called the UL and DL imbalance, which increases simultaneously with the growth of SCells [3]. In this situation, CUDA may no longer be the optimal user access strategy. For the seek of reduced path-loss, it would be a better choice for some UEs to connect to a geometrically closer SCell in the UL. This architecture is called DL and UL decoupling (DUDe) or the UL and DL split [2], which allows UEs to connect to different BSs in the two directions. Similarly, the UL and DL operating frequency bands can also be decoupled. As the frequency of C-band is higher than existing systems, using the existing 4G spectrum of sub-3 GHz to carry 5G NR UL services becomes a natural option. At Mobile World Congress 2019, Huawei presented a "5G Uplink and Downlink Decoupling" scheme which enables C-Band and 1.8GHz co-site deployment with the same coverage [4].

DUDe has numerous advantages. BS decoupling shortens the distance between UEs and their serving BSs, thus reduces the path-loss and improves the signal to interference plus noise power ratio (SINR). The reduced path-loss allows lower transmission power, so the interference to neighboring BSs is reduced. Furthermore, BS decoupling pushes more UEs to underutilized SCells in the UL, which in turn allows more efficient resource utilization of SCells and achieves higher data rates. Frequency decoupling increases the reach of 5G in C-band to enhance the customer experience, and could reduce investment in additional sites. Due to the advantages above, DUDe promotes green communications. From the user perspective, since 5G mobile phones are equipped with more antennas and can support wider bandwidths than 4G equipment, they may cost more energy. Under these circumstances, BS decoupling allows lower transmission power, which helps reduce energy consumption and extend battery life. From the mobile operator perspective, over 90% of network costs are spent on energy, consisting mostly of fuel and electricity consumption. Most of this spend powers the radio access network (RAN), with data centres and fibre transport accounting for a smaller share [5]. New techniques such as sleep node and energy harvesting have attracted more and more attention [6]. In this context, frequency decoupling widens the coverage of BSs in the UL, thus mobile operators can deploy fewer new sites in the 5G era, which reduces energy consumption. Another technology that can increase resource utilization of SCells is cell range extension (CRE) or biased cell association [7]. It adds a cell selection offset to the reference signals of the SCells to increase their coverage and offload more traffic from the MCells. However, since CRE does not consider the UL and DL separately, it will bring some problems. For example, a large

offset may cause high interference in the DL for SCell edge UEs, and the resource of MCells may not be fully utilized. By contrast, DUDe brings in the benefits of having very high offsets in the UL without the interference effects in the DL.

For the non-network side, millimeter wave (mmWave) communication, carrier aggregation (CA), multi-connectivity, device-to-device (D2D) communication, mobile edge computing (MEC), multiple input multiple output (MIMO) [8], etc., are utilized to improve network performance. Among them, mmWave communication, multi-connectivity, D2D communication and MEC can be combined with DUDe to get better UL performances.

MmWave communication and multi-connectivity: Wireless communications are reaching the bottleneck of in-sufficient traditional spectrum resources, mmWave frequency spectrum is envisaged to offer an essential lifeline for future broadband cellular systems in the quest to satisfy the anticipated explosive resources demand. However, the characteristics such as high near-field path-loss, severe oxygen and gaseous water molecules absorption have posed significant challenges to mmWave communication. A recent study on electromagnetic field exposure [9] showed that to satisfy applicable exposure limits at frequencies above 6 GHz, the maximum transmission power in the UL might have to be several dB below the power levels used for current cellular technologies. As the transmission power of mobile devices (MDs) is limited, in order to keep the UL SNR unchanged, the distance between UEs and serving BSs should be shortened, and DUDe can achieve this goal. Moreover, as millimeter waves are sensitive to blockage, they are best suited for indoor hotspots and outdoor small cell scenarios. It would be more realistic to jointly deploy mmWave BSs and ultra-high frequency (UHF) BSs. UHF BSs can provide seamless coverage and support high mobility, while mmWave BSs can provide high data rates. In this case, multi-connectivity can allow a user being simultaneously served by multiple BSs [10, 11]. Take dual connectivity (DC) as an example, each UE is allowed to simultaneously utilize the spectrum from two BSs connected together via non-ideal backhaul links. But as the transmission power of UEs is limited, adopting in the UL is highly controversial. Nevertheless, we might as well combine dual connectivity with DUDe since DUDe reduces the distance between users making it more power-efficient in the UL. The work has been published in the IEEE Transactions on Vehicular Technology [12].

Device-to-device communication: D2D communication refers to direct communication between two mobile users without traversing the BS or core network. In a traditional cellular network, all communications must go through the BS, which is

suitable for conventional low data rate mobile services such as voice call and text messaging in which UEs are far away from each other. However, with the development of some data rate services, such as gaming, video sharing, proximity-aware social networking, UEs could be close enough for direct communications (i.e., D2D). In such scenarios, D2D communications can not only increase the spectral efficiency of the network, but energy efficiency, delay, and fairness as well. Most of the current research focuses on in-band underlay D2D, in which D2D re-uses the licensed spectrum; hence, the spectrum resources are simultaneously used by the cellular UEs (CUEs) and D2D UEs. A few studies consider D2D in HetNets, where SCells and MCells co-exists. In this case, not only the co-channel interference between the CUE and D2D UE (DUE), SCell UE (SUE) and CUE, SUE and DUE should be considered, but the interference between the DUEs/SUEs that share the same subchannels should be considered as well. As the complex interference among UEs, it is necessary to control the interference, apart from various resource allocation and power control methods, DUDe is a new promising technique to solve this problem. DUDe facilitates a more benign environment for D2D receivers by lowering the CUE UL transmission power, which results in less interference, and enables more D2D transmissions. The work has been submitted to the IEEE Transactions on Vehicular Technology.

Mobile edge computing: Low latency is also an important requirement for 5G and beyond networks. With the development of 5G ultra-dense networks, MEC has become a promising technique to minimize the increasing latency and satisfy capacity requirements of mobile communications, where edge servers are deployed at the cellular base-stations, such as macro base-stations (MBSs) and/or small base-stations (SBSs) to finish the computationally-intensive tasks and workloads offloaded from MDs. Generally speaking, computational task offloading is potentially limited by the type of MD-BS association, and almost all the previous works consider offloading an MD's computation task to the MEC servers available at its serving BS. According to CUDA, a specific UE is connected to the BS with the maximum DL received signal strength in both the UL and DL the BS, but the BS with rich communication resources may not have enough computation resources. Fortunately, in DUDe scenario, one MD can have multiple serving BSs, hence more offloading choices can be exploited, and the serving BS can be chosen from the perspective of both communication capacity and computing power. The work has been submitted to the IEEE Transactions on Communications.

From the above analysis, it is clear that investing DUDe in 5G and beyond networks

is necessary. Apart from these, DUDe can be also be applied to other 5G scenarios, for example, **unmanned aerial vehicle (UAV) communications**. The global market for UAVs has grown substantially over the past decade and has become a high point for economic growth in many countries. Hence integrating UAVs with cellular networks is considered pivotal to tapping into new business opportunities for cellular operators. It is worth noting that UAV communication has a significant character which is the UL and DL data rate imbalance. UAV uplinks are dominated by data transmission, requiring high data rates up to hundreds of Mbps. In contrast, UAV downlinks are dominated by control and non-payload communications (CNPC). They are crucial to the UAV operation requiring low latency, ultra-reliability, and high security, but could not be guaranteed due to the interference from the ground users (GUEs) [13]. To overcome this problem, DUDe can be applied to split the UAV data communications from the CNPC communications, as well as the GUE communications from UAV communications. Part of the work has been published in the IEEE Systems Journal [14] and part of the work has been submitted to IEEE Internet of Things Journal.

1.2 Main Contributions

The primary aim of this report is to study how to decouple the access work in HetNets and explore the feasibility of combining DUDe with other cutting-edge communication techniques, such as mmWave communication, multi-connectivity, D2D, UAV communication, mobile edge computing, etc.. The main contributions of this report are listed as follows, more detailed contributions are provided in the introduction part of each chapter.

- In Chapter 3, we investigate the feasibility of decoupling the UL and DL serving BSs from the perspective of maximizing the total network capacity in both single and multi-connectivity scenarios. Specifically, we propose an adaptive decoupling and multi-BS association scheme for mmWave/UHF hybrid HetNets where mmWave SCells, UHF SCells and MCells coexist, and compare its performance for a wide range of metrics with benchmark single and dual connectivity alternatives.

- In Chapter 4, we investigate the performance of DUDe in D2D-underlay HetNets. In turn, a joint cell-association, subchannel allocation, and power control (J-CA-SCA-PC) problem for UL network sum-rate maximization is formulated,

which happens to be non-convex and NP-hard, and thus is computationally-expensive. Thus, in this thesis, we decouple the J-CA-SCA-PC problem and solve it via a low-complexity and near-optimal scheme.

- In Chapter 5, we propose a novel DUDe based access scheme for cellular-enabled UAV communications, in which both dimensions of serving BSs and operating frequencies are utilized. The proposed DUDe scheme eliminates interference between the UAVs and GUE, as well as part of the inter-cell interference among GUEs, leading to: (1) interference-limited GUE communications, and (2) noise-limited UAV and line-of-sight (LOS) GUE communications, which is fundamentally different from the conventional scenario where UAVs and GUEs share the same resources. Then, we devise an optimal low-complexity power allocation algorithm, based on fractional programming and successive convex approximation, to maximize the UL communication energy efficiency (EE) in tandem with the proposed DUDe scheme. Furthermore, in Chapter 6, two power allocation schemes based on Q-learning (QL) and deep Q-learning (DQL) are also proposed to optimize the EE of the DUDe network, and are compared with the fractional power control scheme which is applied in 4G and 5G networks, as well as the optimal power allocation scheme we proposed.

- In Chapter 7, we analyze the application of DUDe on MEC, the communication and computational disparity of SBS and MBS cloudlets are taken into consideration. In contrast to most existing works that consider BS association and subchannel allocation separately, a joint BS association and subchannel allocation algorithm based on a student-project allocation (SPA) matching is proposed in this thesis. Then, an optimal power allocation algorithm is proposed to minimize the sum-latency of the network MDs. The formulated problem is a sum-of-ratios problem, which is non-convex and NP-hard. To efficiently and optimally tackle it, the proposed algorithm tightly approximates the problem as a convex optimization problem, and successively solves it until convergence to the global optimal power allocation solution.

1.3 Thesis Organization

The rest of this thesis is organized as: Chapter 2 introduces the theoretical background and some representative published works. Chapter 3 investigates the compatibility

of mmWave communication and multi-connectivity in DUDe. Chapter 4 proposes a DUDe joint BS association, subchannel allocation and power control scheme for D2D-underlay HetNets. Chapter 5 investigate the performances of DUDe in cellular-enabled UAV networks. Chapter 6 analyzes the application of QL and DQL to UAV power control in the DUDe scenario. Chapter 7 analyzes the application of DUDe on MEC. Chapter 8 provides the conclusion and future work.

1.4 Publication List

- **Journal Papers**

  1. **Shi Y**, Alsusa E, Ebrahim A, and Baidas M W, "Uplink Performance Enhancement Through Adaptive Multi-Association and Decoupling in UHF-mmWave Hybrid Networks", *IEEE Transactions on Vehicular Technology*, 2019, 68(10): 9735-9746.

  2. **Shi Y**, Alsusa E, and Baidas M W, "Joint DL/UL Decoupled Cell-Association and Resource Allocation in D2D-Underlay HetNets", submitted to *IEEE Transactions on Vehicular Technology* on December 31, 2020, under review with major revisions.

  3. **Shi Y**, Alsusa E, and Baidas M W, "An Energy-Efficient Decoupled Access Scheme for Cellular-Enabled UAV Communication Systems", *IEEE Systems Journal*, Accepted.

  4. **Shi Y**, Mutasem Q Hamdan, Emad Alsusa, Khairi A Hamdai and Baidas M W, "Decoupled Access and Reinforcement Machine Learning Power Control for Cellular-Enabled UAV network", submitted to *IEEE Internet of Things Journal* on January 6, 2021, under review.

  5. **Shi Y**, Alsusa E, and Baidas M W, "On the Application of Uplink/Downlink Decoupled Access in Heterogeneous Mobile Edge Computing", submitted to *IEEE Transactions on Communications* on October 20, 2020, under review with major revisions.

- **Conference Papers**

  1. **Shi Y**, Alsusa E, and Ebrahim A, "Single and Dual Connectivity for Decoupled Uplink and Downlink Access in UHF-mmWave Hybrid Networks", *2018 IEEE Global Communications Conference (GLOBECOM)*, IEEE, 2018: 1-6.

2. **Shi Y**, Alsusa E, and Baidas M W, ”Downlink-Uplink Decoupled Access in Heterogeneous Cellular Networks with UAVs,” *2020 IEEE 31st Annual International Symposium on Personal, Indoor and Mobile Radio Communications (PIMRC)*, IEEE, 1-6.

Chapter 2

Background and State of the Art

2.1 Heterogeneous Networks

Mobile communication has experienced tremendous changes in recent decades. From 2G to 4G, the data traffic over networks has increased significantly and will continue to grow with the maturity of new concepts, such as augmented reality, wireless body area network, vehicular network, smart city, and so on. To meet the growing data rate requirement, network operators will have to improve the capacity of networks constantly. In traditional homogeneous networks, where each node, i.e., MCell, has a similar wireless transmission mode, BS type, coverage, topology, etc., the main method to increase network capacity is to increase the number of BSs and expand transmission bandwidth. However, sometimes it is unavailable to add more MCells due to the lack of available sites, for example, in crowded public places and terrain complex areas. Thus, more small cells are introduced to the network. These cells are flexible-deployment, low-cost and low-coverage. They can provide extra connections in hot spots and change the topology of cellular networks. Networks that overlay MCells and SCells are called HetNets.

In fact, there are two definitions of HetNet. One refers to the network with different wireless access schemes, where traditional cellular networks (2G, 3G, 4G), satellite communication, Ad Hoc network, or broadband wireless connection (WLAN, WiMAX) coexist. The other refers to the network with different types of network element nodes, such as femtocells and picocells. For one thing, these nodes can be deployed by users, which makes a random topology of the entire network different from the traditional cellular structure. For another, the BS type, parameter settings, transmission power, and antenna configuration of these nodes can be different from

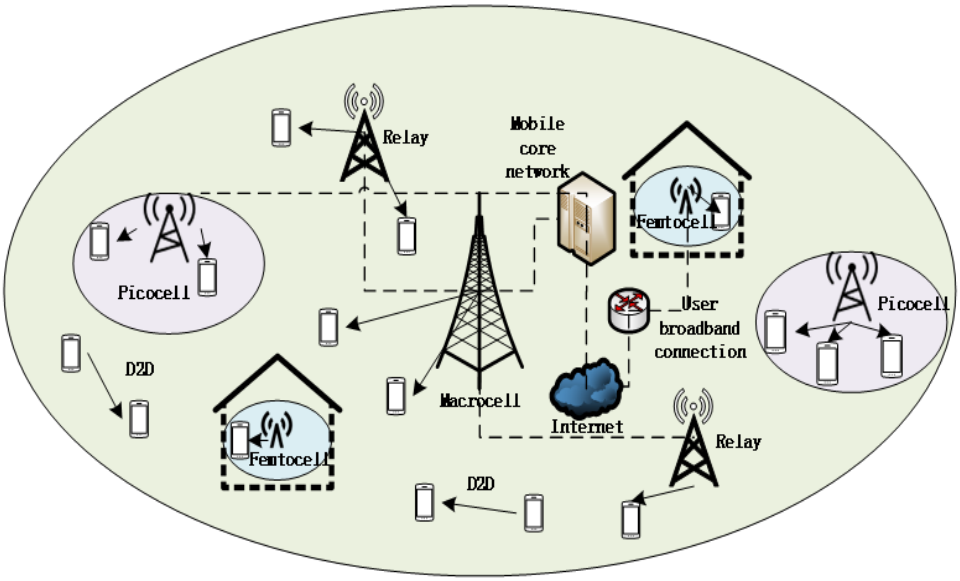

Figure 2.1: A multi-tier network model.

each other, which provides users with diverse communication methods and ubiquitous access services. The definition of HetNet in this thesis is a special case of the latter one, where BSs can transmit over different frequencies with different transmission powers. A HetNet with N different types of BSs is called an N-tier network. A typical structure of HetNet is a Long Term Evolution Advanced (LTE-A) network [15], where MCells provide essential coverage and seamless connections; dense SCells provide supplementary coverage and increase the network capacity. Fig. 2.1 illustrates such a multi-tier network with an MCell overlaid by relays, picocells and femtocells. Arrows indicate wireless links, and the dashed lines denote the backhaul connections. The LTE-A HetNet adopts advanced wireless and wired backhaul technologies, that is, some SCells can configure their backhaul interfaces, or several cells can form a cluster to aggregate and forward network data. SCells can also use relay nodes, i.e.Donor eNB (DeNB), to set up their backhaul links. Fig. 2.2 shows the network topology [16].

2.2 Small Cell

SCell is a general term for a series of low-powered cellular radio access nodes. They are small compared to a mobile MCell, partly because they have a shorter range and

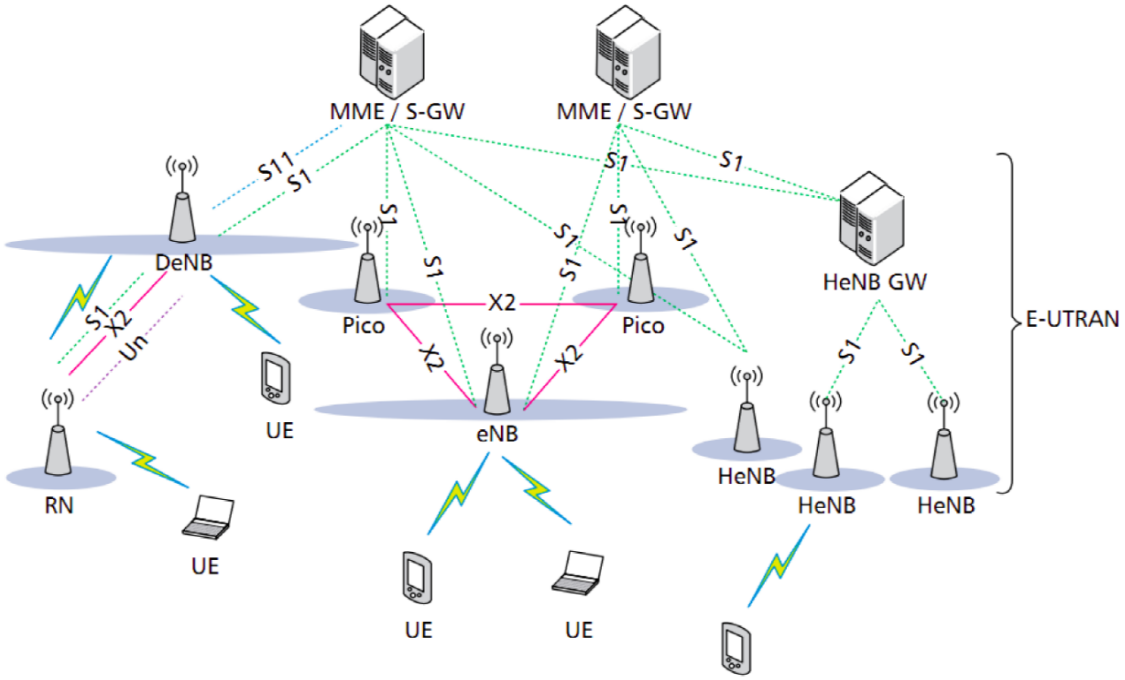

Figure 2.2: LTE-A heterogeneous network topology.

partly because they typically handle fewer concurrent calls or sessions. They can increase the capacity of indoor and outdoor hotspot scenarios and cope with the explosive growth of mobile traffic. Generally, SBS can be divided into two types: fully-functioning BSs (picocells and femtocells) and macro-extension access points (relays and Remote Radio Heads (RRHs)) [17]. The fully-functioning SBS is capable of performing all the functions of a MCell with lower power and a smaller coverage area. Specifically, all functions of the entire protocol stack can be run on the fully-functioning base station [18]. A macro-extension access node is an extension for the MCell to effectively extend the signal coverage, and it performs all or some of the physical layer functions only. In addition, according to the coverage, transmission power, and deployment scenarios, SCells can be classified into the following types [19]:

- Picocells are SBSs deployed and installed by operators, and their coverage is about 300 meters. They are usually deployed in indoor or outdoor hotspots such as shopping centers, bus stops, etc., and can serve dozens of UEs. The transmission power of picocells is around 23-30dBm, and they are mainly used to increase network capacity. The backhaul of picocells is similar to MBS and can provide ideal high-speed, low-latency links over fiber or microwave.

- Femtocells are indoor BSs installed by UEs with a coverage of about tens of

meters. They are usually deployed to cover indoor spots, such as homes, offices, conference rooms, etc., and to serve a small group of UEs. Femtocells can be divided into three categories based on their access control mode: open access, closed access, and hybrid access [20]. In the open-access mode, any UE can get access to the femtocell; in the closed access mode, only the UEs belong to the closed subscriber group (CSG) can get access to the femtocell; in the hybrid access mode, the UEs that not belong to the CSG may camp and acquire some level of service on these cells. However, UEs subscribed to the femtocell may get preferential charging and treatment in comparison with UEs not subscribed to the cell that receive service from it. The transmission power of the femtocells is usually less than 23dBm, and they are mainly used to guarantee the signal strength of home UEs. The femtocells can be connected to the network via any of the users' broadband connections such as digital subscriber line (DSL), cable, or fiber.

- Relays are the access point deployed by operators, which can transmit the UEs' data back and forth from and to the MCell, featuring what is considered as wireless backhauls. They are usually used to extend the coverage of MCells, cover the dead zones, and improve the performance of MCell edge UEs. The transmission power and coverage of the relay node and picocell are the same. The main difference lies in three aspects: first, the picocell is a fully-functioning BS, and the relay is an extension for the MCell; second, the picocell is mainly used to increase the network capacity, and the relay is used to extend the coverage; third, picocell has an ideal backhaul link, and the backhaul is a wireless in-band or out-of-band backhaul.

Table 2.1 summarizes the basic characteristics of the deployment scenarios, coverage, transmission power, and backhaul links of the above-mentioned SCells, and compares them with the MCell [19].

Table 2.1: The Parameters of Various Types of Nodes in the LTE-A Network

Parameters	Max transmission power	Coverage radius	Backhaul interface
Macrocell	46dB	few km	S1 interface
Relay	30dB	200m	wireless
Femtocell	<23dB	<50m	Internet IP
Picocell	23-30dBm	<300m	X2 interface

2.2.1 The Advantages of SCells

To meet the explosion of data and shortage of spectrum resources, there is a real beauty to going small. The advantages of SCells are as follows:

- Flexible to deploy: SCells are smaller in size and hence they are easy to install. Compared to MCells, SCells can be located at hotpots without erecting towers, such as shopping malls and office buildings. They can also be deployed in weak coverage areas such as MCell edges, indoors, tunnels, etc., so as to provide reasonably contiguous coverage.

- Low transmission power: The distance between the user and the SCell is relatively close, so the path-loss is lower and energy efficiency is higher. In addition, since the coverage and transmission power of SCells are low, the spectral efficiency can be improved through the dense deployment of SCells, thereby improving the network capacity.

- Low cost: The deployment of SCells does not require high costs of tower construction, equipment maintenance, etc., so the cost of networking is relatively low. In addition, SCells consume less power. The energy consumption of an MCell is equivalent to 30 Picocells. The deployment of SCells can save 76% of the energy compared with the traditional cellular network [21].

- Better support high-frequency resources: In order to achieve large-scale coverage of the network, the traditional macro cellular network generally uses UHF spectrum resource with low penetration loss and path-loss. For signals above 3 GHz, it will experience severe penetration loss and path-loss during propagation. As the coverage of SCells is small, most of the links are line-of-sight, so the high-frequency resources can be better utilized.

The advantages of the SCell show its strong vitality, which will inevitably become an indispensable part of the future 5G network, but it will also introduce new challenges as follows.

2.2.2 The Challenges of SCell

Although introducing SCells into the homogeneous network can increase network coverage and capacity, it also brings some new challenges as follows:

- Interference management: After deploying SCells to the MCell network, the HetNet can be divided into two layers: MCell layer and SCell layer. There are generally two ways to allocate spectrum resources in this network: the first is that the SCell layer uses the same or partially the same spectrum resource as the MCell layer, called the co-channel deployment; the second is the SCell layer and the MCell layer use orthogonal spectrum resources, which is called orthogonal channel deployment. In the co-channel deployment scenario, there is inter-layer interference between the MCell layer and the SCell layer, and intra-layer interference among cells in each layer. In the orthogonal channel deployment scenario, there is only intra-layer interference, but the spatial bandwidth efficiency is lower than that in the co-channel deployment scenario. Introducing SCells into the traditional homogeneous network causes more interference. Therefore, it is necessary to research the interference management technology in the MCell-SCell hybrid network.

- Mobility management: Mobility management in MCell-Scell hybrid networks involves issues such as cell selection and cell handover. The large deployment of SCells will make mobility management in the network more complicated [22]. Due to the small scale of SCell coverage, the UE with high velocity will cross the SCell in a short time, causing the UE to frequently switch between cells, which increases the signaling overhead [23]. In addition, since the SCell has lower transmission power and smaller coverage than the MCell, the traditional handover process and parameters cannot be directly applied to MCell-SCell hybrid networks [24]. The handover procedure between the SCell and MCell should be modified. As for cell selection, when MCells and SCells are all in the open-access mode, since UEs generally perform cell selection based on the reference signal received power (RSRP) scheme and the transmission power gap between SBSs and MBSs, UEs prefer to access to MBSs, which causes network load imbalance. In summary, the deployment of SCells makes cell selection and cell handover more complicated. It is necessary to conduct in-depth research on these issues.

- Energy efficiency management: Energy efficiency has always been an important indicator of network performance. Compared to traditional MCells, SCells have lower energy consumption. The power consumption is only 15 W to maintain the operation of a non-loaded SBS. However, with a surge of traffic, more and

more SCells will be deployed to weak coverage areas or hotspots, and the energy consumption will greatly increase. It is necessary to study how to improve the energy efficiency of the networks with SCells.

- Backhaul: SCell has a variety of backhaul methods, such as fiber, microwave, DSL. Operators have to design suitable backhaul networks for different types of SCells according to their corresponding requirements, so as to ensure the QoS and reduce the cost of network construction.

2.3 Cell Association Criteria

One of the major issues in mobile cellular networks is how to provide the highest possible quality of service (QoS) with limited resources. The process of allocating resources to each UE and determining associated BS to maximize resource utilization while minimizing interference is called user access or cell association. In the following section, we will introduce four different cell association criteria.

2.3.1 Signal to Interference Plus Noise Power Ratio (SINR) based Cell Association

Average received SINR is the best criterion to measure the channel quality for cell selection. SINR refers to the received signal power over the sum of the interference and noise power. This cell selection criterion can be represented as follows

$$i_{SINR} = \arg\max_{i} \ \gamma_i, \tag{2.1}$$

where i, i_{SINR} and γ_i represent the cell index, the SINR of the i-th cell and the selected cell index based on the max SINR criterion, respectively [25].

2.3.2 Reference Signal Received Power (RSRP) based Cell Association

RSRP based cell association is specified in the LTE by the 3GPP organization in Release 12. When a typical UE accesses the network, each BS in its vicinity transmits a reference signal to it; then the UE measures the strength of this reference signal to estimate the distance of the BS. In fact, after using the inter-cell interference coordination

technology (ICIC) [26], RSRP based cell association is not optimal because it only reflects the signal strength received from each BS but does not reflect the actual channel condition. However, it is still widely used because of its simplicity in the calculation. This criterion is represented as follows

$$i_{RSRP} = \arg\max_{i} \; s_i, \tag{2.2}$$

where i_{RSRP} and s_i represent the selected cell index based on the max RSRP criterion and the RSRP of the i-th cell, respectively [25].

2.3.3 Reference Signal Received Quality (RSRQ) based Cell Association

Another criterion specified in LTE is RSRQ based cell association. It is a variant of RSRP. RSRQ is defined by the RSRP over the total received power, i.e., received signal strength indicator (RSSI) [25]. Under full load conditions, RSRQ is proportional to the following value

$$RSRQ = \frac{RSRP}{RSSI} \propto \frac{S}{S+I+N} = \frac{SINR}{1+SINR} \tag{2.3}$$

where S, I and N represent received signal power, interference power and Gaussian white noise, respectively. The RSRQ based cell association criterion is represented as follows

$$i_{RSRQ} = \arg\max_{i} \; \rho_i, \tag{2.4}$$

where i_{RSRQ} and ρ_i represent the selected cell index based on the max RSRQ criterion and the RSRQ of the i-th cell, respectively [25].

2.3.4 Cell Range Extension

In a HetNet, since there is a huge gap in the transmission power between SCells and MCells, the UL and DL cell bounder are different. As can be seen in Fig. 2.3, MCell DL coverage is larger than its UL coverage, and SCell UL coverage is larger than its DL coverage, which results in the UE in the middle area of the two borders accessing different BSs according to the UL and DL maximum SINR/RSRP/RSRQ criteria. The

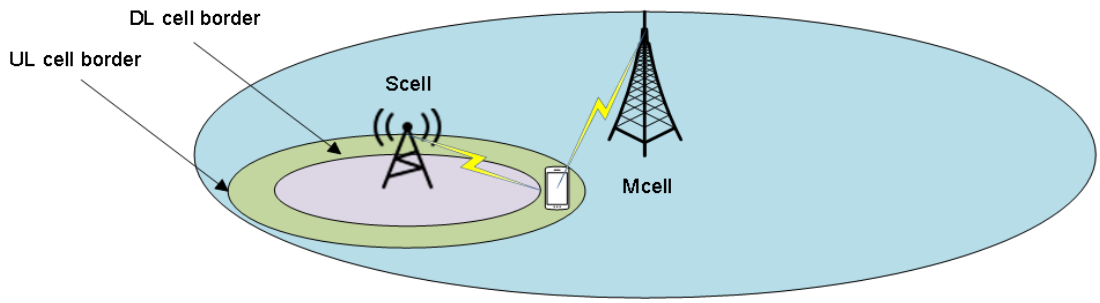

Figure 2.3: The phenomenon of the Uplink and downlink imbalance.

phenomenon that the UL and DL optimal access cells are different is called the UL and DL imbalance.

A possible solution to this problem is cell range extension (CRE) [7]. It adds a positive cell selection offset to the reference signals of the SCells to increase their coverage and offload more traffic from the MCells. Specifically, the three previous criteria mentioned above can be extended to biased versions. For SINR based cell association, the in equation (2.1) can be modified to

$$\gamma_i = \begin{cases} \gamma_{MCell}, \\ \gamma_{SCell} + \alpha_{SINR}. \end{cases} \tag{2.5}$$

That is, bias α_{SINR} is added when calculating the SINR of MCells. Similarly, s_i and ρ_i in equations (2.2) and (2.3) are modified to

$$s_i = \begin{cases} s_{MCell}, \\ s_{SCell} + \alpha_{RSRP}. \end{cases} \tag{2.6}$$

$$\rho_i = \begin{cases} \rho_{MCell}, \\ \rho_{SCell} + \alpha_{RSRQ}. \end{cases} \tag{2.7}$$

Fig. 2.4 shows the effect of cell coverage change after the offset is introduced. As can be seen from the figure, the coverage of the MCell becomes smaller and the coverage of the SCell becomes larger than before. Light-colored areas represent the coverage area with bias. The UEs in these areas are offloaded to the micro base station.

CRE can bring some fairness to the UL, but it will cause some new problems at the same time. For example, if the offset is set too large, the resource of MCells may not be fully utilized. In addition, SCell edge UEs will suffer from high interference in the DL

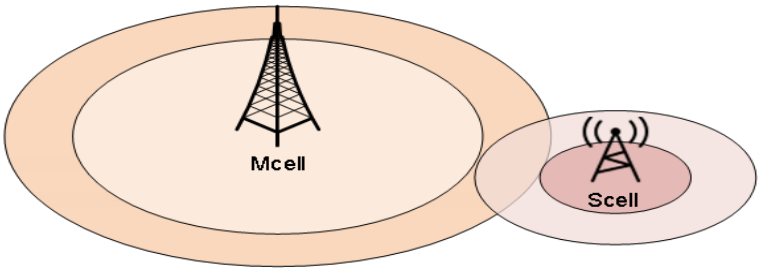

Figure 2.4: The change of BS coverage after introducing a bias.

Table 2.2: Qualitative Comparison among Existing Cell Association Schemes for Multi-tier Networks

	RSRP	RSRQ	CRE
Objective	Maximize received signal power	Maximize SIR	Balance traffic load
Applicability	UL and DL	UL and DL	DL
Channel-aware	✓	✓	✓
Interference-aware	×	✓	✓
Traffic load-aware	×	×	✓
Resource-aware	×	×	×

since the strongest SINR/RSRP/RSRQ is from MCells. Therefore, some techniques, like ICIC [26], have been developed to combat this kind of interference. Only in this way can increase the SCell resource utilization without influence the performance of SCell edge UEs.

A qualitative comparison among these cell association schemes is given in Table 2.2 [27]. The specific key terms used in Table 2.2 are defined as follows. Channel-aware refers to knowing the transmission power at the receiver and knowledge of the instantaneous channel. Interference-aware refers to knowing the instantaneous interference at the receiver. Traffic load-aware refers to knowing the traffic load information. Resource-aware refers to knowing the resource allocation information. The schemes in the table are getting better and better from left to right, but the corresponding required information is also increasing. Their purpose is to allocate UEs as reasonably as possible to each BS for optimal performance. These schemes are tractable and straightforward. However, to ensure optimal performance in multi-tier HetNets, critical parameters such as offset values and transmission power need to be optimized. More importantly, with the development of HetNets, some limitations of these technologies are gradually revealed. Therefore, it is necessary to study new access strategies to meet the requirements of the network structure.

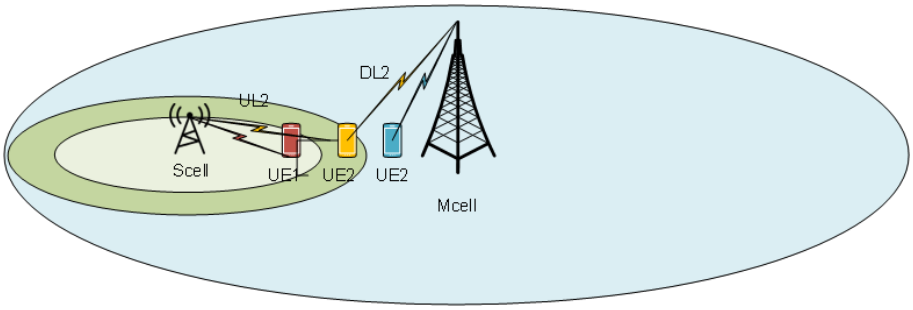

Figure 2.5: A scenario of downlink and uplink decoupling.

2.4 Downlink and Uplink Decoupling

A better method proposed to solve the UL and DL imbalance problem and make better use of the spectrum resources of SCells is DUDe, which allows UEs to connect to different BSs in the UL and DL. DUDe brings in the benefits of having very high offsets in the UL without the interference effects in the DL.

The DUDe strategy is shown in Fig. 2.5. The cell association criterion here is RSRP. Since the MCell has a much larger transmission power than the SCell, it has broader coverage, just like the blue cycle in the figure. According to traditional coupled uplink/downlink access, UE2 and UE3 are associated with the MCell, and UE1 is associated with the SCell. All the UEs are associated with the same BSs in the UL and DL. For UE1 and UE3, they connect to the BS with the strongest RSRP in both DL and UL. However, for UE2, since it is closer to the SCell than to the MCell, the path loss will be lower if it connects to the SCell. If the DUDe strategy is adopted, the DL connection will keep unchanged, but the UL connection will switch from UL1 to UL2. In this way, UE2 is associated with the MCell in the DL and the SCell in the UL. The connection pairs are all the best in both directions. In fact, DUDe not only pushes more UEs to SCells in the UL, but it can also improve the SNR and energy efficiency. If UEs transmit at a fixed power, a connection to a closer BS provides a higher SNR. If the target SNR is fixed, UEs can transmit at a lower power via power control, then the interference to neighboring BSs is reduced, and the UL capacity is increased.

Similarly, the UL and DL operating frequency bands can also be decoupled. As the frequency of C-band is higher than existing systems, using the existing 4G spectrum of sub-3 GHz to carry 5G NR UL services becomes a natural option. At Mobile World Congress 2019, Huawei presented a ”5G Uplink and Downlink Decoupling” scheme, where C-band is used for the DL and a sub-3 GHz band (for example, 1.8 GHz) for the UL, thereby improving UL coverage, as shown in Fig. 2.6 [4]. Since the coverage of

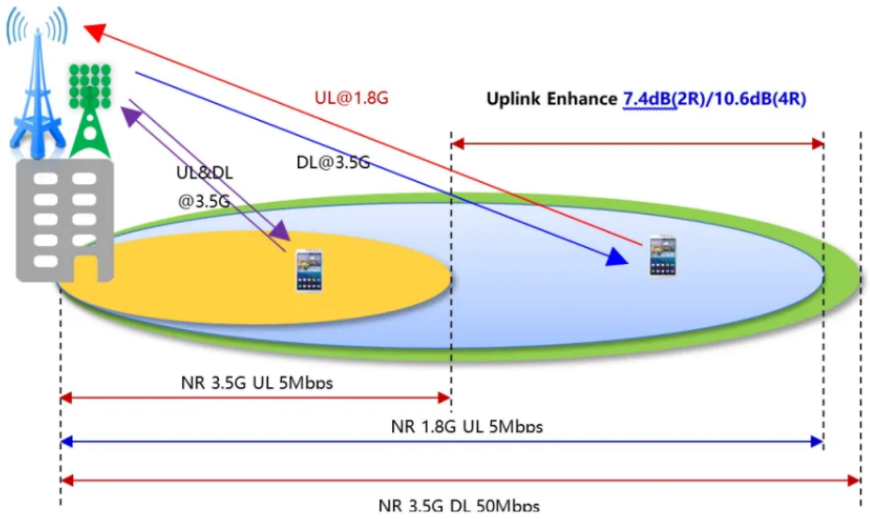

Figure 2.6: Combining DL on C-band with UL on sub-3 GHz band.

BSs in the UL is widened, mobile operators can deploy fewer new sites in the 5G era.

2.5 Millimeter Wave (mmWave) Communications

Wireless communication has reached the bottleneck of insufficient traditional spectrum resources. MmWave communications with abundant available spectrum resources may be a potential choice for next-generation wireless communications. Millimeter-wave refers to electromagnetic waves with wavelengths from 10 mm to 1 m and frequencies from 30 GHz to 300 GHz (the industry has loosely considered any signal with a frequency above 10 GHz to be a mmWave signal). However, the characteristics such as high near-field path loss, severe oxygen and gaseous water molecules absorption have posed significant challenges to mmWave communication. The difficulties in mmWave communications are as follows [28].

- Range and directional communication: According to Friis' transmission law, it can be seen that the free space omnidirectional path-loss is proportional to the square of the frequency [29]. Therefore, mmWave communication systems require highly directional antennas and beamforming to compensate for severe mmWave propagation path-loss [30, 31].

- Shadowing and rapid channel fluctuations: MmWave signals are incredibly vulnerable to shadowing. Shadowing can cause connection interruptions or poor

channel quality. For a given moving speed, the linear relationship between the channel coherence time and the carrier frequency means that the channel coherence time at the mmWave wave is minimal. For example, the Doppler spread at 60km/h at 60 GHz is approximately 3 kHz, that is, the channel will change in the order of hundreds of microseconds, so how to quickly track the mmWave wave channel change is an essential problem in mmWave communications [28, 29]. Luckily, beam steering [28] and dense deployment may solve these problems.

- Multiuser coordination: MmWave communication research and applications mainly focus on point-to-point links (such as cellular backhaul [32]), as well as local area network (LAN) and personal area network (PAN) systems limiting the number of users or having media access control (MAC) protocols that prohibit multiuser simultaneous transmissions [33–36]. For spatial reuse with high spectral efficiency, people need to study new mechanisms to coordinate the simultaneous transmissions on multiple interfering links in mmWave networks.

- Processing power consumption: The power consumption is linear with the sampling rate and exponentially with the number of bits per sample [37, 38]. For low-power and low-cost devices, the high-resolution quantization at wide bandwidths with a large number of antennas is not practical. Especially in high-definition (HD) video transmission, mmWave communications face even more severe technical challenges.

- Oxygen and water molecules absorption: MmWave signals are mainly absorbed by oxygen and water molecules during propagation. Oxygen molecules have different effects on mmWave signals in different frequency bands. Oxygen molecules can attenuate signals by 15 dB/km in 57 to 64 GHz, but the loss in 28GHz, 38GHz and 73GHz are much lower [37, 39]. Humidity and rain fades are common problems for long-range mmWave communications but not an issue when cell sizes are on the order of 200 m [37, 40].

Despite so many challenges above, the mmWave frequency spectrum is a candidate for future broadband cellular communication due to the global bandwidth shortage. Moreover, mmWave communication has some advantages. Because of the highly directional transmission and sensitivity to blockage, mmWave networks are noise-limited rather than interference-limited [29, 41]. In addition, the smaller wavelength of mmWave signals also enables proportionally greater antenna gain for the same physical antenna size. Since mmWave cannot achieve universal coverage, especially in high

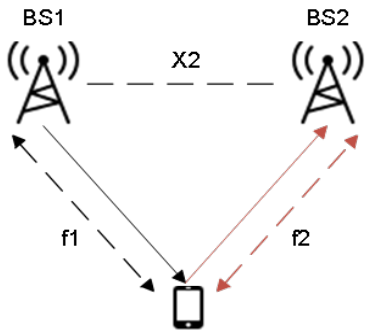

Figure 2.7: Dual connectivity used for DUDe.

blockage areas, we consider a network with mmWave BSs coexisting with ultra-high frequency (UHF) BSs in this thesis.

2.6 Multi-Connectivity

In heterogeneous wireless networks, since the frequency resources and coverage of a single BS are limited, maintaining multiple connections is a better way to meet the user's capacity and coverage requirements, which is called multi-connectivity. In the case of dual connectivity (DC) [42] (Fig. 2.9), each UE is allowed to simultaneously utilize the spectrum from two cells transmitting over different frequencies via non-ideal backhaul links (later releases may add support for infra-frequency band deployments). In DC scenario, the information can be either split or transmitted twice. The two cells are connected via a standard X2 interface. They operate separately, handling their scheduling and control signaling (e.g., HARQ message), thereby significantly relaxing the backhaul requirements [1]. This network architecture with functionality separation is estimated to save more than one-third of the current overall network power consumption [43]. It has been introduced to Release 12 of the 3GPP [44].

Dual connectivity is expected to bring system enhancements as described below.

- Since dual connectivity simultaneously receives or sends multiple data streams, and dynamically accesses the multiple cells with the best radio resources, it can increase user throughput, especially for cell-edge users.

- It enhances mobile robustness. Dense small cell deployments lead to frequent handovers for UEs when moving between SCells. However, if dual connectivity is used, the signaling overhead will be greatly reduced as long as the UE remains in the coverage of the macro cell.

- It alleviates the UL and DL imbalance problem in HetNets. Due to the different transmission powers between MCells and SCells in the DL, UEs sometimes prefer MCell to SCells although connecting to SCells may take advantage of lower path loss. Dual connectivity increases the probability of UEs connecting to SCells.

2.7 Device to Device Communication

2.7.1 Short-Range Communication Technologies

There are a number of different wireless technologies have been developed for very short distances, such as Bluetooth, Wi-Fi Direct, ZigBee, etc. These technical parameters of these short-range wireless communication technologies are shown in Table 2.3 [45]. Among them, D2D communication technology has received great attention. D2D communication refers to direct communication between two mobile users without traversing the BS or core network. Compared to other short-range communication technologies, D2D has a wider communication range, and it operates on a licensed band, therefore can provide a guaranteed rate. D2D communication is more flexible than traditional cellular communication. It can be applied to hotspots such as shopping centers and stadiums to cover the dead zones and improve the network capacity. Moreover, it is a key enabler of IoT. Therefore, it is necessary to study D2D communications in HetNets.

Table 2.3: Comparison of Short Range Technologies

Featured technology	Standard	Spectrum range	Coverage	Max. data rate	Uniformity of service provision
D2D	3GPP	Licensed band	1000 m	1 Gbbps	Yes
Wi-Fi direct	802.11	2.4 GHZ	200 m dB	250 Mbps	No
NFC	ISO 13157	13.56 MHZ	0.2m	424 kpbs	No
ZigBee	802.1504	868/915 MHZ, 2.4 GHZ	10-100 m	250 kpbs	No
Bluetooth	SIG	2.4 GHZ	10-100m	24 Mbps	No

2.7.2 Advantages of D2D communication

The specific advantages of D2D communication are as follows:

- Single-hop communication: D2D communication transforms two-hop communications (via BS) to single-hop communication, which does not require a routing protocol like a multi-hop link, so using a single-hop link has lower complexity and latency.
- Short-range communication: D2D communication is typically used for short-range data transmission, which allows the device to communicate at low transmission power, thereby reducing power consumption and extending the battery life. In addition, since the communication distance is relatively short, a higher transmission rate and a lower delay can be obtained.
- Improve spectrum efficiency: Because of its low transmission power, D2D devices can reuse the CUE spectrum resources without introducing to much interference, thus enhance the spatial bandwidth efficiency through reasonable resource allocation and interference management without lowering the performance of MUE communication.
- Extend cell coverage: Cell edge UEs often encounter poor signal quality while connecting to the BS. If an intermediate UE can act as a relay either between a BS and a UE or between two UEs, the communication quality of the edge UE can be improved and the coverage of cellular service is extended.
- Reduce BS load: Due to the boom of mobile devices, the load of BSs is increasing dramatically. Introducing D2D communication into the network can separate a part of the data exchange that does not need the BS to participate, such as local advertising, proximity-based group gaming, content sharing, etc., and effectively alleviate the load of BSs.

2.7.3 D2D Applications

With the development of the IoT, the applications of D2D are also increasing. Some representative applications are shown in Figure 2.8 [46].

(1) Local service

Local message push: in this service, user data is directly transmitted between terminals. By D2D communication, adjacent UEs can share data among themselves. Friends

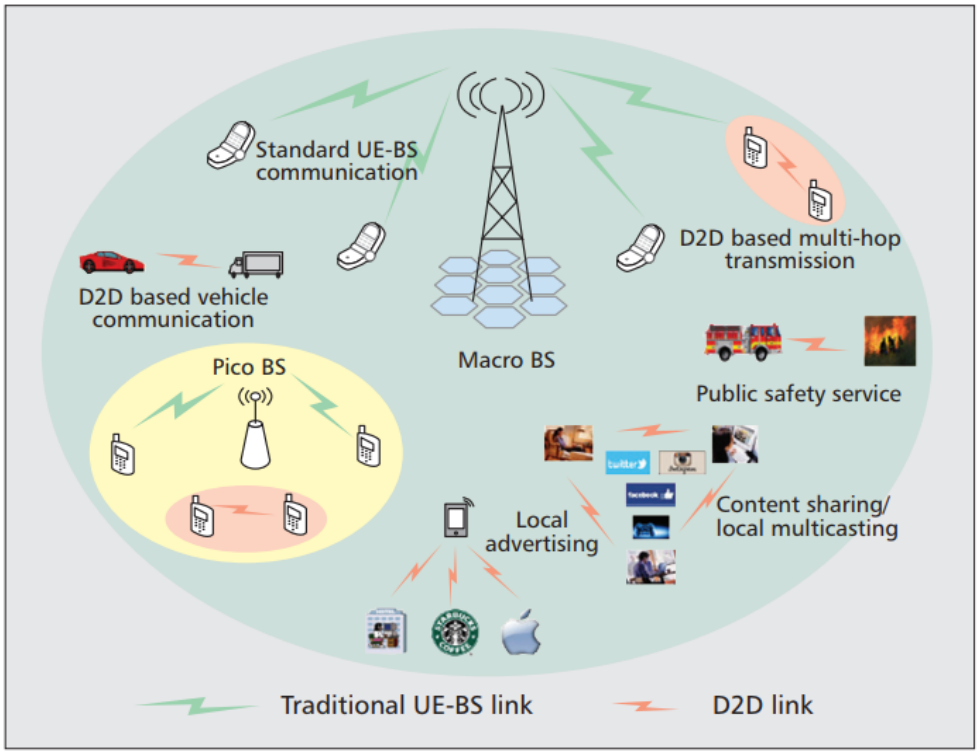

Figure 2.8: D2D application scenarios.

can exchange photos or videos through their smartphones and team up to games. The shops can send the latest promotional information to the surrounding customers.

Network traffic offloading: D2D communication can significantly offload a large amount of data from the traditional cellular transmission. For example, while people are visiting scenic spots, they often want the stories behind them. However, the number of tourists is large, if every visitor in the scenic spot downloads the same content through the cellular network, it will cause a large waste of network resources. If some local servers are deployed in these popular scenic spots to store the introduction materials, when the tourists approach the spot, their mobile phones automatically receive data from the server in D2D mode, which can reduce the pressure of the cellular network while improving the visitor experience.

(2) Internet of Things enhancement

The goal of developing mobile communications is to establish an extensive interconnected network that contains various types of terminals. This is the idea behind developing IoT in cellular communications. New devices will have IoT features, such as autonomous driving, automatically controlling vehicles and various devices. Because there will be many IoT terminals in the 5G network, the access load has become

a serious issue. D2D communication can effectively decrease the access load and latency.

Internet of Vehicles: The Internet of Vehicles plays a vital role in the development of unmanned technology. Driving at a high speed in complex road conditions requires a short response time for the car, but a large amount of access to the internet of vehicles causes a large delay and increases the probability of an accident. If D2D technology is applied to the internet of vehicles, cars can easily complete a series of operations such as autonomously discovering the surrounding vehicles, finding hazards, changing lanes, etc., and truly ensure the safety of people.

Smart home: Instead of accessing all the devices with IoT features to the cellular network, connecting them to an intelligent terminal by D2D first, and then connect the terminal to the cellular network can effectively save the spectrum resources.

(3) Public safety scenarios

In massive emergency scenarios, for example, after a bomb explosion, people use mobile phones to inform their families, network load surges in a short period of time, so the communication requirements of many users cannot be satisfied. In this case, D2D communication can be used to satisfy the basic voice call demands and push the related information to people's mobile phones.

(4) Emergency communications

When natural disasters such as earthquakes and mudslides occur, the cellular communication system may be destroyed. D2D technology is applied to allow users to establish a multi-hop self-organizing network to achieve information transmission between users and provide a solid support for disaster relief.

2.7.4 Key Technologies and Challenges of D2D

Although 3GPP has conducted research on D2D communication technology, D2D communication still has many technical challenges and problems, such as peer discovery, mode selection, security and interference management.

(1) Peer discovery

Looking at the demand of the D2D network, there should be an efficient method for discovering peers before devices communicate with each other. From the user perspective, peer discovery techniques can be classified into two categories: restricted and open. In the first case, devices cannot be discovered by the UEs without their permission. In the second case, devices can be discovered whenever they lie in the proximity of other UEs. From the network perspective, peer discovery can be controlled lightly

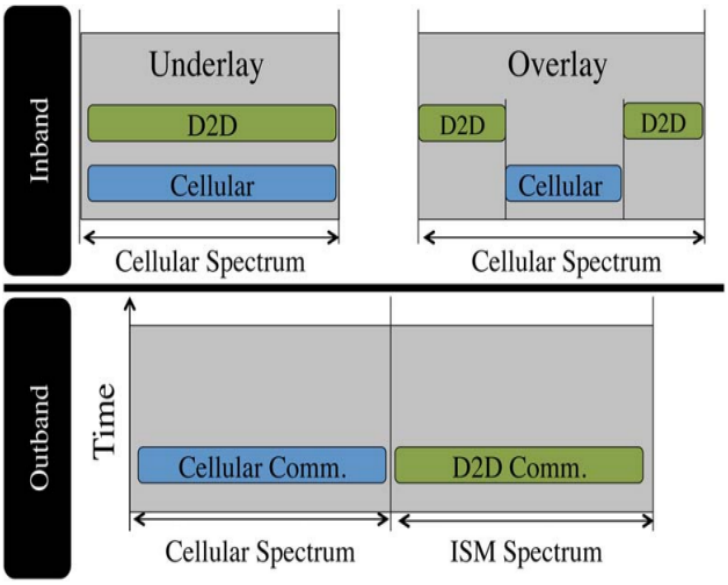

Figure 2.9: Schematic representation of overlay inband, underlay inband, and outband D2D.

or tightly by the BS [46]. Compared to light BS control, tight BS control is more efficient but requires more signaling overhead. Device discovery is the basis for D2D communication and it is necessary to investigate an efficient peer discovery scheme to establish D2D communication quickly.

(2) Mode selection

After the devices discover each other, it is necessary to determine whether D2D communication is preferable compared to cellular communication. Sometimes, even if the requirements of D2D communication are satisfied, the D2D communication mode is not necessarily optimal in terms of performance. Therefore, it is necessary to determine whether D2D communication can be selected through a mechanism to optimize some performance objective, such as spectral efficiency, latency, or transmission power. This process is called mode selection. D2D mode can be divided into two basic modes: inband (on the cellular spectrum) and outband (on the unlicensed spectrum), and the inband mode can be divided into underlay and overlay mode, which means the D2D user shares the spectrum with the cellular user in an orthogonal or non-orthogonal way. If DUEs work in underlay mode, they will cause interference to the CUEs. Fig. 2.9 illustrates the different kinds of D2D communications [47].

In-band Communication: it means that D2D communication uses the licensed

spectrum as cellular communication. The current cellular network has higher control over the licensed band and therefore in-band communication has higher reliability. Some researchers believe that the unlicensed frequency band is uncontrollable due to the large number of UEs, which makes it very difficult to guarantee the UE QoS. In-band D2D communication can be further divided into underlay D2D and overlay D2D according to the way in which the spectrum resources are used. The underlay D2D communication link shares the same spectrum resources as the cellular link, while the overlay D2D communication link uses dedicated spectrum resources for communication. Most of the current research is focused on underlay D2D communication. Next, we will briefly introduce the advantages and disadvantages of in-band D2D communication.

In-band D2D communication has the following advantages: underlay D2D communication can increase the spatial bandwidth efficiency of the system because it can reuse the spectrum resource of CUEs. Because the BSs can effectively control the licensed spectrum, the in-band D2D communication can perform effective QoS management. In-band D2D communication has the following disadvantages: for underlay D2D communication, the reuse of spectrum resources may cause serious interference problems; for overlay D2D communication, due to the use of dedicated spectrum resources, it may cause waste of spectrum resources to some extent.

Out-band D2D communication: refers to D2D communication uses unlicensed frequency bands. The main motivation for selecting out-band D2D communication is that it does not interfere with cellular communication. UEs have to use an extra interface for D2D communication using unlicensed bands. Only devices that have two kinds of interfaces can perform D2D and cellular communications simultaneously. Out-band D2D communication can be divided into the controlled mode when D2D control is done by BSs and the autonomous mode when D2D control is done by users. One of the most significant advantages of out-of-band D2D communication is that it does not cause interference to the CUE, and thus does not have to be allocated dedicated cellular resources like in-band overlay D2D communication. However, there are also some disadvantages, for example, the BS cannot effectively manage the interference of unlicensed frequency bands. At present, research on out-of-band D2D communication is relatively rare compared to in-band D2D communication, but some researchers have begun to explore its advantages and consider whether it can be used as an alternative to in-band D2D communication. The underlay mode DUEs share the same resources as CUEs, thus introduces more interference. As shown in Fig. 2.10(a), when the UL

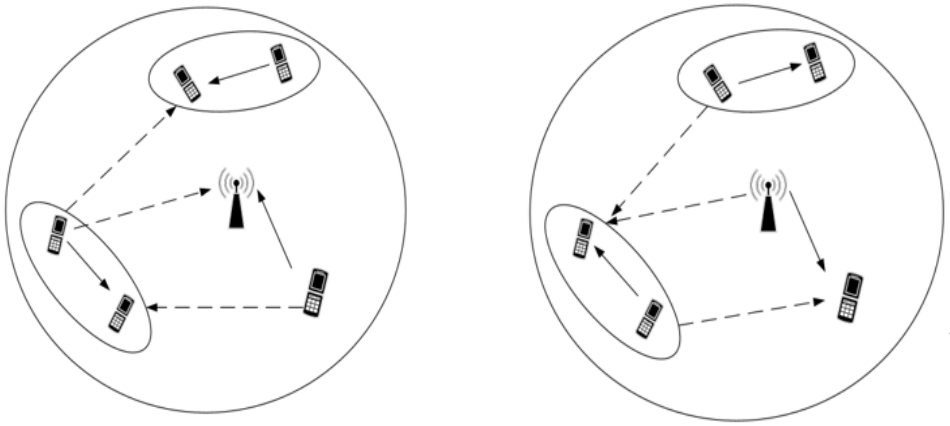

(a) Interference situation when share the uplink resources

(b) Interference situation when share the downlink resources

Figure 2.10: Interference situation in the cell when share the UL and DL resources.

spectrum resource is reused, the D2D receiver receives the interference caused by the CUE using the same resource, if the distance between the CUE and the D2D receiver is close, the interference will be high. Similarly, the communication between the D2D pairs also affects the BSs. The closer the distance between the D2D transmitter and the BS, the more the impact on the BS. When the UL spectrum resource is reused, as shown in Fig. 2.10(b), the CUE will receive the signal sent by the base station, but will also receive the interference caused by the D2D transmitter. Since the transmission power of the BS is high, it will cause interference to nearby D2D users. In order to further improve the spectrum utilization, multiple pairs of D2D users are allowed to reuse the same cellular resources. Whether the UL resources or the downlink resources are reused, interference will occur between D2D user pairs, and the situation becomes more complicated. Since the pressure of data transmission in the DL is larger compared with that in the UL, and BSs can better control the interference, UL spectrum resources are preferentially selected to reuse.

(3) Security issues

Security is an important part of D2D communication. Because the data transmission in D2D communication is via other users' devices, the transmitted data is prone to many security risks. D2D links can be paralyzed by various attacks, such as eavesdropping, denial of service, IP spoofing, and so on. Because of these security issues of D2D communication, it is necessary to ensure the transmission security of D2D communication through strict authentication and key agreement mechanism. Closed access is an effective measure to ensure security. In closed access, the UEs store a list

of reliable devices, such as colleagues, family members, etc.. Devices on the reliable list are free to communicate with each other directly, and the devices out of this list can communicate in cellular mode. For open access, each device can be used as a relay for other devices, and the security cannot be guaranteed. How to ensure security in open access mode is an important issue in current research.

(4) Interference management

Interference management is an important research challenge in D2D communication. As described before, DUEs in overlay mode may cause serious interference to the CUEs. It is necessary to adopt interference management on the D2D communication to improve the system performance. At present, the interference problem in the network is generally solved by resource allocation and power control.

2.8 Cellular-Enabled Unmanned Aerial Vehicular Communication

With the maturity of unmanned aerial vehicle (UAV) services such as cargo delivery, photography and surveillance, the global market for UAVs has substantially increased over the past decade. The UAV industry has become a new driver of economic growth as it taps into new business opportunities for the telecom operators [48]. For one thing, UAVs are aerial terminals that can be served by cellular networks, which can be added to its existing population of users [49, 50]. For another, UAVs can act as flying BSs to boost throughput, coverage, and quality of service (QoS) of cellular networks [51–53]. The former case is considered in this thesis.

At present, most UAVs in the market depend on direct point-to-point communication with ground pilots or ground control stations (GCSs) over the unlicensed spectrum [54]. Although the unlicensed spectrum is free and can satisfy some personal applications like visual LOS aerial photography, it is data rate and coverage are limited, unreliable, insecure, and vulnerable to interference. The surging number of UAVs and ever-increasing requirements for UAV communications call for a more effective and reliable communication strategy. A promising approach that has recently gained popularity is utilizing cellular networks, i.e. cellular-enabled UAV communications.

Providing enhanced communication support for UAVs via LTE has recently been approved by 3GPP, [55], while the feasibility of such approach was demonstrated in [48, 56]. Although 4G networks can meet the requirements of some services, it cannot support services requiring high data rate and/or extremely low latency. The major

challenges of 4G-enabled UAV communications are:

Limited UL capacity: The 4G bandwidth is limited and hard to meet the demand for some data-hungry applications, such as high definition (HD) broadcast and aerial surveillance.

High interference: Most of the channels between UAVs and BSs are LOS, and the antennas on the UAVs are generally omnidirectional, in this case UAVs generate/receive UL/DL interference to/from more BSs than GUEs.

Limited coverage height: The coverage of 4G cells is designed for GUEs. The flight height of UAVs is not within the main lobe of ground BS antennas, thus there are blind areas in the airspace above 120 meters.

High latency: As computing resources are only deployed in the core network, network congestion can cause high latency.

Fortunately, such 4G limitations have been overcome in 5G. With the use of the C-band and mmWave band, the single carrier bandwidth of 5G networks can be 5-20 times higher than that of 4G networks [57]. Besides, MIMO and beamforming technologies can be applied to narrow the beamwidth and improve antenna gain, which compensates for the high mmWave propagation loss, and reduces the intra-cell and inter-cell interference, as well as the interference between the UAVs and GUEs[1]. Furthermore, MEC can be leveraged to reduce latency by integrating the processing and storage modules within the MEC servers to ensure real-time performance. Thus, in this thesis we focus on 5G-enabled UAV communications, and utilize the mmWave band for UAV data transmission to reduce interference to GUEs and improve the network data rate.

2.9 Reinforcement Learning

Reinforcement learning (RL) is a category of machine learning methods that are concerned with how software agents ought to take actions in an environment so as to maximize the notion of cumulative reward. The idea of reinforcement learning algorithms is very simple. Take the game as an example, if a certain strategy can be adopted in the game to get a higher score, then further strengthen the strategy in order to continue to achieve better results.

Some key terms that describe the elements of an RL problem are:

[1] Although some may question the practicability of mmWave-enabled communication, the challenges and solutions have been well addressed in [58, 59].

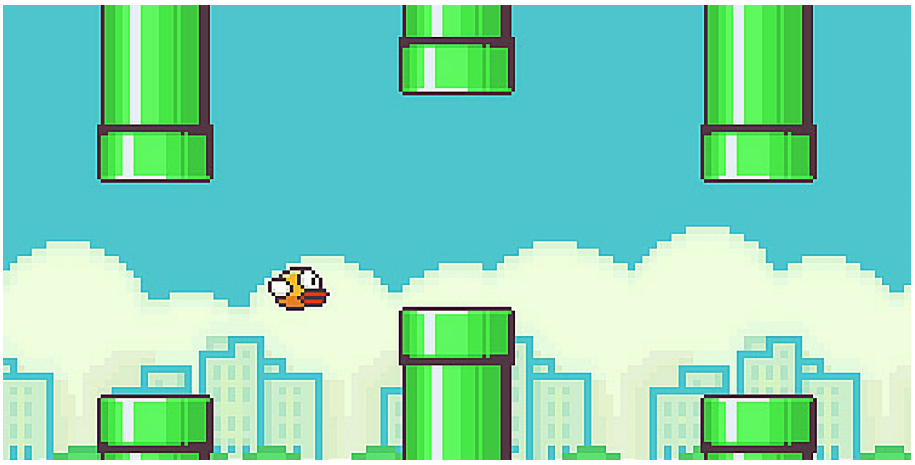

Figure 2.11: Flappy Bird.

- Agent: It is an assumed entity that performs actions in an environment to gain some reward.
- Environment (e): A scenario that an agent has to face.
- Reward (R): An immediate return given to an agent when he or she performs specific action or task.
- State (s): State refers to the current situation returned by the environment.
- Policy (π): It is a strategy which applies by the agent to decide the next action based on the current state.
- Value (V): It is expected long-term return with discount, as compared to the short-term reward.
- Q value or action value (Q): Q value is quite similar to value. The only difference between the two is that it takes an additional parameter as a current action.

Take Flappy Bird as an example, we need to click on the screen to fly the bird as far as possible without hitting a pipe. The farther the bird flies, the higher the bonus. The bird - Agent All kinds of water pipes - Environment The position of the bird - State Click the screen to fly the bird - Action The farther the bird flies, the more points you get - Reward

RL has a lot of applications, the most well-known one is for playing games. AlphaGo Master defeated a world champion in the game of go in 2016, then AlphaGo Zero, a version created without using data from human games, exceeded AlphaGo

Master in 40 days. AlphaStar beat the top player Dario " TLO " Wunsch in StarCraft II. Apart from this, RL can be applied to robotics for industrial automation, text summarization engines, business strategy planning, etc..

RL algorithms can be divided into: model-based and model-free. In model-based algorithms, you need to create a virtual model for each environment. The agent learns to perform in that specific environment. However, if the model is inconsistent with the real world, it will not perform well in the actual use scenario. By contrast, model-free RL aims to acquire an effective behavior policy through trial and error interaction with a black box environment [60], which is easier to implement and adjust to real scenarios. Q-learning (QL) is a commonly used model free method. It updates Q values which denotes value of doing action a in state s by the weighted average of the old value and the new information. The value update rule is

$$Q^{new}(s_t,a_t) \leftarrow \underbrace{Q(s_t,a_t)}_{\text{old value}} + \alpha \overbrace{(\underbrace{r_t}_{\text{reward}} + \gamma \underbrace{\max_a Q(s_{t+1},a)}_{\text{estimate of optimal future value}} - Q(s_t,a_t))}^{\text{temporal difference}}, \tag{2.8}$$

$$\underbrace{\qquad\qquad\qquad\qquad\qquad\qquad\qquad\qquad}_{\text{new value (temporal difference target)}}$$

where $\gamma \in [0,1]$ is the discount factor, which makes rewards from the uncertain far future less important than the ones in the near future that it can be fairly confident about, and $\alpha \in [0,1]$ is the learning rate determines to what extent newly acquired information overrides old information. (2.8) is according to Bellman equation

$$Q(s_t,a_t) = r + \gamma \max_{a_{t+1}} Q(s_{t+1},a_{t+1}). \tag{2.9}$$

It means the maximum return in each state is equivalent to the sum of the maximum immediate reward and and the return (discounted by γ) obtained by following the optimal policy thereafter until the end of the episode (i.e., the maximum expected reward from the next state).

Q-learning only works in environments with discrete and finite state and action spaces. Otherwise calculate and store the Q-value for each state-action combination can be infeasible. To extend Q-learning, we can train a function approximator, for example a neural network with parameters θ, to estimate the Q-values, i.e. $Q(s,a) \approx Q(s,a;\theta)$. This is called deep Q-learning (DQL). To get the parameters θ, we need to

minimize the following loss function

$$L(\theta) = E[(r + \gamma \max_{a'} Q(s', a'; \theta') - Q(s, a; \theta^{-}))^2]. \tag{2.10}$$

where s', a' are the next action and state of s, a, θ^{-} is a snapshot of the network parameters from a few iterations ago. Then, perform a greedy descent step on $r + \gamma \max_{a'} Q(s', a'; \theta') - Q(s, a; \theta^{-}))^2$ with respect to θ. Q-Learning and DQL are off-policy algorithms that learn about the greedy policy $a = \max_a Q(s, a); \theta$ while using a different behaviour policy for acting in the environment. This behaviour policy is usually an ε-greedy policy, where a random action is taken with a probability ε to ensure good coverage of the state-action space, and the greedy action is taken with a probability $1 - \varepsilon$.

2.10 Mobile Edge Computing

Recent years have witnessed how MDs have become an indispensable part of daily life. The development of mobile devices has triggered numerous new applications, such as language recognition, map navigation, augmented reality, face recognition, cloud gaming, and so on. These applications are computation-intensive and latency-sensitive. Due to the limited battery power and computation resources of mobile devices, computationally-intensive tasks and workloads are often offloaded to remote computational servers, under the notion of cloud computing. To avoid long-distance transmission latency from the MDs to cloud servers, MEC has been proposed as a supplement to cloud computing, which enables cloud computing to be done at the edge of a mobile network. Compared with cloud computing, edge computing servers are deployed closer to users. MEC allows processes to take place in BSs, central offices, and other aggregation points on the network. Fig. 2.12 shows the possible locations of MEC in end-to-end network [61]. In this thesis, we consider MEC at MBSs and SBSs.

MEC has become a promising technique to satisfy the latency, capacity and security requirements of many emerging services [62, 63]. At present, the smart factory, smart city, live streaming/gaming and V2X are the most typical applications for MEC. Their requirements for MEC are shown in Fig. 2.13 [61]. They are also the requirements for typical 5G scenarios, i.e. the high bandwidth of eMBB, the ultra-high reliability and low latency communication of URLLC, and the large connections of MIoT. Therefore, MEC and 5G are mutually reinforcing. 5G network realizes the breakout of data traffic

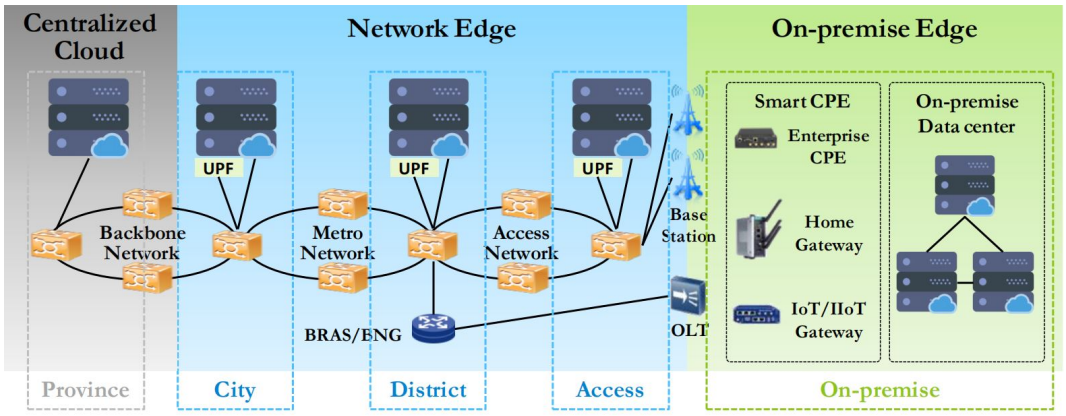

Figure 2.12: The locations of MEC in end-to-end network.

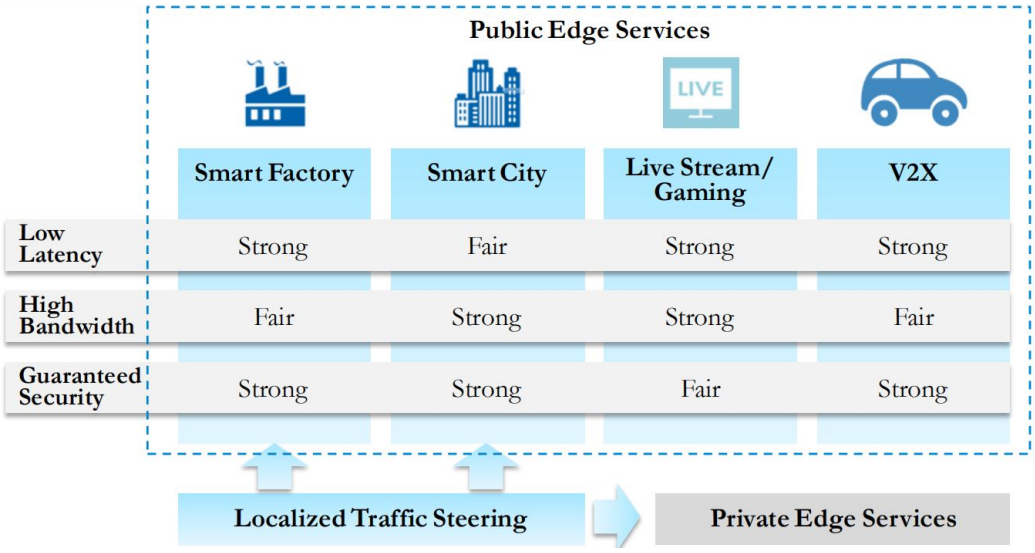

Figure 2.13: Typical use cases and requirements of MEC.

through the flexible deployment of the user plane function (UPF) at the edge of the network, and the flexibility of UPF deployment accelerated the development of edge computing.

2.11 Optimization Problem

In this thesis, we are going to solve a series of resource allocation problems, they are essentially optimization problems. A general optimization problem follows the standard form below:

$$\min_{\mathbf{x}} \quad f_0(\mathbf{x}), \tag{2.11}$$

$$\text{s.t.} \quad f_i(\mathbf{x}) \leq 0, \quad i = 1, ..., m \tag{2.11a}$$

$$h_i(\mathbf{x}) = 0, \quad i = 1, ..., p \tag{2.11b}$$

$$\tag{2.11}$$

where $\mathbf{x} = [x_1, ..., x_n]^T$ is the optimization variables, $f_0(\mathbf{x})$ is the objective function, $f_i(\mathbf{x})$ denote the inequality constraint functions, $h_i(\mathbf{x})$ denote the equality constraint functions. The aim is to find the optimal solution $\mathbf{x}^*$ which realises the smallest value of $f_0(\mathbf{x})$ while satisfying the constraints.

Since the late 1940s, a large effort has gone into developing algorithms for solving various classes of optimization problems, analyzing their properties, and developing good software implementations. However, we can only effectively solve a few classes of them, for example, linear programs, least-squares problems, and convex optimization problems. In fact, linear programs and least-squares problems are special cases of the general convex optimization problem. The standard form of a convex optimization problem is as follows:

$$\min_{\mathbf{x}} \quad f_0(\mathbf{x}), \tag{2.12}$$

$$\text{s.t.} \quad f_k(\mathbf{x}) \leq 0, \quad k = 1, ..., m \tag{2.12a}$$

$$\mathbf{a}_k^T \mathbf{x} = b_k, \quad k = 1, ..., p \tag{2.12b}$$

$$\tag{2.12}$$

where the objective function $f_0(\mathbf{x})$ and inequality constraint functions $f_1, ..., f_m$ are convex, the equality constraints, characterized by $\mathbf{a}_k \in \mathbb{R}^n$ and $b_k \in \mathbb{R}$ for $k = 1, ..., p$,

are affine.

Most problems in the world are non-convex, in this case, what we can do is transforming them into convex optimization problems. There are very effective algorithms that can reliably and efficiently solve large convex optimization problems with hundreds or thousands of variables and constraints, and convex optimization problems have very useful properties such as if the objective function is strictly convex, then the problem has at most one optimal point, and the local minimum is also the global minimum. Once you formulate a practical problem as a convex optimization problem, you can solve it via many effective methods. Unconstrained minimization problems can be solved by decent methods, such as the gradient descent method, steepest descent method, Newton's method, and so on. Equality constrained minimization problems can be reduced to an equivalent unconstrained problem by eliminating the equality constraints, after which descent methods can be applied to solve it. The other way is to solve the dual problem which is unconstrained, and then recover the solution of the original problem from the dual solution. Inequality constrained minimization problems can be solved by interior-point methods [64]. Of course, we can also optimization toolbox solvers to solve the problems, such as CVX, MIDACO, etc.

2.12 Simulation Process

Cellular network simulations can be divided into two categories: link-level and system-level. Link-level simulations are basically a software implementation of one or multiple links between a BS and a UE, with a channel model to reflect the actual transmit of the waveforms generated. The system-level simulation focuses on the performance of the entire network to evaluate the impact of resource scheduling, power control, routing, etc., on the system.

The process of system level simulation can be briefly decried as follows: first, UEs are randomly distributed in one or more cells, and some basic parameters, such as transmission power, bandwidth, are set for the BSs and UEs; then, the channel fading information between all links is calculated according to the UE distribution in the cell, and the UEs feed back the channel state information (CSI) of the channels to the BSs, and BSs perform resource allocation and power control according to the information and the corresponding algorithm. After multiple iterations, the advantages and disadvantages of the algorithm are summarized according to information such as system throughput, latency, fairness, and time complexity.

This thesis carries out system-level simulations using Matlab. The simulation is mainly divided into three parts: network initialization, algorithm simulation and output statistics. The initialization part is to set the coordinates of the UEs and BSs in the network, and perform channel initialization and power initialization for the UEs, and calculate the CSI information among all UEs in the whole system according to the node coordinates and fading. The algorithm simulation part mainly verifies the performance of the algorithm in the network. The output statistics part mainly calculates the throughput, latency and energy efficiency of the whole system, the capacity between the links, etc., and the average of the results of multiple iterations is averaged and visualized to figures or charts.

Chapter 3

Capacity Enhancement Decoupled Access

3.1 Introduction

This chapter investigates the compatibility of mmWave communication and multi-connectivity in DUDe. Increasing communication capacity has always been a major goal from 1G to 5G. However, in 5G era, insufficient traditional spectrum resources has become an bottleneck of wireless communications. In such a situation, mmWave frequency spectrum is envisaged to offer an essential lifeline for future broadband cellular systems in the quest to satisfy the anticipated explosive traffic demands. However, due to the directional transmission of mmWave, where the multi-user interference may fall precipitously, mmWave systems are noise-limited [29, 41]. Nonetheless, the smaller wavelength of mmWave signals enables proportionally greater antenna gain for the same physical antenna array [29]. That said, the propagation characteristics, such as high near-field path-loss, severe oxygen and water molecules absorption, pose great challenges. Fortunately, recent research shows that these problems can be overcome using highly directional antennas and beamforming techniques [30, 31], but as mmWaves are sensitive to blockage, mmWave BSs alone can not achieve universal coverage, using mmWave BSs with ultra-high frequency (UHF)[1] BSs is an appealing approach. UHF frequency bands can provide seamless coverage and high mobility, while mmWave bands can support ultra-high data rates. A recent study in [66] showed that to satisfy acceptable exposure limits at frequencies above 6 GHz, the maximum

[1]UHF refers to the radio frequencies in the range between 300 MHz and 3GHz. Most frequencies used in mobile 4G network are classified in the UHF band [65].

transmission power in the UL should be several dBs below the power levels used in current cellular technologies. Although the SNR can be maintained by mounting antenna arrays on the BS, it is also possible to achieve this by shortening the distance between BSs and UEs to reduce the path-loss. Nonetheless, mmWave signals tend to experience lower SNRs, as the mmWave bandwidth is much wider than UHF bandwidth and the transmission power per Hertz for mmWave is much lower than that of the UHF signals. In this case, DUDe can be applied to shorten the BS-UE distance to improve the UL SNR.

Since its inception, much research has been done on DUDe. For instance, the authors in [2] used real data from Vodafone's LTE network to evaluate the potential throughput gain of DUDe. This technique was found to achieve 100%-200% improvement in the 5^{th} percentile UL throughput, and more so in the 50^{th} percentile throughput in a dense HetNet deployment. The analytical SINR coverage and joint UL-DL rate of DUDe are obtained in [67]. The authors of [68] derived the association probability based on stochastic geometry, and showed that as the density of SCells increases, a large number of UEs choose to receive from an MCell in the DL, and transmit to an SCell in the UL. The UL performance improvement brought by DUDe was investigated in [69]. Their results show that DUDe can improve load balance, and is particularly beneficial to ultra-dense networks. A number of studies have examined the application of DUDe in mmWave-UHF hybrid networks including, e.g. [70], in which the authors have derived the SINR and rate distributions from path-loss based and capacity-based cell association perspectives. Also, in [71], O. W. Bhatti et al. analyzed the performance of DUDe in such networks using real blockage data. However, those studies are based on minimum path-loss (Min-PL) cell association scheme. According to this association criteria, users may prefer UHF BSs to mmWave SBSs due to the high path loss of mmWave, although their spectrum resources are more abundant.

Another way to improve the network data rate is allowing a user to be simultaneously served by multiple BSs [10, 11]. In the case of dual connectivity (DC) for instance, each UE is allowed to simultaneously utilize the spectrum from two BSs connected together via non-ideal backhaul links. In such scenarios, the information can be either split or transmitted twice. This network architecture with functionality separation is estimated to save more than one-third of the current overall network power consumption [43]. However, as the transmission power of UEs is limited, adopting this in the UL could be counterproductive unless combined with DUDe to make it more power efficient. [72] introduced DUDe to dual connectivity, but to the best of our

knowledge, DUDe and dual connectivity in UHF/mmWave hybrid network have not been considered before.

3.1.1 Main Contributions

This chapter investigates the feasibility of mmWave with DUDe in HetNets. In particular, we focus on decoupling the UL and DL serving BSs from the perspective of maximizing the total network capacity. To this end, we propose an efficient joint resource-management and cell-association technique for hybrid HetNets, and compare its performance for a wide range of metrics with benchmark single and dual connectivity alternatives. Specifically, we investigate the performance of single and dual connectivity techniques in both path-loss based and capacity-based approaches in three-tier UHF-mmWave hybrid network, where mmWave SCells, UHF SCells and MCells coexist. For comparison, the special case where all SBSs are of the same type is also considered. To evaluate the potentials of capacity-based cell association scheme, we formulate the problem of joint cell association and network capacity maximization as a mixed-integer nonlinear programming problem, which serves as an upper-bound benchmark of the network capacity. Besides, the complexity and energy efficiency analyses of the proposed technique are also provided.

3.1.2 Organization

The rest of this chapter is organized as follows. In Section 3.2, the assumptions considered in the system model are explained. In Section 3.3, the proposed joint resource-management and cell-association technique with decoupling capability is presented. In Section 3.4, the performance of path-loss based and capacity-based cell association schemes are evaluated in the single and dual connectivity scenarios. Finally, Section 3.5 concludes the chapter.

3.2 System Model

3.2.1 Heterogeneous network model

We consider an orthogonal frequency-division multiple access (OFDMA) HetNet with UHF MCells, UHF SCells, mmWave SCells and UEs following independent homogeneous Poisson Point Processes (HPPP) Φ_m, Φ_{s_1}, Φ_{s_2} and Φ_u with intensities λ_m, λ_{s_1},

λ_{s_2} and λ_u, respectively. The ratio of the SCell density to the MCell density is denoted by β, while the ratio of UHF SCells to all SCells is denoted by γ. The user traffic is based on the full-buffer model.

In 2010, Jeffery G. Andrews et al. first modeled cellular networks based on stochastic geometric theory and proposed an HPPP model [73]. It used a HPPP to model the distribution of nodes in a cellular network and simulated the coverage and average achievable rate of the cellular network.

3.2.2 Cell Association model

We consider macro base stations (MBSs) transmitting over UHF bands, and small base stations (SBSs) transmitting over UHF or mmWave bands. It is also assumed that the UEs can connect to any type of BSs and are capable of operating at UHF and mmWave bands. Also, each UE can connect to one BS or two BSs over different sub-carriers. In the DL, the UEs connect to the best one or two BSs according to the biased reference signal received power (RSRP) criterion [25, 26]. If the UL and DL are coupled, the UEs connect to the same BSs in both link directions; otherwise, the UL BSs will be separately selected using the path-loss based association in [2], or the capacity-based association proposed in this chapter. It is worth emphasizing that the UE can connect up to 2 BSs on each link direction simultaneously (i.e. 4 BSs in total). While it is possible to allow each UE to be associated with more than two BSs for each link direction, it was found that the resulting improvement in sum-rate is negligible. This is because the potential capacity gain for the UEs connecting to more than two BSs is more often outweighed by the amount of interference caused to adjacent BSs; ultimately leading to an overall capacity reduction. Furthermore, complexity significantly increases, as the more BSs a UE is connected to, the more overhead is generated, adding to the side-information to be processed.

The core idea of capacity-based association is to adaptively switch between coupling and decoupling the UL and DL on the basis of maximizing capacity at each link; similarly for when adapting between single and dual connectivity. This association scheme will be further explained in Chapter 4, while in this section, we will briefly describe the Min-PL based association scheme.

In the Min-PL criterion, the UEs are connected to the BS with the lowest path-loss

[2, 72]. A typical UE is associated with a BS at $x^* \in \Phi_l$ in the UL if and only if

$$P_u W_l {L_l}^{-1} \geq P_u W_k L_{min,k}^{-1}, \quad \forall k,l \in \{s_1, s_2, m\}, \tag{3.1}$$

where P_u is the transmission power of UE u, W is the UL cell bias value which is positive referring to expanding the coverage of the cells, L_l is the UL path-loss of the typical UE to the BS l, and $L_{min,k} = \min_{x \in \Phi_k} L_k(x)$ is the minimum UL path-loss of the typical UE to the k^{th} tier BS.

3.2.3 Uplink and Downlink Interference Model

The system bandwidth is equally divided into N orthogonal resource blocks (RBs), where each RB is divided into 12 resource elements (REs). Each RE refers to a subcarrier. The subcarrier spacing is 15 kHz for UHF and 60 kHz for mmWave. UEs in the same cell occupy orthogonal RBs, so there is no intra-cell interference, but UEs in different cells interfere with each other. Moreover, there is no interference between UHF and mmWave cells as their frequency bands are orthogonal. The DL SINR between UE k and its serving BS i at RB n is given by

$$\eta_{i,k,n} = \frac{\Gamma_{i,n} \hbar_{i,k,n} L_{i,k,n}^{-1}}{\eta_0 + \sum_{j=1}^{B} \Gamma_{j,n} \hbar_{j,k,n} L_{j,k,n}^{-1}}, \quad j \neq i, \tag{3.2}$$

where $\Gamma_{i,n}$ is the transmit signal power of the BS i at the RB n, $\hbar_{i,k,n}$ is Rayleigh fading channel for UHF signals and Rician fading channel for mmWave signals. The K-factor is set to be 7dB for LOS and 6dB for non-LOS (NLOS) [74]. The number of paths is 10. The adopted multipath channel model is the same as [75]. $L_{i,k,n}$ is the path-loss, $\sum_{j=1}^{B} \Gamma_{j,n} \hbar_{j,k,n} L_{j,k,n}^{-1}$ is the interference power (for $j \neq i$), B is the number of BSs and η_0 is the additive white Gaussian noise (AWGN). On the other hand, the UL SINR is given by

$$\eta_{k,i,n} = \frac{\Gamma_{k,n} \hbar_{k,i,n} L_{k,i,n}^{-1}}{\eta_0 + \sum_{l=1}^{K} \Gamma_{l,n} \hbar_{l,i,n} L_{l,i,n}^{-1}}, \quad l \neq k, \tag{3.3}$$

where $\Gamma_{k,n}$ is the transmit signal power of UE k at RB n , K is the number of UEs and $\Gamma_{l,n}$ is the transmission power of other UEs.

3.2.4 Resource Allocation

Resource allocation is performed using the aperiodic channel quality indicator (CQI) [76] reported from the UEs. In LTE and LTE-A systems, the CQI is often used for packet scheduling (PS). Specifically, PS refers to selecting the scheduling time and frequency for each UE. UEs report the CQI value for each RB to their serving BS. The BSs utilize these CQI reports to select the preferred RBs for each UE. The CQI report from a given UE includes information regarding the SINR for each physical RB from the received pilot power and total interference every measurement period.

3.2.5 Propagation Model

The path-loss $L(d)$ is modeled as

$$L(d) = 20\log\left(\frac{4\pi f}{c}\right) + 10\theta\log(d) + \chi, \tag{3.4}$$

where d is the distance between the UEs and BSs, f is the operating frequency, c is the light speed, θ is the path-loss exponent, and χ is the zero-mean log normal shadowing. Line-of-sight (LOS) mmWave, none-line-of-sight (NLOS) mmWave and UHF links have different values of α and χ. We adopt the same blockage model as in [77]. If the distances between the users and mmWave SCells are less than the threshold μ = 200 m, then these links are assumed LOS with probability ω = 0.2, otherwise, these links are assumed NLOS. The parameters μ and ω are environment-dependent.

It is assumed that the UHF BSs are equipped with omni-directional antennas, the mmWave BSs are equipped with directional antenna arrays to compensate for the high path-loss, and the UEs are equipped with omni-directional antennas [70, 77]. The antenna gain at a mmWave BS is formulated by

$$G_b(\theta) = \begin{cases} G_M, & |\theta| \leq \theta_b/2, \\ G_m, & \text{otherwise}, \end{cases} \tag{3.5}$$

where $\theta_b = 10^\circ$ is the beamwidth of the main lobe, $G_M = 18$dBi and $G_m = -2$dBi denote the gains of main lobe and side lobe, respectively. The mmWave UEs are assumed to be in perfect alignment with their serving cells, while the beam directions of interfering mmWave links are independently and uniformly distributed in $[-\pi, \pi]$. Moreover, the antenna gain of an interfering mmWave link is G_M with a probability of

$p_M = \theta_b/2\pi$, and is G_M with a probability of $p_m = 1 - p_M$.

3.2.6 Energy Efficiency Model

As DUDe will not affect DL cell association, and the BSs are generally assumed to have an abundance of power supply, we only consider the energy efficiency (EE) in the UL [78], which is defined as

$$EE = \frac{\sum_{u\in\Phi_u} \tau_u}{\sum_{u\in\Phi_u} P_u}, \tag{3.6}$$

where τ_u is the data rate of UE u, P_u is the UL transmission power of UE u. P_u (expressed in dBm) can be written as [79, 80]

$$P_u = \min\{P_{\max}, 10\log_{10} M + \alpha\tilde{L} + P_0 + \Delta_{mcs}\}, \tag{3.7}$$

where $P_{\max}$ is the maximum transmission power of UEs, P_0 is the power baseline value reflecting the noise level in the UL, Δ_{mcs} is a parameter which depends on the modulation and coding scheme chosen, M is the number of RBs assigned to the UE, $\alpha \in \{0, 0.4, 0.5, 0.6, 0.7, 0.8, 0.9, 1\}$ is a compensation factor for $\tilde{L}$, which is the total UL signal loss, including path-loss, shadowing, fast fading, etc.

3.3 Capacity-Based Cell Association

In this section we describe the proposed capacity maximization approach. Due to the random nature of the user positions, some BSs may occasionally be highly loaded while others are underutilized. Moreover, the high path-loss of mmWaves makes them often less favorable to UEs than UHF BSs even though they offer much more bandwidth. To increase the participation of mmWave SBSs, association schemes that maximize frequency reuse and capacity should be sought. To this end, we extend the joint network capacity and QoS Maximization (NCQM) method presented in our previous work for conventional HetNets [81] to the case of hybrid-networks with DUDe. Specifically, we refine the criteria and adapt it to encompass the new dimensions of the considered network including dual connectivity and mmWave-BSs. The presented scheme can be divided into two parts. The coupling/decoupling association (CDA) part determines when to decouple the UL and DL, while the single/multi-BS association (SMBA) part determines when to select dual connectivity over single connectivity

per user per link. Using this scheme, some UEs are offloaded to the BSs which can provide more RBs rather than those with lower path-loss.

3.3.1 Coupling/Decoupling Association

In the UL, UEs are initially connected to the same BSs as those in the DL. It is worth noting that one UE can connect to one or two BSs. Thus a association and interference matrix $\Theta \in \mathbb{R}^{B\times K}$ can be constructed as

$$\Theta_{i,k} = \begin{cases} 2, & \text{UE } k \text{ is connected to BS } i, \\ 1, & \text{if } P_{i,k} > \eta_0 + \sigma, \\ 0, & \text{otherwise,} \end{cases} \tag{3.8}$$

where $P_{i,k}$ is the UL interference power, σ is the interference threshold and η_0 is the noise power, $\Theta(i,k)$ represents the relation between UE k and BS i, as follows: a) UE k is served by BS i ($\Theta(i,k) = 2$); b)UE k interferes with BS i ($\Theta(i,k) = 1$); and c) UE k do not interfere with BS i ($\Theta(i,k) = 0$). Since there are N RBs overall, the average number of RBs that BS i can provide to each UE is given by

$$\Omega_i = \left\lfloor \frac{N}{\sum_{k=1}^{K}\{\Theta_{i,k} = 1\} + \sum_{k=1}^{K}\{\Theta_{i,k} = 2\}} \right\rfloor, \tag{3.9}$$

If UE k can get Ω_i and Ω_j RBs from its serving BS i and a neighboring BS j separately, then a candidate pair matrix $\Lambda \in \mathbb{R}^{B\times K}$ can be constructed as

$$\Lambda_{j,k} = \begin{cases} 1, & \Omega_j > \Omega_i,\ i \neq j \\ 0, & \text{otherwise.} \end{cases} \tag{3.10}$$

If $\Lambda(j,k) = 1$, then UE k and BS j is a candidate link. With this in mind, the achievable capacity for each $\Lambda_{j,k}$ is obtained as

$$C_{j,k} = \sum_{n\in\Omega_{j,k}} W \log_2(1+\gamma_{k,j,n}), \tag{3.11}$$

where W is the bandwidth of each RB, $\Omega_{j,k}$ is the index set of RBs that BS can provide to UE k. If $C_{j,k} > C_{i,k}$, calculate the updated network capacity $C_{tot}(j,k)$ with the

candidate association pair (j,k), the way to calculate the network capacity is

$$C_{tot} = \sum_{i=1}^{B} \sum_{k=1}^{K} \sum_{n \in \Omega_{i,k}} W \log_2(1+\gamma_{k,i,n})\}. \tag{3.12}$$

The candidate pair with the highest overall network capacity will replace the original association pair (i,k). This algorithm is guaranteed to converge when it cannot find any more pairings that would improve the overall capacity. The steps above are formulated in a pseudo-code structure in Algorithm 1.

As the capacity for each candidate pair and the overall network capacity need to be calculated many times, the time complexity of this association scheme can be higher than that of Min-PL. According to [82], the time-complexity of the Shannon capacity formula is unknown, therefore we assume it to be $O(1)$. Assuming the number of candidate pairs and deployed UEs are given by K_a and K_b respectively, and the number of candidate pairs satisfying $C_{j,k} > C_{i,k}$ is K_c, then the computational complexity of this scheme is expressed as $(K_c+1)K_bO(1) + K_aO(1) = (K_cK_b + K_b + K_a)O(1)$. Parameters K_a and K_c increase with the number of BSs and UEs.

Algorithm 1 Coupling/Decoupling Association (CDA)

Initialization: calculate Θ, Ω_i, Ω_j and current network data rate $C_{tot}^{'}$.
Set $C_{tot} = C_{tot}^{'}$;
for $k = 1$ until K **do**
  $\omega = (0,0)$;
  for $i = 1$ until B **do**
    if $\Theta_{i,k} = 2$ **then**
      Calculate $C_{i,k}$;
    end if
    for $j = 1$ until B **do**
      if $\Theta_{j,k} = 1$ & $\Omega_j > \Omega_i$ **then**
        $\Lambda_{j,k} = 1$ and calculate $C_{j,k}$;
        if $C_{j,k} > C_{i,k}$ **then**
          Calculate the updated network data rate $C_{tot}(j,k)$ with the candidate association pair (j,k);
          if $C_{tot}(j,k) > C_{tot}$ **then**
            $C_{tot} = C_{tot}(j,k)$;
            $\omega = (j,k)$;

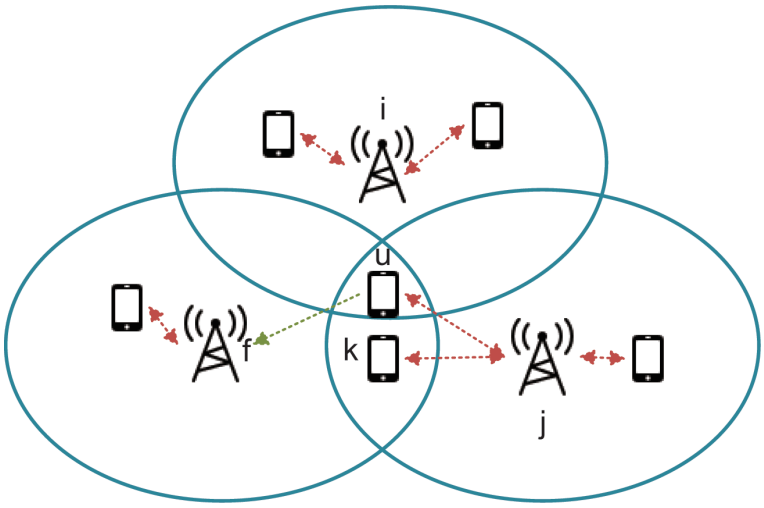

Figure 3.1: Illustration of SMBA association scheme.

else
  Reject the candidate association pair (j,k);
end if
end if
end if
end for
end for
if $\omega \neq (0,0)$ **then**
  Replace the original association pair (i,k) with ω;
  Recalculate Θ, Ω_i, Ω_j;
  Set $C'_{tot} = C_{tot}$;
end if
end for

3.3.2 Single/Multi-BS Association

The association scheme in this part is different from the dual connectivity association scheme in [72] in the sense that UEs can connect to one more BS if higher capacity can be achieved. Only a small portion of the UEs may be connected to two BSs, and thus UEs can connect in a single or dual hybrid connectivity. Assuming UE u is connected to BS j, and BS f is its neighbouring BS, then UE u may also connect to BS f if conditions C1, C2 and C3 are all satisfied, which are stated as follows.

C1: The additional RBs from BS f do not overlap with the existing RBs provided

by BS j as follows

$$\delta_{f,u} + \delta_{j,u} < N, \tag{3.13}$$

where $\delta_{f,u}$ and $\delta_{f,u}$ are the numbers of RBs from BSs f and j separately. If BSs j and f are in different frequency bands, i.e., UHF and mmWave, there is no need to check this condition.

C2: The second connection does not interfere with any other BS (BS i, j and f in Fig. 3.1) that covers UE u within its area, as follows

$$\phi + \delta_{f,u} + \delta_{j,u} < N, \tag{3.14}$$

where ϕ is the number of RBs occupied by BS i or j. Similar to C1, BSs i, f, and j may be in different frequency bands, and UEs transmit over different bands will not interfere with each other.

C3: The second connection does not interfere with any UE (UE k in Fig. 3.1) interfered by BS f, as follows

$$\phi_f + \delta_{f,u} + \lambda_k < N, \tag{3.15}$$

where ϕ_f and λ_k are the numbers of RBs already occupied by BS f and UE k, separately. The achieved capacity for each candidate pair satisfying all the conditions is calculated according to (3.11) and the priority of selection is given to the candidate pair with the highest capacity. This process repeats until the overall capacity in (3.12) cannot be increased any more, so this algorithm is also convergent. These steps are formulated in a pseudo code structure in Algorithm 2. Assuming the number of candidate pairs that satisfy all the conditions is K_s, then the computational complexity can be expressed as $(K_s+1)K_bO(1)$, where the parameter K_s increases with the number of BSs and UEs.

The DUDe technique and our proposed schemes have some impact on the network architecture and signaling overhead. For instance, a central unit is necessary to collect the information from all BSs in the group (A group consists of one, or several, MBSs and some SBSs.) and calculate the parameters needed in our algorithm, such as how many UEs are within the coverage area of each BS in the UL, the number of allocated resources per UE, and the path-loss of each link, so that the central unit can control the

BS handover. Besides, the UL-related control signaling needs to be transmitted from the DL node, while the DL-related control signaling from the UE needs to be received by the UL node, and forwarded to the DL node over the network infrastructure [1].

To construct the association and interference matrix Θ, each BS needs to send its local association and interference map Θ_i to the central unit. If we assume there are B BSs in the coverage of the central unit, BS i has K_i users, and the number of bits needed to encode $\Theta_{i,k}$ is D, then the total number of bits required for all the BSs to forward Θ_i to the central unit is $\sum_{i=1}^{B} K_i D$.

Algorithm 2 Single/Multi-BS Association (SMBA)

Initialization: calculate Θ, Ω_i, Ω_j and current network data rate $C_{tot}^{'}$.
Set $C_{tot} = C_{tot}^{'}$;
for $k = 1$ until K **do**
  $\omega = (0,0)$;
  for $i = 1$ until B **do**
    for $j = 1$ until B **do**
      if $\Theta_{j,k} = 1$ & C1 & C2 & C3 **then**
        Calculate the updated network data rate $C_{tot}(j,k)$ with the candidate association pair (j,k) added;
        if $C_{tot}(j,k) > C_{tot}$ **then**
          $C_{tot} = C_{tot}(j,k)$;
          $\omega = (j,k)$;
        else
          Reject the candidate association pair (j,k);
        end if
      end if
    end for
  end for
  if $\omega \neq (0,0)$ **then**
    Add the original association pair ω;
    Recalculate Θ, Ω_i, Ω_j;
    Set $C_{tot}^{'} = C_{tot}$;
  end if
end for

3.3.3 Joint Cell Association and Network Capacity Maximization

The capacity-based association schemes (CDA&SMBA) do not necessarily guarantee global optimal network capacity. In order to quantify the upper-bound of the UL network sum-rate, the problem of joint cell association and network capacity maximization (J-CA-NC-MAX) is formulated as a mixed integer nonlinear programming problem. Particularly, the aim is to associate the K UEs with the B BSs, such that each UE is associated with at least (most) ρ (ψ) BSs in the UL. Also, the sum of transmission powers of the UEs associated with each BS must satisfy $P_{\max}$. The J-CA-NC-MAX problem is formulated as follows.

J-CA-NC-MAX

$$\max \quad C_{tot} = \sum_{j=1}^{B} \sum_{k=1}^{K} \sum_{n \in \beta_{j,k}} W \log_2(1+\gamma_{k,j,n}), \tag{3.16a}$$

$$\text{s.t.} \quad \sum_{k=1}^{K} I_{j,k} P_{j,k} \leq P, \quad \forall j \in \{1,2,\ldots,B\}, \tag{3.16b}$$

$$\sum_{j=1}^{B} I_{j,k} \leq \psi, \quad \forall k \in \{1,2,\ldots,K\}, \tag{3.16c}$$

$$\sum_{j=1}^{B} I_{j,k} \geq \rho, \quad \forall k \in \{1,2,\ldots,K\}, \tag{3.16d}$$

$$0 \leq P_{j,k} \leq P, \quad \forall k \in \{1,2,\ldots,K\}, \forall j \in \{1,2,\ldots,B\}, \tag{3.16e}$$

$$I_{j,k} \in \{0,1\}, \quad \forall k \in \{1,2,\ldots,K\}, \forall j \in \{1,2,\ldots,B\}, \tag{3.16f}$$

where $\beta_{j,k}$ is the index of RBs occupied by the association pair (j, k), while $I_{j,k}$ is a binary decision variable, defined as

$$I_{j,k} = \begin{cases} 1, & \text{if UE } k \text{ is associated with BS } j, \\ 0, & \text{otherwise.} \end{cases} \tag{3.17}$$

In this work, it is assumed that each UE is associated with at least one BS and at most two BSs (i.e. $\rho = 1$ and $\psi = 2$). Lastly, it should be noted that the J-CA-NC-MAX problem is non-convex, and thus is computationally-intensive and time-consuming even for moderate size of networks (i.e. not practical). However, it is considered in this work as an upper-bound benchmark for the network capacity. The J-CA-NC-MAX is

solved via MIDACO, with tolerance set to 0.001 [83].

3.4 Performance Analysis

In this section, the performance of the proposed schemes in both single and dual connectivity scenarios are evaluated and compared with the state-of-the-art alternatives. The 5G NR frame structure supports both TDD and FDD transmissions, but for the mmWave band, it only supports TDD at present [57]. Thus, TDD is applied in this chapter. We assume half of the time is used for the UL and we do not consider the overhead due to switching between transmission directions. We know that the network traffic in the DL tends to be much larger than that in the UL, but we believe that with the rise of new services and applications of 5G and IoT, the UL transmission is expected to increase [1]. Besides, DUDe increases the UL data rate without impacting the DL data rate; thus, only the UL data rate is considered in this chapter. In the dual connectivity scenario, we consider at most two uplink associations. For the Min-PL scheme, UEs can connect to the first and second best serving BSs with the lowest pathloss. In the case of the SMBA scheme, UEs can connect to one more BS if higher capacity can be achieved from the decoupling. The list of all the association schemes are shown in Table 3.1, while the simulation parameters are listed in Table 3.2. To analyze the improvements, data rate and load situations in the MCells and SCells have been selected as metrics. Monte Carlo simulation is utilized to evaluate the different association and connectivity schemes.

3.4.1 Decoupling Access in Three-Tier HetNet

We consider three-tier UHF-mmWave hybrid networks in this section, where mmWave SCells, UHF SCells and MCells coexist. Fig. 3.2 illustrates the average number of UEs per cell in the UL for the different association schemes. The figure reveals that the decoupled association schemes offload more UEs to underutilized SCells in the

Table 3.1: Cell Association Schemes

Conectivity	Coupled association	Decoupled association
Single	Coupled (biased RSRP)	Min-PL, CDA, SMBA, CDA&SMBA
Dual	Coupled-Dual (biased RSRP)	Min-PL-Dual, CDA-Dual

Table 3.2: Simulation Parameters

Parameters	UE	MCell	UHF SCell	MmWave SCell
Maximum transmission power	23 dBm	46 dBm	30 dBm	30 dBm
Downlink/Uplink bias	N/A	0/0 dB	3/0 dB	5/0 dB
Spatial distribution	HPPP			
Spatial density	$250/km^2$	$5/km^2$	$\gamma\beta\lambda_m$	$(1-\gamma)\beta\lambda_m$
Lognormal shadowing	N/A	$\mu = 0$, $\sigma =$ 4 dB	$\mu = 0$, $\sigma =$ 4 dB	LOS $\mu = 0$, $\sigma = 8.66$ dB, NLOS $\mu = 0$, $\sigma = 9.02$ dB [29]
Path-loss exponent	N/A	3	3	LOS 2.55, NLOS 5.76 [29]
Operating frequency	N/A	2 GHz	2 GHz	28 GHz
Bandwidth	N/A	20 MHz	20 MHz	200 MHz [84]
Subcarrier spacing	N/A	15 kHz	15 kHz	60 kHz [84]
OFDM symbol period	N/A	66.67 us	66.67 us	16.67 us [85]
Power control	Transmit at the maximum power level			
Noise density	-174 dbm/Hz			

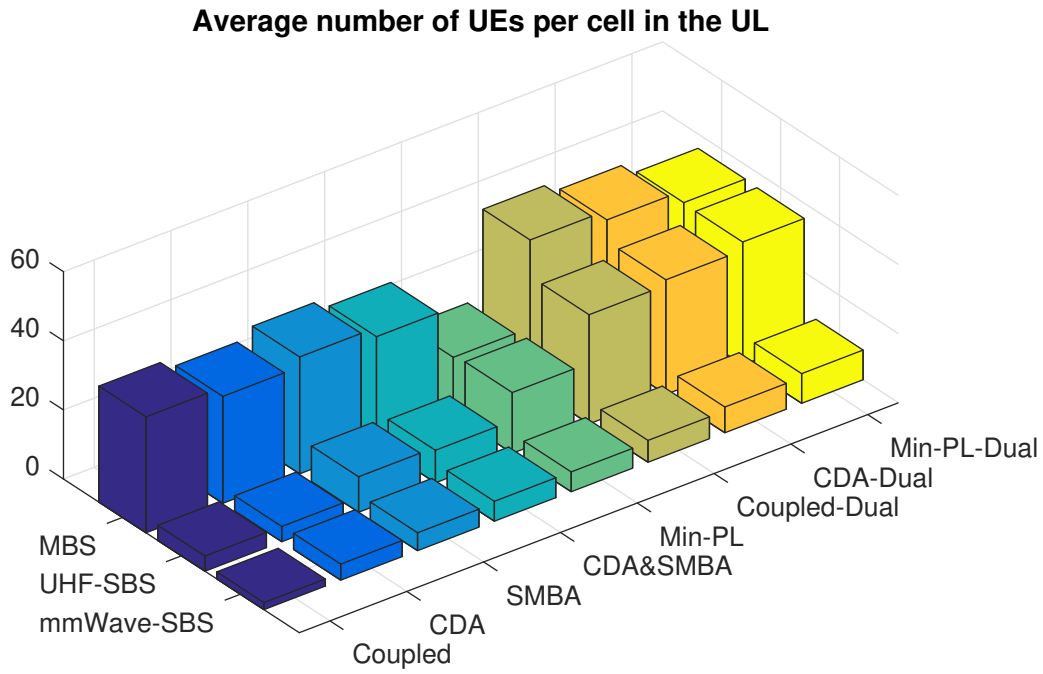

Figure 3.2: Average number of UEs per cell in the UL for different association schemes in single and dual connectivity scenarios ($\beta = 2$, $\gamma = 0.5$).

UL direction, and thus potentially freeing more MCell resources for users out of SCell coverage. Additionally, although the numbers of mmWave and UHF SCells are equal,

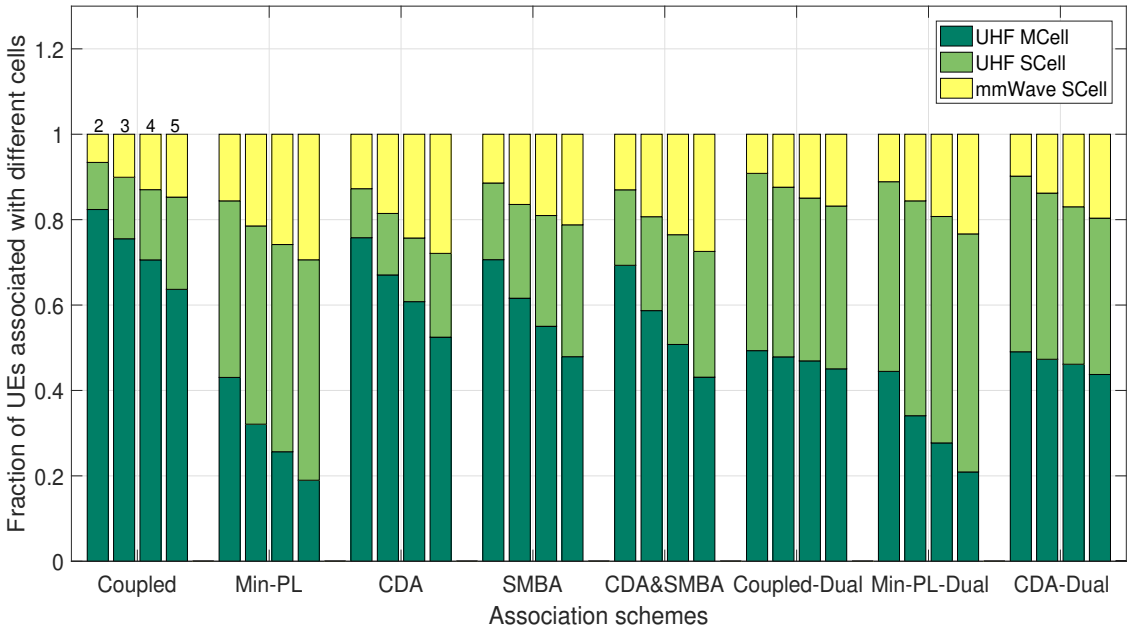

Figure 3.3: Ratio of UEs associated with different BSs at different ratios of SCell density to MCell density and association schemes ($\gamma = 0.5$).

it is obvious that more UEs connect to UHF SCells. This is because the path-loss of mmWave signals is higher, and there may be no LOS link between the BSs and UEs. Even if the directional antenna array is applied, as the mmWave bandwidth is much wider than UHF bandwidth, the transmission power per Hertz for mmWave is much lower than UHF, and thus it will also decrease the SNR. Besides, compared with the capacity-based (CDA, SMBA) association schemes, the receive signal power based (Min-PL) association scheme provides higher probability for the UEs to connect to the small BSs (SBSs) in both single and dual connectivity scenarios. The reason is that in the CDA and SMBA schemes, UEs initially connect to the same BSs as those in the DL.

Fig. 3.3 shows the fraction of UEs associated with MCells, UHF SCells and mmWave SCells in the UL direction at various SCell to MCell densities. The numbers 2, 3, 4, 5 on the top of bars refer to the different ratios of SCells to MCells density. In general, decoupling schemes make use of a bigger proportion of SCells, which in turn results in an increase of SCell UEs. For the coupled association scheme and CDA scheme, the ratio of association pairs with MBSs in dual connectivity is lower than that in single connectivity. This is because the number of MBSs is much lower than that of SBSs

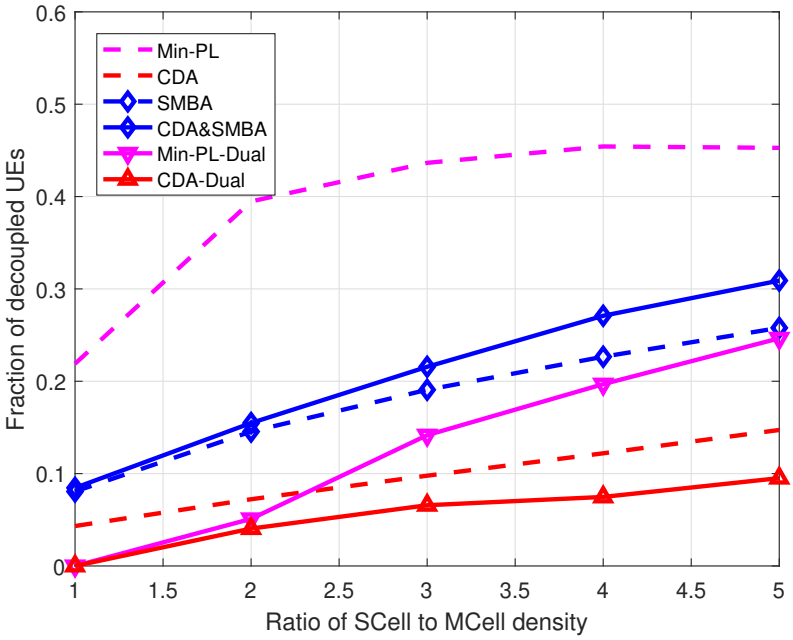

Figure 3.4: Ratio of UEs decoupled in the UL and DL vs. ratio of SCell density to MCell density ($\gamma = 0.5$).

and most UEs are associated with MCells in the DL, in the case when there is only one MBS nearby, then the second association pair must be with an SBS. Accordingly, the ratio of association pairs with UHF SBSs in dual connectivity is higher than that in single connectivity, but the ratio of association pairs with the mmWave SBSs in the dual connectivity scenario is almost the same as that in the single connectivity scenario, which is because of the severity of the near-field path-loss of mmWaves. In other words, the UEs prefer UHF SBSs to mmWave SBSs when both are available.

Fig. 3.4 shows the DUDe ratio at various SCell to MCell density ratios. When the SCell density increases, there will be more overlapped regions, which provides more flexibility for users to be handed-off to less loaded cells, and hence the number of DUDe UEs increases. Moreover, the DUDe ratio becomes lower when each UE connects to two BSs. For CDA and SMBA, as their initial association pairs are the same as those in the UL, their DUDe ratios tend to be lower. In contrast, the UL association pairs based on Min-PL are independent and experience a higher DUDe rate in single and dual connectivity scenarios. It also explains why based on Min-PL more UEs connect to SBSs in Fig. 3.3.

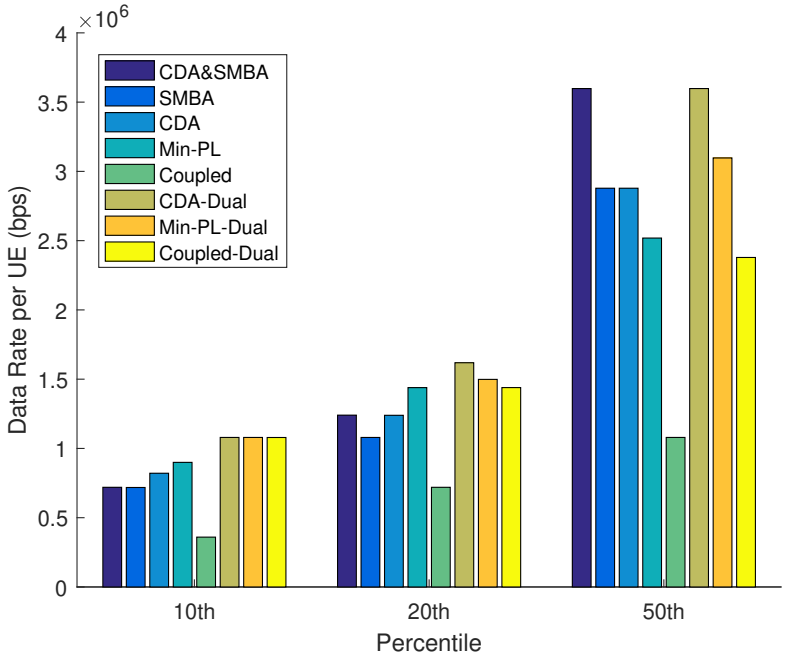

(a) 10th, 20th, 50th percentile data rates

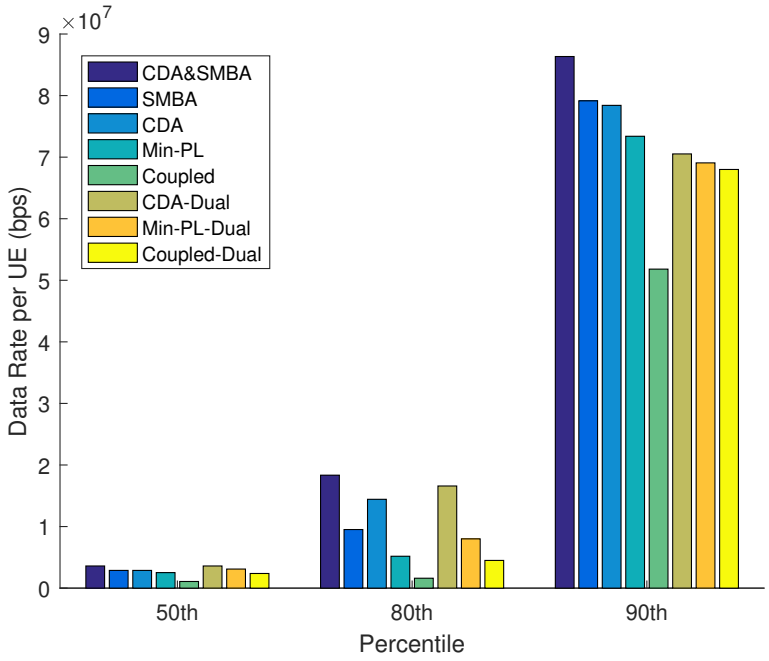

(b) 50th, 80th, 90th percentile data rates

Figure 3.5: 10th, 20th, 50th, 80th, 90th percentile UE UL data rates based on different cell association schemes in single and dual connectivity scenarios ($\beta = 5, \gamma = 0.5$).

Figs. 3.5 (a) and (b) show the 10th, 20th, 50th, 80th, 90th percentile UE UL data rates based on eight cell association schemes. A percentile is a measure used in statistics indicating the value below which a given percentage of observations in a group of observations fall [86]. For example, the 20th percentile is the value (or score) below which 20% of the observations may be found. Because of the wide bandwidth of mmWave, a few UEs associated with mmWave SBSs have extremely high data rates, and so the 80th and 90th percentile data rates are extremely high. The data rate based on the coupled scheme is the lowest in both single and dual connectivity scenarios. This can be explained by the fact that higher coverage of SCells in the DUDe cases results in a better distribution of UEs among the nodes, which provides better utilization of the resources. Additionally, connecting to a nearer BS can yield a higher SINR, and thus achieve higher throughput. Capacity-based cell association schemes (CDA, SMBA, CDA&SMBA) achieve higher 50th, 80th and 90th percentile data rates than the Min-PL scheme. It is because SCells serve fewer UEs in this case than with Min-PL, though these UEs achieve higher data rates at the expense of the 10th and 20th percentile per UE data rates. Furthermore, for Min-PL, CDA and coupled schemes, dual-BS association can achieve higher 10th, 20th, 50th, 80th percentile data rates than single-BS association.

Fig. 3.6 shows the impact of varying the SCell density within the MCell coverage area on the UL network sum-rate. The densities of UEs and MCells remain constant across the different cases. As the number of deployed SCells increases, the network sum-rate grows. This is because adding more SCells means more UEs are offloaded from the MCell to the SCells where they are granted more resources compared to the resources offered by the congested MCells. Additionally, decoupled association schemes provide better performance in comparison with the coupled scheme. Furthermore, capacity-based association schemes (CDA, SMBA, CDA&SMBA) have higher network sum-rate than Min-PL which do not consider cell loads. It is worth noting that dual connectivity does not necessarily improve the sum-rate, especially when the number of BSs is small. An explanation for this could be that increasing the association pairs may increase interference and decrease the available RBs for the users near the BSs. Determining whether to increase the number of connections from the perspective of capacity gain seems more reasonable. Furthermore, CDA and Min-PL have a tangible effect in the single connectivity scenario, but for dual connectivity, its effect is limited. This may be because the frequency resource has been utilized

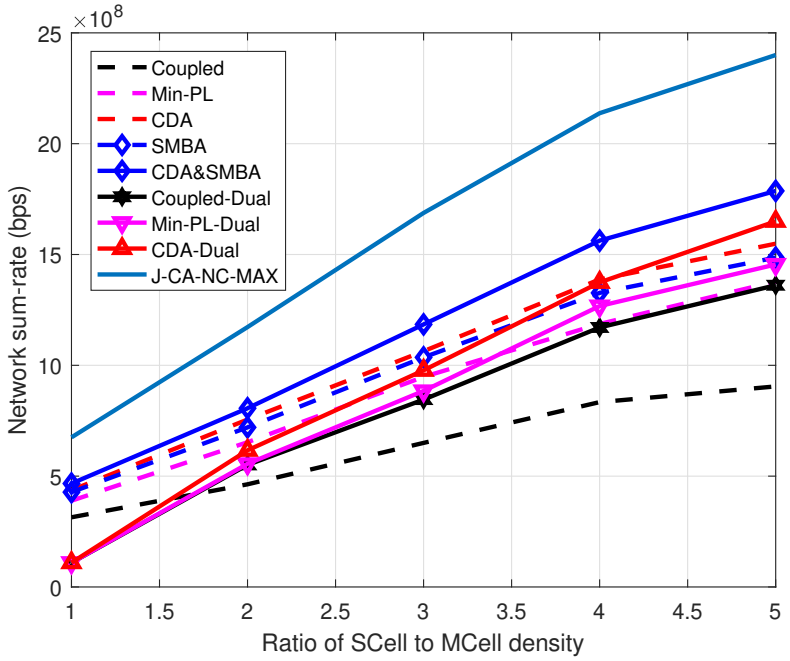

Figure 3.6: Network sum-rate in the UL vs. ratio of SCell density to MCell density in single and dual connectivity scenarios ($\gamma = 0.5$).

efficiently in dual and hybrid connectivity. On the other hand, it is evident that the J-CA-NC-MAX scheme serves as an upper-bound to the network sum-rate due to the following reasons. First, the sum-rates of CDA and SMBA are dependent upon the initial association pairs, which are chosen to be the same as those in the UL, but in fact, they can also be set by the Min-PL scheme or randomly. In turn, different initial association pairs can lead to different final sum-rates. Second, the higher network sum-rate achieved by the J-CA-NC-MAX scheme is at the expense of some UEs' data rates being lower, which impairs the fairness of the network UEs. However, for the CDA and SMBA schemes, the data rate of each UE will not be lower than the coupled association scheme.

Fig. 3.7 shows the UL network sum-rate when the UHF SCells make up different proportions of all the SCells. It can be seen that the different dual-BS association schemes follow a similar trend. Specifically, the sum-rate increases first and then decreases under different ratios of UHF SCell to total SCell densities. As might be anticipated, wireless networks with both UHF and mmWave SCells have better coverage than those with mmWave SCells. However, for the other association schemes, the network sum-rate decreases when the number of mmWave BSs decreases. This is because of the

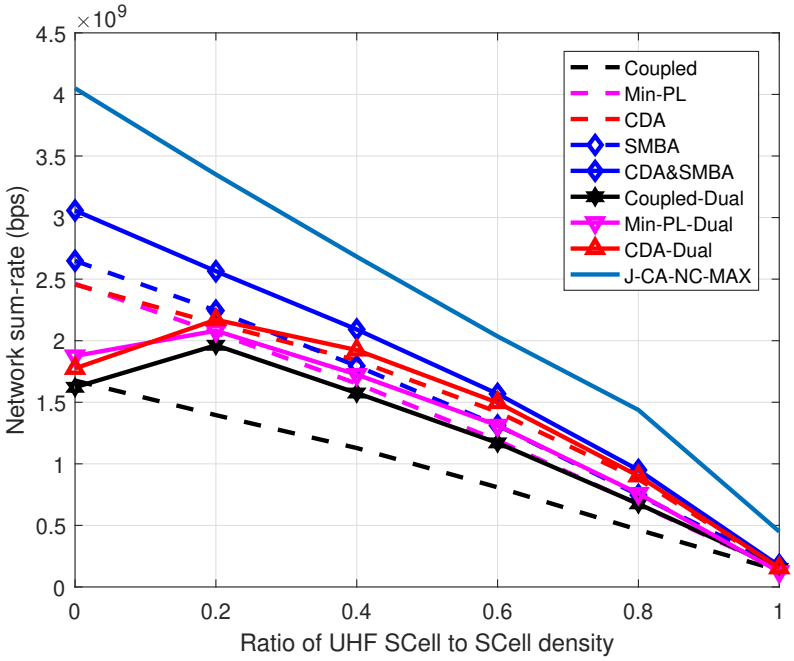

Figure 3.7: Network sum-rate in the UL vs. ratio of UHF SCell density to SCell density in single and dual connectivity scenarios ($\beta = 5$).

decrease in the bandwidth available. Moreover, CDA can achieve higher sum-rate in the single and dual hybrid connectivity scenario than in the dual connectivity scenario, and the advantage of decoupled association is less effective in the dual connectivity. This is due to the fact that the UEs distribution among the BSs is more balanced in the dual connectivity scenario.

Fig. 3.8 shows the UL energy efficiency when the UHF SCells make up different proportions of all the SCells. It can be seen that for the same association scheme, single connectivity is more energy efficient than dual connectivity, because the path-loss between a UE and its second serving BS is relatively higher. Moreover, in most cases, decoupled association schemes have higher energy efficiency than the coupled association scheme, since DUDe shortens the distance between UEs and BSs. The CDA scheme reconciles the RB utilization and interference, and thus, it has higher energy efficiency than the Min-PL scheme in the single and dual connectivity scenarios. For single connectivity and single-dual hybrid connectivity, the energy efficiency increases with the number of mmWave SCells. It is because there is almost no interference among mmWave UEs and when the density of mmWave SBSs is high, the directional

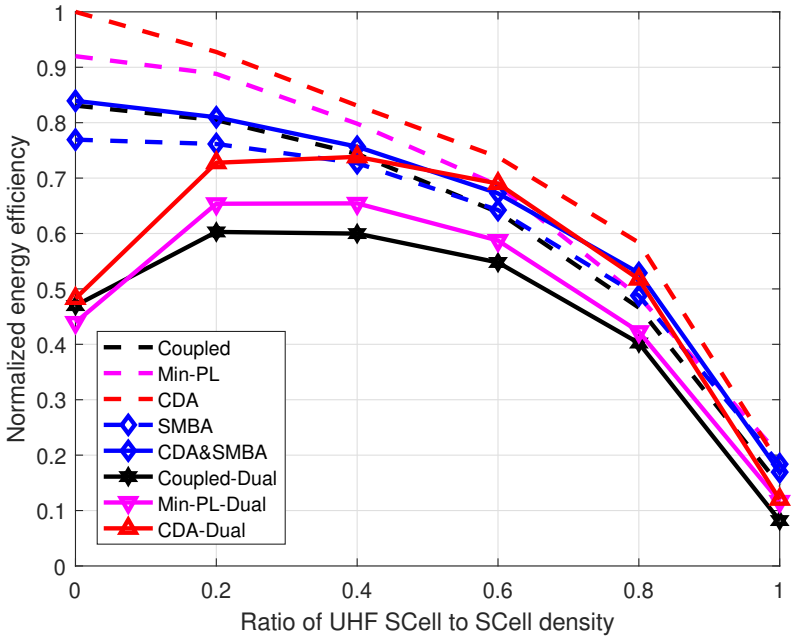

Figure 3.8: Normalized network energy efficiency when the UHF SCells make up different proportions of all the SCells ($\beta = 5$).

antenna can compensate for the high path-loss of mmWave signals, and thus, the HetNet with more mmWave SBSs can achieve higher sum-rate. By contrast, the energy efficiency of the dual connectivity schemes increases first and then decreases. This is because mmWave signals are sensitive to blockage, and since the distance between a UE and its LOS mmWave serving BS can be long, deploying more UHF SBSs can shorten the UE-BS distance, but at the same time aggravate the co-channel interference.

Fig. 3.9 shows the number of handovers (switching among the serving BSs) for the different schemes, when there are 40 UEs, 1 MBS and at most 5 SBSs. The Min-PL and coupled association schemes can complete the BS association in one iteration. For CDA and SMBA, however, it takes a number of iterations to converge, though in the meantime, the UEs can connect to their DL serving BSs in the UL first, and in each iteration, only one association pair is changed without affecting the other existing associations. It can be seen that the number of handovers increases with the number of BSs. The CDA scheme requires more iterations to converge in the single connectivity scenario than in the dual connectivity scenario because the UEs distribution among the BSs is more balanced in the dual connectivity scenario.

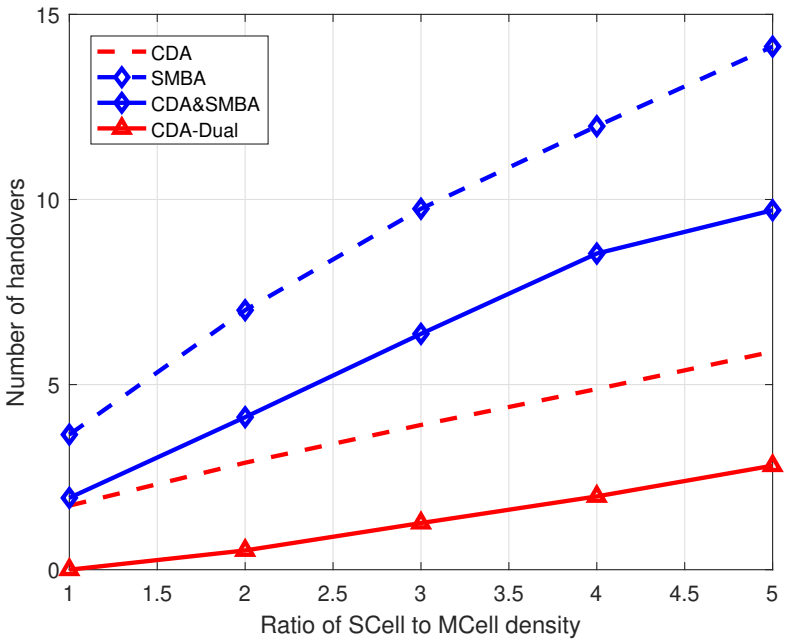

Figure 3.9: Number of handovers in the UL vs. ratio of SCell density to MCell density in single and dual connectivity scenarios ($\gamma = 0.5$).

3.4.2 Decoupling Access in Two-Tier HetNet

In order to promote system integration, we also consider the special case where all SBSs are of the same type, i.e., $\gamma = 1$ or $\gamma = 0$. Although many of the results are similar to those in the three-tier HetNet, there are some subtle differences. For HetNets consisting of UHF MCells and mmWave SCells (Fig. 3.10 (a)), the ratio of mmWave SCell UE in the dual connectivity scenario is higher than that in the single connectivity scenario. Due to the high path-loss and blockage of mmWave, the coverage of mmWave SCell is smaller than that of UHF MCells in the UL. However, if there is only one MBS nearby then the second association pair must be with a mmWave SCell. Additionally, by comparing Fig. 10 (a) with Fig. 10(b), it is evident that the ratio of mmWave SCell is doubled, but the mmWave SCell UEs increase more than twice. This also verifies that the UEs prefer UHF BSs to mmWave SBSs when both are available.

Compared to Fig. 3.11 (b), it is obvious that the sum-rate of the HetNets with only UHF SCells (Fig. 3.11 (a)) is much lower than those with mmWave SCells, and this is because the mmWave bandwidth is much wider than UHF bandwidth. Moreover, the sum-rate based on Min-PL, CDA and coupled schemes increases more slowly with

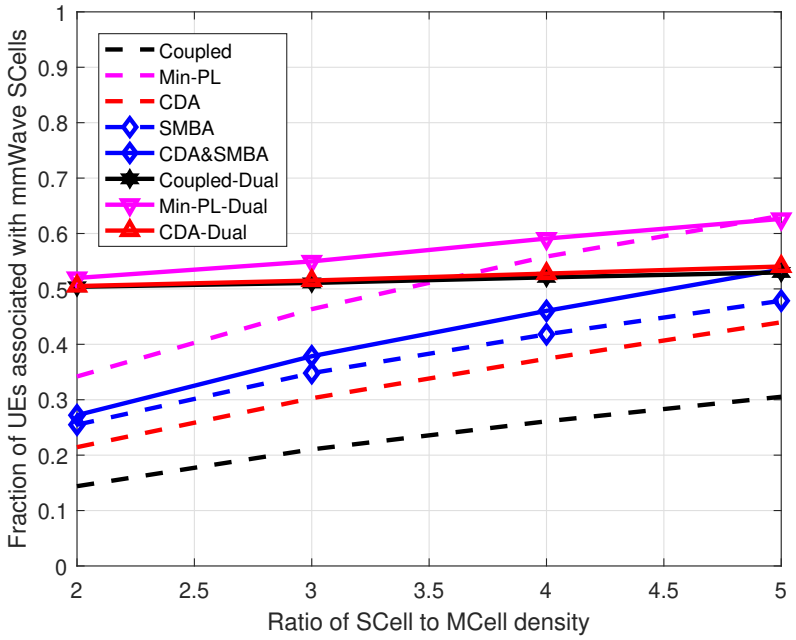

(a) $\gamma = 0$

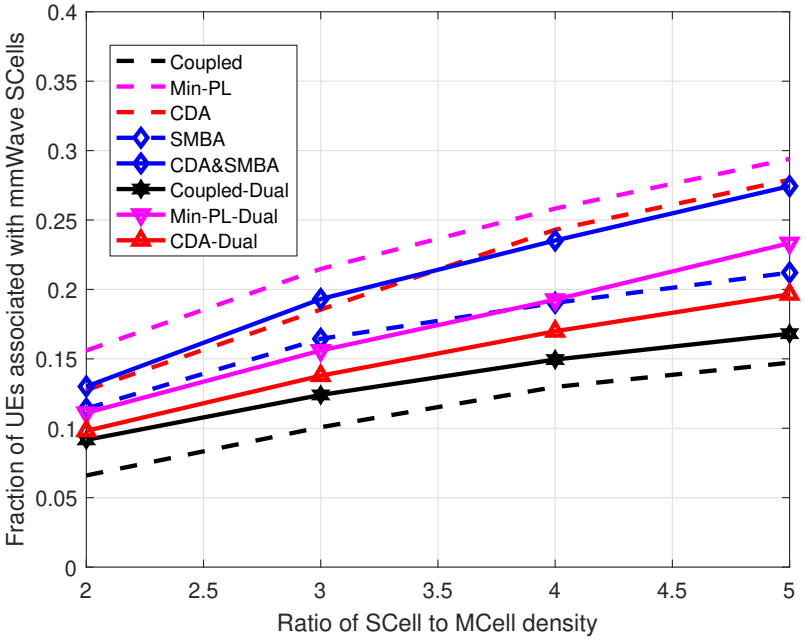

(b) $\gamma = 0.5$

Figure 3.10: Ratio of UEs associated with mmWave SCells in the UL vs. ratio of SCell density to MCell density with different ratios of mmWave SCells.

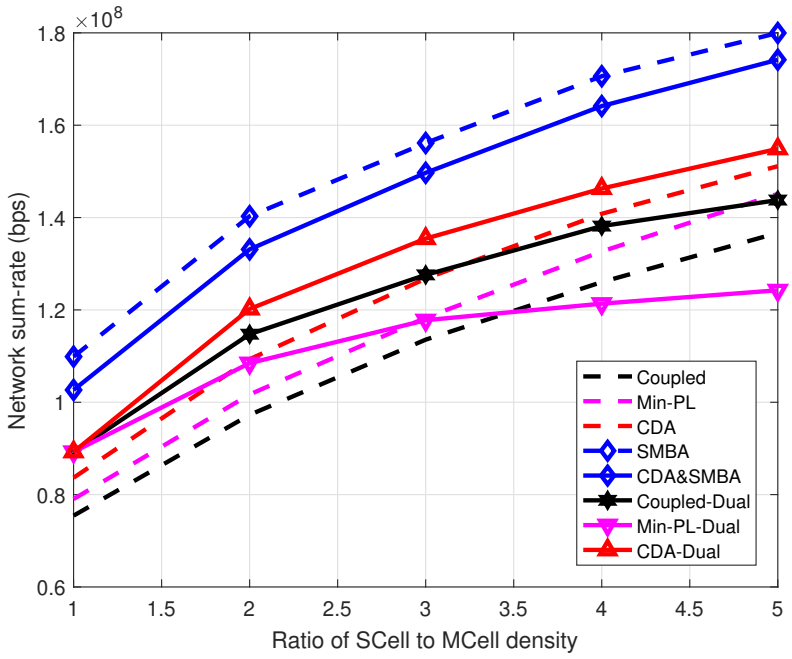

(a) $\gamma = 1$

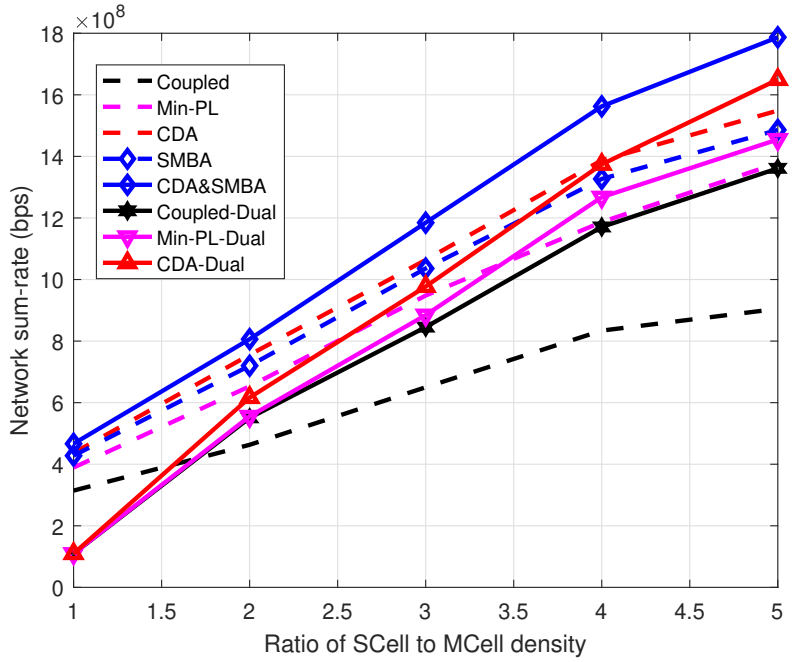

(b) $\gamma = 0.5$

Figure 3.11: Network data rate in the UL vs. ratio of SCell to MCell density with different ratios of mmWave SCells.

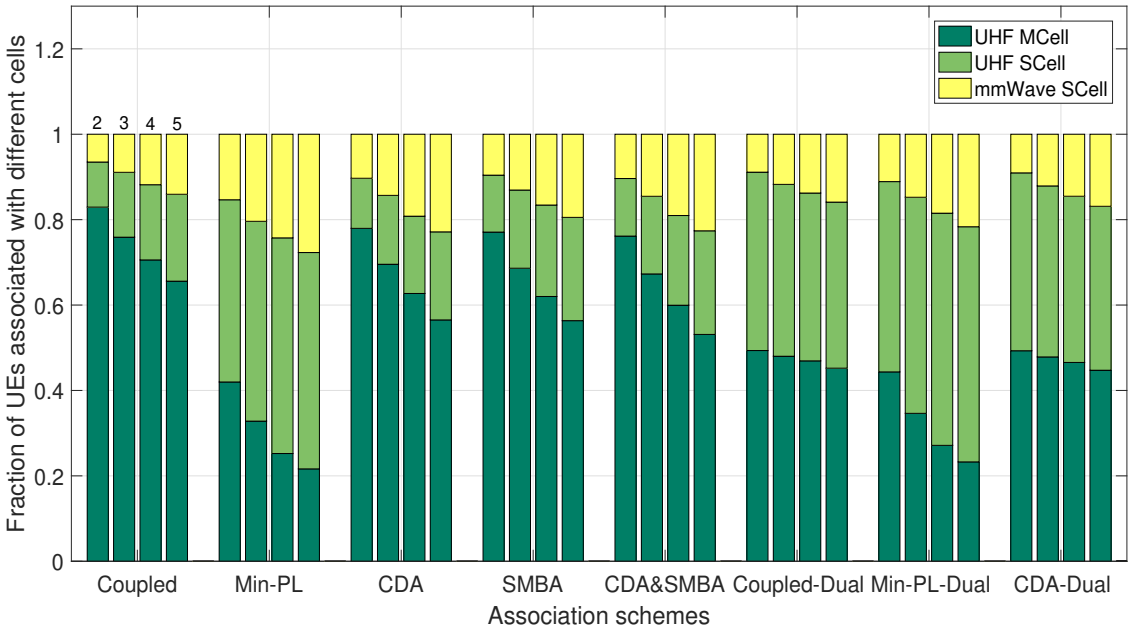

Figure 3.12: Ratio of UEs associated with different BSs at different ratios of SCell density to MCell density and association schemes (less density scenario, $\gamma = 0.5$).

the increase in the SCell to MCell density in the dual connectivity scenario than in the single connectivity scenario, which is different from the result in Fig. 3.11 (b). This is because increasing the number of BSs transmitting over UHF bands increases not only resource utilization but also collaterally interference, and the dual connectivity can make the interference even higher. Moreover, the sum-rate based on the coupled scheme is higher than the Min-PL scheme in the dual connectivity scenario. This is because a few UEs near SBSs acquire rich resources and thus achieve a very high data rate with the coupled scheme.

3.4.3 Reduced Density Scenario

The BS and UE densities are reduced by half in Fig. 3.12, but the number of BSs and UEs is kept constant. Compared with Fig. 3.3, the number of UEs associated with the mmWave BSs decreases while the number of UEs associated with UHF BSs increases. When the BS density decreases, the average distance between UEs and BSs becomes longer, making it more difficult for UEs to access the mmWave BSs. Besides, compared with Fig. 3.6, the network sum-rate in Fig. 3.13 dropped due to the decreased BS density. Furthermore, the network sum-rate for the dual connectivity

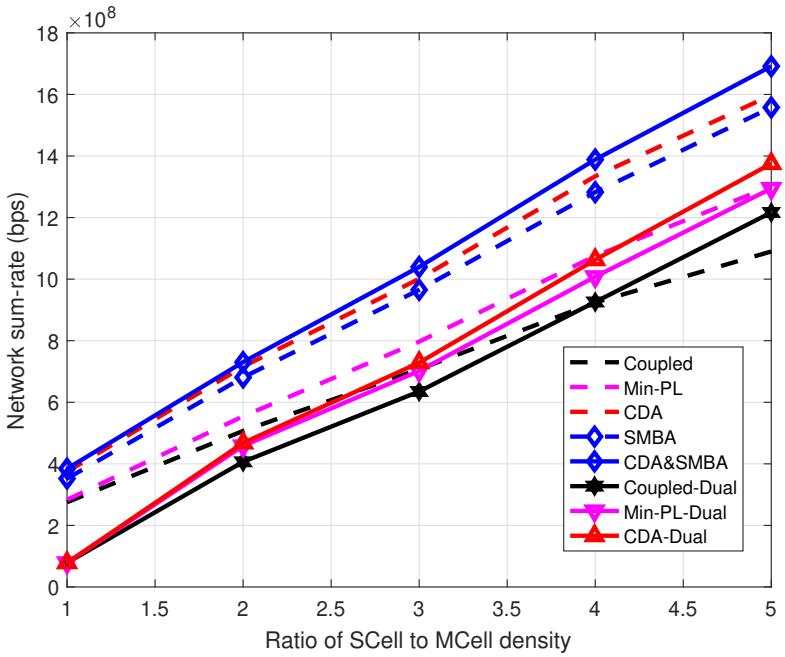

Figure 3.13: Network sum-rate in the UL vs. ratio of SCell density to MCell density in single and dual connectivity scenarios (less density scenario, $\gamma = 0.5$).

association schemes is severely degraded. It is because the distance to the second best BS becomes longer, thus connecting to a far away BS is not energy efficient and will decrease the available RBs for the UEs near the BSs. In these circumstances, the sum-rate of the CDA and SMBA schemes in the dual connectivity scenario is even lower than those in the single connectivity scenario.

3.5 Summary

This chapter proposed a DUDe based resource allocation and multi-BS association technique to improve the performance of hybrid HetNets. Both capacity maximization and minimum path-loss based approaches were considered using single and dual connectivity. The results provide an insight into the performance of DUDe combined with mmWave and dual connectivity techniques for various performance metrics of interest. It was shown that capacity-based cell association schemes (CDA, SMBA, CDA&SMBA) can achieve higher data rates than path-loss based cell association. CDA scheme reconciles the RB utilization and interference, thus has higher energy

efficiency than the Min-PL scheme in the single and dual connectivity scenarios. Moreover, it has been demonstrated that dual connectivity does not necessarily improve the sum-rate, especially when the density of UHF BSs is low. Determining whether to increase the number of connections from the perspective of capacity gain seems more reasonable. The advantage of decoupled association is less effective in dual connectivity, because the UEs distribution among the BSs is more balanced in the dual connectivity scenario than in the single connectivity scenario. Finally, the available mmWave bandwidth is much wider than UHF bandwidth, and so the network sum-rate mostly depends on the density of mmWave BSs, but UHF SBSs and MBSs are still important to provide umbrella coverage to guarantee a consistent service.

Chapter 4

Interference Management for D2D based on DUDe

4.1 Introduction

This chapter analyzes the application of DUDe to D2D-underlay HetNets. Most of the current research focuses on in-band underlay D2D, in which D2D re-uses the licensed spectrum; hence, the spectrum resources are simultaneously used by the cellular and D2D UEs (DUEs). This mode is advantageous due to the reuse of the spectral resource of the cellular UEs (CUEs). Besides, as the BSs can effectively control the licensed spectrum usage, in-band D2D can be effective in QoS management. Many studies on D2D assume homogeneous networks or only consider one MCell [87–89]. This is the most common scenario for D2D communication and has been extensively studied. At present, mode selection, resource allocation, and power control are mainly used to manage the interference in macrocell and D2D hybrid networks.

Mode Selection: the DUE in the coverage of the MCell can select the cellular mode or the D2D mode for communication. The cellular mode means that data transmission between UEs is through the MBS, and the D2D mode is direct communication between UEs without MBS forwarding. The D2D mode can be divided into two basic modes: underlay and overlay, which means that DUEs share the spectrum with CUEs in an orthogonal or non-orthogonal way. If DUEs work in underlay mode, it will cause interference to the CUEs. A large and growing body of literature has investigated the mode selection for D2D communication.

The paper [90] discussed the mode selection for D2D communication underlaying a cellular network in a single cell scenario, and a mode selection algorithm based

on DUE throughput was proposed. By calculating the throughput when DUE uses cellular, underlay and overlay mode respectively, the mode that maximizes the DUE throughput is selected for communication. Then, based on the learning from the single cell studies, this mode selection algorithm was extended to a multi-cell scenario. Although this mode selection algorithm can greatly improve system throughput, the computational complexity is high. Especially when there are a large number of DUEs in the network, this algorithm becomes impractical.

In [91], authors formulated a stochastic optimization problem that aims to maximize the average sum-rate of the network, while satisfying the QoS requirement of each UE. By solving the problem, they developed an optimal opportunistic subchannel scheduling algorithm, which performs both subchannel scheduling and transmission mode selection opportunistically. However, this paper only considered the cellular mode and the underlay mode, and underlay mode was not studied.

In [92], relay nodes are introduced into the macro cellular network, and a distance-dependent mode selection algorithm is proposed, which aims at selecting the optimal transmission mode with the overall maximized capacity, and the QoS of CUEs is satisfied at the cost of nearly the least information for decision-making. It needs merely a few parameters instead of traversal analysis in [90], which is much more significant in practical application.

From the papers above, it can be seen that a reasonable mode selection mechanism can bring great gain to the network. Besides, from a realistic point of view, we should focus more on the underlay mode, since the underlay mode can only be applied when free spectrum resource is available. Therefore, when introducing D2D communication into an MCell-SCell hybrid network, we should put emphasis on the underlay mode.

Resource Allocation: it is an important way to control the interference, especially when DUEs reuse the CUE resources. There have been a lot of studies on resource allocation in the MCell-D2D hybrid network. They are mainly based on game theory [93–96], mixed integer nonlinear programming [97], interference avoidance [98, 99] and fractional frequency reuse [100]. Besides, the distance between the transmitter and receiver of a D2D pair is often shorter than that of an MBS-MUE pair, it is likely that the D2D link has a higher channel gain than the MBS-MUE link. Therefore, when the network sum rate is optimized, the MUE rate could be sacrificed [101]. However, in general, the priority of the MUE QoS is higher than that of the DUE, so the requirements of the MUE QoS must be satisfied when optimizing the network sum rate.

Through the analysis to the documents, we find that most of the current literature pays particular attention to the resource allocation in D2D underlay mode. These papers aim at different scenarios, adopt different optimization indicators, and utilize different methods to reduce the interference when DUEs reuse the resources of CUEs. There have been a lot of studies on interference management in HetNets composed of MCells, SCells, and D2D pairs.

Power Control: it refers to reducing the interference in the system by adjusting the transmission power of nodes in the network. At present, there are two categories of power control schemes in D2D communication: static power control and [102, 103] ,dynamic power control [104–107].

Static power control means that the transmission power of UEs are determined and fixed the D2D links are established. In [102], the SINR thresholds of MUEs and the DUEs are predefined, and then the transmission powers of the UEs are calculated . In [103], a distance-dependent resource allocation algorithm is proposed. In this algorithm, the transmission power of DUEs is fixed, and MUEs use open loop power control method to determine the transmission power. Since the static power control scheme does not have to adjust the UE transmission power according to the network status, its signalling overhead is relatively small, but because it is not flexible enough, the network performance cannot be fully improved.

Dynamic power control means that the MBSs or UEs can dynamically adjust their transmission power according to their channel states [104–107]. In [105], a close loop power control scheme is proposed, which uses open loop fraction power control scheme to calculate the initial transmission power of the DUE, compares the SINR at the receiver with a predefined target SINR, then adjusts the transmission power of the DUE to satisfy target SINR, but this method cannot guarantee the QoS of the MUE. In [106], authors solve the DUE power allocation problem through a subgradient-based algorithm by applying the Lagrangian dual theory. This algorithm can find an optimal DUE transmission power, but since it pursues DUE rate maximization but only guarantees the minimum rate of the MUE, the fairness between the MUE and the DUE cannot be guaranteed. In [107], a centralized and a distributed power control algorithms are proposed. The goal of centralized power control is twofold: ensure that the CUEs have sufficient coverage probability by limiting the interference created by underlaid D2D users while scheduling as many D2D links as possible. For the distributed power control method, the optimal on-off power control strategy is proposed, which maximizes the sum-rate of the D2D links. Compared with the static power control scheme, the

dynamic power control scheme can better improve the system performance but has more signalling overhead and higher computational complexity.

However, as HetNets are becoming the mainstream, it is necessary to optimize the performance of D2D in HetNets. Different from the two-tier MCell-D2D networks, D2D-underlay HetNets are composed of MCell, SCell and D2D pairs. Many of the research so far considers MCells and SCells that use different frequency bands [108–110]; so there is no interference between these cell types, resulting in a two-tier network scenario. There are relatively few studies that consider both SUEs and DUEs reusing the spectrum of MCells, and they can be further divided into two categories. Some researchers assume the resource of one MUE cannot be reused by multiple D2D/SUE links simultaneously within the MCell. For example, in [111], a coalition formation algorithm and a constrained deferred acceptance algorithm were devised to solve the subchannel allocation problem, where the subchannel of a MUE can be reused by at most one SUE/DUE. In order to optimize spatial reuse gain and enable as many as possible D2D terminals to access the network, a few papers have focused on the scenario where the resource of one MUE may be reused by multiple D2D/SUE links simultaneously within the MCell, as long as the interference is low enough. For instance, in [112], the authors devised a dynamic programming approach for efficiently matching communicating endpoints and assigning spectrum resources. In [113], regional restrictions on MBSs, SBSs, and D2D pairs were conducted to solve the resource allocation problem. In [114], mode selection, resource allocation and power control of DUEs in HetNets were studied, but only considered a relatively simple scenario with only one MUE, one femto-cell UE, and one D2D pair.

Overall, most of the current research focuses on in-band underlay D2D, in which D2D re-uses the licensed spectrum; hence, the spectrum resources are simultaneously used by the cellular and D2D UEs. This mode is advantageous due to the reuse of the spectral resource of the cellular users (CUEs). Besides, as the BSs can effectively control the licensed spectrum usage, in-band D2D can be effective in QoS management. However, in an in-band underlay D2D scenario, interference management is a major challenge, as there exists not only inter-tier interference among MCell UEs (MUEs), SCell UEs (SUEs) and D2D UEs (DUEs), but also intra-tier interference among UEs associated with different BSs sharing the same subchannel. Apart from mode selection, resource allocation and power control which been mentioned in many published studies, DUDe is a new promising technique to solve this problem.

DUDe allows the UEs to connect to a geometrically closer SCell in the UL, rather

than the same one in the DL, which shortens the distance between UEs and their serving BSs in the UL, reduces path-loss, and lowers transmission power and interference to neighboring BSs. Besides, DUDe pushes more UEs to under-utilized SCells in the UL, which allows more efficient resource utilization of SCells, and higher data rates. At the same time, DUDe can facilitate a more benign environment for D2D receivers by lowering the CUE UL transmission power, which results in less interference, and enables more D2D transmissions. Although there have been some research on DUDe, few attention has been paid to the performance of DUDe in D2D scenarios. Specifically, the authors in [115] focused on how to calculate the total power saved by UEs and the extra area that can be utilized to enable D2D pairs because of DUDe; however, neither subchannel allocation nor transmission power optimization have been taken into consideration. The authors in [116] proposed a fractional frequency reuse scheme based on DUDe cell association, where inner and outer subregions of MCells are pre-assigned to different sub-bands, and MCell-edge UEs are associated with SCells in the UL to mitigate the interference. However, fractional frequency reuse scheme reduces the available resources in each subregions. Thus, the quality of services is degraded, especially when the number of UEs at a certain subregion is extremely high, as the BS may not able to accommodate all the UEs. Furthermore, the UEs adjust their transmission powers via channel inversion power control, which cannot optimize the data rate.

4.1.1 Main Contributions

This chapter fills a gap in the literature on DUDe-based D2D communications in HetNets. In this work, we consider a HetNet scenario which is closer to reality, where the resource of one MUE could be reused by multiple D2D/SUE links simultaneously within the MCell as long as the interference is kept sufficiently low. In contrast to other research considering UEs connecting to the same BS in the UL and DL, we investigate the performance of DUDe in D2D-underlay HetNets. In turn, a joint cell-association, subchannel allocation, and power control (J-CA-SCA-PC) problem for UL network sum-rate maximization is formulated, subject to maximum transmission power and minimum rate constraints. However, J-CA-SCA-PC happens to be non-convex and NP-hard, and thus is computationally-expensive. Hence, this work decouples problem J-CA-SCA-PC, and solves it via a low-complexity and near-optimal scheme. Specifically, the main contributions of this work can be summarized as follows:

- Formulated a joint cell-association, subchannel allocation and power control problem for network sum-rate maximization in D2D-underlay HetNets, subject to maximum transmission power and minimum rate constraints.

- Proposed a DUDe cell association scheme for D2D underlay HetNets. Particularly, as we consider the scenario where the resource of one MUE could be reused by multiple D2D/SUE links simultaneously, it is necessary to manage the interference carefully. In turn, UE clustering and subchannel allocation is achieved via a greedy coloring scheme and a modified Munkres algorithm of low-order polynomial time-complexity [117]. Furthermore, a difference of convex (D.C.) functions based power allocation algorithm is devised with proven complexity and convergence to maximize the network sum-rate, while satisfying the UE transmission power and data rate constraints.

- Compared the proposed scheme to various coupled/decoupled cell-association, subchannel allocation, and power control schemes. In addition, it should be noted that decoupling cell-association, subchannel allocation, and power control does not necessarily guarantee global optimality, in comparison to the formulated J-CA-SCA-PC problem. Thus, the proposed scheme is also compared with the upper bound, obtained by solving problem J-CA-SCA-PA via a global optimization package. Numerical results show that the proposed scheme efficiently yields near-optimal network sum-rate in comparison to the J-CA-SCA-PA scheme, while posing a reasonable tradeoff between complexity and optimality. Moreover, it has been shown to achieve about 20% higher network sum-rate, 30% higher CUE sum-rate, and 15% higher DUE sum-rate than its coupled counterparts.

As the outset, it may seem rather intuitive that DUDe can improve the performance of D2D communications compared to the coupled schemes. However, to the best of our knowledge, no prior work has devised a low-complexity but near-optimal joint decoupled cell-association, subchannel allocation, and power control scheme for sum-rate maximization in D2D-underlay HetNets, or performed extensive comparisons with state-of-the-art and upper-bound benchmark schemes.

4.1.2 Organization

The rest of this chapter is organized as follows. The system model is presented in Section 4.2, while the proposed scheme is presented in Section 4.3. The performance of our algorithm and state-of-art alternatives are evaluated in Section 4.4. The conclusions are drawn in Section 4.5.

4.2 System Model

We consider an orthogonal frequency-division multiple access (OFDMA)-based HetNet composed of a MCell, S SCells, C CUEs and D D2D pairs. The positions of SCells, CUEs and D2D transmitters follow uniform distribution with densities of λ_s, λ_c and λ_d, respectively. Assuming all UEs have low mobility, the channel state information (CSI) between UEs and BSs, as well as between D2D pairs remains stationary [118][1]. The UEs' traffic is based on the full-buffer model. Furthermore, we assume in-band underlay D2D communication, where the D2D pairs and SUEs share N UL subchannels with the MUEs, and each MUE's resource can be reused by multiple CUEs and DUEs[2]. Let $I_C = \{1,2,...,C\}$, $I_D = \{C+1,C+2,...,C+D\}$ and $\mathcal{N} = \{1,2,...,N\}$ indicate the index sets of CUEs, DUEs and subchannels, respectively. For convenience, let $I = \{1,2,...,C,C+1,C+2,...,C+D\}$ denote the index set of all UEs (i.e. CUEs and DUEs). The MBSs and SBSs are all closed-access, meaning that each cell can only schedule the UEs that belong to it. We assume that frequency division duplexing (FDD) is applied in the HetNet, and all BSs and D2D pairs transmit over ultra-high frequency (UHF) bands [1]. A UE within the coverage of both an MBS and an SBS could be served by either a MBS or a SBS. Lastly, we consider unicast data transmissions, where UEs can transmit data to only one endpoint at a time.

4.2.1 Transmission Data Rate

As DUDe only increases the UL data rate, we only consider UL transmission here, while accounting for interference between all CUEs and DUEs, as shown in Fig. 4.1.

[1]A CUE may be associated with a MBS (i.e. MUE) or a SBS (i.e. SUE). Moreover, UEs is used to collectively refer to CUEs and DUEs.

[2]We assume each UE occupies one subchannel, but it can be extended to multiple subchannels by assuming that virtual UEs exist at the positions of actual UEs. If a UE is not assigned any subchannel, then its communication is blocked.

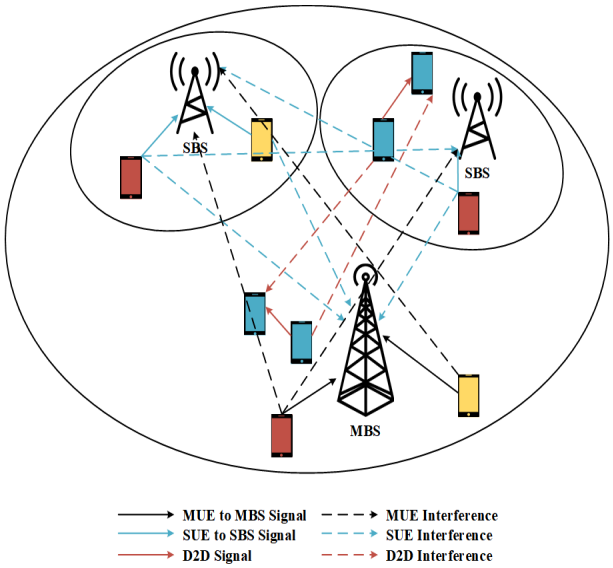

Figure 4.1: Interference between MUEs, SUEs and DUEs

Particularly, UEs in different colors are assigned different subchannels; only UEs occupying the same color cause interference to each other. Now, let $\mathcal{M} = \{0, 1, \ldots, M\}$ denote the set of BSs, where BS $m = 0$ corresponds to the MBS, and the rest (i.e. $m = 1, \ldots, M$) are SBSs. For convenience, let $\chi_{i,n}$ (for $i \in I_C$) be a binary decision variable, defined as

$$\chi_{i,m} = \begin{cases} 1, & \text{if CUE } i \text{ is associated with BS } m, \\ 0, & \text{otherwise,} \end{cases} \tag{4.1}$$

where it should be noted that each CUE $i \in I_C$ can be associated with one BS (i.e. $\sum_{m \in \mathcal{M}} \chi_{i,m} = 1$). Also, let $\rho_{i,n}$ (for $i \in I_C$) and $\rho_{k,n}$ (for $k \in I_D$) be defined as

$$\rho_{i,n} = \begin{cases} 1, & \text{if subchannel } n \text{ is allocated to CUE } i, \\ 0, & \text{otherwise,} \end{cases} \tag{4.2}$$

and

$$\rho_{k,n} = \begin{cases} 1, & \text{if subchannel } n \text{ is allocated to DUE } k, \\ 0, & \text{otherwise,} \end{cases} \tag{4.3}$$

respectively. We assume that each CUE $i \in I_C$ and DUE $k \in I_D$ can be allocated to one subchannel $n \in \mathcal{N}$. That is, $\sum_{n \in \mathcal{N}} \rho_{i,n} = 1$, and $\sum_{n \in \mathcal{N}} \rho_{k,n} = 1$, $\forall i \in I_C$, and $\forall k \in I_D$,

respectively. Thus, the data rate of CUE $i \in I_C$ is

$$R_i^C = B\log_2\left(1+\sum_{m\in\mathcal{M}}\sum_{n\in\mathcal{N}}\chi_{i,m}\frac{\rho_{i,n}p_i h_{i,m,n}}{I_{i,m,n}+\sigma^2}\right), \tag{4.4}$$

where B is the subchannel bandwidth. Moreover, $\sigma^2 = N_0 B$ is the variance of the additive white Gaussian noise (AWGN), N_0 is the noise spectral density, and p_i is the transmission power of CUE i. Also, $h_{i,m,n}$ is the fading channel gain between transmitter i and receiver m on subchannel n, including path-loss, where Rayleigh fading channels are assumed in this work. The interference $I_{i,m,n}$ received at BS m on subchannel n for CUE i is

$$I_{i,m,n} = \sum_{j\in I_C, j\neq i}\rho_{j,n}p_j h_{j,m,n} + \sum_{k\in I_D}\rho_{k,n}p_k h_{k,m,n}, \tag{4.5}$$

Similarly, the transmission data rate of DUE $k \in I_D$ on subchannel $n \in \mathcal{N}$ is written as

$$R_k^D = B\log_2\left(1+\sum_{n\in\mathcal{N}}\frac{\rho_{k,n}p_k h_{k,k,n}}{I_{k,n}+\sigma^2}\right), \tag{4.6}$$

where $h_{k,k,n}$ is the channel gain between the D2D transmitter k and its receiver k on subchannel n. The interference received at D2D receiver k on subchannel n is given by

$$I_{k,n} = \sum_{i\in I_C}\rho_{i,n}p_i h_{i,k,n} + \sum_{l\in I_D, l\neq k}\rho_{l,n}p_l h_{l,k,n}. \tag{4.7}$$

4.2.2 Path-loss and Energy-Efficiency Models

The path-loss $L(d)$ is modeled as

$$L(d) = 20\log\left(\frac{4\pi f}{c}\right) + 10\theta\log(d) + \psi, \tag{4.8}$$

where f is the operating frequency, c is the speed of light, θ is the path-loss exponent, d is the distance between the transmitter and receiver, and ψ is the zero-mean log normal shadowing. It is assumed that the UHF BSs are equipped with omni-directional antennas.

The network energy-efficiency (EE) in the UL is determined as [78]

$$EE = \frac{\sum_{i\in I_C} R_i^C + \sum_{k\in I_D} R_k^D}{\sum_{i\in I_C} p_i + \sum_{k\in I_D} p_k}. \tag{4.9}$$

4.3 Resource Allocation in D2D-Underlay HetNets with DUDe

4.3.1 Problem Formulation

In this work, our focus is to maximize the network sum-rate with constraints on the minimum data rate and maximum transmission power per UE. Therefore, the joint cell-association, subchannel allocation, and power control (J-CA-SCA-PC) problem can be formulated as[3]

J-CA-SCA-PC: (4.10)

$$\max_{\boldsymbol{\chi},\boldsymbol{\rho},\mathbf{p}} \quad R \triangleq \sum_{i\in I_C} R_i^C + \sum_{k\in I_D} R_k^D \tag{4.10a}$$

$$\text{s.t.} \quad R_i^C \geq R_{min}^C, \qquad \forall i \in I_C, \tag{4.10b}$$

$$R_k^D \geq R_{min}^D, \qquad \forall k \in I_D, \tag{4.10c}$$

$$0 \leq p_i \leq p_{max}^C, \qquad \forall i \in I_C, \tag{4.10d}$$

$$0 \leq p_k \leq p_{max}^D, \qquad \forall k \in I_D, \tag{4.10e}$$

$$\sum_{m\in\mathcal{M}} \chi_{i,m} = 1, \qquad \forall i \in I_C, \tag{4.10f}$$

$$\sum_{n\in\mathcal{N}} \rho_{i,n} = 1, \qquad \forall i \in I_C, \tag{4.10g}$$

$$\sum_{n\in\mathcal{N}} \rho_{k,n} = 1, \qquad \forall k \in I_D, \tag{4.10h}$$

$$\rho_{i,n}, \rho_{k,n} \in \{0,1\}, \quad \forall i \in I_C, \forall k \in I_D, \forall n \in \mathcal{N}, \tag{4.10i}$$

$$\chi_{i,m} \in \{0,1\}, \qquad \forall i \in I_C, \forall m \in \mathcal{M}, \tag{4.10j}$$

where R_{min}^C and R_{min}^D are the minimum data rate values per CUE and DUE, respectively. Moreover, p_{max}^C and p_{max}^D are the maximum transmission power per CUE and DUE,

[3]The use of "joint" generally refers to the overall problem we are considering, which is solved by decoupling it into three sub-problems, i.e. cell-association, subchannel allocation, and power control.

respectively. Additionally, $\boldsymbol{\chi}$, $\boldsymbol{\rho}$ and $\mathbf{p}$ are the network cell-association, subchannel allocation, and transmission power matrices of all CUEs and DUEs, respectively. In problem **J-CA-SCA-PC**, (4.10a) is the objective function, representing the network sum-rate. Constraints (4.10b) and (4.10c) correspond to the minimum CUE and DUE data rates, respectively. Constraints (4.10d) and (4.10e) represent the upper and lower bounds of the CUE and DUE transmission powers, respectively. Constraint (4.10f) ensures that each CUE is associated with one BS, while Constraints (4.10g) and (4.10h) respectively ensure that each CUE and DUE is assigned one subchannel. The last two constraints define the range of values the binary decision variables take.

Remark 1. *Problem **J-CA-SCA-PC** is a mixed-integer non-linear programming (MINLP) problem. More importantly, it is non-convex (and NP-hard [112, 119, 120]) due to the binary decision variables for subchannel allocation, and also the existence of the interference among the CUEs and D2D pairs sharing the same subchannel. A possible approach is to exhaustively search for every possible BS, subchannel and UEs combination, and compute the corresponding optimal power allocation for each combination (which is still non-convex). However, this approach is impractical, and excessively complex.*

Alternatively, we decouple problem **J-CA-SCA-PC** into three sub-problems: (1) cell-association, (2) subchannel allocation, and (3) power control. Firstly, we fix the UL transmission powers, and decide on the serving BS for each UE. After that, we allocate a suitable subchannel to each UE, while fixing their transmission powers and serving BSs. Finally, the transmission powers are optimized based on the obtained cell-association and subchannel allocation to maximize the network sum-rate. This approach is widely used in the literature, such as [89, 110].

4.3.2 Cell-Association

As for traditional UL and DL coupled cell-association, CUEs connect to the BS with the maximum biased DL RSRP [25, 26] in the UL and DL. However, we decouple the UL and DL in this chapter, and allow the CUEs to be associated with a BS according to the minimum path-loss (Min-PL) criterion in the UL [2]. In the Min-PL criterion, the CUEs are connected to the BS with the lowest path-loss [2]. Particularly, CUE $i \in I_C$ is associated with BS $m \in \mathcal{M}$ in the UL if

$$p_{i,m} W_m {L_{i,m}}^{-1} \geq p_{i,m'} W_{m'} L_{i,m'}^{-1}, \quad \forall m, m' \in \mathcal{M}, \tag{4.11}$$

where W is the UL cell bias value, which is positive referring to expanding the coverage of the cells, $L_{i,m}$ is the UL path-loss between CUE i and BS m. Moreover, $p_{i,m}$ and $p_{i,m'}$ (expressed in dBm) are UL transmission powers of UE i, which are related to the UE-BS distances, and set according to the fractional power control (FPC) scheme in [79], as

$$p_i = \min\{p_{\max}, 10\log_{10}M + \alpha L + p_0\}, \tag{4.12}$$

where p_{max} is the maximum transmission power per UE, and M is the number of sub-channels assigned to the UE. Moreover, p_0 is a target received power at BSs, and $0 < \alpha < 1$ is a compensation factor for UL path-loss L. Particularly, α allows the UE to partially compensate the path-loss, as the higher the path-loss the lower the received power. In turn, increasing α increases the received power at the cell-edge UEs, which also increases inter-cell interference [121]. In this chapter, $\alpha = 0.6$, as it balances the cell-edge and cell-centre UEs' data rates.

4.3.3 Resource Block Allocation

Once cell-association is obtained, and in order to allow as many CUEs/DUEs as possible to access to the network, we assume the SUEs and DUEs can reuse the subchannels of MUEs, and one subchannel can be reused by multiple UEs simultaneously in different cells, which makes it necessary to control inter-tier and co-tier interference[4]. Now, we first assign an unoccupied subchannel to each MUE, and then cluster all the SUEs and DUEs using the graph coloring theory to control the interference[5]. The UEs whose mutual interference is under a certain threshold are clustered into one group, and the UEs in the same group are allocated the same subchannel.

We define $G = (V, E)$ as a graph corresponding to the interference in the network, where $V = V_i$ (for $1 \leq i \leq C+D$), and $E = e_{i,j}$ (for $i \neq j$ and $1 \leq i, j \leq C+D$) represent the vertices and edges of the graph, respectively. Specifically, a vertex represents a UE requesting a subchannel. An edge connects two different vertices, which means these two UEs cannot be allocated to the same subchannel due to strong mutual interference. The criteria for judging whether there is strong interference between UE i and UE j

[4]Resource block allocation is based on the aperiodic channel quality indicator (CQI) reported from the UEs [76].

[5]We assume a control node in the network knows the whole interference map.

($i \neq j$) on subchannel n are

$$\frac{p_i L_{i,m}}{p_j L_{j,m}} > \frac{\gamma_m}{\phi}, \tag{4.13}$$

and

$$\frac{p_j L_{j,l}}{p_i L_{i,l}} > \frac{\gamma_l}{\phi}, \tag{4.14}$$

where $i, j \in I$, the receiver of UE i is BS/UE m, while the receiver of UE j is BS/UE l. Moreover, $L_{i,m}$ denotes the path-loss between transmitter i and receiver m, while γ_i and γ_j are the signal-to-interference (SIR) thresholds at the serving BS/UE of UEs i and j. Also, ϕ is a parameter proportional to the density of the UEs, which is used to adjust the SIR thresholds as the potential interference level after subchannel allocation is proportional to the number of UEs. More specifically, the higher number of UEs in the network is, the more UEs will reuse a subchannel, and thus, the SIR threshold determining if two UEs can reuse a subchannel should be lower. If either (4.13) or (4.14) is not satisfied, these two UEs cannot share the same subchannel. We use different colors to represent different subchannels, and assign a color to each vertex. Notably, two vertices on the same edge cannot use the same color.

The greedy coloring algorithm is utilized to solve this graph coloring problem, whose time-complexity is $O(|V| + |E|)$ [122]. Particularly, the vertices are ranked in descending order by their degrees[6]. The colors are represented by the numbers $\{0, 1, 2, \dots\}$, and each vertex is given the color with the smallest number that is not already used by one of its neighbors. Then, the vertices with more edges incident to them are served first, and so on. The vertices in the same color represent the UEs in the same group. Intuitively, the UEs in a group are located far apart, so as to ensure that the mutual interference of the UEs within each group is kept under a certain threshold. It should also be noted that the higher the SIR threshold, the more the clusters, and the fewer the UEs in each group; however, the number of groups cannot exceed that of the subchannels.

[6]In graph theory, the degree (or valency) of a vertex of a graph is the number of edges that are incident to the vertex.

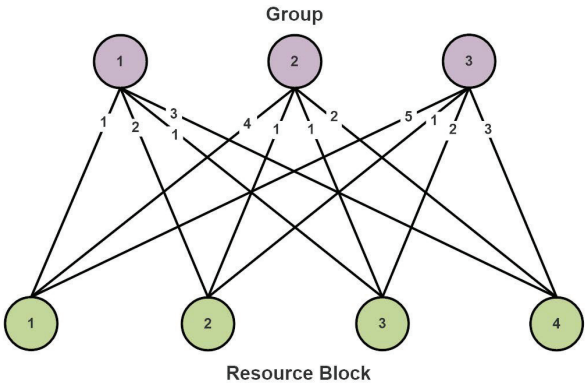

Figure 4.2: Weighted bipartite graph matching.

After clustering the SUEs and DUEs into G groups, the next step is to allocate one subchannel to each group. Particularly, the subchannel allocation can be modeled as a weighted bipartite graph matching, as shown in Fig. 4.2, where the two vertex sets $\mathcal{G} = \{1,2,...,G\}$ and $\mathcal{N} = \{1,2,...,N\}$ represent the grouped user equipment (GUE) (i.e. SUEs and/or DUEs) set and the subchannel set, respectively. Moreover, let $w_{g,n}$ be a weight representing the sum-rate gain when subchannel n is allocated to GUE $g \in \mathcal{G}$, as

$$w_{g,n} = \left(\sum_{i \in I_C^g} R_{i,n}^C + \sum_{k \in I_D^g} R_{k,n}^D \right) - R_n, \tag{4.15}$$

where I_C^g and I_D^g refer to the CUE and DUE index sets of the g^{th} group, whereas $R_{i,n}^C$ and $R_{k,n}^D$ represent the data rates of CUE $i \in I_C^g$ and DUE $k \in I_D^g$ over subchannel n, respectively. Moreover, R_n is the data rate on subchannel n when group g has not occupied it yet, which could be zero.

To solve this problem, the Munkres algorithm is utilized to effciently find the optimal one-to-one UE group-subchannel assignment [123]. Particularly, it optimally performs subchannel assignment for the clustered UE groups, such that the network sum-rate is maximized, while ensuring low complexity. In turn, a $G \times N$ capacity gain matrix $W = [w_{g,n}]$ is constructed. However, as the number of groups could be less than the number of subchannels, the traditional Munkres algorithm for square matrices is not suitable, so we utilize the modified Munkres algorithm to solve the assignment problem for rectangular matrices [117, 124]. Specifically, given the $G \times N$ cost matrix $W' = [-w_{g,n}]$ of real members, and find a set of k independents $k = \min(G,N)$, which are in different rows and columns, such that the sum of the elements is minimum[7].

[7]The Munkres algorithm is initially used to solve the minimal assignment problem, i.e. find

The modified Munkres algorithm is outlined in Algorithm 3, which has a low-order polynomial run-time with a worst-case complexity of $O(N^3)$ [125], and the proof of convergence of Algorithm 3 can be found in [126].

4.3.4 Power Control

After subchannel allocation, the final step is to maximize the network sum-rate while satisfying the minimum UE data rate and maximum transmission power constraints. In OFDMA networks, due to the orthogonality of subchannels, the interference between two different subchannels can be ignored. Thus, maximizing the network sum-rate is equivalent to maximizing the sum-rate over each subchannel. This network sum-rate maximizing power control (PC) problem can be formulated as

$$\underline{\textbf{PC:}} \tag{4.16}$$

$$\max_{\mathbf{p}} \quad R(\mathbf{p}) = \sum_{n\in\mathcal{N}} R_n(\mathbf{p}) \tag{4.16a}$$

$$= \sum_{n\in\mathcal{N}} \left(\sum_{i\in I_C^n} R_{i,n}^C(\mathbf{p}) + \sum_{i\in I_D^n} R_{k,n}^D(\mathbf{p}) \right)$$

$$\text{s.t.} \quad R_{i,n}^C(\mathbf{p}) \geq R_{min}^C, \quad \forall i \in I_C^n, \forall n \in \mathcal{N}, \tag{4.16b}$$

$$R_{k,n}^D(\mathbf{p}) \geq R_{min}^D, \quad \forall k \in I_D^n, \forall n \in \mathcal{N}, \tag{4.16c}$$

$$0 \leq p_i \leq p_{max}^C, \quad \forall i \in I_C^n, \tag{4.16d}$$

$$0 \leq p_k \leq p_{max}^D, \quad \forall k \in I_D^n, \tag{4.16e}$$

where I_C^n and I_D^n are the index sets of the CUEs and DUEs allocated to subchannel n, respectively. Moreover, $R_{i,n}^C(\mathbf{p})$ is the data rate of CUE i on subchannel n, which can be expressed as

$$R_{i,n}^C(\mathbf{p}) = B\log_2\left(1+\frac{p_i h_{i,i,n}}{\sum_{j\in I_C^n, j\neq i} p_j h_{j,i,n} + \sum_{l\in I_D^n} p_l h_{l,i,n} + \sigma^2}\right), \tag{4.17}$$

a maximum cardinality matching $\mathcal{E}$ of minimum cost, where the cost of matching $\mathcal{E}$ is given by $c(\mathcal{E}) = \sum_{e\in\mathcal{E}} w(e)$. As for the maximal assignment, the best way is to replace the values $w_{g,n}$ with $-w_{g,n}$.

Algorithm 3 Modified Munkres' Algorithm

Initialization: $W^{'}$
Rotate the matrix if necessary so that the number of columns exceeds the number of rows and let $k = \min(G,N)$;
Find the smallest element of each row of the matrix and subtract it from every element in its row;
Find a zero in the resulting matrix;
if there is no 0^* in its row or column **then**
    Star it;
    Repeat for each element in the matrix;
end if
while (1) **do**
    Cover each column containing a 0^*;
    if k columns are covered **then**
        break;
    else
        while (1) **do**
            if there exists an uncovered zero **then**
                while (1) **do**
                    Prime it;
                    if (there is no 0^* in the row containing this $0^{'}$) **then**
                        Construct a series of alternating primed and starred zeros as follows,
                        while there exists a $0^{'}$ that has 0^* in its column **do**
                            Let Z_0 represent the uncovered $0^{'}$ found in Step 15, Z_1 denote the 0^* in the column of Z_0 (if any), and Z_2 denote the $0^{'}$ in the row of Z_1;
                        end while
                        Unstar each 0^* of the series;
                        Star each $0^{'}$ of the series;
                        Erase all primes and uncover every line in the matrix;
                        Go to step 9;
                    else
                        Cover this row and uncover the column containing the 0^*;
                        break;
                    end if
                end while
            else
                Add the smallest uncovered value to every element of each covered row, and subtract it from every element of each uncovered column;
                break;
            end if
        end while
    end if
end while
Done: if $w_{g,n}$ is a 0^*, then the element associated with row g is allocated to that associated with column n.

where $h_{i,i,n}$ is the channel gain between CUE i and its serving BS i on subchannel n, while $h_{j,i,n}$ is the channel gain between CUE j (j not necessarily equals i) and the serving BS of CUE i on subchannel n. Moreover, the data rate of DUE k over subchannel n is written as

$$\begin{aligned} &R_{k,n}^{D}(\mathbf{p}) \\ &= B\log_2\left(1+\frac{p_k h_{k,k,n}}{\sum_{j\in I_C^n} p_j h_{j,k,n}+\sum_{l\in I_D^n, l\neq k} p_l h_{l,k,n}+\sigma^2}\right). \end{aligned} \tag{4.18}$$

The power allocation problem on each subchannel is non-convex due to the interference terms in the rate function of each CUE and DUE, and thus is difficult to optimally solve. However, note that the sum-rate function $R_n(\mathbf{p})$ can be re-written as

$$R_n(\mathbf{p}) = f_n(\mathbf{p}) - g_n(\mathbf{p}), \tag{4.19}$$

where

$$\begin{aligned} f_n(\mathbf{p}) = B\sum_{i\in I_C^n}\log_2\left(\sum_{j\in I_C^n} p_j h_{j,i,n}+\sum_{l\in I_D^n} p_l h_{l,i,n}+\sigma^2\right) \\ +B\sum_{k\in I_D^n}\log_2\left(\sum_{j\in I_C^n} p_j h_{j,k,n}+\sum_{l\in I_D^n} p_l h_{l,k,n}+\sigma^2\right), \end{aligned} \tag{4.20}$$

and

$$\begin{aligned} g_n(\mathbf{p}) = B\sum_{i\in I_C^n}\log_2\left(\sum_{j\in I_C^n, j\neq i} p_j h_{j,i,n}+\sum_{l\in I_D^n} p_l h_{l,i,n}+\sigma^2\right) \\ +B\sum_{i\in I_D^n}\log_2\left(\sum_{j\in I_C^n} p_j h_{j,k,n}+\sum_{l\in I_D^n, l\neq k} p_l h_{l,k,n}+\sigma^2\right). \end{aligned} \tag{4.21}$$

It can straightforwardly be verified that $f_n(\mathbf{p})$ and $g_n(\mathbf{p})$ are concave functions in $\mathbf{p}$ [127], and thus the sum-rate function $R_n(\mathbf{p})$ is a D.C. function. As $g_n(\mathbf{p})$ is slowly sensitive to a change in $\mathbf{p}$, it can be well-approximated by its first order Taylor expansion at a fairly large neighborhood of $\mathbf{p}^{(\ell)}$ in each iteration ℓ, as

$$g_n(\mathbf{p}) \approx g_n\left(\mathbf{p}^{(\ell)}\right) + \nabla g_n^T\left(\mathbf{p}^{(\ell)}\right)\left(\mathbf{p}-\mathbf{p}^{(\ell)}\right), \tag{4.22}$$

where $\nabla g_n^T\left(\mathbf{p}^{(\ell)}\right)$ is the gradient of $g_n\left(\mathbf{p}^{(\ell)}\right)$ at $\mathbf{p}^{(\ell)}$, and $(\cdot)^T$ denotes the transpose operator [128]. In turn, the sum-rate function in (4.19) can be approximated as

$$\bar{R}_n(\mathbf{p}) \approx f_n(\mathbf{p}) - \left(g_n\left(\mathbf{p}^{(\ell)}\right) + \nabla g_n^T\left(\mathbf{p}^{(\ell)}\right)\left(\mathbf{p}-\mathbf{p}^{(\ell)}\right)\right), \tag{4.23}$$

which can be verified to be concave in $\mathbf{p}$, since it is a difference between a concave function and a linear function [129]. Additionally, note that Constraint (4.16b) can be written in linear form ($\forall i \in I_C^n$) as

$$p_i h_{i,i,n} \geq \bar{R}_{min}^C \left(\sum_{j\in I_C^n, j\neq i} p_j h_{j,i,n} + \sum_{l\in I_D^n} p_l h_{l,i,n} + \sigma^2\right), \tag{4.24}$$

where $\bar{R}_{min}^C \triangleq 2^{R_{min}^C/B} - 1$. Similarly, Constraint (4.16c) can be re-expressed ($\forall k \in I_D^n$) as

$$p_k h_{k,k,n} \geq \bar{R}_{min}^D \left(\sum_{j\in I_C^n} p_j h_{j,k,n} + \sum_{l\in I_D^n, l\neq k} p_l h_{l,k,n} + \sigma^2\right), \tag{4.25}$$

and $\bar{R}_{min}^D \triangleq 2^{R_{min}^D/B} - 1$. Based on the above, the D.C. programming-based power control problem for sum-rate maximization over each subchannel $n \in \mathcal{N}$ can be expressed as

$$\underline{\textbf{DC-PC } (\boldsymbol{n},\boldsymbol{\ell})\textbf{:}} \tag{4.26}$$

$$\max_{\mathbf{p}} \quad f_n(\mathbf{p}) - \left(g_n\left(\mathbf{p}^{(\ell)}\right) + \nabla g_n^T\left(\mathbf{p}^{(\ell)}\right)\left(\mathbf{p}-\mathbf{p}^{(\ell)}\right)\right) \tag{4.26a}$$

$$\text{s.t.} \quad (4.24), (4.25), (4.16d), \text{and } (4.16e), \tag{4.26b}$$

which can be verified to be a concave maximization problem with a linear constraints set. Thus, **DC-PC $(\boldsymbol{n},\boldsymbol{\ell})$** can be solved efficiently via any standard optimization package [129]. Now, to efficiently solve problem **DC-PC $(\boldsymbol{n},\boldsymbol{\ell})$** in each iteration ℓ, the Frank-Wolfe iterative algorithm is employed [130]. Specifically, a feasible solution $\mathbf{p}^{(0)}$ is initialized, and then a sequence of improved solutions $\left\{\mathbf{p}^{(l)}\right\}$ is generated until convergence, as outlined in Algorithm 4.

Algorithm 4 D.C. Programming-Based Power Control

1: **Initialization:** Set error tolerance $\varepsilon \in (0,1)$, initialize iteration index $\ell = 0$, select a feasible $\mathbf{p}^{(0)}$, and calculate $R_n\left(\mathbf{p}^{(0)}\right)$.
2: **repeat**
3: Set $\ell = \ell + 1$;
4: Solve problem **DC-PC (n,ℓ)** to obtain the solution $\mathbf{p}^*$;
5: Set $\mathbf{p}^{(l)} = \mathbf{p}^*$, and calculate $R\left(\mathbf{p}^{(l)}\right)$;
6: **until** $\left|R_n\left(\mathbf{p}^{(\ell)}\right) - R_n\left(\mathbf{p}^{(\ell-1)}\right)\right| \leq \varepsilon$ or $\left|\mathbf{p}^{(\ell)} - \mathbf{p}^{(\ell-1)}\right| \leq \varepsilon$.
7: **Output:** $\mathbf{p}^\star = \mathbf{p}^{(\ell)}$.

The computational-complexity of Algorithm 4 is $O\left(\left(\left|I_C^n\right| + \left|I_D^n\right|\right)^3\right)$ [128], and since there is a total of N subchannels, then the overall computational-complexity of solving problem **PC** is $O\left(N\left(\left|I_C^n\right| + \left|I_D^n\right|\right)^3\right)$. As for convergence, note that the solution $\mathbf{p}^{(\ell+1)}$ obtained in the $(\ell+1)^{th}$ is based on the solution of the previous iteration (i.e. $\mathbf{p}^{(\ell)}$). Also, since **DC-PC (n,ℓ)** is a concave maximization problem, then the following inequality holds [128]

$$\begin{aligned} & f_n\left(\mathbf{p}^{(\ell+1)}\right) - g_n\left(\mathbf{p}^{(\ell+1)}\right) \geq \\ & f_n\left(\mathbf{p}^{(\ell)}\right) - \left(g_n\left(\mathbf{p}^{(\ell)}\right) + \nabla g_n^T\left(\mathbf{p}^{(\ell)}\right)\left(\mathbf{p}^{(\ell+1)} - \mathbf{p}^{(\ell)}\right)\right) \geq \\ & f_n\left(\mathbf{p}^{(\ell)}\right) - g_n\left(\mathbf{p}^{(\ell)}\right), \end{aligned} \tag{4.27}$$

which implies that the sum-rate function $R_n\left(\mathbf{p}^{(\ell)}\right)$ improves at each iteration ℓ. Moreover, since the constraints set is linear, and hence convex (i.e. closed and compact) [129], then by Cauchy theorem, the sequence $\left\{\mathbf{p}^{(\ell)}\right\}$ always converges [131]. This happens when $\left|R_n\left(\mathbf{p}^{(\ell)}\right) - R_n\left(\mathbf{p}^{(\ell-1)}\right)\right| \leq \varepsilon$ or $\left|\mathbf{p}^{(\ell)} - \mathbf{p}^{(\ell-1)}\right| \leq \varepsilon$, as there is no improvement, for some $\varepsilon > 0$.

Remark 2. *It should be noted that decoupling cell-association, subchannel allocation, and power control does not necessarily guarantee global optimality, in comparison to the formulated **J-CA-SCA-PC** problem. However, it will shortly be demonstrated that decoupling cell-association in the DL and UL, while Min-PL for UL cell-association, graph-coloring and Munkres algorithm for subchannel allocation, and D.C. programming-based power allocation poses a reasonable tradeoff between complexity and optimality.*

Table 4.1: Resource Allocation Schemes

Scheme	**Cell-Association**	**Subchannel Allocation**	**Power Control**
C-G-FPC	Biased RSRP	Greedy	Fractional power control
D-G-FPC	Min-PL	Greedy	Fractional power control
D-R-FPC	Min-PL	Random	Fractional power control
D-GCM-FPC	Min-PL	Greedy coloring & Munkres	Fractional power control
C-G-DCP	Biased RSRP	Greedy	D.C. programming
D-G-DCP	Min-PL	Greedy	D.C. programming
D-R-DCP	Min-PL	Random	D.C. programming
D-GCM-DCP	Min-PL	Greedy coloring & Munkres	D.C. programming
C-GCM-DCP	Biased RSRP	Greedy coloring & Munkres	D.C. programming

4.4 Performance Evaluation

In this section, the performance of the proposed (D) decoupled cell-association is evaluated and compared to the coupled (C) cell-association scheme for different combinations of subchannel allocation and power control schemes. Particularly, the proposed subchannel allocation scheme—based on greedy coloring and the Munkres (GCM) algorithm—is compared with the Random (R), and Greedy (G) subchannel allocation schemes[8]. Moreover, the proposed D.C. programming-based power control (DCP) is compared with the FPC scheme [79]. The different schemes are listed in Table 4.1[9].

[8]In the Random scheme, subchannels are randomly allocated to the UEs, while in the Greedy scheme, the subchannel with the highest SINR is allocated to each UE [132].

[9]The initial feasible transmission power values of the DCP scheme are set according to the FPC scheme. Particularly, the minimum data rate per CUE/DUE is 500 kbps, in alignment with the maximum transmission power values given in Table II. Specifically, this is the minimum data rate that all the UEs can achieve according to the FPC scheme. When maximizing the network sum-rate, the data rate of some UEs may be sacrificed to reduce the interference to other UEs; however, the minimum data rate constraint is used to guarantee the data rate of each UE will not drop below the minimum requirement. In practice, and in the case that the channel conditions are severe and/or the available transmission power is insufficient to satisfy the minimum rate constraints, some CUEs/DUEs may experience an outage.

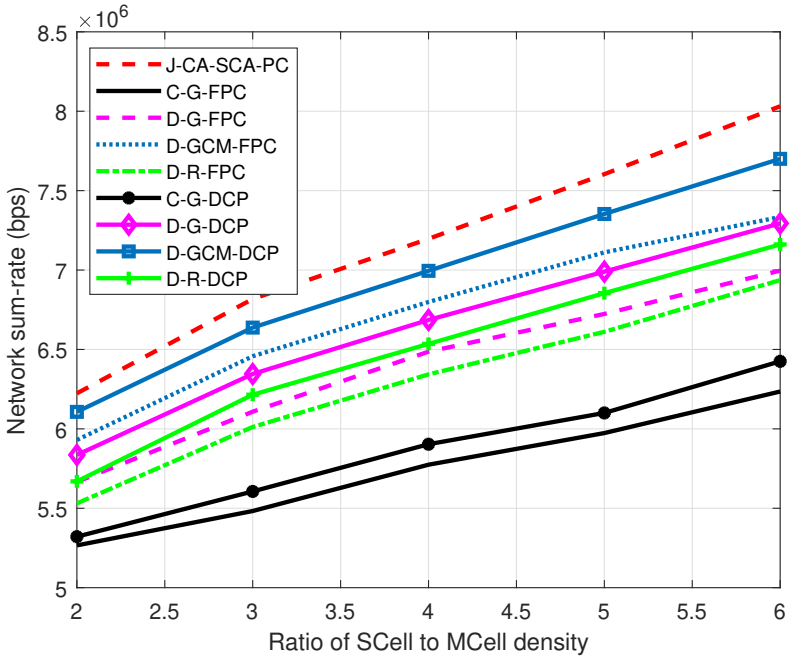

Figure 4.3: Network sum-rate vs. ratio of SCell to MCell density.

As per **Remark 1**, obtaining the global optimal solution of problem **J-CA-SCA-PC** may be possible in theory; but may be practically infeasible due to the excessive computational complexity. Nevertheless, to highlight the near-optimality of our proposed algorithmic designs, we simulate a small HetNet with one MBS, 2-6 SBSs, 3 CUEs and 3 D2D pairs, which are randomly and uniformly deployed in a $450m \times 450m$ square network area. The number of subchannels is assumed to be 2. Clearly, there is an exponential number of possible combinations for the cell-association, and subchannel allocation of the UEs. On top of that, the power control is non-convex for all the UEs sharing the same subchannel. In turn, problem **J-CA-SCA-PC** is implemented in a commercial global optimization package, known as MIDACO [83, 133][10]. As shown in Fig. 4.3, the network sum-rate of the proposed **D-GCM-DCP** scheme is very close to that of the **J-CA-SCA-PA** scheme (as per **Remark 2**), especially when the possible BS-subchannel-UE combination number is low. More importantly, our proposed scheme is superior to the other cell-association, subchannel allocation and power control schemes.

Remark 3. *From this point onwards, and due to the excessive computational-complexity*

[10]Note that the **J-CA-SCA-PC** scheme serves as an upper-bound benchmark scheme for network sum-rate maximization. Moreover, in MIDACO, the tolerance has been set to 10^{-3}, which implies that the global optimal solution is accurate up to three decimal places.

Table 4.2: Simulation Parameters

Parameters	**CUE**	**DUE**	**MCell**	**SCell**
Maximum transmission power	20 dBm	17 dBm	46 dBm	30 dBm
Minimum data rate per UE	500 kbps	500 kbps	N/A	N/A
Spatial density	$150/km^2$	$150/km^2$	$5/km^2$	$25/km^2$
D2D maximum distance	30 m			
Spatial distribution	HPPP			
Lognormal shadowing	$\mu = 0$, $\sigma = 4$ dB			
Path-loss exponent	3			
Operating frequency	2 GHz			
UL bandwidth	5 MHz			
Subcarrier spacing	15 kHz			
Number of subchannels	25			
Noise spectral density	-174 dbm/Hz			

*of the **J-CA-SCA-PC** scheme, it is omitted from the following simulation results, which are based on a larger HetNet, with the full simulation parameters as given in Table 4.2. Particularly, the simulation parameters are applicable to both LTE and 5G cellular networks [57].*

Fig. 4.4 shows the relationship between the number of SCells and the network sum-rate. It can be seen that decoupled association schemes achieve at around 20% higher sum-rates than the coupled association ones. This is because DUDe shortens the distance between the UEs and their serving BSs, which in turn reduces the path-loss. As FPC is utilized, uplink transmission power and interference are also reduced accordingly. Similarly, deploying more SCells offloads more UEs from the MCell to the SCells, which shortens the distance between the UEs and BSs, and as a result, the network sum-rate increases with the number of SCells. This figure also shows that our subchannel allocation algorithm—based on greedy coloring and Munkres' algorithm—outperforms the Greedy and Random subchannel allocation schemes. Moreover, the proposed power allocation scheme based on D.C. programming also improves the network sum-rate in comparison to FPC. However, the performance gain of optimizing subchannel allocation and power control is less remarkable in comparison to the decoupled access. Specifically, the C-GCM-DCP scheme achieves 7% higher network sum-rate than the C-G-FPC scheme, while the D-GCM-DCP achieves 20% higher sum-rate. This may be because DUDe has reduced the interference significantly that there is not much room left for further improvement via

subchannel allocation and power control; although we used a near-optimal subchannel allocation and power control scheme.

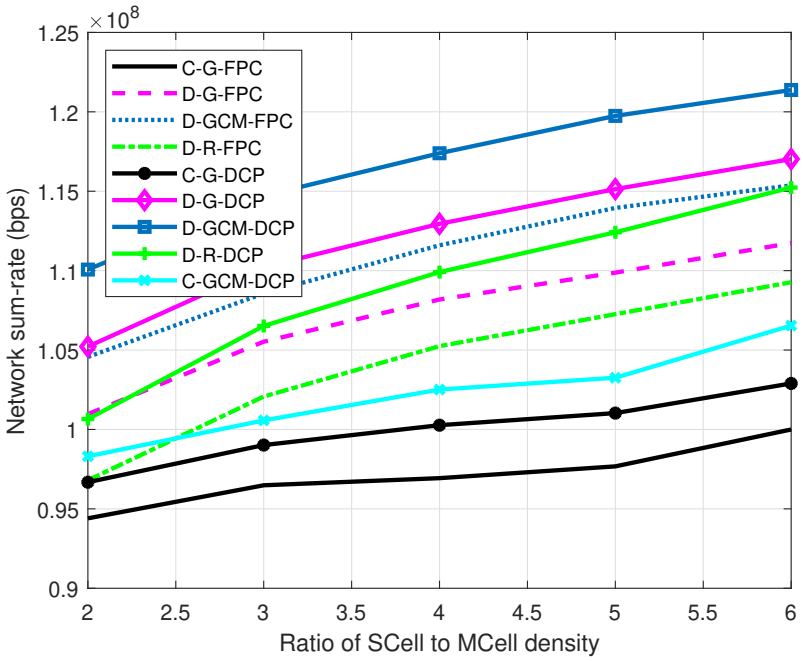

Figure 4.4: Network sum-rate vs. ratio of SCell to MCell density.

Fig. 4.5 shows the relationship between the number of SCells and the CUE sum-rate. The D-GCM-FPC and D-GCM-DCP schemes can achieve around 30% higher CUE sum-rate than C-G-FPC and C-G-DPC schemes. It is interesting to find that our power allocation scheme reduces the CUE sum-rate, which lies in the fact that the distance between a D2D transmitter and receiver is often shorter than that between a CUE and its serving BS (i.e. the D2D link has higher SINR). Thus, to maximize the network sum-rate, when the D2D link and CUE link share the same subchannel, more power is allocated to the D2D link and the CUE link suffers more interference, and thus, the impact of the D.C. programming-based power allocation on the CUE sum-rate is negative. However, the distance gap decreases when the number of SCells increases, and so the impact of the D.C. power allocation scheme also decreases, and the CUE sum-rate gap of the schemes with and without D.C. power allocation decreases.

Fig. 4.6 shows the 10^{th}, 20^{th}, 50^{th}, 80^{th}, and 90^{th} percentile data rates per UE. It can be seen that the D-GCM-FPC and D-GCM-DCP schemes can achieve about twice higher 10^{th} percentile data rate than the C-G-FPC and C-G-DPC schemes. The D.C. power allocation increases the 80^{th}, and 90^{th} percentile data rates, but decreases

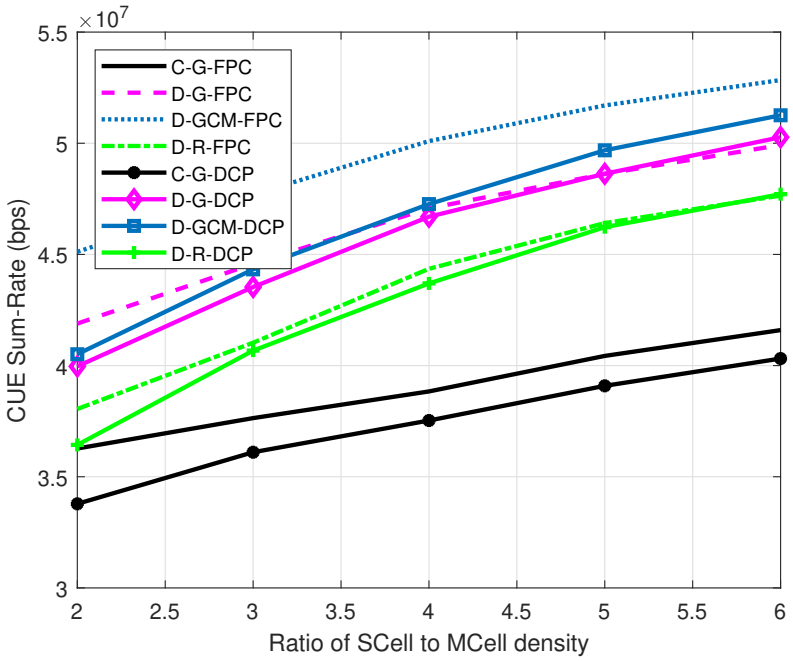

Figure 4.5: CUE sum-rate vs. ratio of SCell to MCell density.

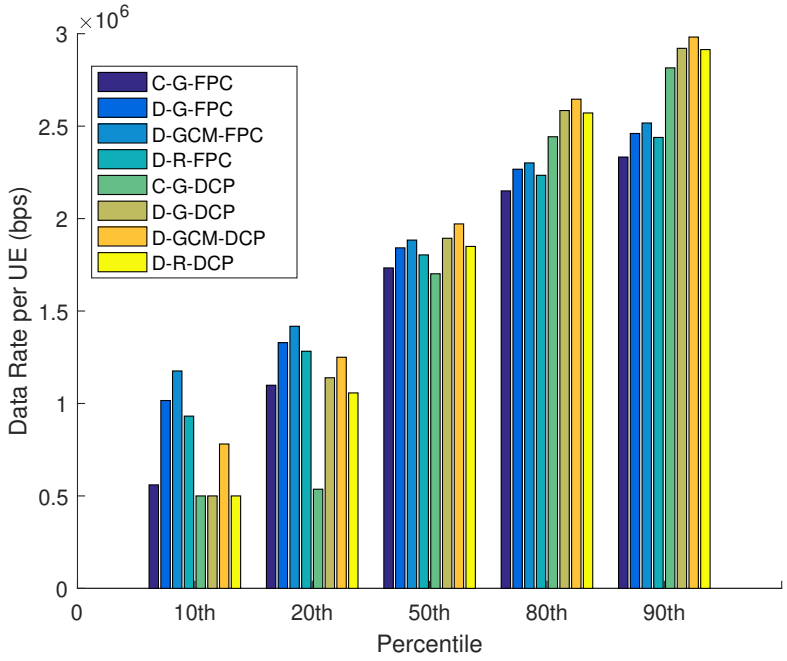

Figure 4.6: 10^{th}, 20^{th}, 50^{th}, 80^{th}, and 90^{th} percentile UE data rates based on different schemes.

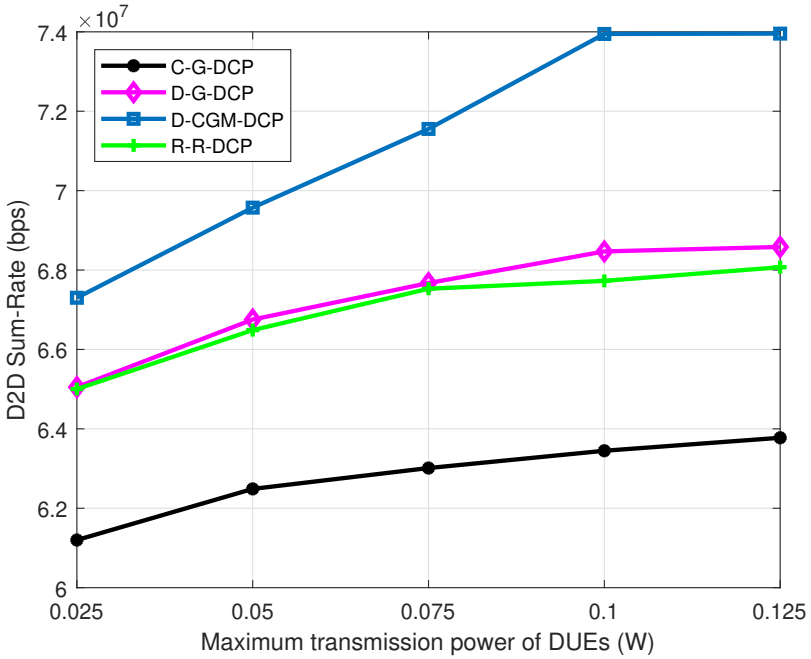

Figure 4.7: DUE sum-rate vs. maximum transmission power of DUEs.

the 10^{th} and 20^{th} percentile per UE data rates. In other words, it improves the data rates of the links with high channel quality at the expense of those with low channel quality. Furthermore, the coupled association schemes have the lowest data rate and our decoupled GCM algorithms have the highest data rate irrespective of the power allocation scheme.

Fig. 4.7 shows the relationship between the maximum transmission power of DUEs and the D2D sum-rate. According to the FPC scheme, as long as the maximum transmission power is sufficiently high, the transmission power of each UE is only affected by their path-loss, and so we only consider the performance of the schemes with the aid of power optimization based on D.C. programming. It can be seen that the D2D sum-rate increases with the maximum transmission power, which means that the sum-rate improvement mainly depends on the transmission power increase. However, when the transmission power becomes higher, its effect on the data rate becomes less, because interference becomes more dominant. The DUEs sum-rate of the proposed scheme is about 15% higher than the coupled scheme.

Fig. 4.8 shows the relationship between the number of UEs and the normalized energy-efficiency. Although with the aid of D.C. power allocation, UEs can achieve higher data rate (as shown in Fig. **??**), their energy-efficiency reduces. This is because

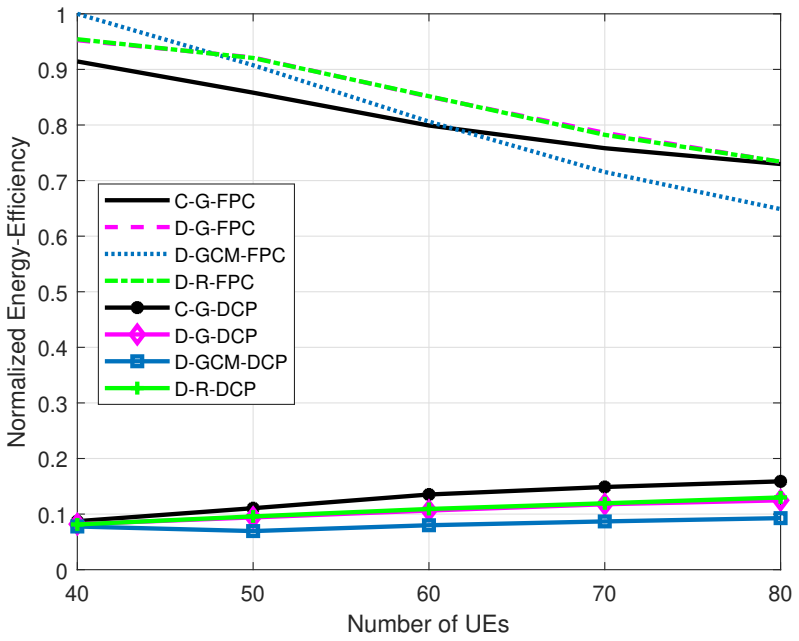

Figure 4.8: Normalized energy-efficiency vs. number of UEs.

the D.C. power allocation scheme will allocate as much power as possible to UEs, so as to improve their data rates, but the interference grows with the UE transmission power, especially when the transmission power and UE density are high. Besides, it is surprising to find that the energy-efficiency of the schemes with D.C. power optimization does not decrease when the number of UEs increases. A possible explanation for this is that in high density scenarios, interference bottleneck happens before the transmission power bottleneck, such that the transmission power of the UEs decreases with the increase of UEs.

Lastly, and to shed light on the convergence of the proposed scheme, Fig. 4.9 illustrates the average number of iterations of Algorithms 1 and 2. It can be seen that Algorithm 1 increases slightly with the increase in the number of CUEs and DUEs[11]. This implies that the devised greedy coloring and modified Munkres algorithm is efficient when assigning the UEs to the subchannels. As for Algorithm 2 (over all 25 subchannels), one can see that with the increase the number of CUEs and DUEs the average number of iterations increases relatively higher than Algorithm 1. This is due to the relatively higher complexity of Algorithm 2 in comparison to Algorithm

[11]The number of DUEs make up half of the total number of CUEs and DUEs.

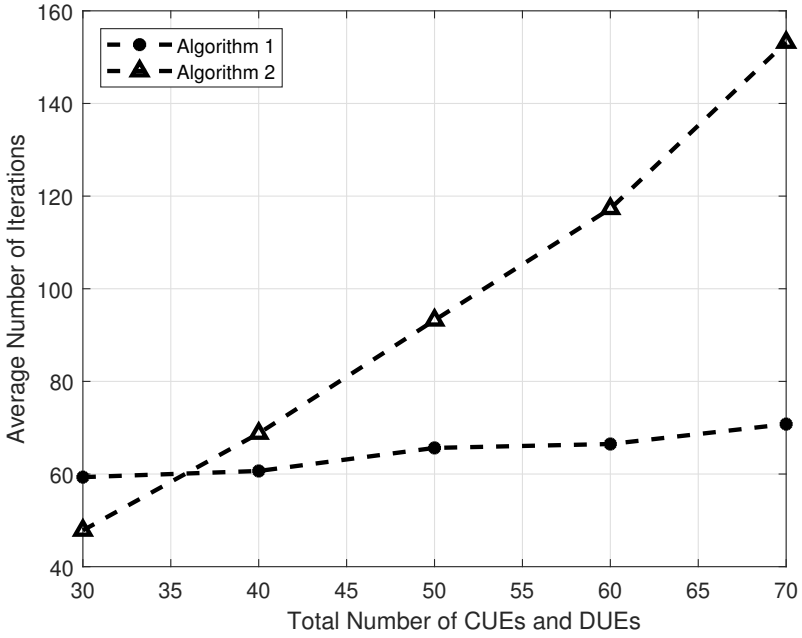

Figure 4.9: Average number of iterations of Algorithms 1 and 2.

1 (i.e. $O\left(N\left(\left|I_C^n\right|+\left|I_D^n\right|\right)^3\right)$ in comparison to $O\left(N^3\right)$). More importantly, the complexity over each subchannel is $O\left(\left(\left|I_C^n\right|+\left|I_D^n\right|\right)^3\right)$, which implies that if Algorithm 2 can be executed in parallel over all subchannels, then the complexity can be greatly reduced. This in turn proves the efficient execution of the proposed scheme to obtain a near-optimal network sum-rate.

4.5 Summary

A joint DL/UL decoupled cell-association, subchannel allocation and power control scheme for D2D-underlay HetNets has been proposed, and its performance has been compared with state-of-the-art alternatives. In the proposed scheme, the Min-PL based DUDe has been used for cell-association in the UL. Moreover, a greedy coloring and a modified Munkres algorithm have been employed to solve the subchannel allocation problem. After that, D.C. programming is utilized to maximize the network sum-rate while meeting UE maximum transmission power and minimum date rate constraints. Numerical results show that the DUDe association schemes achieve higher data rate than their coupled counterparts. The proposed subchannel allocation scheme has been shown to outperform the Greedy and Random subchannel allocation schemes, and

power allocation using D.C. programming dramatically improves the network sum-rate. It was also found that power optimization based on D.C. programming tends to allocate more power to UEs with higher channel quality at the expense of the UEs with lower channel quality. However, care must be taken as energy-efficiency may decrease if the power optimization stage continues to allocate power to the UEs even when the data rate improvement is marginal. Overall, the results showed that the proposed joint scheme can achieve about 20% higher network sum-rate, 30% higher CUE sum-rate, and 15% higher DUE sum-rate than its coupled counterparts.

Chapter 5

DUDe Cellular-Enabled UAV Communications

5.1 Introduction

This chapter investigates the performances of applying DUDe to cellular-enabled UAVs communications. Research in cellular-enabled UAV communication is still in its infancy. The authors in [49] designed a cellular-enabled UAV communication system from the perspective of connectivity-constrained trajectory optimization, where each UAVs' starting point and destination are fixed and a target quality-of-connectivity with the cellular network should be guaranteed. The average secrecy rates of the UAV-to-ground (U2G) and ground-to-UAV transmissions are maximized in [50] by jointly optimizing the UAV's transmission power and the trajectory. Although the formulated problems are non-convex, the authors proposed iterative algorithms to solve them by applying successive convex optimization and the block coordinate descent methods. The authors in [134] proposed a cooperative non-orthogonal multiple access (NOMA) scheme to mitigate the severe UL interference due to the LOS U2G channels. Specifically, some BSs with better channel conditions are selected to decode the UAV's signals first, and then forward the decoded signals to their backhaul-connected BSs for interference cancellation. The throughput of ground passive receivers is maximized by cancelling the highest received jamming power at each passive receiver via successive interference cancellation in [135]. The hovering position for the UAV and the power allocation scheme to meet the data rate constraints of the users is derived in [136]. Generally speaking, most of the existing research focuses on trajectory design and resource allocation to minimize the interference between UAVs and GUEs [137–140].

However, they ignored an important character of UAV communications, which is the UL and DL data rate imbalance. UAV uplinks are dominated by data transmission, requiring high data rates up to hundreds of Mbps. Contrarily, the UAV downlinks are dominated by control and non-payload communication (CNPC) communications with low data rates, which consists of command and control (C&C) data, air traffic control (ATC) relay data, and sense and avoid (S&A) data [48]. They are crucial to the UAV operation requiring low latency, ultra-reliability, and high security, but could not be guaranteed due to the interference from cellular networks [13]. To overcome this problem, we propose a DL-UL decoupled (DUDe) access scheme, which prevents the UAVs-GUEs interference via decoupled BS association and frequency band allocation, and can solve the UL/DL imbalance problem. In this sense, our decoupled scheme can be viewed as an add-on functionality to any existing interference reduction technique.

Conventional DUDe was originally proposed in [2] to allow UEs to be served by different BSs on the UL and DL directions in contrast to legacy 1G-4G systems where the same BS must serve the user on both directions. DUDe not only shortens the distance between the UEs and serving BSs in the UL—which can improve communication energy-efficiency (EE)—but also makes better use of the spectral resources of small BSs. References [69] show that DUDe can improve load balancing, and is particularly beneficial to ultra-dense networks. Current researches focus on decouple the UL and DL serving BSs, inspired by this, and in comparison to existing work, we consider decoupling the DL/UL not only on the basis of BSs but also on the basis of operating frequencies. By utilizing different frequency bands for LOS links and NLOS links, as well as CNPC links and data links, the interference between UAVs and GUEs can be eliminated from the very beginning.

5.1.1 Main Contributions

The main contributions of this chapter can be summarised as follows:

- We propose a novel DUDe based access scheme for cellular-enabled UAV communications, in which both dimensions of serving BSs and operating frequencies are utilised. The proposed DUDe eliminates interference between the UAVs and GUE, as well as part of the inter-cell interference among GUEs, leading to: (1) interference-limited GUE communications, and (2) noise-limited UAV and LOS GUE communications, which is fundamentally different from the the conventional scenario where UAVs and GUEs share the same resources. To the best of

our knowledge, the proposed DUDe scheme has not been introduced to cellular-enabled UAV systems before.

- We devise an optimal low-complexity power allocation algorithm, based on fractional programming and successive convex approximation, to maximise the UL communication EE in tandem with the proposed DUDe scheme.

- Finally, the performance of the proposed DUDe access scheme and power allocation algorithm are compared with benchmark schemes in terms of EE, sum-rate and data rate per UE. It is demonstrated that the proposed DUDe can achieve several times higher sum-rates in both UL and DL directions than the coupled benchmark counterparts, while the optimal power allocation algorithm can provide 15% higher GUE sum-rate and twice higher GUE EE than conventional fractional power control.

5.1.2 Organization

In the rest of the chapter, Section 5.2 presents the system model. Section 5.3 proposes the DUDe access scheme for cellular-enabled UAV networks. Section 5.4 utilizes fractional programming to optimize the EE of the proposed scheme. Section 5.5 evaluates the performance of the proposed scheme, and compares it with coupled benchmarks. Finally, Section 5.6 presents the conclusions.

5.2 System Model

5.2.1 Network Model

In this work, an OFDMA HetNet composed of MCells, SCells, UAVs and GUEs is considered. The positions of MCells, SCells and GUEs follow uniform distribution with densities of λ_m, λ_s and λ_g, respectively. The horizontal locations of the UAVs also follow uniform distribution with intensity λ_u, and their altitudes are randomly and uniformly distributed in the altitude of 50-200 m[1]. Lastly, we assume a full-buffer UE traffic model[2]

[1]It is assumed that the UAVs are independent users, and the resource allocation problem is considered from the network operator's perspective. Thus, the positions of the UAVs are assumed to be fixed, and the trajectory or/and position optimization is assumed to be outside the HetNet control. Nevertheless, interested readers in scenarios where trajectory optimisation is possible are kindly referred to [138–141].

[2]UE is collectively used to refer to a GUE or a UAV.

Table 5.1: Antenna parameters

Frequency Band	UHF	mmWave	mmWave
Number of antenna elements	1	4	16
Half-power beamwidth (degree) θ_b	360	49.6	24.8
Main-lobe gain (dBi) G_M	0	6	12
Side-lobe gain (dBi) G_m	0	-0.8839	-1.1092

5.2.2 Propagation Model

The path-loss $L(d)$ can be modeled as

$$L(d) = 20\log\left(\frac{4\pi d_0 f}{c}\right) + 10\phi\log\left(\frac{d}{d_0}\right) + \chi, \tag{5.1}$$

where d_0 denotes close-in reference distance, f is the operating frequency, c is the speed of light, d represents UE-BS distance, ϕ is path-loss exponent, and χ is the log-normal shadowing.

5.2.3 Antenna Elements

In this work, the BSs and both types of UEs are assumed to support UHF and mmWave bands. Each BS and UE are assumed to have one UHF omnidirectional antenna. On the other hand uniform planar square arrays (UPA) with half-wavelength antenna element spacing are assumed for mmWave transmissions to compensate for the high path-loss. The antenna parameters are shown in Table 5.1 [142–144]. Moreover, the antenna gain at the mmWave BS is

$$G_b(\theta) = \begin{cases} G_M, & |\theta| \leq \theta_b/2, \\ G_m, & \text{otherwise}, \end{cases} \tag{5.2}$$

where θ_b is the mainlobe beamwidth, G_M is the mainlobe gain, and G_m is the sidelobe gain. We assume the mmWave UEs are in perfect alignment [144] with their serving BSs. The antenna gain of a UE-BS link is the product of the antenna gains at the receiver and the transmitter.

5.2.4 Blockage Model

For GUE communications, the generalized blockage ball model is considered [77], as it is widely used in many studies [70, 145]. If the UE-BS distance is less than μ =

200 m, this link is assumed to be LOS with probability $\omega = 0.2$, otherwise, this link is assumed to be NLOS. For UAV communications, the blockage model in [146] is applied, where the LOS probability is

$$P(LOS,\theta) = \frac{1}{1+\exp(-b(\theta-a))}, \tag{5.3}$$

with θ being the elevation angle of the UAV at the BS antenna, and a and b are S-curve parameters related to the environment.

5.2.5 Resource Block Allocation

Resource block (RB) allocation is performed using the aperiodic channel quality indicator (CQI) [76] reported from the UEs. In LTE and LTE-A systems, the CQI is often used for packet scheduling (PS). Specifically, PS refers to selecting the scheduling time and frequency for each UE. UEs report the CQI value for each RB to their serving BS. The BSs utilize these CQI reports to select the preferred RBs for each UE. The CQI report from a given UE includes information regarding the SINR for each physical RB from the received pilot power and total interference every measurement period. The greedy RB allocation algorithm in [132] is adopted in this chapter. We assume the RBs of each BS are equally assigned to its UEs, which can be easily extended to the unequal case. For each UE, all the RBs that are not yet assigned are sorted by SINR (from the viewpoint of the UE), and those with high SINR are preferentially assigned to the UE.

5.2.6 Transmission Data Rate

The transmission data rate between transmitter $i \in I = \{1,2,...,I\}$ and its receiver $m \in \mathcal{M} = \{0,1,2,...,M\}$ on RB $n \in \mathcal{N} = \{0,1,2,...,N\}$ is given by

$$\mathbb{R}_{i,m,n} = B\log_2\left(1+\frac{P_{i,n}G_{i,m}|h_{i,m,n}|^2}{\sum_{j\in I, j\neq i}P_{j,n}G_{j,m}|h_{j,m,n}|^2+\sigma^2}\right), \tag{5.4}$$

where B is the RB bandwidth, $G_{i,m}$ is the antenna gain, $\sigma^2 = N_0 B$ is the variance of the AWGN, N_0 is the noise spectral density, $P_{i,n}$ is the transmission power of transmitter i on RB n, and $h_{i,m,n}$ is the channel gain between transmitter i and receiver m on RB n, including path-loss and fading. As we consider both UL and DL in this chapter, a

transmitter can be a UE or BS[3]. In this chapter, one transmitter can occupy multiple RBs. Moreover, the total data rate of transmitter i is the sum of its data rate on each allocated RB. We assume different fading models for mmWave and UHF communications; specifically, Nakagami$-m$ fading [147] and Rayleigh fading [148], respectively.

5.3 DUDe Access in Cellular Networks Serving UAVs and GUEs

Table 5.2: Transmission Parameters of the Different Schemes

Scheme	DUDe				Coupled (UHF)		Coupled (mmWave)	
Direction	DL		UL		DL	UL	DL	UL
Frequency	mmWave	UHF	mmWave	UHF	UHF		mmWave	
Bandwidth	200 MHz	20 MHz	200 MHz	20 MHz	20 MHz		200 MHz	
Time	50%		50%		50%	50%	50%	50%
UE	GUE	GUE	UAV	GUE	GUE	UAV+GUE	GUE	UAV+GUE
Association	Biased RSRP		Min-PL		Biased RSRP		Biased RSRP	

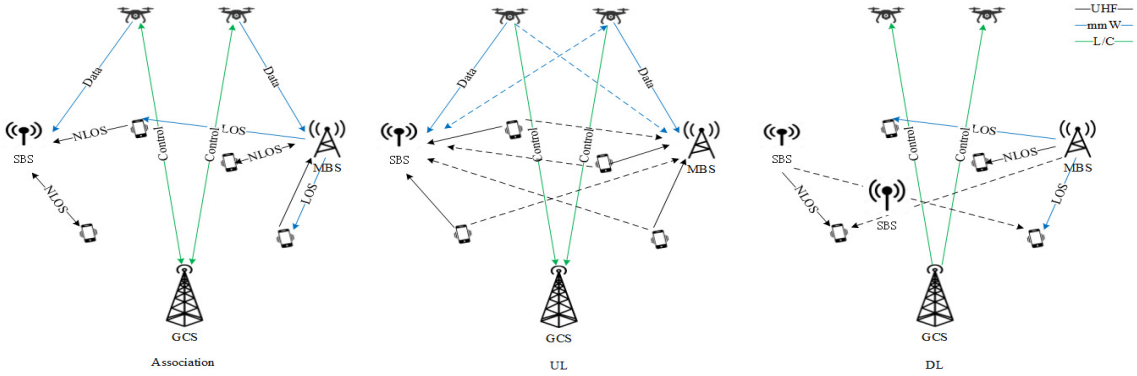

Figure 5.1: Cell Association and Interference map of the proposed scheme.

In conventional cellular networks, the UL and DL are coupled, and UEs connect to the BS with the highest biased reference signal received power (RSRP) [25] in the DL, and transmit to the same BS in the UL. The operating frequency is also the same in the two link directions. This is known as coupled uplink/downlink access (CUDA) [1]. In homogeneous networks, the CUDA mode is optimal, because the best serving BS in the UL and DL are the same. However, with the development of 4G and 5G networks, more low-cost SCells are deployed, which makes cellular networks heterogeneous. Due to the transmission power gap between SCells and MCells, MCells usually

[3]It should be noted that if RB n is not allocated to UE i, then $P_{i,n}$ is set to zero.

have wider coverage than SCells in the DL, hence more UEs are associated with them. However, this is not the case in the UL. Most UEs are battery-powered with similar transmission power, as a result, their coverage is also similar. The CUDA scheme makes the UL channel quality of the MCell edge UEs terrible. As the operating frequencies keep getting higher, the situation becomes even worse. This is called UL and DL imbalance [3]. For the sake of reducing the path-loss, a better choice is to allow MCell edge UEs to connect to a geometrically closer SCell rather than the coupled MCell in the UL, which is the essence of the DUDe technique [2]. Furthermore, since cellular GUEs require higher data rate in the DL than in the UL, allowing them to transmit over high-frequency bands in the DL and low-frequency bands in the UL is another way to improve the UL coverage while guaranteeing a high throughput in the DL, which is akin to decoupling in terms of the operating frequency.

Likewise, UAV UL and DL communication also have different requirements as explained in Section I. Therefore, splitting the UAV data links from the control links is intuitive. The GCSs operating on the L/C bands can be utilized for CNPC links, which can provide a wide coverage, and thus avoid frequently switching of serving BSs during the flight. There is approximately 17 MHz (960-977 MHz) at the L-band, and 61 MHz (5.03-5.091 GHz) at the C-band presently allocated for UAV CNPC links [149]. Transmitting on a dedicated band can also avoid interference and guarantee the reliability of control links. Meanwhile, cellular BSs can be utilized for data transmission. Instead of choosing the serving cellular BSs according to the DL biased RSRP, using a minimum path-loss (min-PL) scheme is a better choice, where UEs are connected to the BS with the lowest path-loss [2] in the UL. Particularly, UE $i \in I$ is associated with BS $m \in \mathcal{M}$ in the UL if

$$p_{i,m} W_m {L_{i,m}}^{-1} \geq p_{i,m'} W_{m'} L_{i,m'}^{-1}, \quad \forall m, m' \in \mathcal{M}, \tag{5.5}$$

where W is the UL cell bias value, which is positive and refers to expanding the coverage of the cells. Moreover, $L_{i,m}$ is the UL path-loss between UE i and BS m. Due to the high capacity requirement of the UAV UL data transmission as well as the LOS dominant characteristic, mmWave bands can be utilized for UAV data links. With the development of directional antennas and beam-forming technologies, the received signal strength of mmWave communications can be guaranteed and inter-cell interference can be significantly reduced. Correspondingly, to reduce the interference between UAVs and GUEs in the UL, UHF bands are utilized for the GUE UL transmission (The mmWave band is utilized for the UL-dominant UAV data transmission). Thus, the UL

coverage can also be guaranteed. As for GUE DL transmission, UHF bands are utilized to provide umbrella coverage. Additionally, in order to improve the network capacity, mmWave bands are used in the DL LOS links. Besides, the serving BSs of GUEs are also decoupled, which are decided according to the biased RSRP scheme in the DL and min-PL scheme in the UL. The whole band allocation and cell association strategy of the proposed DUDe scheme is given in Table 5.2.

Since the current 5G NR frame structure only supports time division duplexing (TDD) mode for mmWave transmission [57], for consistency, TDD is utilized for both UHF and mmWave transmission in this chapter. According to the LTE standard, the DL/UL configuration is semi-static, but in the actual LTE-TDD deployment, cells operating over the same frequency are set for the same DL/UL configuration. 5G NR standard supports the dynamic and flexible setting of the DL/UL configuration in a TDD mode, and adjacent cells at the same frequency can have similar or different DL/UL configuration. However, for simplicity, the static consistent DL/UL configuration is considered in this chapter so that cross-link interference [150] is avoided. The cell association and interference map of the proposed scheme is shown in Fig. 5.1, where the dotted lines refer to interference.

5.4 Energy-Efficiency Maximization

The EE of the GUEs and UAVs under the proposed scheme is optimized in this section. As per Fig. 5.1, the intra-cell interference can be ignored since all sub-carriers are orthogonal to each other in OFDM, but because of frequency reuse, inter-cell interference still exists. In the DL, the GUEs transmitting over the UHF band cause interference to each other (i.e. an interference-limited scenario). On the other hand, GUEs transmitting over the mmWave band also suffer from interference, but due to beamforming and the fact that mmWave signals are sensitive to blockage, the interference level is negligibly small (i.e. a noise-limited scenario [29, 41]). Moreover, the larger bandwidth of the mmWave signal necessitates a wider band receiving filter hence more noise passes through with the desired signal. In such a case, the noise power becomes more dominant than the interference and thus the SNR can be used as an approximation for the SINR; hence mmWave communication networks can be modeled as noise-limited systems [151, 152]. In the UL, all UAVs transmit over the mmWave band, while all GUEs transmit over the UHF band, and the interference relationship is quite similar to that in the DL. Due to the DUDe structure, the interference

between UAVs and GUEs is eliminated, which is quite different from the assumptions in most research. Taking the high mobility of UAVs into consideration, we propose a practical low complexity power allocation scheme which can optimize EE in the UL direction, while the DL scenario can be easily analogized. Specifically, we consider EE maximization at the GUEs (UHF band) and the UAVs (mmWave band) separately, subject to a minimum data rate and maximum transmission power requirements per UE.

5.4.1 GUEs Energy-Efficiency Maximization

The transmission data rate of GUE i to its serving BS m over RB n is written as

$$\mathbb{R}^G_{i,m,n}(\mathbf{P}) = B\log_2\left(1+\frac{\overbrace{P_{i,n}|h_{i,m,n}|^2}^{\gamma^G_{i,n}}}{\sum\limits_{j\in I^G, j\neq i} P_{j,n}|h_{j,m,n}|^2+\sigma^2}\right), \tag{5.6}$$

where $\gamma^G_{i,n}$ is the received SINR at the BS, I^G is the index set of GUEs over the UHF band, and $\mathbf{P}$ is the power allocation matrix of all GUEs over all RBs. Thus, the total rate of GUE i in the UL is obtained as

$$\mathbb{R}^G_i(\mathbf{P}) = \sum_{n\in\mathcal{N}_{UHF}} \mathbb{R}^G_{i,m,n}(\mathbf{P}). \tag{5.7}$$

Similarly, the total power consumption of GUE i is

$$\mathbb{P}^G_i = \sum_{n\in\mathcal{N}_{UHF}} P_{i,n}, \tag{5.8}$$

where $\mathcal{N}_{UHF}$ is the index set of UHF RBs. The transmitter is considered to be OFF when the UE is not allowed to transmit or during periods when the UE is not transmitting a sub-frame [153]. The GUEs energy-efficiency maximization (GUEs-EE-MAX) problem can be formulated as

GUEs-EE-MAX: (5.9)

$$\max_{\mathbf{P}} \quad \mathbb{EE}^G = \frac{\sum_{i\in I^G} \mathbb{R}_i^G(\mathbf{P})}{\sum_{i\in I^G} \mathbb{P}_i^G(\mathbf{P})} \tag{5.9a}$$

$$\text{s.t.} \quad \mathbb{R}_i^G(\mathbf{P}) \geq R_{\min}^G, \forall i \in I^G, \tag{5.9b}$$

$$\mathbb{P}_i^G \leq P_{\max}^G, \qquad \forall i \in I^G, \tag{5.9c}$$

$$P_{i,n} \geq 0, \qquad \forall i \in I^G, \forall n \in \mathcal{N}_{UHF}. \tag{5.9d}$$

where $R_{\min}^G$ and $P_{\max}^G$ are the minimum rate and maximum transmission power per GUE, respectively. In problem **GUEs-EE-MAX**, (5.9a) defines the EE objective function as the ratio of the GUEs sum-rate to the total power consumption. Constraint (5.9b) ensures that the total rate of each GUE satisfies the minimum rate requirement, while Constraint (5.9c) defines the maximum value of the total transmission power of each GUE. We assume that all the UEs have the same minimum rate and maximum transmission power requirements, but it can be easily extended to the scenario where different UEs have different requirements. Lastly, Constraint (5.9d) ensures the non-negativity of the transmission power of each GUE over each RB. The feasibility of problem **GUEs-EE-MAX** depends on the values of $R_{\min}^G$ and $P_{\max}^G$, where $R_{\min}^G$ is used to guarantee the data rate of each UE will not drop below the minimum requirement, when energy-efficiency is maximized. On the other hand, if $R_{\min}^G$ is too high, the power allocation scheme may not satisfy the minimum data rate of each UE, in which case problem **GUEs-EE-MAX** becomes infeasible. Thus, in our work, $R_{\min}^G$ is set according to the data rate that can be achieved via the fractional power control (FPC) scheme. The FPC scheme is applied in 4G and 5G cellular networks [79, 154], where the transmission power of GUE i on RB n is given by

$$P_{i,n} = \frac{1}{M} \min\{P_{\max}, 10\log_{10} M + wL + P_0\}, \tag{5.10}$$

in which $P_{\max}$ is the maximum transmission power per UE, M is the number of allocated RBs per UE, P_0 is the target received power, and $w \in \{0, 0.4, 0.5, 0.6, 0.7, 0.8, 0.9, 1\}$ is the compensation factor for path-loss L. Based on (5.10), the initial transmission power will not exceed $P_{\max}^G$. Thus, problem **GUEs-EE-MAX** is always feasible in our work.

Remark 4. *The rate function of each GUE is **non-convex** due to the interference terms, and thus the $\mathbb{EE}^G$ function is not necessarily **convex** [155]. Moreover, the constraints set is not convex due to the minimum rate constraint.*

To efficiently solve problem **GUEs-EE-MAX**, consider the following lower-bound

approximation [156]

$$\log_2(1+\gamma) \geq \alpha \log_2 \gamma + \beta, \tag{5.11}$$

where $\gamma, \bar{\gamma} \geq 0$, and the bound is tight for $\gamma = \bar{\gamma}$. Moreover,

$$\alpha = \frac{\bar{\gamma}}{1+\bar{\gamma}}, \text{ and } \beta = \log_2(1+\bar{\gamma}) - \alpha \log_2 \bar{\gamma}. \tag{5.12}$$

Thus, the lower-bounded objective function is obtained as in (5.13). Then, by adopting the transformation $Q_{i,n} = \log_2 P_{i,n}$, the lower-bounded EE function $\overline{\mathbb{EE}}^G(\mathbf{P})$ is rewritten as in (5.14).

$$\frac{\sum_{i\in I^G} \mathbb{R}_i^G(\mathbf{P})}{\sum_{i\in I^G} \mathbb{P}_i^G(\mathbf{P})} = \frac{\sum_{i\in I^G}\sum_{n\in\mathcal{N}_{UHF}} B\log_2\left(1+\gamma_{i,n}^G\right)}{\sum_{i\in I^G}\left(\sum_{n\in\mathcal{N}_{UHF}} P_{i,n}\right)} \geq \frac{\sum_{i\in I^G}\sum_{n\in\mathcal{N}_{UHF}} B\left(\alpha_{i,n}\log_2\left(\gamma_{i,n}^G\right)+\beta_{i,n}\right)}{\sum_{i\in I^G}\left(\sum_{n\in\mathcal{N}_{UHF}} P_{i,n}\right)} \triangleq \overline{\mathbb{EE}}^G(\mathbf{P}) \tag{5.13}$$

$$\begin{aligned}
\overline{\mathbb{EE}}^G(\mathbf{Q}) &= \frac{\sum_{i\in I^G}\sum_{n\in\mathcal{N}_{UHF}} B\left(\alpha_{i,n}\log_2\left(\frac{2^{Q_{i,n}}|h_{i,m,n}|^2}{\sum_{j\in I^G, j\neq i} 2^{Q_{j,n}}|h_{j,m,n}|^2+\sigma^2}\right)+\beta_{i,n}\right)}{\sum_{i\in I^G}\left(\sum_{n\in\mathcal{N}_{UHF}} 2^{Q_{i,n}}\right)} \\
&= \frac{\sum_{i\in I^G} \overbrace{\sum_{n\in\mathcal{N}_{UHF}} B\left(\alpha_{i,n}\left(Q_{i,n}+\log_2|h_{i,m,n}|^2-\log_2\left(\sum_{j\in I^G, j\neq i} 2^{Q_{j,n}}|h_{j,m,n}|^2+\sigma^2\right)\right)+\beta_{i,n}\right)}^{\overline{\mathbb{R}}_i^G(\mathbf{Q})}}{\underbrace{\sum_{i\in I^G}\left(\sum_{n\in\mathcal{N}_{UHF}} 2^{Q_{i,n}}\right)}_{\overline{\mathbb{P}}_i^G(\mathbf{Q})}} \\
&\triangleq \frac{\overline{\mathbb{R}}^G(\mathbf{Q})}{\overline{\mathbb{P}}^G(\mathbf{Q})}
\end{aligned} \tag{5.14}$$

Remark 5. *For each rate function $\overline{\mathbb{R}}_i^G(\mathbf{Q})$ in (5.14), the negative log-sum-exp term is concave in $\mathbf{Q}$ [155], and thus $\overline{\mathbb{R}}_i^G(\mathbf{Q})$ is concave, $\forall i \in I^G$. More importantly, the sum of the concave functions is also concave [157], and hence, the lower-bounded rate function $\overline{\mathbb{R}}^G(\mathbf{Q})$ is* ***concave*** *in $\mathbf{Q}$.*

Remark 6. *In (5.14), the total transmission power $\overline{\mathbb{P}}_i^G(\mathbf{Q})$ of each GUE $i \in I^G$ is convex in $\mathbf{Q}$, while implies that $\overline{\mathbb{P}}^G(\mathbf{Q})$ is also convex in $\mathbf{Q}$.*

Based on all the above, the *transformed* GUEs EE maximization problem is expressed as

T-GUEs-EE-MAX: (5.15)

$$\max_{\mathbf{Q}} \quad \overline{\mathbb{EE}}^{G} = \frac{\sum_{i\in I^G} \overline{\mathbb{R}}_i^G(\mathbf{Q})}{\sum_{i\in I^G} \overline{\mathbb{P}}_i^G(\mathbf{Q})} \tag{5.15a}$$

$$\text{s.t.} \quad \overline{\mathbb{R}}_i^G(\mathbf{Q}) \geq R_{\min}^G, \qquad \forall i \in I^G, \tag{5.15b}$$

$$\sum_{n\in\mathcal{N}_{UHF}} 2^{Q_{i,n}} \leq P_{\max}^G, \forall i \in I^G. \tag{5.15c}$$

Remark 7. *The constraints set of problem **T-GUEs-EE-MAX** can be verified to be **convex** in* $\mathbf{Q}$.

Based on **Remarks 5**, **6** and **7**, the transformed lower-bounded EE function $\overline{\mathbb{EE}}^{G}(\mathbf{Q})$ is a ratio of a concave function to a convex function in $\mathbf{Q}$, with a convex constraints set. Particularly, problem **T-GUEs-EE-MAX** takes the form of a **concave-convex** fractional programming problem [155], and thus can be **globally optimally** solved via the Dinkelbach's algorithm [158]. Particularly, define the auxiliary function

$$\mathbb{F}^G(\lambda) \triangleq \max_{\mathbf{Q}} \left\{ \overline{\mathbb{R}}^G(\mathbf{Q}) - \lambda \overline{\mathbb{P}}^G(\mathbf{Q}) \right\}, \tag{5.16}$$

for $\lambda \geq 0$, which is the unique maximizer of $\mathbb{F}^G(\lambda)$, for fixed values of $\alpha_{i,n}$ and $\beta_{i,n}$, $\forall i \in I^G$ and $\forall n \in \mathcal{N}_{UHF}$ [159]. Hence, problem **T-GUEs-EE-MAX** is solved via the algorithm outlined in **Algorithm 6**.

Algorithm 5 Dinkelbach's Algorithm

1: **Initialization:** Set error tolerance $\varepsilon \in (0,1)$, iteration index $\ell = 0$, and $\lambda^{(0)} = 0$.
2: **repeat**
3: Compute $\mathbf{Q}^{(\ell)} = \arg\max_{\mathbf{Q}} \left\{ \overline{\mathbb{R}}^G(\mathbf{Q}) - \lambda^{(\ell)} \overline{\mathbb{P}}^G(\mathbf{Q}) \right\}$;
4: Calculate $\mathbb{F}^G\left(\lambda^{(\ell)}\right) = \overline{\mathbb{R}}^G\left(\mathbf{Q}^{(\ell)}\right) - \lambda^{(\ell)} \overline{\mathbb{P}}^G\left(\mathbf{Q}^{(\ell)}\right)$;
5: Update $\lambda^{(\ell+1)} = \frac{\overline{\mathbb{R}}^G\left(\mathbf{Q}^{(\ell)}\right)}{\overline{\mathbb{P}}^G\left(\mathbf{Q}^{(\ell)}\right)}$;
6: Set $\ell = \ell + 1$;
7: **until** $\left|\mathbb{F}^G\left(\lambda^{(\ell)}\right)\right| \leq \varepsilon$.
8: **Output:** $\hat{\mathbf{Q}} \triangleq \mathbf{Q}^{\star}$.

Algorithm 6 Solution of Problem **T-GUEs-EE-MAX**

1: **Initialization:** Set error tolerance $\varepsilon \in (0,1)$, iteration index $\ell = 0$, $\alpha_{i,n} = 1$, $\beta_{i,n} = 0$, $\forall i \in I^G$ and $\forall n \in \mathcal{N}_{UHF}$, select a feasible $\hat{\mathbf{P}}^{(0)}$, and calculate $\widehat{\mathbb{EE}}^G\left(\hat{\mathbf{P}}^{(0)}\right)$.
2: **repeat**
3: Set $\ell = \ell + 1$;
4: Update $\alpha_{i,n}^{(\ell)}$ and $\beta_{i,n}^{(\ell)}$ by (10), $\forall i \in I^G$, and $\forall n \in \mathcal{N}_{UHF}$;
5: Compute $\hat{\mathbf{Q}}^{(\ell)}$ by solving problem **T-GUEs-EE-MAX** via **Algorithm 5**;
6: Set $\hat{\mathbf{P}}^{(\ell)} = 2^{\hat{\mathbf{Q}}^{(\ell)}}$
7: Evaluate $\widehat{\mathbb{EE}}^G\left(\hat{\mathbf{P}}^{(\ell)}\right)$;
8: **until** $\left|\widehat{\mathbb{EE}}^G\left(\hat{\mathbf{P}}^{(\ell)}\right) - \widehat{\mathbb{EE}}^G\left(\hat{\mathbf{P}}^{(\ell-1)}\right)\right| \leq \varepsilon$.
9: **Output:** $\mathbf{P}^\star$

Lemma 1. ***Algorithm 5*** *monotonically converges to the global optimal solution* $\hat{\mathbf{Q}}$ *of problem* ***T-GUEs-EE-MAX***[4].

Proof: Refer to Appendix A.1.

After that, the obtained solution is transformed into its original form as $\hat{\mathbf{P}} = 2^{\hat{\mathbf{Q}}}$, and hence the value of the original objective function in (5.9a) is calculated as

$$\widehat{\mathbb{EE}}^G\left(\hat{\mathbf{P}}\right) = \frac{\sum_{i \in I^G} \mathbb{R}_i^G\left(\hat{\mathbf{P}}\right)}{\sum_{i \in I^G} \mathbb{P}_i^G\left(\hat{\mathbf{P}}\right)}, \tag{5.17}$$

which is based on fixed values of $\alpha_{i,n}$ and $\beta_{i,n}$. Additionally, $\hat{\mathbf{Q}}$ is obtained from **Algorithm 5** based on a lower-bounded objective function. Hence, to obtain the solution of problem **GUEs-EE-MAX**, $\alpha_{i,n}$ and $\beta_{i,n}$ must be repeatedly updated $\forall i \in I^G$ and $\forall n \in \mathcal{N}_{UHF}$, while solving problem **T-GUEs-EE-MAX** via **Algorithm 5**, as shown in Algorithm 6.

Lemma 2. ***Algorithm 6*** *converges in a finite number of iterations to the global optimal solution* $\mathbf{P}^\star$ *of problem* ***GUEs-EE-MAX****.*

Proof: Refer to Appendix A.2.

5.4.2 UAVs Energy-Efficiency Maximization

Different from GUE communications, UAV communications can be seen as noise-limited [29, 41]. Thus, the transmission data rate between UAV $i \in I^A$ and its serving

[4] **Algorithm 5** has a linear convergence rate and polynomial-time complexity [160].

BS m on RB n is given by[5]

$$\mathbb{R}^A_{i,m,n}(P_{i,n}) = B\log_2\left(1+\frac{P_{i,n}G_{i,m}|h_{i,m,n}|^2}{\sigma^2}\right), \tag{5.18}$$

where I^A is the index set of UAVs transmitting over the mmWave band. In turn, the total data rate of UAV i in the UL is determined as

$$\mathbb{R}^A_i(\mathbf{P}) = \sum_{n\in\mathcal{N}_{mmW}} \mathbb{R}^A_{i,m,n}(P_{i,n}), \tag{5.19}$$

where $\mathcal{N}_{mmW}$ is the index set of mmWave RBs.

Remark 8. *The data rate function $\mathbb{R}^A_{i,n}(P_{i,n})$ is **concave** in $P_{i,n}$, and hence the sum-rate function $\mathbb{R}^A_i$ is a sum of concave functions, and thus is also **concave** in $\mathbf{P}$ [157].*

The total power consumption of UAV i is given by

$$\mathbb{P}^A_i = \sum_{n\in\mathcal{N}_{mmW}} P_{i,n}. \tag{5.20}$$

Hence, the UAVs energy-efficiency maximization (UAVs-EE-MAX) problem is expressed as

UAVs-EE-MAX: (5.21)

$$\max_{\mathbf{P}} \quad \mathbb{EE}^A = \frac{\mathbb{R}^A(\mathbf{P})}{\mathbb{P}^A(\mathbf{P})} \tag{5.21a}$$

$$\text{s.t.} \quad \mathbb{R}^A_i(\mathbf{P}) \geq R^A_{\min}, \forall i \in I^A, \tag{5.21b}$$

$$\mathbb{P}^A_i \leq P^A_{\max}, \qquad \forall i \in I^A, \tag{5.21c}$$

$$P_{i,n} \geq 0, \qquad \forall i \in I^G, \forall n \in \mathcal{N}_{mmW}. \tag{5.21d}$$

where $R^A_{\min}$ and $P^A_{\max}$ are the minimum rate and maximum transmission power per UAV, respectively[6].

[5]Recall that all UAVs transmit over the mmWave band, and beamforming is applied, and thus inter-cell interference can be neglected [29, 41].

[6]In a similar manner to problem **GUEs-EE-MAX**, the feasibility of problem **UAVs-EE-MAX** can be guaranteed. In the simulations, this has been achieved by setting the initial transmission power of each UE as that of the FPC scheme.

Remark 9. *The objective function* $\mathbb{EE}^A(\mathbf{P})$ *is a ratio of a* ***concave*** *function* $\mathbb{R}^A(\mathbf{P})$ *to a linear function in* $\mathbf{P}$.

Based on **Remark 9**, problem **UAVs-EE-MAX** takes the form of a **concave-linear fractional programming problem** [155]. More importantly, each stationary point of the objective function $\mathbb{EE}^A(\mathbf{P})$ is the global maximizer [155]. Therefore, define the auxiliary function

$$\mathbb{F}^A(\lambda) \triangleq \max_{\mathbf{P}} \left\{ \mathbb{R}^A(\mathbf{P}) - \lambda \mathbb{P}^A(\mathbf{P}) \right\}. \tag{5.22}$$

Hence, problem **UAVs-EE-MAX** can be globally optimally solved via **Algorithm 5**, but by replacing $\overline{\mathbb{R}}^G(\mathbf{Q})$, $\overline{\mathbb{P}}(\mathbf{Q})$, and $\mathbb{F}^G(\lambda)$ by $\mathbb{R}(\mathbf{P})$, $\mathbb{P}(\mathbf{P})$, and $\mathbb{F}^A(\lambda)$, respectively[7].

5.4.3 Computational Complexity

The computational-complexity of the Dinkelbach-based algorithm (i.e. **Algorithm 5**) with stopping criteria ε is $O\left(\frac{1}{\varepsilon^2}\log(K)\right)$, where K is the number of terminals (i.e. $K = |I^G|$) [158]. In **Algorithm 6**, a concave optimization problem is solved in each iteration via **Algorithm 5**, and hence **Algorithm 6** has polynomial time-complexity, then the overall complexity of **Algorithm 6** is $O\left(\left(\frac{1}{\varepsilon^2}\log(|I^G|)\right)^2\right)$. Since problem UAVs-EE-MAX is solved via **Algorithm 5**, its computational complexity is $O\left(\frac{1}{\varepsilon^2}\log(|I^A|)\right)$. For comparison, Table 5.3 gives the complexities of some other optimal power allocation schemes in similar scenarios. It is evident that the complexity of our proposed scheme is relatively lower than the other schemes.

Table 5.3: Complexity of Different Schemes

Paper	Complexity
[161]	$O(MN)$, where M is the number of UEs, N is the number of time-slots.
[162]	$O(FKM)$, where F is the number of resource blocks, K is the number of vehicle to vehicle links, M is the number of vehicle to UAV links.
[163]	$O(NMK)$, where N is the number of smart devices, M is the number of UAVs and K is the number of subchannels.

[7]The proof of **Lemma 1** of problem **T-GUEs-EE-MAX** is tenable to problem **UAVs-EE-MAX**, and thus is not provided to avoid unnecessary repetition.

5.5 Performance Evaluation

In this section, the performance of the GUEs and UAVs under the proposed DUDe access scheme is evaluated and compared with benchmark schemes in terms of energy-efficiency, sum-rate, and data rate per UE. In the simulations, the total DL and UL transmission time is assumed to be the same. Considering the current UAV regulations [13], we set the altitude of UAVs to be 50-200 meters[8]. As the data rate of the UAV CNPC links is limited, and will not cause any interference to other links, it is ignored in the simulations for simplicity. As for benchmarks, we consider both UAVs and DUEs transmitting over the UHF or mmWave band, with access according to the CUDA (coupled) scheme. In the UL, fractional power control (FPC) is applied. In the DL, the transmission power is uniformly distributed over the whole bandwidth. The transmission parameters of the different schemes are given in Table 5.4.

Table 5.4: Simulation Parameters

Parameters	GUE	UAV	MCell	SCell
Maximum transmission power	23 dBm	23 dBm	46 dBm	30 dBm
Downlink/Uplink bias	N/A	N/A	0/0 dB	3/0 dB
Spatial distribution	Uniform distribution			
Altitude of UAVs	50-200 m			
S-curve parameters	$a = 9.6$, $b = 0.28$ [144, 146]			
Blockage ball model parameters	$\mu = 200$ m, $\omega = 0.2$ [77]			
Spatial density	250 per km^2	50 per km^2	5 per km^2	20 per km^2
Path-loss exponent	UHF: GUE-UAV 2, GUE-BS 3, $d_0 = 1$ m [148]; mmWave: LOS 2.55, NLOS 5.76, $d_0 = 5$ m [29, 164]			
Lognormal shadowing	UHF: $\mu = 0$, $\sigma = 4$ dB [148]; mmWave: LOS $\mu = 0$, $\sigma = 8.66$ dB, NLOS $\mu = 0$, $\sigma = 9.02$ dB [29]			
Nakagami-m parameters	$m_L = 3$, $m_N = 2$ [144, 147]			
Operating frequency	2 GHz & 28 GHz	28 GHz	2 GHz & 28 GHz	2 GHz & 28 GHz
Bandwidth	UHF: 20 MHz; mmWave: 200 MHz [84]			
Subcarrier spacing	UHF: 15 kHz; mmWave: 60 kHz [84]			
Power control	FPC with $p_0 = -85$ dBm, and $\alpha = 0.8$ [55], fixed power consumption $\rho^G = \rho^A = -50$ dBm [153]			
Noise spectral density	-174 dbm/Hz			

5.5.1 Proposed DUDe Access Scheme Simulations

Fig. 5.2 depicts the 10^{th}, 20^{th}, 50^{th}, 80^{th}, and 90^{th} percentile data rate per UE in the DL and UL. A percentile indicates the value below which a given percentage of observations falls [86]. For example, the 10^{th} percentile is the value (or score) below which 10% of the observations may be found. The 10^{th} percentile data rate of mmWave UEs in the UL is around 1.6×10^8 bps, which means, 10% of mmWave UEs' UL data rates are below 1.6×10^8 bps. It can be seen that the decoupled scheme can achieve several times higher data rates in both the UL and DL than its coupled counterparts.

[8] 3GPP identified that cellular networks should cater for UAVs flying between ground level and 300 meters [13, 55].

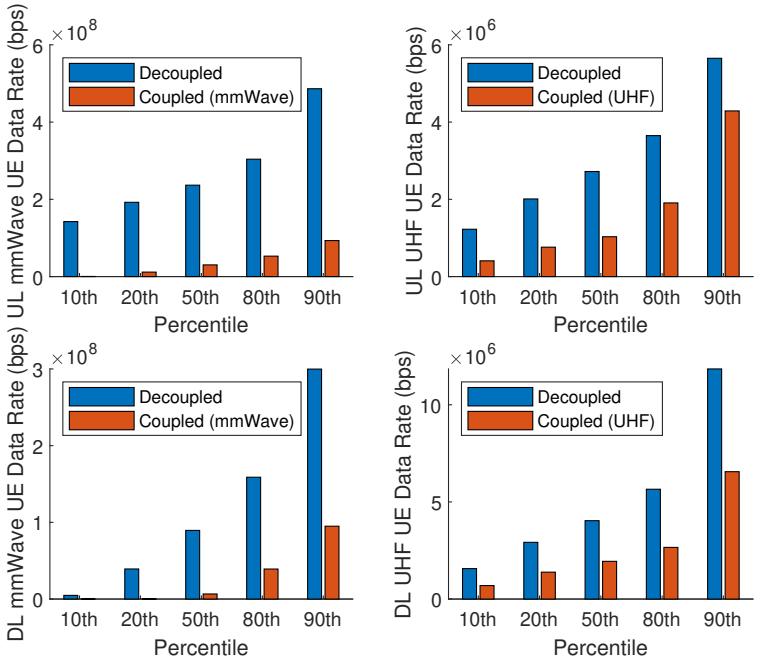

Figure 5.2: 10^{th}, 20^{th}, 50^{th}, 80^{th}, and 90^{th} percentile data rate per mmWave link and UHF link in the UL and DL.

This is partly because the decoupled scheme occupies wider bandwidth (as shown in Table 5.2), but it is worth noting that the bandwidth of the decoupled scheme is only 10% wider than the mmWave coupled scheme. The huge rate gap between the decoupled and coupled mmWave schemes is due to the DUDe access. According to the DUDe scheme, the mmWave band is monopolized by UAVs in the UL and LOS GUEs in the DL. For comparison, according to the mmWave coupled scheme, the mmWave band is shared by the GUEs and UAVs in the UL, and NLOS and LOS GUEs in the DL. In this case, the DUDe scheme can make better use of the mmWave band and provide higher data rates. Besides, DUDe also shortens the UE-BS distance in the UL, which increases the received signal strength and thus improves the SINR. It can also be seen that, due to the wider bandwidth, the mmWave band can provide high data rate for LOS links. Although mmWave signals suffer from high path-loss, it can be compensated for by beamforming. As such, the interference among the UAVs is very low and can be seen as noise-limited.

Fig. 5.3 illustrates the impact of the UAV altitude on the UL sum-rate and EE, where—for instance—50/80 refers to the altitude range 50-80 m. As for the coupled mmWave and UHF schemes, the sum-rate and EE of UAVs decreases when the altitude increases, which is due to the increase in path-loss. However, for the decoupled

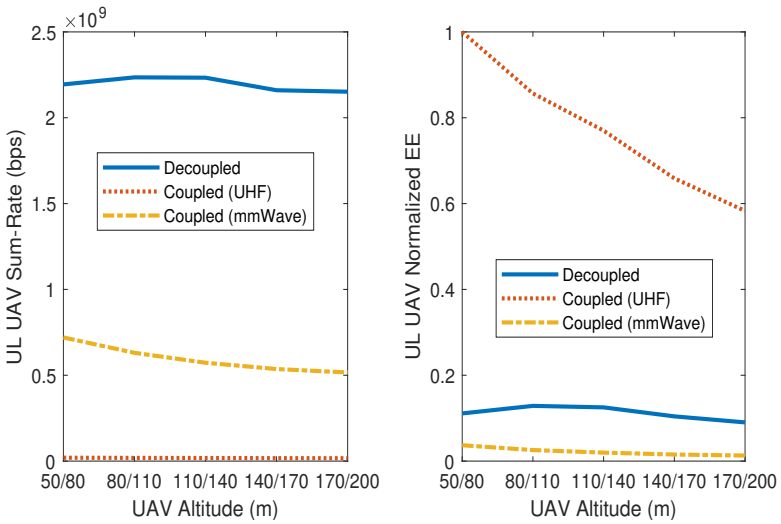

Figure 5.3: UL UAV sum-rate and normalized EE vs. UAV altitude.

scheme, the sum-rate and EE slightly increase at first as the LOS probability increases with altitude. Although the path-loss also increases, since many UAVs are associated with nearby SCells (while more UAVs are associated with MCells in the coupled schemes), and thus the impact of path-loss does not surpass the impact of LOS probability. It can also be seen that the EE of the coupled UHF scheme is higher than that of the coupled mmWave scheme and the decoupled mmWave/UHF hybrid scheme. This is because, in contrast to the coupled benchmark which uses UHF, our decoupled scheme uses mmWave frequency for the UAVs, which has higher sensitivity to path-loss as opposed to UHF frequencies. It is also important highlight that while the coupled technique provides 10 times better EE in this case (as shown in Fig. 5.3 (b), our decoupled technique provides over 100 times better sum-rate, as can be seen from Fig. 5.3 (a). To further elaborate, when comparing the GUE performances, as shown in Fig. 5, in which case both our decoupled technique and the coupled counterparts use UHF frequencies, our proposed technique is superior in terms of sum-rate and EE.

Fig. 5.4 shows the relationship between the number of UAVs/GUEs and UL and DL sum-rates, where 2/10 refers to 2 UAVs and 10 GUEs, and there are 1 MBS and 4 SBSs here. The UL sum-rate of the coupled mmWave scheme is the highest at first, then it is exceeded by the sum-rate of the decoupled scheme. This is because, for the decoupled scheme, only the UAVs transmit over the mmWave band in the UL, while the GUEs transmit over UHF band. Moreover, when the number of BSs is greater than the number of UAVs, the mmWave resource cannot be not fully utilized; whereas for the coupled mmWave scheme, both GUEs and UAVs transmit over the mmWave band

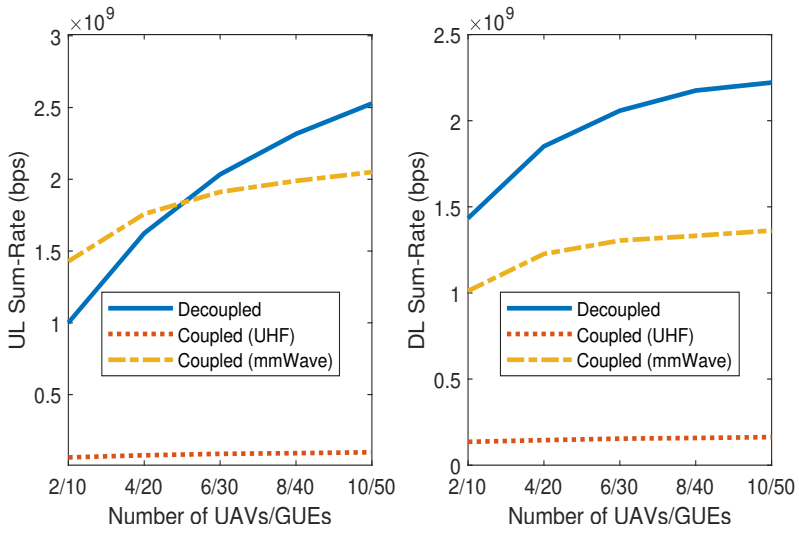

Figure 5.4: Network sum-rate in the UL and DL vs. number of UAVs/GUEs.

hence can achieve better spectral utilisation. This is corroborated by the results when the number of UAVs for the decoupled case exceeds the number of base-stations it becomes superior to the coupled counterpart. As for the DL, although there are more UEs, most of them are associated with MCells, and some BSs are not activated at first, and so the DL network sum-rate increases with the increase in the number of UEs.

5.5.2 Energy-Efficiency Maximization

In this subsection, the performance of the proposed optimal (OPT) EE-maximizing power allocation is compared to that of FPC. Fig. 5.5 compares the UL GUE sum-rate and normalized EE of the proposed decoupled access scheme to the coupled UHF scheme, both of which use the UHF band for GUE UL transmission. It can be seen that the proposed OPT power allocation scheme can achieve around 15% higher GUE sum-rate and twice higher EE than the FPC scheme. Furthermore, the performance of the coupled schemes is worse than that of the corresponding decoupled scheme. This is because in the decoupled schemes, the UHF band is monopolized by GUEs in the UL, while in the coupled UHF scheme, it is shared by the GUEs and UAVs. Moreover, DUDe shortens the UE-BS distance, and hence improves the SINR.

Fig. 5.6 is similar to Fig. 5.5 except it compares the UL UAV performance. It can be seen that the OPT power allocation scheme achieves much higher EE than the FPC scheme. However, since the UAVs utilize the mmWave band in the decoupled schemes, the transmission is noise-limited rather than interference-limited, and the

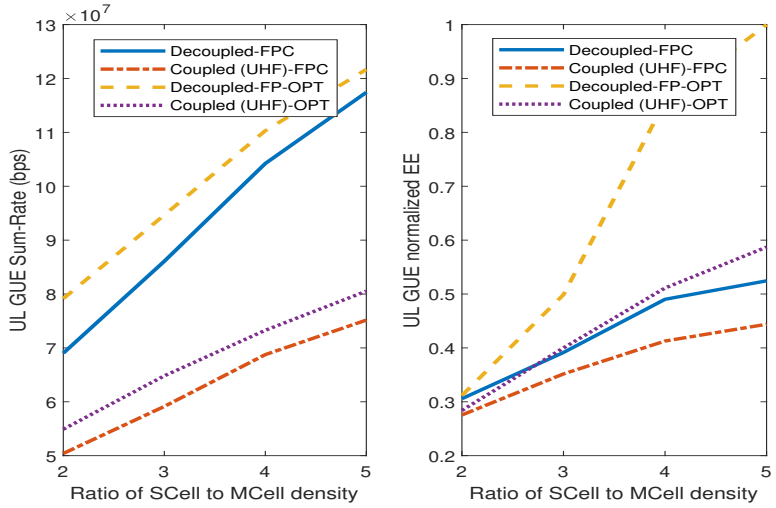

Figure 5.5: UL GUE sum-rate and normalized EE vs. ratio of SCell density to MCell density.

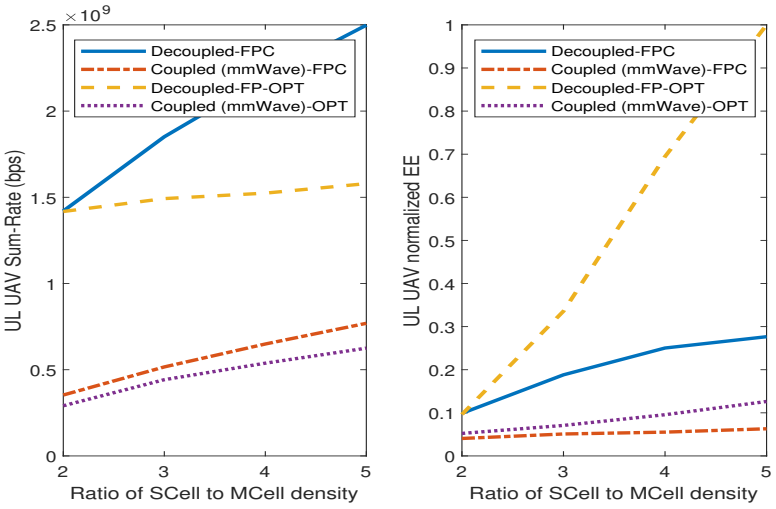

Figure 5.6: UL UAV sum-rate and normalized EE vs. ratio of SCell density to MCell density.

optimal transmission power that maximizes the UAVs' EE is much lower than that of the GUEs transmission. The OPT power allocation scheme cannot attain high sum-rate and EE simultaneously. Nonetheless, similar to Fig. 5, the performance of the decoupled schemes is superior to the corresponding coupled schemes.

Fig. 5.7 illustrates the 10^{th}, 20^{th}, 50^{th}, 80^{th}, and 90^{th} percentile data rate per GUE and UAV in the UL, where the ratio of SCell density to MCell density is 4. The UAV data rate shows a relatively average distribution; however, the GUE data rate distribution is more uneven. This is because the OPT power allocation scheme tends to allocate more power to those UEs with higher channel condition and/or lower path-loss. Due to the minimum data rate constraint, the two power allocation schemes achieve similar 10^{th} percentile data rate per UAV, while the 90^{th} percentile data rate of the OPT power allocation scheme is lower than the FPC scheme. This validates the conclusions in Fig. 5.6 in another way.

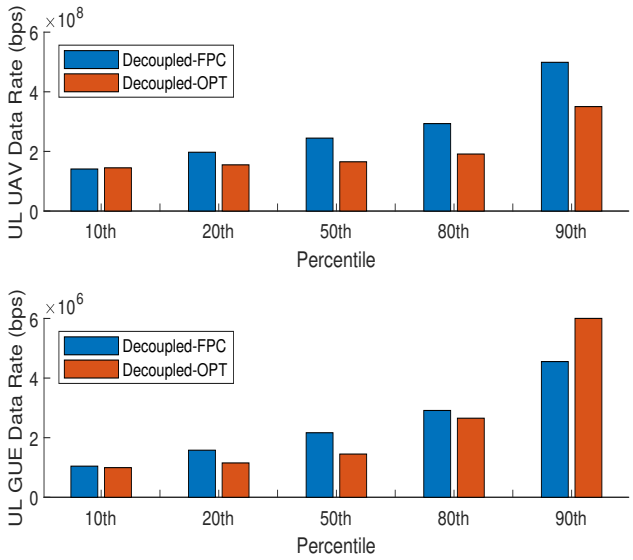

Figure 5.7: 10^{th}, 20^{th}, 50^{th}, 80^{th}, and 90^{th} percentile data rate per UAV and GUE in the UL.

5.6 Summary

A new access scheme in heterogeneous cellular networks with UAVs has been proposed in this chapter. Particularly, to meet the different requirements of UAV data links and CNPC links, as well as GUE uplinks and downlinks, we separate the UAV CNPC links from the high-capacity data communication links, and separate the GUE uplinks

from the downlinks. All the CNPC signals are connected to the GCSs operating in the L/C band, while the data signals are communicated to cellular BSs via the mmWave band. To further reduce interference between the UAVs and GUEs, the GUE downlinks and uplinks are also decoupled in terms of operating frequency and serving BS. The results demonstrated that the proposed access scheme can achieve several times higher sum-rates in both UL and DL than its coupled counterparts. Furthermore, an optimal power allocation algorithm has been devised to optimize the EE of the DUDe scheme, and shown to achieve 15% higher GUE sum-rate and twice higher GUE EE than the conventional fractional power control scheme. Finally, it was shown that for noise-limited UAV communications, there is a trade-off between sum-rate and EE as simultaneously maximizing both is unattainable.

Chapter 6

Q-Learning and DQL based Power Control for UAVs

6.1 Introduction

This chapter solve the same EE optimization problem as in Section 5.4, but use reinforcement learning methods. Due to the rapid changes in the UAV wireless environment, such as air-to-ground channels, spatial and time variations of non-stationary signal behaviour, and detection of UAVs via UAVs-enabled protocols, conventional optimization methods with ideal assumptions (e.g. perfect CSI) may not work in practical and real-time applications. Hence, it is necessary to augment classical algorithms and solutions with artificial intelligence (AI) and machine learning (ML)-based techniques [165]. Moreover, when both UAVs and GUEs transmission resources are optimized, the network access schemes can be designed to overcome the classical methods' excessive overhead and delays, while incorporating ML techniques to achieve an acceptable/sub-optimal EE solution in rapidly changing wireless environments.

Reinforcement learning (RL) algorithms are among the most promising ML techniques to use in radio resource management (RRM) for UAV-enabled cellular communications [166]. This is due to the nature of RL, which is based on maximizing a reward function by exploring the action(s) domain—via trial-and-error interactions—to allow the learner to discover the best choices based on the received rewards [167]. In turn, RL has become a base for resource allocation in wireless networks, due to its simplicity and ability to provide reliable and efficient learning through interaction with the network. Q-learning (QL) is a model-free RL approach, which is based on finite

states and actions to obtain acceptable/near-optimal solutions with low computational-complexity [168]. However, in QL, the sizes of the state and action spaces grow exponentially for each additional unknown network feature and/or parameter, leading to the curse of dimensionality, especially in the training phase. Alternatively, deep Q-learning (DQL) has been proposed, which utilizes a deep neural network (DNN), called deep Q-network (DQN) along with other techniques (e.g. replay memory) to perform a stable and efficient training, and reliably estimate the Q-function [169]. Particularly, DQL is based on quickly performing predictions using only a small number of simple operations to obtain an output, which greatly reduces execution time. Consequently, deep RL approaches have found numerous applications in cellular networks [170–172]. Add to this the 3GPP technical requirements for the enhancement of UAVs [173], which only proposes AI/ML to control the UAVs, but did not discuss how AI/ML can be used in the scheduling and resource allocation. This motivates us to investigate the potentials of AI/ML techniques in cellular-enabled UAVs by applying QL and DQL as resource allocation tools.

6.1.1 Related Works

Recently, a number of research works have proposed learning-based resource allocation for cellular-enabled UAV networks [171]. For instance, in [174], an interference management scheme is proposed with the aim of achieving a tradeoff between maximizing EE and minimizing wireless latency and interference to the ground network. Specifically, a DQL algorithm based on echo state network (ESN) cells is devised to allow each UAV to map each observation of the network state to an action, and hence learn its optimal path, transmission power and cell association. The proposed algorithm has been shown to minimize the interference to the GUEs and the transmission delay of the UAVs. A 3D energy-efficient and fair UAV scheduling scheme based on deep RL (DRL) is proposed in [175] to allow the UAVs to hover around and serve the users, and also recharge their batteries. The proposed algorithm has been shown to outperform existing scheduling algorithms in terms of coverage, energy-efficiency and fairness. In [176], a novel DRL-based control algorithm is devised for energy-efficient coverage and connectivity, which is demonstrated to outperform baseline schemes in terms of coverage, fairness and energy consumption. In [177] and [178], the proposed QL- and DRL-based methods have been applied to UAV-BSs with energy constraints to achieve energy-efficiency and coverage fairness to the GUEs, while reducing the collision incidents and co-channel interference (CCI). To the best of our knowledge,

none of the prior works in the literature have considered decoupled access in cellular-enabled UAVs with RL-based power control for energy-efficiency maximization.

6.1.2 Main Contributions

The main contributions of this chapter can be summarized as follows:

- A novel and simple QL algorithm is proposed for EE-maximizing power control, while alleviating the excessive computational delays of the classical fractional programming and successive convex approximation solutions. This algorithm has outperformed the benchmark schemes in terms of EE.

- A novel DQL algorithm is proposed to optimize the EE and overcome the large state-action matrix in the QL algorithm. Although the DQL performance is slightly worse than the QL, it outperforms the conventional fractional power control (FPC) scheme.

- The performance of the proposed DUDe QL and DQL power control schemes are compared with state-of-art alternatives in terms of EE, sum-rate and data rate per UE. It is demonstrated that the proposed DUDe can achieve several times higher sum-rates and EE than the coupled benchmark counterparts. The QL (DQL) power control scheme improves EE by around 100% (70%) for the UHF band, and by around 160% (130%) for the mmWave band, in comparison to conventional FPC scheme.

6.1.3 Organization

The rest of this chapter is organized as follows. Section 6.2 outlines the QL and DQL algorithms for EE maximization, while Section 6.3 discusses their implementation. Section 6.4 evaluates the performance of the proposed QL and DQL power control schemes, and compares them with several benchmarks. Finally, Section 6.5 draws the conclusions.

The System Model in this chapter is the same as in Section 5.2, and the EE optimization problem is based on the DUDe access scheme proposed in Section 5.3.

6.2 RL-Based Optimization of Energy-Efficiency

6.2.1 Q-Learning (QL)

In this work, the power control is centralized, and the QL agent is assumed to be located at the MBS, where the learning process is modeled as a Markov decision process (MDP). Now, let $\mathcal{S}$ be the set of possible transmission power states over the assigned RBs, and $\mathcal{A}(\mathbf{s})$ be the discrete set of actions in terms of the transmission powers over the assigned RBs in state $\mathbf{s}$. Assuming discrete time-steps t resembling the training rounds, the QL agent takes $\mathbf{a}^{(t)} \in \mathcal{A}\left(\mathbf{s}^{(t)}\right)$ based on some policy ϕ. Particularly, $\phi(\mathbf{s},\mathbf{a})$ represents the probability of taking action vector $\mathbf{a}$ in state $\mathbf{s}$[1]. By applying $\mathbf{a}^{(t)} \in \mathcal{A}\left(\mathbf{s}^{(t)}\right)$ and transitioning from state $\mathbf{s}^{(t)}$ to $\mathbf{s}^{(t+1)}$, a reward $r^{(t+1)} \triangleq \left(\mathbf{s}^{(t)},\mathbf{a}^{(t)}\right)$ is given to characterize the benefit from taking action vector $\mathbf{a}^{(t)}$ in state $\mathbf{s}^{(t)}$. The well-known QL algorithm aims to find the optimal policy ϕ^* that maximizes an expected reward function. Thus, let the future cumulative discounted reward at time-step t be given by [179]

$$\mathcal{R}^{(t)} = \sum_{\tau=0}^{\infty} \delta^{\tau} r^{(t+\tau+1)}, \tag{6.1}$$

where $\delta \in [0,1)$ is the discount factor for future rewards. Also, let the Q-function associated with policy ϕ as the expected reward when $\mathbf{a}$ is taken in state $\mathbf{s}$, as

$$Q_{\phi}(\mathbf{s},\mathbf{a}) = \mathbb{E}\left[\mathcal{R}^{(t)} | \mathbf{s}^{(t)} = \mathbf{s}, \mathbf{a}^{(t)} = \mathbf{a}\right], \tag{6.2}$$

which satisfies the Bellman optimality equation as [180]

$$\begin{aligned} &Q_{\phi}(\mathbf{s},\mathbf{a}) = \\ &\mathcal{R}(\mathbf{s},\mathbf{a}) + \delta \sum_{\mathbf{s}' \in \mathcal{S}} \mathcal{P}^{\mathbf{a}}_{\mathbf{s},\mathbf{s}'} \left(\sum_{\mathbf{a}' \in \mathcal{A}(\mathbf{s}')} \phi\left(\mathbf{s}',\mathbf{a}'\right) Q_{\phi}\left(\mathbf{s}',\mathbf{a}'\right) \right), \end{aligned} \tag{6.3}$$

with $\mathcal{R}(\mathbf{s},\mathbf{a}) = \mathbb{E}\left[r^{(t+1)} | \mathbf{s}^{(t)} = \mathbf{s}, \mathbf{a}^{(t)} = \mathbf{a}\right]$ being the expected reward of $(\mathbf{s},\mathbf{a}) \in \mathcal{S} \times \mathcal{A}$. Moreover, $\mathcal{P}^{\mathbf{a}}_{\mathbf{s},\mathbf{s}'} = \Pr\left(\mathbf{s}^{(t+1)} = \mathbf{s}' | \mathbf{s}^{(t)} = \mathbf{s}, \mathbf{a}^{(t)} = \mathbf{a}\right)$ represents the transition probability from state $\mathbf{s}$ to state $\mathbf{s}'$ upon applying $\mathbf{a}$. In turn, the optimal Q-function associated with ϕ^* is obtained as

[1] It should be noted that both $\mathbf{s}$ and $\mathbf{a}$ are of dimension $1 \times N$, where N is the number of the reused RBs in the system.

$$Q_{\phi^*}(\mathbf{s},\mathbf{a}) = \mathcal{R}(\mathbf{s},\mathbf{a}) + \delta \sum_{\mathbf{s}' \in \mathcal{S}} \mathcal{P}^{\mathbf{a}}_{\mathbf{s},\mathbf{s}'} \max_{\mathbf{a}'} Q_{\phi^*}\left(\mathbf{s}',\mathbf{a}'\right). \tag{6.4}$$

The QL agent assigned a Q matrix for each UE in the network, denoted $\mathbf{Q}(\mathbf{s},\mathbf{a})$, which serves as a lookup table for each action-value combination. Moreover, the QL algorithm updates each entry in the $\mathbf{Q}$ matrix in each time-step t as

$$\begin{aligned}\mathbf{Q}\left(\mathbf{s}^{(t)},\mathbf{a}^{(t)}\right) \leftarrow (1-\eta)\mathbf{Q}\left(\mathbf{s}^{(t)},\mathbf{a}^{(t)}\right) \\ +\eta\left(r^{(t+1)} + \delta \max_{\mathbf{a}} \mathbf{Q}\left(\mathbf{s}^{(t+1)},\mathbf{a}\right)\right),\end{aligned} \tag{6.5}$$

where $0 < \eta \leq 1$ is the learning rate to control the speed of reaching a solution. To avoid being stuck at non-optimal policies and to deal with the exploitation versus exploration tradeoff issue [181], the ε-greedy policy is used for each time-step t, which implies that the QL agent takes action $\mathbf{a}^*$ that maximizes the Q-function with probability $1-\varepsilon+\frac{\varepsilon}{|\mathcal{A}(\mathbf{s})|}$ for exploitation, and a random action with probability $\varepsilon+\frac{\varepsilon}{|\mathcal{A}(\mathbf{s})|}$ for exploration [181].

Algorithm 7 Q-Learning

1: **Initialization:** $\mathbf{Q}(\mathbf{s},\mathbf{a})$ with zero values, δ, η, and ε.
2: **for** each time-step t **do**
3: For the current state $\mathbf{s}^{(t)}$, pick the action vector $\mathbf{a}^{(t)}$ using the ε-greedy policy, as

$$\mathbf{a}^{(t)} \leftarrow \begin{cases} \arg\max_{\mathbf{a}} \mathbf{Q}\left(\mathbf{s}^{(t+1)},\mathbf{a}\right), & \text{with prob. } 1-\varepsilon+\frac{\varepsilon}{|\mathcal{A}(\mathbf{s}^{(t)})|}, \\ \text{a random action vector}, & \text{with prob. } \varepsilon+\frac{\varepsilon}{|\mathcal{A}(\mathbf{s}^{(t)})|}. \end{cases}$$

4: Perform action $\mathbf{a}^{(t)}$, obtain reward $r^{(t+1)} = r\left(\mathbf{s}^{(t)},\mathbf{a}^{(t)}\right)$ and observe the new state $\mathbf{s}^{(t+1)}$.
5: Update $\mathbf{Q}\left(\mathbf{s}^{(t)},\mathbf{a}^{(t)}\right)$ as

$$\begin{aligned}\mathbf{Q}\left(\mathbf{s}^{(t)},\mathbf{a}^{(t)}\right) \leftarrow (1-\eta)\mathbf{Q}\left(\mathbf{s}^{(t)},\mathbf{a}^{(t)}\right) \\ +\eta\left(r^{(t+1)} + \delta \max_{\mathbf{a}} \mathbf{Q}\left(\mathbf{s}^{(t+1)},\mathbf{a}\right)\right).\end{aligned}$$

6: Set $t \leftarrow t+1$ and current state $\mathbf{s}^{(t)} \leftarrow \mathbf{s}^{(t+1)}$.
7: **end for**
8: **Output:** State $\mathbf{s}$ and action $\mathbf{a}$ vectors.

In this work, the reward function $r(\mathbf{s},\mathbf{a})$ takes one of the predefined values $v_1 > v_2 > v_3$, described as

$$r(\mathbf{s},\mathbf{a}) = \begin{cases} v_1, & (\mathbb{EE} \geq \zeta_{\min}) \cap (\mathbb{R}_i \geq R_{\min}) \cap (\mathbb{P}_i \leq P_{\max}), \\ v_2, & (\mathbb{EE} \geq \zeta_{\min}) \cup (\mathbb{R}_i \geq R_{\min}) \cap (\mathbb{P}_i \leq P_{\max}), \\ v_3, & \text{otherwise}, \end{cases} \tag{6.6}$$

where $\mathbb{EE}$ is the energy-efficiency value, $\mathbb{R}_i$ is the data rate of UE i, and $\mathbb{P}_i$ the total transmission power of that UE over all used RBs, with thresholds $\zeta_{\min}$, $R_{\min}$, and $P_{\max}$, respectively. Every time an the action vector $\mathbf{a}$ is selected, the MBS calculates the rewards, and measures how well the action vector contributes to the maximization of the UEs energy-efficiency, while ensuring the minimum date rate and maximum transmission power constraints are satisfied. The QL algorithm is outlined in **Algorithm 7**, which summarizes the process of evaluating the Q values, and obtaining the GUEs and UAVs allocated RBs states, and transmission power action vectors. Each UE independently learns its own policy, treating other agents as part of the environment, i.e. independent Q-learning [182].

The QL algorithm is guaranteed to converge when all actions are repeatedly sampled and the rewards are bounded [168, 183]. More importantly, the QL algorithm has two serious issues: (1) the amount of memory need to store and update the $\mathbf{Q}(\mathbf{s},\mathbf{a})$ matrix grows exponentially as the number of states and actions increases, and (2) some states may rarely be visited, which excessively increases the time needed to explore all state-action combinations to obtain a good estimate of $\mathbf{Q}(\mathbf{s},\mathbf{a})$, which is impractical. Independent Q-learning makes the environment become non-stationary from the point of view of each UE. Since it contains other UEs who are themselves learning, the convergence can not be guaranteed. Fortunately, substantial empirical evidence has shown that independent Q-learning often works well in practice [184].

6.2.2 Deep Q-Learning (DQL)

As for DQL, and as mentioned earlier, a DNN called DQN is utilized to estimate the Q-function instead of the $\mathbf{Q}(\mathbf{s},\mathbf{a})$ matrix in the QL algorithm. In this work, a multi-layer deep forward neural network is utilized to replace the classical state-action matrix and find the optimal policy. This is achieved by exploiting correlations in the space of the input raw data and identifying the important features that distinguish such input [185]. Moreover, an experience-replay mechanism is used to store the reciprocal experience and randomly pick a group of samples from the stored experience to train the DQL instead of the direct successive samples of the QL algorithm. Furthermore, a second

neural network is added to provide the target Q-values. These values will be used to calculate the loss value for each action at DQL training round [171].

Now, let the DQN be denoted $\mathbf{Q}(\mathbf{s},\mathbf{a};\boldsymbol{\theta})$, where $\boldsymbol{\theta}$ is a real-valued vector completely characterizing the function $\mathbf{Q}(\mathbf{s},\mathbf{a};\boldsymbol{\theta})$, such that $\mathbf{Q}(\mathbf{s},\mathbf{a};\boldsymbol{\theta}) \approx Q_{\phi^*}(\mathbf{s},\mathbf{a})$. In turn, the search for the best Q-function translates to finding the best $\boldsymbol{\theta}$ of finite dimensions via training. In particular, the DQL agent gathers experiences and forms a data set $\mathcal{D}$ in the form of $\left(\mathbf{s}^{(t)},\mathbf{a}^{(t)},r^{(t+1)},\mathbf{s}^{(t+1)}\right)$ by collecting experiences until-step t. To this end, two DQNs are defined, namely the target DQN with $\boldsymbol{\theta}^{(t)}_{\text{target}}$, and the train DQN with $\boldsymbol{\theta}^{(t)}_{\text{train}}$. Moreover, $\boldsymbol{\theta}^{(t)}_{\text{target}}$ is updated to become equivalent to $\boldsymbol{\theta}^{(t)}_{\text{train}}$ over a specific number of time-steps [179]. In each time-step t, the DQN is trained by minimizing a least squares loss function (i.e. a gradient-descent) based a random mini-batch from $\mathcal{D}$, which is expressed as [186]

$$\mathcal{L}\left(\boldsymbol{\theta}^{(t)}_{\text{train}}\right) = \mathbb{E}\left[y^{(t)} - Q\left(\mathbf{s}^{(t)},\mathbf{a}^{(t)};\boldsymbol{\theta}^{(t)}_{\text{train}}\right)\right]^2, \tag{6.7}$$

where $y^{(t)}$ is the target value function, given by

$$y^{(t)} = r\left(\mathbf{s}^{(t)},\mathbf{a}^{(t)}\right) + \delta \max_{\mathbf{a}} Q\left(\mathbf{s}^{(t+1)},\mathbf{a};\boldsymbol{\theta}^{(t)}_{\text{target}}\right). \tag{6.8}$$

Due to the possible instability (or divergence) of the DQL, the aperiodic store experience is used to improve the learning stability of the DQL [187]. In addition, ε is updated using the decay rate υ as $\varepsilon = \varepsilon(1-\upsilon)$, while slowly smoothing the target parameters in every training round with ξ, as

$$\begin{aligned} \boldsymbol{\theta}^{(t)}_{\text{train}} &= \xi\boldsymbol{\theta}^{(t-1)}_{\text{train}} + (1-\xi)\boldsymbol{\theta}^{(t)}_{\text{train}} \\ \boldsymbol{\theta}^{(t)}_{\text{target}} &= \xi\boldsymbol{\theta}^{(t-1)}_{\text{target}} + (1-\xi)\boldsymbol{\theta}^{(t)}_{\text{target}}, \end{aligned} \tag{6.9}$$

ultimately reducing the correlations between the target and estimated Q-values, and thus stabilizing the DQL algorithm.

For DQL, the reward function $r(\mathbf{s},\mathbf{a})$ takes one of the predefined values and $v_1 > v_2$, as

$$r(\mathbf{s},\mathbf{a}) = \begin{cases} v_1, & (\mathbb{EE} \geq \zeta_{\min}) \cap (\mathbb{R}_i \geq R_{\min}) \cap (\mathbb{P}_i \leq P_{\max}), \\ v_2, & \text{otherwise}, \end{cases} \tag{6.10}$$

which maintains the minimum capacity and maximum transmission power for each UE, while maximizing the EE. The DQL algorithm is summarized in **Algorithm 8**, which is guaranteed to converge efficiently [179, 188].

Algorithm 8 Deep Q-Learning

1: **Initialization:** Experience memory $\mathcal{D}$, δ, ε, υ, and ξ. Also, initialize training parameters $\boldsymbol{\theta}_{\text{train}}$, and target parameters as $\boldsymbol{\theta}_{\text{target}} = \boldsymbol{\theta}_{\text{train}}$.
2: **for** each time-step t **do**
3: For the current state $\mathbf{s}^{(t)}$, pick the action vector $\mathbf{a}^{(t)}$ using the ε-greedy policy, as

$$\mathbf{a}^{(t)} \leftarrow \begin{cases} \arg\max_{\mathbf{a}} \mathbf{Q}\left(\mathbf{s}^{(t+1)}, \mathbf{a}; \boldsymbol{\theta}_{\text{target}}^{(t)}\right), & \text{with prob. } 1-\varepsilon+\frac{\varepsilon}{\left|\mathcal{A}\left(\mathbf{s}^{(t)}\right)\right|}, \\ \text{a random action vector}, & \text{with prob. } \varepsilon+\frac{\varepsilon}{\left|\mathcal{A}\left(\mathbf{s}^{(t)}\right)\right|}. \end{cases}$$

4: Perform action $\mathbf{a}^{(t)}$, obtain reward $r^{(t+1)} = r\left(\mathbf{s}^{(t)}, \mathbf{a}^{(t)}\right)$ and observe the new state $\mathbf{s}^{(t+1)}$.
5: Store $\left(\mathbf{s}^{(t)}, \mathbf{a}^{(t)}, r^{(t+1)}, \mathbf{s}^{(t+1)}\right)$ in experiences memory $\mathcal{D}$.
6: Pick a random mini-batch of from $\mathcal{D}$.
7: Determine the target value function $y^{(t)}$ as

$$y^{(t)} = r\left(\mathbf{s}^{(t)}, \mathbf{a}^{(t)}\right) + \delta \max_{a} Q\left(\mathbf{s}^{(t+1)}, \mathbf{a}; \boldsymbol{\theta}_{\text{target}}^{(t)}\right).$$

8: Update parameters $\boldsymbol{\theta}_{\text{train}}^{(t)}$ by minimizing the loss function

$$\mathcal{L}\left(\boldsymbol{\theta}_{\text{train}}^{(t)}\right) = \mathbb{E}\left[y^{(t)} - Q\left(\mathbf{s}^{(t)}, \mathbf{a}^{(t)}; \boldsymbol{\theta}_{\text{train}}^{(t)}\right)\right]^2.$$

9: Update the target parameters $\boldsymbol{\theta}_{\text{train}}^{(t)}$ and $\boldsymbol{\theta}_{\text{target}}^{(t)}$ using ξ as

$$\boldsymbol{\theta}_{\text{train}}^{(t)} = \xi \boldsymbol{\theta}_{\text{train}}^{(t-1)} + (1-\xi)\boldsymbol{\theta}_{\text{train}}^{(t)}$$
$$\boldsymbol{\theta}_{\text{target}}^{(t)} = \xi \boldsymbol{\theta}_{\text{target}}^{(t-1)} + (1-\xi)\boldsymbol{\theta}_{\text{target}}^{(t)}.$$

10: Set $t \leftarrow t+1$ and current state $\mathbf{s}^{(t)} \leftarrow \mathbf{s}^{(t+1)}$.
11: Update $\varepsilon = \varepsilon(1-\upsilon)$.
12: **end for**
13: **Output:** State $\mathbf{s}$ and action $\mathbf{a}$ vectors.

Since a multi-layer deep neural network is utilized in this work, Fig. 6.1 illustrates the operation of the proposed power control scheme using DQL. The state and action vectors each have $1 \times (N \times I)$ elements to describe each possible state and action, where N is the number of the reused RBs in each frequency band, and I is the total number of UEs in the UHF or mmWave band. Both $\mathbf{s}$ and $\mathbf{a}$ represent inputs to the DNN, while the output is the estimate of expected long-term reward based on a given status $\mathbf{s}$ of the DQL. The input layers for both $\mathbf{s}$ and $\mathbf{a}$ are followed by multiple deep layers; starting with fully connected layer, described by $\mathbf{y_1} = \mathbf{w_s} \cdot \mathbf{s} + \mathbf{b_s}$, where the input vector $\mathbf{s}$ is weighted by vector $\mathbf{w_s}$ and $\mathbf{b_s}$ is the bias vector. The next layer is the Rectified Linear Unit (ReLU) used to suppress any negative output value of the previous fully connected layers to zero, and the output is $\mathbf{y_2} = \max(\mathbf{y_1}, 0)$, then another fully connected layer is

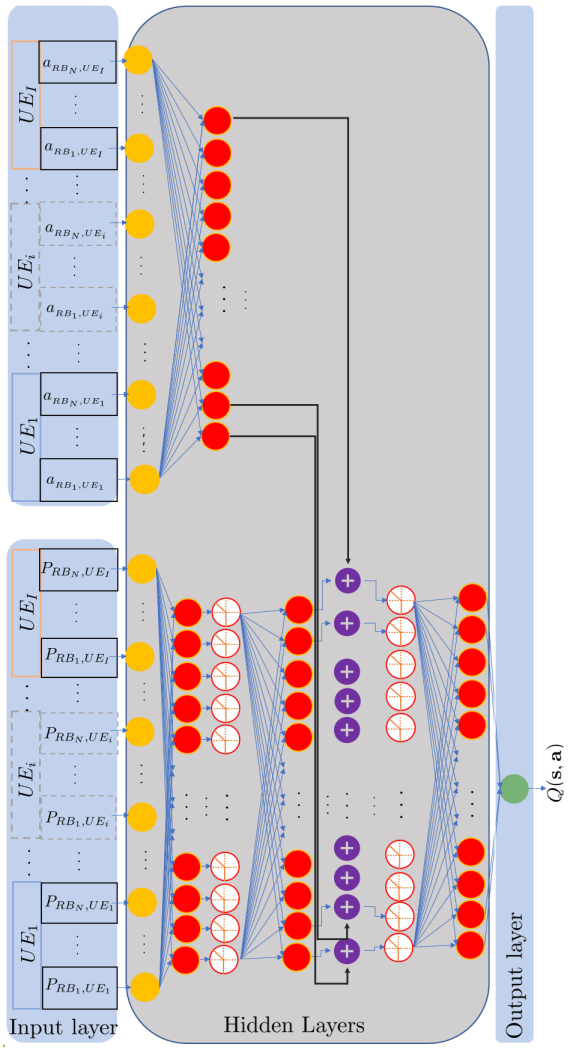

Figure 6.1: Proposed power control scheme using DQL

applied. In order to update **s** by adding the actions **a**, the Add layer has been used to obtain the output. Finally, to remove any negative power, a ReLU layer has been used. Lastly, a fully connected layer with a single output is used to provide the state-action function $Q(\mathbf{s},\mathbf{a})$, as illustrated in Fig. 6.2.

6.3 Implementation of QL and DQL

This section discusses the implementation of the QL and DQL algorithms. It should be noted that since the UHF and mmWave UEs do not interfere with each other, the QL/DQL algorithm is executed for the UE over each band separately to obtain the transmission power values for GUEs and UAVs EE maximization.

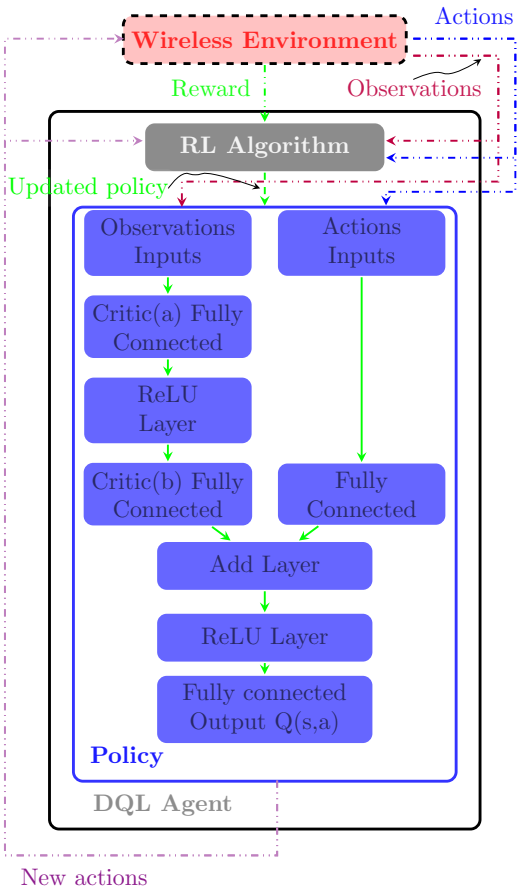

Figure 6.2: DQL Model

Now, the state vector **s** contains the power value of the user RBs, say UE i, starting with a low power value (e.g. $P_{i,n} = 10^{-6}$ W) up to the maximum transmission power value $P_{\max} = 0.1$ W, but each UAV or GUE's maximum transmission power is 0.2 W, since we assume one user can occupy multiple RBs. Each action in the action vector **a** involves multiplying the RB power by one of three values in $\{0.1, 1, 10\}$ as per the ε-greedy policy, which facilitates the exploration and exploitation to maximize the Q-function. Upon applying an action vector, the states vector is updated to values in the range $\left[10^{-6}, 0.1\right]$ W, which designates the transmission power values of either UHF or mmWave UEs.

In this work, the final or exit state is not known a priori, since the optimal value for the EE is not known before executing the QL (or DQL) algorithm. However, convergence to a certain Q value or reaching the maximum number of iterations terminates the search process, and the final obtained Q value resembles the best EE value. In turn, the learning rate η, discount factor δ, and maximum number of iterations $T_{\max}$ govern

the convergence speed and accuracy of the obtained EE solution. Particularly, a higher learning rate η allows better solution exploration, and a value of $\delta \to 1$ puts more emphasis on long-term higher rewards. Also, the higher $T_{\max}$ is, the better the exploration and exploitation, which guarantees the optimal states for UEs transmission powers. Hence, the values of η, δ and $T_{\max}$ pose a trade-off between accuracy of the obtained solution and speed of convergence. To highlight this, Table 6.1 summarizes the parameters for two scenarios, which will be considered in the performance evaluation in Section 6.7.

Table 6.1: QL Parameters

Parameters	Scenario 1	Scenario 2
Possible States of One RB	$s \in [10^{-6}, 10^{-5}, 10^{-4}, 10^{-3}, 10^{-2}, 10^{-1},]$ W	
Possible Actions of One RB	$a \in \{0.1, 1, 10\}$ W	
Reward Function Values	$v_1 = 10$ $v_2 = 1$ $v_3 = -10$ $\zeta^G_{\min} = \zeta^A_{\min} = 4$ MBits/J $R^G_{\min} = 0.4$ MBits/s $R^A_{\min} = 4$ MBits/s $P^G_{\max} = P^A_{\max} = 0.2$ W	
Discount Factor δ	0.1	
ε-Greedy Parameter	0.333	
Learning Rate η	0.1	0.01
$T_{\max}$	10,000	25,000

In a similar manner to the QL algorithm, the DQL is evaluated based on two scenarios, as shown in Table 6.2.

6.4 Performance Evaluation

In this section, the performance of the coupled UHF and coupled mmWave with FPC are compared to the DUDe access scheme in terms of sum-rate, energy-efficiency, and data rate per UE. Specifically, the performance of the QL and DQL power control schemes based on DUDe access are evaluated and compared with the optimal scheme proposed in last chapter and fractional power control schemes used in 4G and 5G networks, namely **Decoupled-Optimal** and **Decoupled-FPC**, respectively[2]. Since the

[2]The optimal EE-maximizing power control schemes are based on the solutions of problems **GUEs-EE-MAX** and **UAVs-EE-MAX**, as discussed in subsections 5.4.1, and 5.4.2, respectively.

Table 6.2: DQL Parameters

Parameters	Scenario 1	Scenario 2
States Input Layer	Input Size: 5 Users × 3 RBs = 15 Neurons Output: 24 Neurons—Normalization: None	
Actions Input Layer	Input Size: 15 Neurons—Output: 50 Neurons Normalization: None	
States Critic(a) Fully Connected Layer	Input Size: 50 Neurons—Output: 50 Neurons Normalization: None	
States Critic(b) Fully Connected Layer	Input Size: 50 Neurons—Output: 50 Neurons Normalization: None	
Action Critic Fully Connected Layer	Input Size: 50 Neurons—Output: 50 Neurons Normalization: None	
ReLU Layers for Critic & Action Paths	$f(x) = \max(0, x)$	
Add layer	Adding neurons element wise	
Fully Connected Output $Q(\mathbf{s}, \mathbf{a})$	Input Size: 50 Neurons—Output: 1 Neuron Normalization: None	
Possible States	$s \in \left[10^{-6}, 10^{-5}, 10^{-4}, 10^{-3}, 10^{-2}, 10^{-1},\right]$ W	
Possible Actions of One RB	$a \in \{0.1, 1, 10\}$ W	
Reward Function Values	$v_1 = 10$ $v_2 = -10$ $\zeta^G_{\min} = \zeta^A_{\min} = 4$ MBits/J $R^G_{\min} = 0.4$ MBits/s $R^A_{\min} = 4$ MBits/s $P^G_{\max} = P^A_{\max} = 0.2$ W	
Decay Rate υ	0.005	
Smoothing Factor ξ	0.001	
Discount Factor δ	0.1	
ε-Greedy Parameter	0.333	
Learning Rate η	0.1	0.01
$T_{\max}$	10,000	25,000

UAV CNPC links require low data rate, and will not interfere with other links, they are not considered in the simulations, for simplicity. Table 6.3 summarizes the simulated transmission parameters.

Fig. 6.3 illustrates the 10^{th}, 30^{th}, 50^{th}, 70^{th}, and 90^{th} percentile data rate per GUE and UAV in the UL, where the ratio of SBS to the MBS is 4. In Fig. 6.3 (a), the UEs data rates shows that due to EE optimization the 70% and 90% percentile data rates in **Decoupled-Optimal**, QL and DQL are lower than the decoupled FPC. Although the minimum rates are respectively 4×10^6 and 4×10^5 bps for the GUEs and UAVs, some

Table 6.3: Simulation Parameters

Parameters	GUE	UAV	MBS	SBS
Maximum transmission power	23 dBm	23 dBm	46 dBm	30 dBm
DL/UL Bias	N/A	N/A	0/0 dB	3/0 dB
Spatial Distribution	Uniform Distribution			
Altitude of UAVs	50-200 m [13, 55]			
S-curve Parameters	$a = 9.6$, $b = 0.28$ [144, 146]			
Blockage Ball Model Parameters	$\mu = 200$ m, $\omega = 0.2$ [77]			
Spatial Density	30 per km^2	30 per km^2	5 per km^2	20 per km^2
Path-Loss Exponent	UHF: GUE-UAV 2, GUE-BS 3, $d_0 = 1$ m [148]; mmWave: LOS 2.55, NLOS 5.76, $d_0 = 5$ m [29, 164]			
Lognormal Shadowing	UHF: $\mu = 0$, $\sigma = 4$ dB [148]; mmWave: LOS $\mu = 0$, $\sigma = 8.66$ dB, NLOS $\mu = 0$, $\sigma = 9.02$ dB [29]			
Nakagami-m Parameters	$m_L = 3$, $m_N = 2$ [144, 147]			
Operating Frequency	2 GHz & 28 GHz	28 GHz	2 GHz & 28 GHz	2 GHz & 28 GHz
Bandwidth	UHF: 1.2 MHz; mmWave: 4.8 MHz			
Subcarrier Spacing	UHF: 15 kHz; mmWave: 60 kHz [84]			
Power Control	FPC with $P_0 = -85$ dBm, and $\alpha = 0.8$ [55]			
Noise Spectral Density	-174 dBm/Hz			

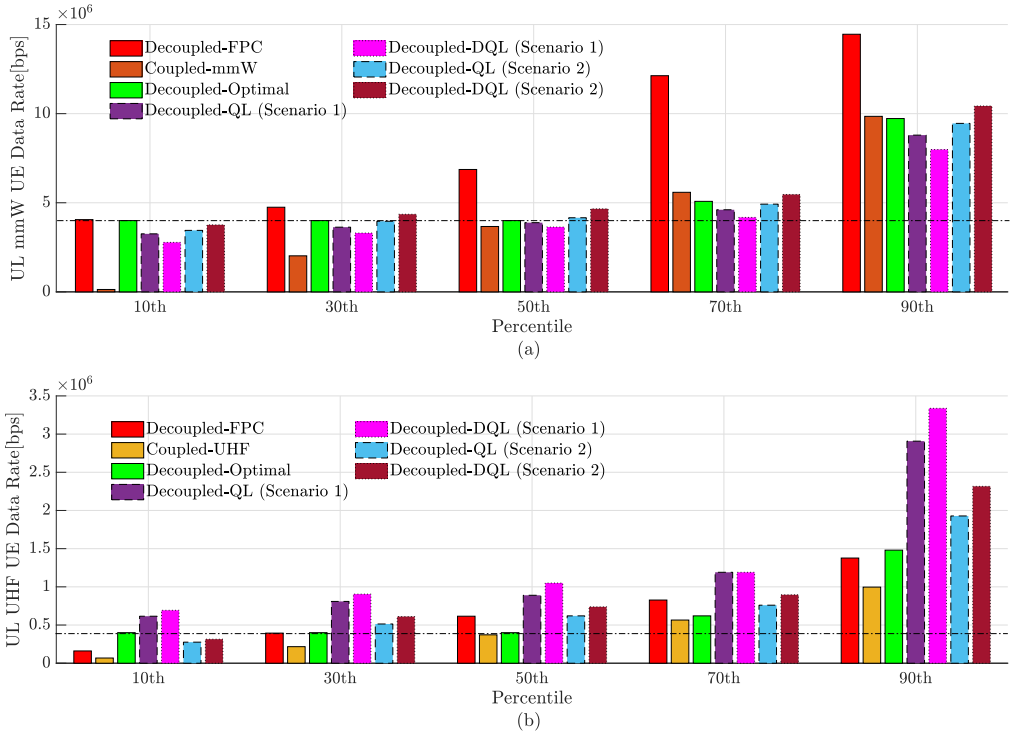

Figure 6.3: 10^{th}, 30^{th}, 50^{th}, 70^{th}, and 90^{th} percentile data rate per user in the UL: (a) mmWave band and (b) UHF band - SBS to MBS ratio = 4

of the UEs under the QL and DQL schemes are below the thresholds. This is because the EE thresholds (i.e. $\zeta^G_{\min}$ and $\zeta^A_{\min}$) appear as soft thresholds (as per (6.6) and (6.10)), which leads to a tradeoff between the data rate and EE. Additionally, Fig. 6.3 (a) shows that both QL and DQL algorithms improve their learning policies and assign power to UEs to increase their data rates when the number of training iterations is increased and

their learning rates are decreased. This can be verified by comparing **Scenarios 1** and **2** for the **Decoupled-QL** and **Decoupled-DQL** schemes, and this is due to the fact that more states are visited in search for the best state. More importantly, this implies that improving the learning increases the rate of the UEs for EE-maximization in the mmWave band since it is noise-limited. Contrarily, Fig. 6.3 (b) depicts an opposite pattern, since the UHF band is interference-limited, and thus, **Scenario 2** decreases the rate of the UEs to improve the EE, in comparison to **Scenario 1**.

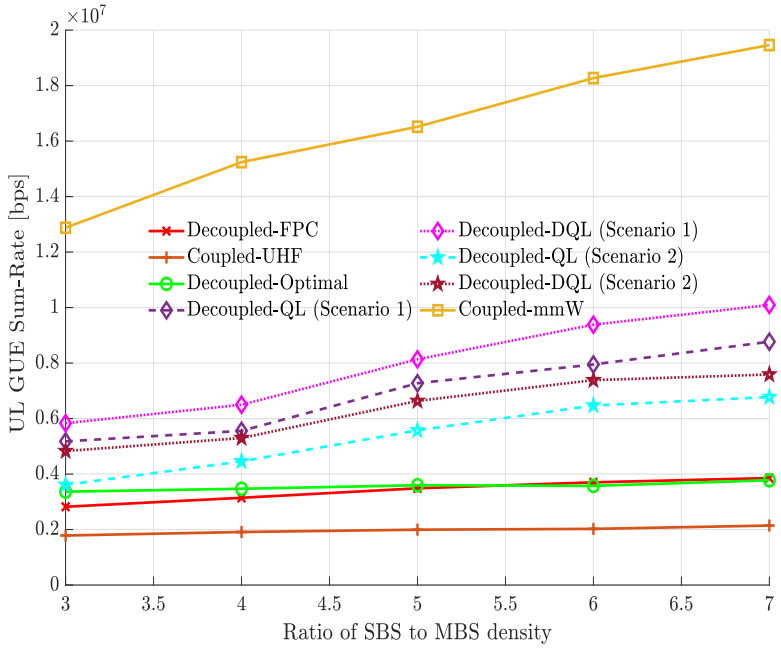

Figure 6.4: UL GUE sum-rate vs. ratio of SBS to MBS.

In Fig. 6.4, it can be seen that the GUEs sum-rate of the decoupled schemes are at least 60% higher than the **Coupled-UHF** scheme. This is because the decoupled schemes have wider bandwidth for GUE UL communications (as shown in Table 5.2), shorten the distances between the GUEs and BSs, and eliminate the interference between UAVs and GUEs. The sum-rate of the **Coupled-mmW** scheme is the highest, since it utilizes the mmWave band for GUE UL communication, while the other schemes utilize the UHF band, and the mmWave bandwidth is wider than the UHF bandwidth. The sum-rate of the **Decoupled-Optimal** scheme remains relatively constant with the increase in the SBS to MBS ratio, since it mainly aims to achieve the optimal energy-efficiency, as will shown in Figs. 6.6 and 6.7. In comparison to the **Decoupled-Optimal** scheme, both the **Decoupled-QL** and **Decoupled-DQL** schemes yield higher data rates at the expense of higher transmission power, which will translate

to lower EE values. To see this, for both schemes, **Scenario 2** yields lower sum-rate than **Scenario 1**, as increasing the training iterations and reducing the learning rate lower the sum-rate to improve the EE by carefully selecting the transmission power.

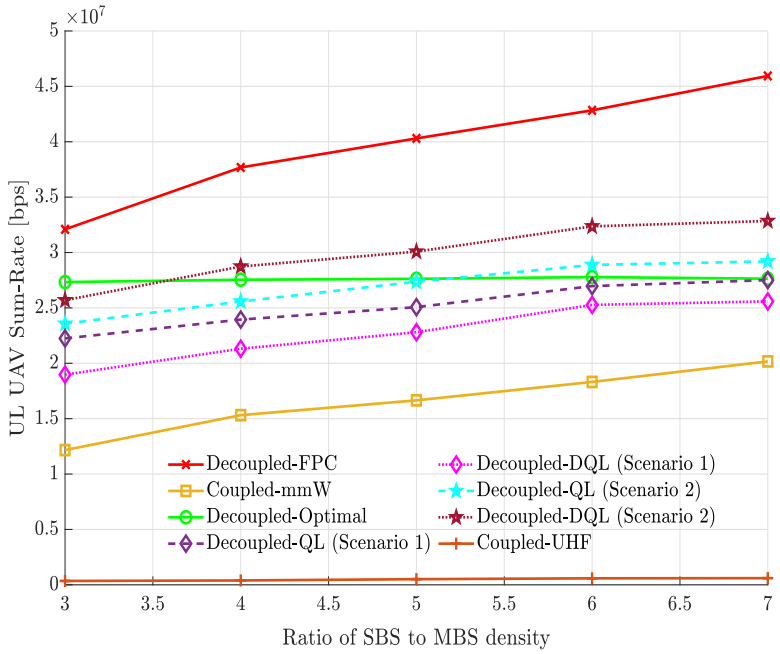

Figure 6.5: UL UAV sum-rate vs. ratio of SBS to MBS.

Similarly, in Fig. 6.5, the UAV sum-rates of the **Coupled-UHF** and **Coupled-mmW** schemes are much lower than the decoupled schemes, since the UAVs under those two schemes are allocated narrower bandwidth and suffer from higher path-loss. Besides, the UAVs under the **Coupled-UHF** scheme also suffer from ICI, while the UAVs under the other schemes are allocated the mmWave band, and thus, their ICI is minimal. In comparison to the **Decoupled-Optimal** scheme, both the **Decoupled-DQL** and **Decoupled-QL** tend to explore if increasing the sum-rates may help in achieving better EE for the UAV UL transmissions and this is appear as a small increase in the sum-rate when the SBS to MBS ratio increases. Adding to this, **Scenario 2** improves the sum-rates for both the **Decoupled-DQL** and **Decoupled-QL** in comparison to **Scenario 1**.

As for EE, as shown in Fig. 6.6 and Fig. 6.7, the decoupled schemes can achieve up to several times higher EE than the coupled schemes, as they prevent the interference between UAVs and GUEs, reduce the interference among GUEs, and shorten the UE-BS distances. Also, Figs. 6.6 and 6.7 demonstrate that the EE improvement for the **Decoupled-Optimal**, **Decoupled-QL** and **Decoupled-DQL** schemes as the SBS to

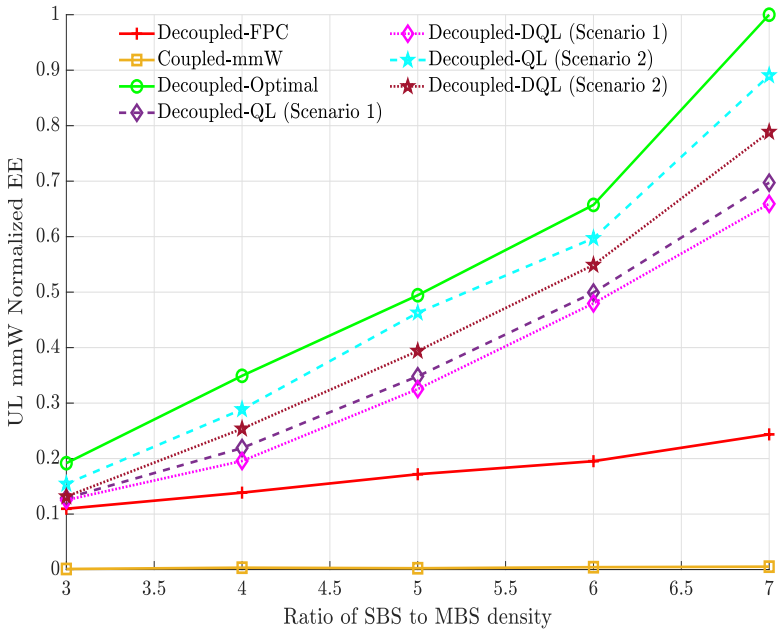

Figure 6.6: UL mmWave UEs normalized EE vs. ratio of SBS to MBS.

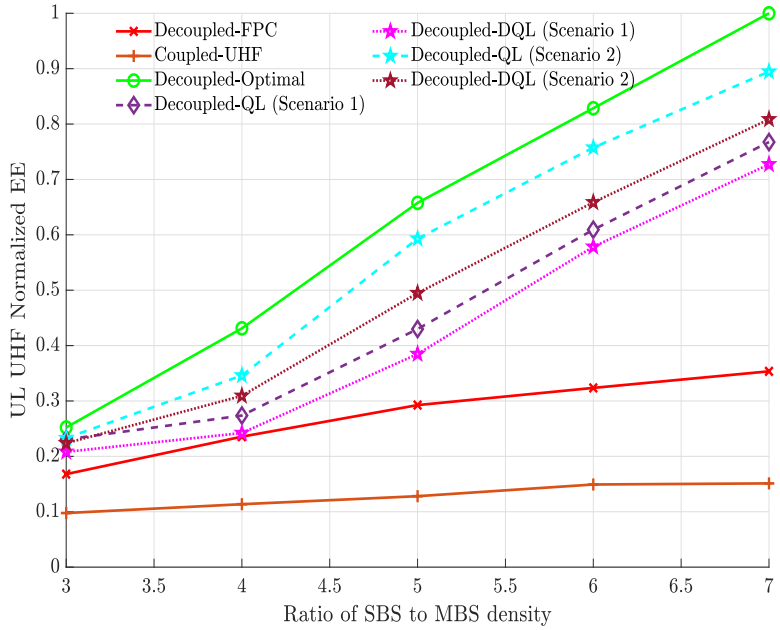

Figure 6.7: UL UHF UEs normalized EE vs. ratio of SBS to MBS.

MBS ratio increases. This is attributed to the decrease in the number of UEs associated with the same SBS or MBS, and the decrease in UE-BS distances. In addition, the **Decoupled-QL** and **Decoupled-DQL** schemes yield an improvement in the EE as the

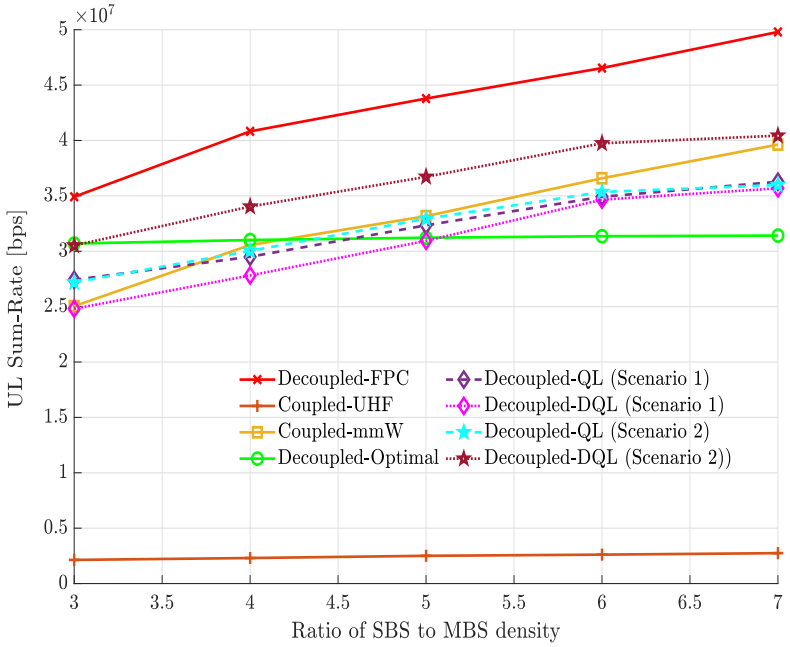

Figure 6.8: Network UL sum-rate vs. ratio of SBS to MBS.

training iterations increase and the learning rate decreases, which can be verified by comparing **Scenario 1** and **Scenario 2** for both schemes.

Fig. 6.8 illustrates the total UL sum-rate, where one can see that the sum-rate of the **Decoupled-QL** and **Decoupled-DQL** schemes improves as the ratio of SBS to MBS increases. Also, the sum-rate for the **Decoupled-QL (Scenario 2)** scheme shows has a minor improvement over the **Decoupled-QL (Scenario 1)** scheme, while **Decoupled-DQL (Scenario 2)** shows around 5 Mbps improvement over **Decoupled-DQL (Scenario 1)**. Lastly the QL and DQL algorithms are limited by the maximum number of iterations in search for the best trade-off between sum rate, minimum user rate, and the EE, which also control how long it takes to run the optimization process.

6.5 Summary

In this chapter, two power control schemes based on QL and DQL have been proposed to improve the EE of an cellular-enabled UAV network in DUDe scenario. Then, the proposed QL and DQL schemes have been compared with the FPC scheme (which is applied in 4G and 5G networks), and the optimal EE-maximizing benchmark power allocation scheme proposed in last chapter. The results revealed that the proposed DUDe access schemes can achieve several times higher sum-rates and EE than their coupled

counterparts. Moreover, it is shown that although RL methods can achieve optimal results in theory, in practical scenarios with predominant dynamic environments, and limited time to execute the optimization process, QL and DQL with limited number of iterations may only achieve a near-optimal EE performance. Nonetheless, the proposed QL (DQL) algorithm has been shown to achieve better EE performance than the baseline FPC scheme by around 100% (70%) for UHF band, and by around 160% (130%) for the mmWave band, in comparison to conventional FPC scheme.

Chapter 7

DUDe Access in Mobile Edge Computing

7.1 Introduction

This chapter analyzes the application of DUDe on MEC. Different from cloud computing, MEC is limited by real-time delay constraints and limited computing resources [189]. If too many tasks are offloaded to one MEC server, then this may lead to severe congestion and latency. If an MD's task is offloaded to a BS that is too far away, then data transmission may be drastically impaired due to excessive path-loss, which adversely affects communication resource utilization. Thus, the main problems of MEC resource allocation can be divided into computation offloading decision (whether to offload or not), user association/offloading node selection (where to offload), subchannel assignment, and transmission power control (interference management). Some existing research works focus on MEC with multi-user single-server scenarios, while others consider MEC with homogeneous multi-server scenarios. However, only a few studies have been conducted to investigate the heterogeneous servers scenario, where servers are located at the SBS, MBS or cloud, and have different computing and communication capabilities, hence the focus of this chapter.

Generally speaking, the optimization objectives in most works can be divided into three categories:

(1) Energy consumption minimization: To improve the battery lifetime, the energy consumption of MDs and/or BSs is optimized, subject to constraints on latency.

(2) Latency minimization: For those applications with stringent latency constraints,

Table 7.1: Summary of MEC Scenarios and Objectives

Ref.	MD		Edge Servers		Objectives		
	Single	Multiple	Single	Multiple	Energy	Latency	Energy & Latency
[190]		✓		✓			✓
[191]		✓		✓		✓	
[192]		✓	✓		✓		
[193]		✓	✓				✓
[194]		✓	✓			✓	
[195]	✓		✓		✓		
[196]	✓			✓			✓
[197]	✓			✓			✓
[198]		✓		✓	✓		
[199]		✓		✓		✓	

it is necessary to shorten the latency while satisfying the transmission power and/or energy consumption constraints.

(3) Joint energy consumption and latency minimization: The weighted sum of energy consumption and latency is minimized.

A summary of different MEC scenarios and objectives studied in the literature is given in Table 7.1, where it should be noted that [190, 191] pertain to the heterogeneous servers scenario, while the rest are for homogeneous servers.

In MEC-based systems, computational tasks offloading is potentially limited by the type of MD-BS association, and almost all the previous works consider offloading a MD's computation task to the MEC servers available at its serving BS. However, with the deployment of more and more low-cost SBSs, the traditional homogeneous networks become HetNets. Due to the transmission power disparity of SBSs and MBSs, the DL coverage of MBSs is usually much greater than that of SBSs. Consequently, more MDs are associated with MBSs in the DL. Offloading too many MDs to the MBSs may cause severe network congestion and latency. Furthermore, unlike BSs, MDs have similar transmission powers and transmission coverage. If the associated cell in the UL is the same as that in the DL, the link quality of the MCell edge MDs will be poor, and may cause high UL transmission latency. Although cell range extension can offload more MDs to the SBSs [7], it may impair the DL transmission performance. For the sake of balanced offloading and reduced path-loss, it would be a better choice for some MDs to connect to a geometrically closer SCell in the UL

rather than the same BS in the DL, i.e. DUDe access [2]. Moreover, since different types of BSs have different computation capabilities, choosing the serving BS from the computation resource perspective is also necessary.

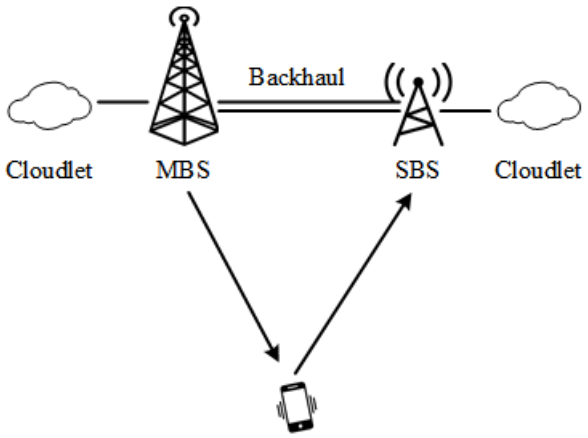

Figure 7.1: A DUDe MEC model.

As shown in Fig. 7.1, according to the DUDe access, a MD's UL and DL serving BSs may not necessarily be the same. Accordingly, the MD's tasks can be executed at the MEC server available at the UL and/or DL serving BS. In such a case, the BSs should be able to communicate with each other, which is possible for 4G and beyond cellular networks, since the BSs are inter-connected via traditional backhaul connections (e.g. via the X2 interface, in accordance with 3GPP LTE terminology) [1]. Despite the extra backhaul delay, the DUDe MEC scheme is also capable of providing a fairly lower offloading latency as compared to the conventional offloading scheme with coupled association [200]. Hence, it is necessary to study optimal or near-optimal resource allocation algorithms for DUDe MEC systems. To the best of our knowledge, only one paper applied DUDe to MEC-based networks [200], which presents a DUDe MEC framework and compares it with the CUDA scheme; however, it does not propose any offloading or resource allocation algorithms.

7.1.1 Main Contributions

The main contributions of this chapter can be summarized as follows:

- A DUDe joint BS association and subchannel allocation algorithm is proposed. Different from most studies that consider BS association and subchannel allocation separately, this work jointly performs BS association and subchannel allocation by utilizing the student-project allocation (SPA) matching model [201].

Furthermore, the constraint that one MD must connect to the same BS in the UL and DL is broken, and the UL serving BS is chosen according to both the communication and computation capacity of BSs.

- Given the obtained BS association and subchannel allocation, an optimal power allocation algorithm is devised to minimize the sum-latency of the network MDs. The formulated problem is a sum-of-ratios problem, which is non-convex and NP-hard. To efficiently and optimally tackle it, the proposed algorithm tightly approximates the problem as a convex optimization problem, and successively solves it until convergence to the global optimal power allocation solution.

- Finally, the performance of the proposed algorithms are compared with benchmark schemes in terms of latency, energy-efficiency (EE) and data rate. Specifically, the simulation results demonstrate that the latency of the proposed DUDe access and power control scheme is much lower than that of the CUDA scheme by up to 60%, and its EE and data rate are also increased.

7.1.2 Organization

The rest of the chapter is organized as follows. Section 7.2 presents the system model adopted in this chapter. Section 7.3 proposes the DUDe joint BS association and subchannel allocation scheme, which considers the communication and computation capacity of the different types of BSs. Section 7.4 proposes an optimal power allocation scheme to minimize the network sum-latency. Section 7.5 evaluates the performance of the proposed scheme and compares it with coupled benchmarks. Finally, Section 7.6 gives a summary and critique of the proposed algorithms as well as the findings.

7.2 System Model

7.2.1 Network Model

In this work, a two-tier OFDMA HetNet—composed of one MBS and several SBSs—is considered, and the Rayleigh fading channel model is adopted. The positions of the MBS and the SBSs are uniformly distributed, where the density of the SBSs is λ_s. The MDs' locations also follow a uniform distribution with a density of λ_u. Let $\mathcal{K} = \{1,\ldots,k,\ldots,K\}$ and $\mathcal{N} = \{1,2,...,N\}$ be the index sets of the MDs and subchannels, respectively. Also, let $\mathcal{M} = \{0,1,\ldots,M\}$ denote the set of $M+1$ BSs, where BS $m = 0$

corresponds to the MBS, and the rest (i.e. $m = 1, \ldots, M$) are SBSs. Both tiers operate on the same frequency band, and are based on FDD. Moreover, an MD can only occupy one subchannel, and MDs in different cells can reuse the same subchannel. As such, there is inter-cell interference, but no intra-cell interference.

7.2.2 Transmission Model

The transmit powers of all SBSs are assumed to be identical, but the transmit power of the MBS is greater than the SBSs. In the DL, the maximum transmit power is equally allocated over the whole bandwidth; while in the UL, the initial transmit power of MD k is set according to the fractional power control (FPC) as [202, 203], which is applied in 4G and 5G

$$P_k^{ul} = \min\{P_{\max}, wPL + P_0\}, \tag{7.1}$$

where P_{max} is the maximum transmission power of each MD, P_0 is the target received power, and $w \in \{0, 0.4, 0.5, 0.6, 0.7, 0.8, 0.9, 1\}$ is the compensation factor for path-loss PL. The path-loss $PL(d)$ can be modeled as

$$PL(d) = 20\log\left(\frac{4\pi d_0 f}{c}\right) + 10\phi\log\left(\frac{d}{d_0}\right) + \chi, \tag{7.2}$$

where d_0 denotes the close-in reference distance, f is the operating frequency, c is the speed of light, d represents the MD-BS distance, ϕ is the path-loss exponent, and χ is the log-normal shadowing.

7.2.3 MEC Model

In this work, full offloading is adopted, while assuming that there is only one computation task to be processed for each MD during a computation offloading period. As the UL serving BS may be different from the DL serving BS, the tasks can be executed at the cloudlet attached to the UL serving BS or the DL serving BS or both of them. However, for simplicity, it is assumed that all the tasks are executed at the UL cloudlets in this chapter. The MBS's cloudlet is assumed to have higher computation capacity than the SBSs' cloudlets, which are denoted F^M and F^S (in CPU cycles per second),

respectively[1]. Also, each SBS is connected to the MBS via a backhaul link with finite capacity[2] C^{bh}. Let the computational task of each MD $k \in \mathcal{K} = \{1,2,...,K\}$ be defined as a tuple $\mathcal{T}_k \triangleq (B_k^C, B_k^I, B_k^O)$, where B_k^C is the required number of CPU cycles to complete MD k's task, B_k^I is the number of bits of the offloaded task, and B_k^O is the number of output bits representing the result of the task execution. For simplicity, the output bits and the computation data size are assumed to be proportional to the input task size. Particularly, let $B_k^0 = \alpha_k B_k^I$, where α_k is the proportion of output to input bits [189]. Moreover, $B_k^C = \beta_k B_k^I$, where β_k is the number of CPU cycles per bit, and depends on the type of executed task. To offload a task, MD k first transmits the B_k^I input bits to its UL serving BS, and the cloudlet of which executes the B_k^C CPU cycles. Finally, the B_k^O output bits are transmitted back to the MD[3].

7.2.4 Latency Model

The total offloading latency for a typical MD k is given by

$$L_k = L_k^{ul} + L_k^{exe} + L_k^{bh} + L_k^{dl}, \tag{7.3}$$

where L_k^{exe} is the time delay for the cloudlet to execute MD k's task, L_k^{ul} is the UL transmission latency, and L_k^{dl} is the DL transmission latency[4]. Moreover, there are two cases for the backhaul latency L_k^{bh}, which are defined as

- UL serving BS $\neq$ DL serving BS: $L_k^{bh} = B_k^O / C^{bh}$;
- UL serving BS = DL serving BS: $L_k^{bh} = 0$.

7.2.5 Communication Model

Let $\chi_{k,m}$ be a binary decision variable, defined as

$$\chi_{k,m}^l = \begin{cases} 1, & \text{if MD } k \text{ is associated with BS } m \text{ in } l \text{ direction,} \\ 0, & \text{otherwise,} \end{cases} \tag{7.4}$$

[1]Assume each cloudlet's computational resources are equally shared among all tasks when two or more tasks are offloaded to the same cloudlet.

[2]Interference-free wireless backhaul links are assumed, and the backhaul links will not cause interference to MD-BS links.

[3]Note that if the UL and DL serving BSs are different, the B_k^O output bits are communicated to the DL serving BS via the backhaul link.

[4]There is a waiting time before a cloudlet begins to execute a task, but most works assume it to be zero [189, 200].

where $l \in \{ul, dl\}$. Moreover, it should be noted that each MD $k \in \mathcal{K}$ can be associated with one BS in each link direction (i.e. $\sum_{m \in \mathcal{M}} \chi^{l}_{k,m} = 1$). Also, let $\lambda_{k,n}$ be defined as

$$\lambda^{l}_{k,n} = \begin{cases} 1, & \text{if subchannel } n \text{ is allocated to MD } k \text{ in } l \text{ direction,} \\ 0, & \text{otherwise.} \end{cases} \tag{7.5}$$

Thus, the data rate of MD $k \in \mathcal{K}$ in the UL is

$$R^{ul}_{k} = B \sum_{m \in \mathcal{M}} \sum_{n \in \mathcal{N}} \chi^{ul}_{k,m} \lambda^{ul}_{k,n} \log_2 \left(1 + \frac{P^{ul}_{k,m,n} h^{ul}_{k,m,n}}{I^{ul}_{k,m,n} + \sigma^2} \right), \tag{7.6}$$

where B is the RB bandwidth, and $\sigma^2 = N_0 B$ is the variance of the AWGN, with N_0 being the noise spectral density. Moreover, $P^{ul}_{k,m,n}$ is the transmission power of MD k when associated with BS m over subchannel n, and $h^{ul}_{k,m,n}$ is the corresponding channel gain in the UL. The interference $I^{ul}_{k,m,n}$ received at BS m on RB n for MD k is written as

$$I^{ul}_{k,m,n} = \sum_{j \in \mathcal{K}, j \neq k} \lambda^{ul}_{j,n} P^{ul}_{j,m,n} h^{ul}_{j,m,n}. \tag{7.7}$$

Similarly, the data rate at MD k in the DL is expressed as

$$R^{dl}_{k} = B \sum_{m \in \mathcal{M}} \sum_{n \in \mathcal{N}} \chi^{dl}_{k,m} \lambda^{dl}_{k,n} \log_2 \left(1 + \frac{P^{dl}_{k,m,n} h^{dl}_{k,m,n}}{I^{dl}_{k,m,n} + \sigma^2} \right), \tag{7.8}$$

where $P^{dl}_{k,m,n}$ is the transmission power of BS m to MD k over subchannel n, and $h^{dl}_{m,k,n}$ is the corresponding channel gain. The interference received at MD k on RB n is given by

$$I^{dl}_{m,k,n} = \sum_{i \in \mathcal{M}, i \neq m} \lambda^{dl}_{k,i} P^{dl}_{i,k,n} h^{dl}_{i,k,n}. \tag{7.9}$$

Notably, MD k's UL and DL data rates R^{ul}_{k} and R^{dl}_{k} are related to MD k's serving BS, transmission power, and the interference level over the assigned subchannel in each link direction.

The latency (in seconds) necessary to complete the UL transmission for MD k is

defined as

$$L_k^{ul} = \frac{B_k^I}{R_k^{ul}}, \tag{7.10}$$

while the DL transmission time is

$$L_k^{dl} = \frac{B_k^O}{R_k^{dl}}. \tag{7.11}$$

The backhaul delay is only related to the data size [200], and thus, the backhaul latency is determined as

$$L_k^{bh} = \frac{B_k^{bh}}{C^{bh}}, \tag{7.12}$$

where B_k^{bh} is MD k's backhaul data size, defined as

$$B_k^{bh} = \begin{cases} B_k^O, & \text{decoupled access,} \\ 0, & \text{coupled access.} \end{cases} \tag{7.13}$$

The execution latency for a typical MD k is

$$L_k^{exe} = \frac{B_k^C}{F_k}, \tag{7.14}$$

where $F_k = \bar{F}_k/\bar{K}$, with $\bar{F}_k$ being the computation capacity (in CPU cycles/second) of the cloudlet attached to MD k's UL serving BS (i.e. $\bar{F}_k = F^M$ for MBS, and $\bar{F}_k = F^S$ for SBS), and $\bar{K}$ is the number of MDs associated with that BS. Lastly, the total latency of MD k is calculated as

$$L_k = \frac{B_k^I}{R_k^{ul}} + \frac{B_k^C}{F_k} + \frac{B_k^{bh}}{C^{bh}} + \frac{B_k^O}{R_k^{dl}}. \tag{7.15}$$

7.2.6 Problem Formulation

In this work, the cell association, subchannel allocation and transmission power control are considered in the UL only, as DUDe can only improve the UL performance. As for DL, biased RSRP cell association is along with greedy subchannel allocation, and equal power allocation over all subchannels, and all BSs transmit with their maximum power.

In the UL, our objective function is to minimize the sum-latency, which is defined as $Z(\boldsymbol{X}, \boldsymbol{\Lambda}, \boldsymbol{P}) \triangleq \Sigma_{k \in \mathcal{K}} L_k$. Specifically, $\boldsymbol{X} = \{\chi_{k,m}^{ul}\}$, $\boldsymbol{\Lambda} = \{\lambda_{k,n}^{ul}\}$, and $\boldsymbol{P} = \{P_{k,m,n}^{ul}\}$.

Moreover, the constraints are as follows:

- transmission power of each MD does not exceed the maximum transmission power P_{max}.
- Each MD can associate with only one BS in each link direction.
- Each MD-BS link can be assigned one subchannel.

Therefore, the formulated problem can be expressed as

$$\underline{\textbf{Q1:}} \tag{7.16}$$

$$\min_{\boldsymbol{X},\boldsymbol{\Lambda},\boldsymbol{P}} \quad Z(\boldsymbol{X},\boldsymbol{\Lambda},\boldsymbol{P}) \tag{7.16a}$$

$$\text{s.t.} \quad \sum_{m\in\mathcal{M}} \chi_{k,m} = 1, \qquad \forall k \in \mathcal{K}, \tag{7.16b}$$

$$\sum_{n\in\mathcal{N}} \lambda_{k,n} = 1, \qquad \forall k \in \mathcal{K}, \tag{7.16c}$$

$$0 \le P^{ul}_{k,m,n} \le P_{max}, \forall k \in \mathcal{K}, \forall m \in \mathcal{M}, \forall n \in \mathcal{N}. \tag{7.16d}$$

Problem **Q1** is non-convex and NP-hard. To efficiently solve it, it is split into two subproblems: (1) joint cell association and subchannel allocation (JCASA), and (2) power control (PC). Specifically, the FPC scheme is applied to allocate the initial UL transmission power $\boldsymbol{P}^{(0)}$. Then, the JCASA problem can be obtained as

$$\underline{\textbf{Q2:}} \tag{7.17}$$

$$\min_{\boldsymbol{X},\boldsymbol{\Lambda}} \quad Z\left(\boldsymbol{X},\boldsymbol{\Lambda},\boldsymbol{P}^{(0)}\right) \tag{7.17a}$$

$$\text{s.t.} \quad (7.16b), (7.16c), \tag{7.17b}$$

which is a combinatorial problem. After obtaining the cell association and subchannel allocation solutions $\boldsymbol{X}^*$, and $\boldsymbol{\Lambda}^*$—by solving problem **Q2**—the PC problem can be formulated as

$$\underline{\textbf{Q3:}} \tag{7.18}$$

$$\min_{\boldsymbol{P}} \quad Z(\boldsymbol{X}^*, \boldsymbol{\Lambda}^*, \boldsymbol{P}) \tag{7.18a}$$

$$\text{s.t.} \quad (7.16d). \tag{7.18b}$$

which is a non-convex and non-linear programming problem.

In Section 7.3, the JCASA problem (i.e. problem **Q2**) is modeled and solved via the student-project allocation (SPA) matching model. After that, the sum-latency minimizing power allocation algorithm for solving problem **Q3** is devised in Section 7.4.

7.3 JCASA Based on SPA

7.3.1 Student-Project Allocation Matching Model

In the two-sided SPA matching problem, the students have preferences over the projects, while the lecturers have preferences over the students [201]. In this chapter, we consider the MDs $\mathcal{U} = \{u_1, \ldots, u_k, \ldots, u_K\}$ as the students, the subchannels $\mathcal{C} = \{c_1, \ldots, c_{N\times(M+1)}\}$ as the projects[5], and the BSs $\mathcal{S} = \{s_0, s_1, \ldots, s_m, \ldots, s_M\}$ as the lecturers. Each MD u_k ranks the subchannels by preference according to the SINR, i.e. if MD u_k prefers subchannel c_i to c_j, then this implies that the SINR on subchannel c_i—based on the allocated power—is higher than that on c_j. The top $N \times M_k$ subchannels with the highest SINR form an acceptable subchannel set $\mathcal{C}_k \subseteq \mathcal{C}$, where M_k is an adaptive parameter that decides if the subchannels offered by the nearest M_k BSs are acceptable. Then, each BS s_m ranks the set of MDs that find a project offered by it acceptable, and forms a list denoted by $\mathcal{U}_m \subseteq \mathcal{U}$, which consists of the set of MDs that have the suitable task size. Specifically, since the MBS has higher computation capability, it prefers the MDs that demand more computing resources, which helps reduce the network computation latency. If an MBS prefers MD u_i to u_j, then the number of CPU cycles needed to process MD u_i's task is more than that of MD u_j. On the other hand, if an SBS prefers MD u_i to u_j, then the number of CPU cycles needed to process MD u_i's task is less than that of MD u_j. For each subchannel c_n, let $\mathcal{U}_m^n$ denote its preference list, which is obtained from $\mathcal{U}_m$ by deleting those MDs who do not find c_n acceptable.

Each BS s_m is assumed to have a capacity constraint Ω_m, indicating the maximum number of MDs that it can serve at the same time, which should not exceed the total

[5]The N subchannels are assumed to be offered by the $M+1$ BSs as unique subchannels. In turn, the N subchannels are replicated at each BS, such that a subchannel can be assigned to users associated with different base-stations. Thus, there are $N \times (M+1)$ subchannels in total.

number of subchannels N (i.e. $1 \leq \Omega_m \leq N$, $\forall s_m \in \mathcal{S}$). In practice, Ω_m is set as $\nu_m K/(M+1)$, which represents the average number of MDs per BS. Moreover, $\frac{M+1}{K} \leq \nu_m \leq \frac{M+1}{K}N$ is set to a high value if a BS s_m is rich with computation resources, and vice versa. Also, each subchannel has a capacity constraint of 1, indicating each subchannel can be occupied by one MD when associated with a BS.

Definition 7.3.1 (Assignment)**.** *An assignment $\mathcal{M}$ is a subset of $\mathcal{U} \times \mathcal{C}$ such that:*

(1) $(u_k, c_n) \in \mathcal{M}$ *(i.e. MD u_k finds subchannel c_n acceptable.*

(2) $|(u_k, c_n) \in \mathcal{M} : c_n \in \mathcal{C}| \leq 1$ *(i.e. MD u_k is assigned at most one subchannel).*

If $(u_k, c_n) \in \mathcal{M}$, where BS s_m offers subchannel c_n, then MD u_k is assigned to subchannel c_n, and associated with BS s_m. For any MD u_k, $\mathcal{M}(u_k)$ refers to the subchannel it is assigned to. For any subchannel c_n, $\mathcal{M}(c_n)$ refers the MD assigned to it. For any BS s_m, $\mathcal{M}(s_m)$ denotes the set of MDs associated with BS s_m.

Definition 7.3.2 (Matching)**.** *A matching $\mathcal{M}$ is an assignment, such that $|\mathcal{M}(u_k)| \leq 1$, $|\mathcal{M}(c_n)| \leq 1$ and $|\mathcal{M}(s_m)| \leq \Omega_m$, $\forall u_k \in \mathcal{U}$, $\forall c_n \in \mathcal{C}_m$, and $\forall s_m \in \mathcal{S}$.*

Consequently, under matching $\mathcal{M}$, each MD u_k is assigned to at most one subchannel, no subchannel $c_n \in \mathcal{C}$ is assigned to more than one MD, and no BS s_m is assigned to more than Ω_m MDs.

Definition 7.3.3 (Subscription)**.** *A subchannel $c_n \in \mathcal{C}_m$ is said to be under-subscribed, full, or over-subscribed if $|\mathcal{M}(c_n)| < 1$, $|\mathcal{M}(c_n)| = 1$, or $|\mathcal{M}(c_n)| > 1$, respectively. Similarly, a BS $s_m \in \mathcal{S}$ is considered to be under-subscribed, full, or over-subscribed if $|\mathcal{M}(s_m)| < \Omega_m$, $|\mathcal{M}(s_m)| = \Omega_m$, or $|\mathcal{M}(s_m)| > \Omega_m$, respectively.*

Definition 7.3.4 (Blocking)**.** *The pair $|(u_k, c_n) \in (\mathcal{U} \times \mathcal{C}) \backslash \mathcal{M}$ is said to block a matching $\mathcal{M}$ if:*

(a) $c_n \in \mathcal{C}_k$ (i.e. u_k finds c_n acceptable).

(b) Either u_k is unassigned in $\mathcal{M}$, or u_k prefers c_n to $M(u_k)$.

(c) Either

(c1) c_n is under-subscribed and s_m is under-subscribed, or

(c2) c_n is under-subscribed, s_m is full, and either $u_k \in \mathcal{M}(s_m)$ or s_m prefers u_k to the worst MD in $\mathcal{M}(s_m)$, or

(c3) c_n is full and s_m prefers u_k to the worst MD in $\mathcal{M}(c_n)$, where s_m is the BS who provides c_n.

Definition 7.3.5 (Stable matching)**.** *A matching $\mathcal{M}$ is considered stable if $\mathcal{M}$ contains no blocking pairs.*

Different from most previous works, which consider BS association and subchannel allocation separately, the SPA algorithm performs them jointly and simultaneously. Initially, all MDs are free, and all subchannels and BSs are unsubscribed. As long as there is an MD, u_k, that is free and with a non-empty preference list, it can apply to the first subchannel c_n on $\mathcal{C}_k$. Let s_m be the BS that offers c_n. Immediately, u_k becomes provisionally assigned to c_n (and to s_m). If c_n is over-subscribed, then s_m rejects the worst MD u_r assigned to c_n and the pair (u_r, c_n) will be deleted. Similarly, if BS s_m is over-subscribed, then s_m rejects its worst assigned MD u_r and the pair (u_r, c_t) will be deleted from $\mathcal{M}$, where c_t was the subchannel assigned to u_r. On the other hand, if c_n is full and u_r is the worst MD assigned to c_n, then delete (u_t, c_n), where u_t is each successor of u_r on $\mathcal{U}_m^n$. Similarly, if s_m is full and u_r is the worst MD assigned to s_m, then delete (u_t, c_v), where u_t is each successor of u_r on $\mathcal{U}_m$ and c_v is each subchannel offered by s_m that u_t finds acceptable. The SPA algorithm is described in **Algorithm 9**[6].

The SPA algorithm converges with polynomial-time complexity of O $(|\mathcal{U}| \times |\mathcal{C}|)$, where $|\mathcal{U}| = K$ and $|\mathcal{C}| = N \times (M+1)$ are the number of MDs and subchannels, respectively. The stable matching resulting from the SPA algorithm is optimal with respect to each assigned MD [201]. This is because each user is assigned to its most preferred subchannel available on its preference list, and no stable pair is deleted during the execution of the SPA algorithm [201]. In turn, each user is simultaneously assigned to the best channel it can get in any stable matching.

7.3.2 Swap Matching

SPA-based JCASA is with externalities (also known as peer effects) [204]. The preference lists of the MDs and subchannels are initially constructed without considering the inter-cell interference over each subchannel, since no BS association or subchannel allocation initially exists. Thus, although **Algorithm 9** yields a stable matching, as soon

[6]The BS association and subchannel allocation are applied after the execution of the SPA algorithm outlined in **Algorithm 1**. It should be noted that the accept and/or reject processes only occur during the execution of **Algorithm 1** at a network centralized controller (e.g. a MBS), and not during the network operation. That is, the network operation takes place after the completion of the execution of the proposed scheme shown in Fig. 2. Therefore, it will not cause call drops or failed handovers, and there is no data exchange between MDs and BSs during the execution of the SPA algorithm. Additionally, once a subchannel is occupied during the network operation, it will not be re-allocated to other MDs.

Algorithm 9 SPA based JCASA

Input: Preference lists $\mathcal{U}_m$, $\mathcal{U}_m^n$ and $\mathcal{C}_k$, for $\forall s_m \in \mathcal{S}$, $\forall c_n \in \mathcal{C}$ and $\forall u_k \in \mathcal{U}$.
Initialization: All MDs are free, and all subchannels and BSs are unsubscribed.
while (Some MD u_k is free and has a non-empty list $\mathcal{C}_k$) **do**
    c_n = first subchannel on $\mathcal{C}_k$;
    s_m = the BS that offers c_n;
    provisionally assign subchannel c_n and BS s_m to MD u_k;
    if (c_n is over-subscribed) **then**
        u_r = worst MD assigned to subchannel c_n;
        s_m = the BS that offers subchannel c_n;
        s_m rejects u_r and break assignment (u_r, c_n);
    else
        if (s_m is over-subscribed) **then**
            u_r = worst MD assigned to BS s_m;
            c_t = the subchannel assigned to MD u_r;
            s_m rejects u_r and break assignment (u_r, c_t);
        end if
    end if
end while
if (c_n is full) **then**
    u_r = worst MD assigned to subchannel c_n;
    u_l = each of the successor of u_r on $\mathcal{U}_m^n$;
    Break assignment (u_l, c_n);
end if
if (s_m is full) **then**
    u_r = worst MD assigned to BS s_m;
    u_l = each successor of u_r on $\mathcal{U}_m$;
    c_v = each subchannel offered by s_m that u_t finds acceptable;
    Break assignment (u_l, c_v);
end if
Output: Stable matching $(u_k, c_n) \in \mathcal{U} \times \mathcal{C}$.

as the subchannels are assigned to the MDs, the appearance of inter-cell interference terms may not necessarily preserve the stability of the assignment. For this reason, swap matching is adopted among the MDs associated with the same BS.

Definition 7.3.6 (Swap-Blocking Pair)**.** *Two subchannels c_n (assigned to MD u_k) and $c_{n'}$ (assigned to MD $u_{k'}$, or not occupied)—for $n' \neq n$ and $k' \neq k$—offered by BS s_m form a swap-block pair if:*

(a) MD u_k can get higher data rate on subchannel $c_{n'}$,

(b) subchannel $c_{n'}$ is assigned to MD $u_{k'}$, but MD $u_{k'}$ can get higher data rate on subchannel c_n, and the sum UL transmission latency of MDs u_k and $u_{k'}$ is lower, and

(c) sum-latency of all MDs transmitting over subchannel c_n and $c_{n'}$ is lower after the swap[7]*.*

Given a matching $\mathcal{M}$, when a swap-blocking pair (c_n, $c_{n'}$) exists, MDs u_k and $u_{k'}$ swap their subchannels, while keeping the other MD and subchannel assignments unchanged. In turn, the updated matching is obtained as

$$\begin{aligned}\overline{\mathcal{M}} = &\left\{\mathcal{M} \setminus \left\{\left(u_k, \mathcal{M}\left(u_k\right)\right), \left(u_r, \mathcal{M}\left(u_r\right)\right)\right\}\right\} \\ &\cup \left\{\left(u_k, \mathcal{M}\left(u_r\right)\right), \left(u_r, \mathcal{M}\left(u_k\right)\right)\right\},\end{aligned} \tag{7.19}$$

On the other hand, if $c_{n',m}$ is not occupied, then

$$\overline{\mathcal{M}} = \left\{\mathcal{M} \setminus \left\{\left(u_k, \mathcal{M}\left(u_k\right)\right)\right\}\right\} \cup \left\{\left(u_k, \mathcal{M}\left(u_r\right)\right)\right\}. \tag{7.20}$$

Definition 7.3.7 (Two-Sided Exchange-Stability)**.** *A matching $\overline{\mathcal{M}}$ is said to be two-sided exchange-stable if it does not contain any swap-blocking pairs [205].*

The swap matching algorithm is described as follows. Each MD searches if there is a subchannel that can provide a higher data rate. If there is such a subchannel, check if it can form a swap-blocking pair. If a swap-blocking pair is found, then a swap-operation is performed, and the matching is updated. The process is given in **Algorithm 10**. It is obvious that **Algorithm 10** converges to a matching $\overline{\mathcal{M}}$ in a finite

[7] Note that swapping users within one BS may trigger swaps for users in other BS. This is due to the frequency re-use.

number of iterations, since the number of subchannel pairs that can be swapped for each MD pair is finite. Note that there are $\binom{N}{2} = \frac{1}{2}\left(N^2 - N\right)$ subchannel pairs. Thus, the worst-case complexity is of order $O\left(N^2\right)$ per user pair.

Algorithm 10 Swap Matching for MDs over the same BS

Input: Matching $\mathcal{M}$
for Each MD assign to c_n **do**
  if there is a subchannel $c_{n'}$ that can provide higher data rate **then**
    if $(c_n, c_{n'})$ is a swap-blocking pair **then**
      Perform a swap-operation;
      Update matching $\overline{\mathcal{M}}$;
    end if
  end if
end for
Output: Updated matching $\overline{\mathcal{M}}$.

7.4 Power Allocation

Since this work is focussed on minimizing the sum-latency, and does not optimize the DL latency, problem **Q3** can be simplified as

$$\underline{\textbf{Q4:}} \tag{7.21}$$

$$\min_{\mathbf{P}} \quad \sum_{k\in\mathcal{K}} \left(\frac{B_k^I}{R_k^{ul}(\mathbf{P})} + \frac{B_k^C}{F_k} + \frac{B_k^{bh}}{C^{bh}} \right) \tag{7.21a}$$

$$\text{s.t.} \quad 0 \le P_k^{ul} \le P_{max}, \quad \forall k \in \mathcal{K}. \tag{7.21b}$$

For each MD, when $\mathbf{X}$,$\boldsymbol{\lambda}$ are fixed, the term $\frac{B_k^C}{F_k} + \frac{B_k^{bh}}{C^{bh}}$ is also fixed. Thus, **Q4** can be converted to

$$\underline{\textbf{Q5:}} \tag{7.22}$$

$$\min_{\mathbf{P}} \quad \sum_{k\in\mathcal{K}} \frac{B_k^I}{R_k^{ul}(\mathbf{P})} \tag{7.22a}$$

$$\text{s.t.} \quad 0 \le P_k^{ul} \le P_{max}, \quad \forall k \in \mathcal{K}. \tag{7.22b}$$

Problem **Q5** is non-convex and NP-hard. Alternatively, it can be transformed as

$$\underline{\textbf{Q6:}} \tag{7.23}$$

$$\min_{\mathbf{P},\boldsymbol{\tau}} \quad \sum_{k\in\mathcal{K}} \tau_k \tag{7.23a}$$

$$\text{s.t.} \quad \frac{B_k^I}{R_k^{ul}(\mathbf{P})} \leq \tau_k, \qquad \forall k \in \mathcal{K}, \tag{7.23b}$$

$$0 \leq P_k^{ul} \leq P_{max}, \quad \forall k \in \mathcal{K}. \tag{7.23c}$$

Proposition 1. *If* $(\mathbf{P}^*, \boldsymbol{\tau}^*)$ *is the solution of Problem* ***Q6****, then there exists* $\boldsymbol{\lambda}^* = [\lambda_1, \lambda_2, ..., \lambda_k]$ *such that* $\mathbf{P}^*$ *satisfies the KKT conditions of the following problem upon setting* $\boldsymbol{\lambda} = \boldsymbol{\lambda}^*$ *and* $\boldsymbol{\tau} = \boldsymbol{\tau}^*$*,*

$$\underline{\textbf{\textit{Q7:}}} \tag{7.24}$$

$$\min_{\mathbf{P}} \quad \sum_{k\in\mathcal{K}} \lambda_k (B_k^I - \tau_k R_k^{ul}(\mathbf{P})) \tag{7.24a}$$

$$\text{s.t.} \quad 0 \leq P_k^{ul} \leq P_{max}, \quad \forall k \in \mathcal{K}. \tag{7.24b}$$

Proof: The Lagrangian of Problem **Q6** is expressed as

$$\mathcal{L}(\boldsymbol{\lambda}, \mathbf{P}, \boldsymbol{\tau}) = \sum_{k\in\mathcal{K}} \tau_k + \sum_{k\in\mathcal{K}} \lambda_k \left(B_k^I - \tau_k R_k^{ul}(\mathbf{P}) \right). \tag{7.25}$$

If $(\mathbf{P}^*, \boldsymbol{\tau}^*)$ is the solution of Problem **Q6**, then there exists $\boldsymbol{\lambda}^*$ satisfying the following KKT conditions, $\forall k \in \mathcal{K}$, such that

$$\frac{\partial \mathcal{L}(\boldsymbol{\lambda}, \mathbf{P}, \boldsymbol{\tau})}{\partial \tau_k} = 1 - \lambda_k^* R_k^{ul}(\mathbf{P}^*) = 0, \tag{7.26}$$

$$\frac{\partial \mathcal{L}(\boldsymbol{\lambda}, \mathbf{P}, \boldsymbol{\tau})}{\partial P_k} = -\sum_{k\in\mathcal{K}} \lambda_k^* \tau_k^* \frac{\partial R_k^{ul}(\mathbf{P}^*)}{\partial P_k} = 0, \tag{7.27}$$

$$\lambda_k^* (B_k^I - \tau_k^* R_k^{ul^*}(\mathbf{P})) = 0, \tag{7.28}$$

$$B_k^I - \tau_k^* R_k^{ul^*}(\mathbf{P}) \leq 0, \tag{7.29}$$

$$\lambda_k^* \geq 0, \tag{7.30}$$

and

$$0 \leq P_k^{ul} \leq P_{max}. \tag{7.31}$$

According to (7.26), it can be verified that

$$\lambda_k^* = \frac{1}{R_k^{ul}(\mathbf{P}^*)} > 0. \tag{7.32}$$

Furthermore, (7.28) implies that

$$\tau_k^* = \frac{B_k^I}{R_k^{ul}(\mathbf{P}^*)} > 0. \tag{7.33}$$

Lastly, since (7.26), (7.27) and (7.31) are also the KKT conditions of Problem **Q7**, Proposition 1 is proved.

Based on **Proposition 1**, when $\boldsymbol{\lambda} = \boldsymbol{\lambda}^*$ and $\boldsymbol{\tau} = \boldsymbol{\tau}^*$, P^* satisfies the following constraints

$$\lambda_k = \frac{1}{R_k^{ul}(\mathbf{P}^*)}, \quad \forall k \in \mathcal{K}, \tag{7.34}$$

and

$$\tau_k = \frac{B_k^I}{R_k^{ul}(\mathbf{P}^*)}, \quad \forall k \in \mathcal{K}. \tag{7.35}$$

In this way, Problem **Q6** is transformed into **Q7**, which can be solved in two steps. Firstly, fix $\boldsymbol{\lambda}$ and $\boldsymbol{\tau}$, and obtain $\mathbf{P}$ by solving Problem **Q7** via **Algorithm 12**, which will be discussed shortly. Then, fix $\mathbf{P}$, and update $\boldsymbol{\lambda}$ and $\boldsymbol{\tau}$ via the modified Newton's algorithm until convergence [206, 207]. The process is given in **Algorithm 11**, where

$$\rho_k(\lambda_k) = \lambda_k R_k^{ul}(\mathbf{P}^*) - 1, \quad \forall k \in \mathcal{K}, \tag{7.36}$$

and

$$\kappa_k(\tau_k) = \tau_k R_k^{ul}(\mathbf{P}^*) - B_k^I, \quad \forall k \in \mathcal{K}. \tag{7.37}$$

In order to solve Problem **Q7**, which is non-convex since the rate function $R_k^{ul}(\mathbf{P})$ is non-convex, it is transformed into a convex problem. Note that the rate function in (7.6) can be more conveniently be written as (7.38).

$$R_k^{ul}(\mathbf{P}) = B \sum_{m \in \mathcal{M}} \sum_{n \in \mathcal{N}} \chi_{k,m}^{ul} \lambda_{k,n}^{ul} \log_2 \left(1 + \frac{P_k^{ul} h_{k,m,n}^{ul}}{\sum\limits_{j \in \mathcal{K}, j \neq k} \lambda_{j,n}^{ul} P_j^{ul} h_{j,m,n} + \sigma^2} \right) \tag{7.38}$$

Algorithm 11 Optimal Power Allocation

1: **Initialization:** $\mathbf{P}^{(0)}$, $t=0$, $\zeta \in (0,1)$, $\varepsilon \in (0,1)$, calculate λ_k and τ_k by (7.34) and (7.35), respectively.
2: **repeat**
3: Update $\mathbf{P}^{(t+1)}$ via **Algorithm 4**;
4: Update λ_k and τ_k as follows

$$\lambda_k^{(t+1)} = \lambda_k^{(t)} - \frac{\zeta^{i^{(t+1)}} \rho_k\left(\lambda_k^{(t)}\right)}{R_k^{ul}\left(\mathbf{P}^{(t+1)}\right)}, \quad \forall k \in \mathcal{K},$$

and

$$\tau_k^{(t+1)} = \tau_k^{(t)} - \frac{\zeta^{i^{(t+1)}} \kappa_k\left(\tau_k^{(t)}\right)}{R_k^{ul}\left(\mathbf{P}^{(t+1)}\right)}, \quad \forall k \in \mathcal{K},$$

where $i^{(t+1)}$ is the smallest integer among $i \in \{1,2,3,...\}$ satisfying

$$\begin{aligned}
&\sum_{k\in\mathcal{K}} \left| \rho_k \left(\lambda_k^{(t)} - \frac{\zeta^i \rho_k\left(\lambda_k^{(t)}\right)}{R_k^{ul}\left(\mathbf{P}^{(t+1)}\right)} \right) \right|^2 \\
&\quad + \sum_{k\in\mathcal{K}} \left| \kappa_k \left(\tau_k^{(t)} - \frac{\zeta^i \kappa_k\left(\tau_k^{(t)}\right)}{R_k^{ul}\left(\mathbf{P}^{(t+1)}\right)} \right) \right|^2 \\
&\quad \leq \left(1-\varepsilon\zeta^i\right)^2 \sum_{k\in\mathcal{K}} \left(\left| \rho_k\left(\lambda_k^{(t)}\right) \right|^2 + \left| \kappa_k\left(\tau_k^{(t)}\right) \right|^2 \right);
\end{aligned}$$

5: Set $t = t+1$;
6: **until** the following conditions are satisfied:

$$\lambda_k^{(t)} R_k^{ul}\left(\mathbf{P}^{(t)}\right) - 1 = 0, \quad \forall k \in \mathcal{K},$$

and

$$\tau_k^{(t)} R_k^{ul}\left(\mathbf{P}^{(t)}\right) - B_k^I = 0, \quad \forall k \in \mathcal{K};$$

7: **Output:** Optimal $\mathbf{P}^* = \mathbf{P}^{(t)}$.

Now, consider the lower-bound approximation [156]

$$\log_2(1+\gamma) \geq \mu_1 \log_2(\gamma) + \mu_2, \tag{7.39}$$

where $\gamma \geq 0$, and the bound is tight for $\gamma = \bar{\gamma}$. Moreover,

$$\mu_1 = \frac{\bar{\gamma}}{\bar{\gamma}+1}, \tag{7.40}$$

and

$$\mu_2 = \log_2(1+\bar{\gamma}) - \mu_1 \log_2(\bar{\gamma}). \tag{7.41}$$

By using the variable substitution $P_k^{ul} = 2^{Q_k^{ul}}$, the rate function can be lower-bounded as (7.42).

$$\begin{aligned} & R_k^{ul}(\mathbf{P}) \geq \overline{R}_k^{ul}(\mathbf{Q}) \\ & \triangleq B\left(\sum_{m\in\mathcal{M}}\sum_{n\in\mathcal{N}} \chi_{k,m}^{ul}\lambda_{k,n}^{ul}\left(\mu_{1,k}\log_2\left(\frac{2^{Q_k^{ul}}h_{k,m,n}^{ul}}{\sum\limits_{j\in\mathcal{K},j\neq k}\lambda_{j,n}^{ul}2^{Q_j^{ul}}h_{j,m,n}+\sigma^2}\right)+\mu_{2,k}\right)\right) \\ & = B\left(\sum_{m\in\mathcal{M}}\sum_{n\in\mathcal{N}} \chi_{k,m}^{ul}\lambda_{k,n}^{ul}\left(\mu_{1,k}Q_k^{ul}+\mu_{1,k}\log_2(h_{k,m,n}^{ul})-\mu_{1,k}\log_2\left(\sum_{j\in\mathcal{K},j\neq k}\lambda_{j,n}^{ul}2^{Q_j^{ul}}h_{j,m,n}+\sigma^2\right)+\mu_{2,k}\right)\right) \end{aligned} \tag{7.42}$$

Hence, Problem **Q7** can be rewritten as

Q8: (7.43)

$$\min_{\mathbf{Q}} \quad \bar{L}(\mathbf{Q}) = \sum_{k\in\mathcal{K}} \lambda_k(B_k^I - \tau_k\overline{R}_k^{ul}(\mathbf{Q})) \tag{7.43a}$$

$$\text{s.t.} \quad 0 \leq 2^{Q_k^{ul}} \leq P_{max}, \quad \forall k \in \mathcal{K}. \tag{7.43b}$$

Remark 10. *For the rate function $\overline{R}_k^{ul}(\mathbf{Q})$ in (7.42), the negative log-sum-exp term is concave in $\mathbf{Q}$ [155]. Thus, $\overline{R}_k^{ul}(\mathbf{Q})$ is concave and $\lambda_k\left(B_k^I - \tau_k\overline{R}_k^{ul}(\mathbf{Q})\right)$ is convex. More importantly, the sum of the convex functions is also convex [157], and hence, the lower-bounded objective function $\sum_{k\in\mathcal{K}}\lambda_k\left(B_k^I - \tau_k\overline{R}_k^{ul}(\mathbf{Q})\right)$ is convex in $\mathbf{Q}$. Also, the constraint set of Problem **Q8** is convex.*

Accordingly, Problem **Q8** can be solved optimally for fixed values of $\mu_{1,k}$ and $\mu_{2,k}$ via any standard convex optimization package. By iteratively updating $\mu_{1,k}$ and $\mu_{2,k}$ via (7.40) and (7.41), respectively, in which case $\mathbf{P}^{(t+1)}$ in **Algorithm 11** is obtained via **Algorithm 12**. Hence, the global optimal solution of problem **Q5** can be obtained.

The complexity of **Algorithm 11** is mainly dependent on Step 3, as all the other steps are based on explicit expressions. Since a convex optimization problem is solved in each iteration in **Algorithm 12**, it has polynomial-time complexity [157]. As for convergence, **Algorithm 11** is guaranteed to converge in a finite number of iterations [206].

Finally, a flow-chart of the proposed joint BS association, subchannel allocation, and power control scheme is given in Fig. 7.2. Particularly, the proposed scheme

Algorithm 12 Solution of Problem **Q8**

1: **Initialization:** Set error tolerance $\varepsilon \in (0,1)$, iteration index $t = 0$, $\mu_{1,k} = 1$, $\mu_{2,k} = 0$, $\forall k \in \mathcal{K}$, select a feasible $\mathbf{Q}^{(0)}$, and calculate $\bar{L}(\mathbf{Q}^{(0)})$.
2: **repeat**
3: Set $t = t + 1$;
4: Update $\mu_{1,k}^{(t)}$ and $\mu_{2,k}^{(t)}$ by (7.40) and (7.41), $\forall k \in \mathcal{K}$;
5: Compute $\bar{L}(\mathbf{Q}^{(t)})$ by solving Problem **Q8**;
6: **until** $\left|\bar{L}(\mathbf{Q}^{(t)}) - \bar{L}(\mathbf{Q}^{(t-1)})\right| \leq \varepsilon$
7: **Output:** $\mathbf{P}^{\star} = 2^{\mathbf{Q}^{(t)}}$

starts by performing BS association and subchannel allocation via the SPA algorithm given in **Algorithm 9**. After that, if at least one swap-blocking pair is found, then the corresponding MDs' subchannels are swapped via **Algorithm 10**. Then, optimal power allocation is applied using **Algorithms 11** and **12**. After the power allocation, if a swap-blocking pair is found, **Algorithm 10** is applied again, which is followed by optimal power allocation, and so on. This is to ensure stability after power allocation until no further swap-blocking pairs can be found[8].

7.5 Performance Evaluation

In this section, the performance of the proposed DUDe access scheme is evaluated and compared with benchmark schemes in terms of latency and energy-efficiency (EE). The network energy-efficiency in the UL is determined as [78]

$$EE = \frac{\sum_{k\in\mathcal{K}} R_k^{ul}}{\sum_{k\in\mathcal{K}}\sum_{m\in\mathcal{M}}\sum_{n\in\mathcal{N}} P_{k,m,n}^{ul}}. \tag{7.44}$$

In what follows, the proposed SPA algorithm along with swap matching (SM), and optimal power allocation (OPA) are compared to the CUDA scheme, which is based on biased RSRP for cell association, greedy (G) subchannel allocation [132][9], and FPC. Moreover, a decoupled access scheme, called Min-PL-F-FPC is also compared, which is based on minimum path-loss (min-PL) cell association [2], greedy subchannel allocation, and FPC. In the min-PL criterion, the MDs are connected in the UL to the

[8]Generally speaking, it has been determined that the possibility of finding a swap-blocking pair to perform swap matching is very low after the first loop.

[9]In the greedy subchannel allocation algorithm, subchannels with high SINR are preferentially assigned to the MDs [132].

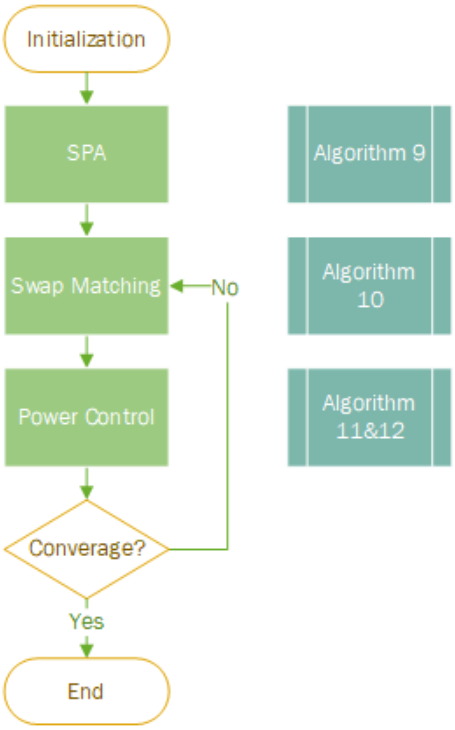

Figure 7.2: Flow-chart of the proposed scheme.

BS with the lowest path-loss. Particularly, a typical MD $k \in \mathcal{K}$ is associated with BS $m \in \mathcal{M}$ in the UL if

$$P^{ul}_{k,m} W_m PL_{k,m}{}^{-1} \geq P^{ul}_{k,m'} W_{m'} PL^{-1}_{k,m'}, \quad \forall m, m' \in \mathcal{M}, \tag{7.45}$$

where W is the UL cell bias value, which is positive and refers to expanding the coverage of the cells. Moreover, $PL_{k,m}$ is the UL path-loss between MD k and BS m. Table 7.2 summarizes the evaluated resource allocation schemes, while the simulation parameters are given in Table 7.3.

Fig. 7.3 depicts the relationship between the UL sum transmission latency and the

Table 7.2: Resource Allocation Schemes

Scheme	**Cell-Association**	**Subchannel Allocation**	**Power Control**
CUDA	Biased RSRP	Greedy	FPC
Min-PL-G-FPC	Min-PL	Greedy	FPC
SPA-FPC	SPA		FPC
SPA-SM-FPC	SPA-SM		FPC
SPA-SM-OPA	SPA-SM		OPA

Table 7.3: Simulation Parameters

Parameters	**MD**	**MBS**	**SBS**
Maximum transmission power	23 dBm	46 dBm	30 dBm
Spatial density	250/km^2	5/km^2	25/km^2
Spatial distribution	Uniform distribution		
Lognormal shadowing	$\mu = 0$, $\sigma = 4$ dB [148]		
Path-loss exponent	3 [148]		
Operating frequency	2 GHz		
UL bandwidth	5 MHz [84]		
DL bandwidth	5 MHz [84]		
Subcarrier spacing	15 kHz [84]		
Number of subchannels	25		
Noise spectral density	-174 dBm/Hz		
Target received power P_0	-80 dBm		
PL compensation factor w	0.7		
Computation capacity	N/A	36 GHz	3.6GHz [200]
Backhaul link capacity C^{bh}	10 Mbits/s [200]		
Offloaded task size B_k^I	(5 Mbits, 10 Mbits)		
Output to input bits proportion α_k	0.2 [189]		
CPU cycles per bit β_k	330, 960, or 1900 [198]		
M_k	2	N/A	N/A
ν_m	N/A	2	0.8

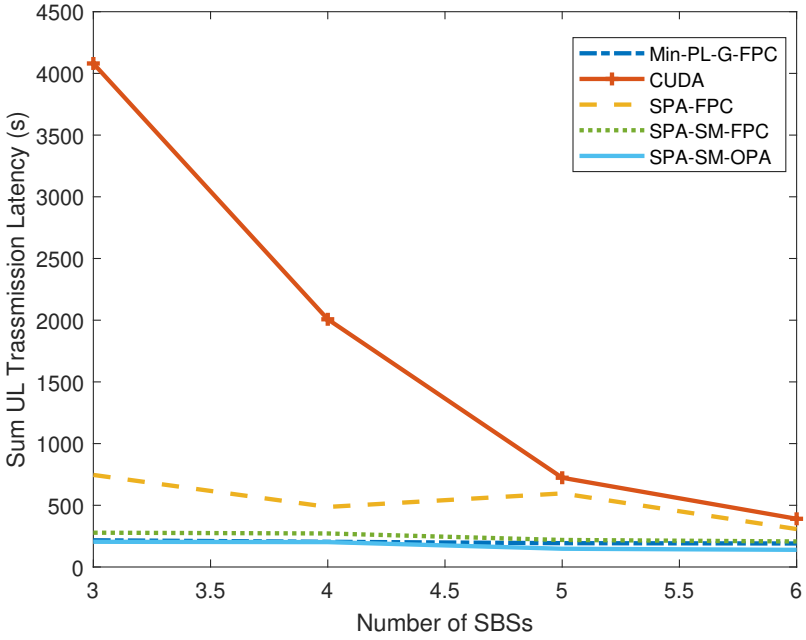

Figure 7.3: UL sum transmission latency.

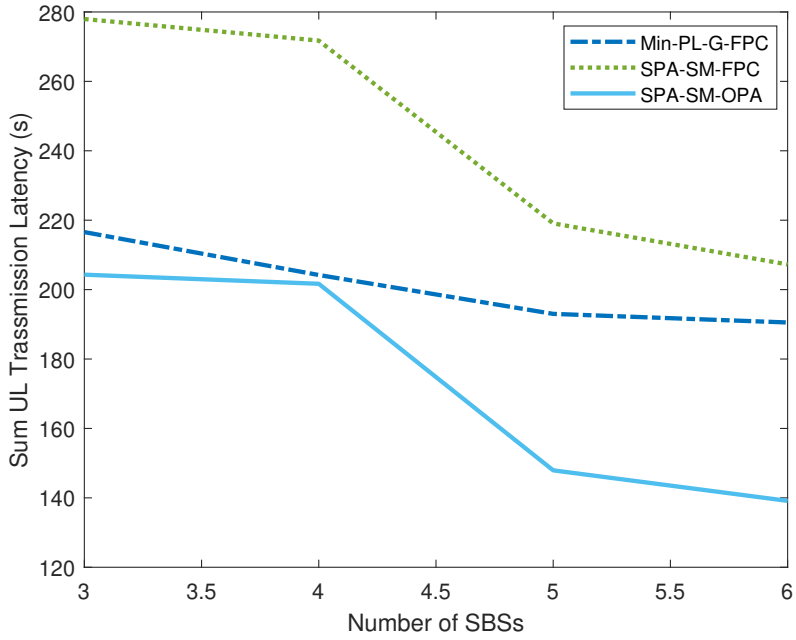

Figure 7.4: UL sum transmission latency.

number of SBSs. As can be seen, the UL transmission latency of the CUDA scheme is several times higher than all its decoupled counterparts. This is because the decoupled schemes shorten the MD-BS distance, and reduce the interference in the network. Due to peer effects, the sum-latency of the SPA scheme decreases with the number of SBSs, which demonstrates the importance of swap matching. Since the latency of the CUDA and SPA-FPC schemes are significantly higher than other schemes, Fig. 7.4 focuses on the Min-PL-G-FPC, SPA-SM-FPC, and SPA-SM-OPA schemes. Particularly, the UL transmission latency of the SPA-SM-FPC is higher than the Min-PL scheme, since some computation-intensive tasks are offloaded to the MBS cloudlet to reduce the computation latency, but the communication latency increases at the same time. Furthermore, with the aid of the proposed OPA scheme, the transmission latency of SPA-SM-OPA decreases by as much as 20% and is lower than the latency of the Min-PL-G-FPC scheme.

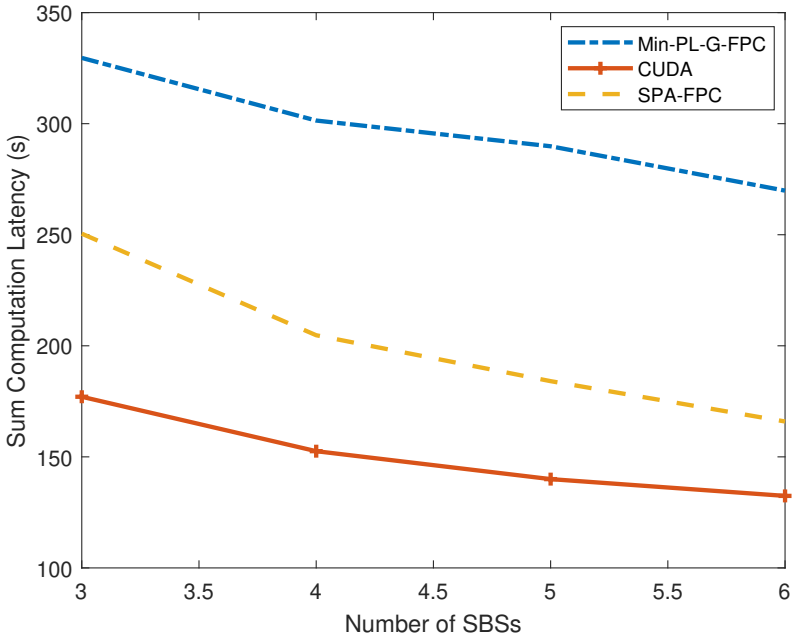

Figure 7.5: Sum computation latency of Min-PL-G-FPC, CUDA and SPA-FPC schemes.

Fig. 7.5 illustrates the sum computation latency of the different schemes. Since the SPA-FPC, SPA-SM-FPC, and SPA-SM-OPA schemes choose the same UL serving BS for each MD, and have the same computation latency, only the SPA-FPC scheme is considered. When the number of SBSs increases, there are more computational resources, and so the computation latency decreases. It can be seen that the SPA-FPC

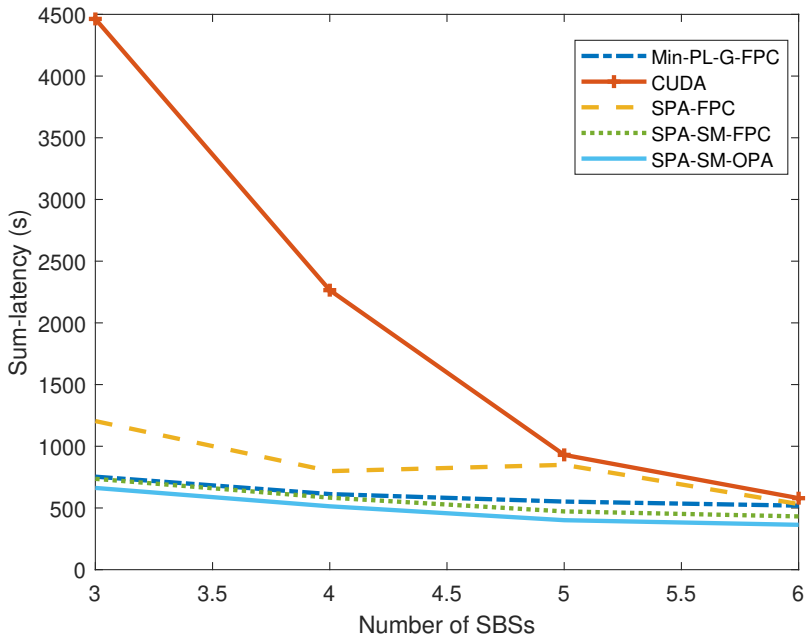

Figure 7.6: Sum-latency.

scheme has the lowest computation latency, because most computation-intensive tasks are offloaded to the MBS cloudlet that has high computation capability. Most of the MDs are associated with the MBS by the CUDA scheme, and so the computation latency for the CUDA scheme is also low. As for the Min-PL-G-FPC scheme, it offloads most MDs to the SBSs and does not offload all the computation-intensive tasks to the MBS cloudlet, thus its computation latency is the highest.

Fig. 7.6 illustrates the sum-latency of all schemes, which is the sum of UL and DL transmission latency, backhaul latency, and computation latency. As the DL latency of all the schemes is the same and the backhaul latency is very small compared to communication and computation latency, the sum-latency mainly depends on the UL transmission latency and computation latency. It is clear from Fig. 7.6 that the latency of all the DUDe schemes is much lower than that of the CUDA scheme. The sum-latency of the SPA-SM-OPA scheme is the lowest, and only 15% to 60% of the CUDA scheme. According to Fig. 7.7, the sum-latency of SPA-SM-OPA scheme is around 15% lower than that of the Min-PL-G-FPC scheme.

Another important metric to consider in this scenario is the fairness metric. Fig. 7.8 and 7.9 utilizes the Jain's fairness index [208] to evaluate the UL transmission latency and computation latency fairness, respectively. As the BSs are uniformly distributed in our simulations, the Min-PL scheme that selects the UL serving BS from the

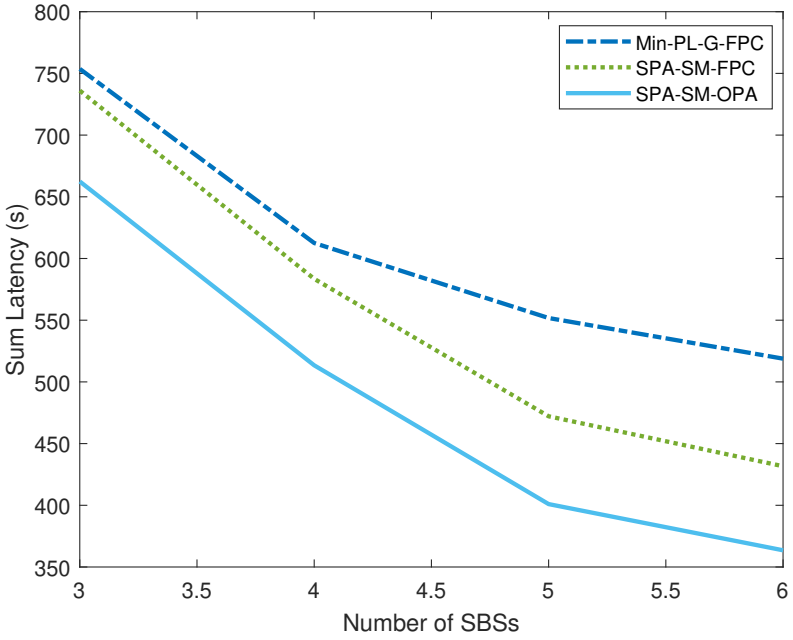

Figure 7.7: Sum-latency of Min-PL-G-FPC, SPA-SM-FPC and SPA-SM-OPA.

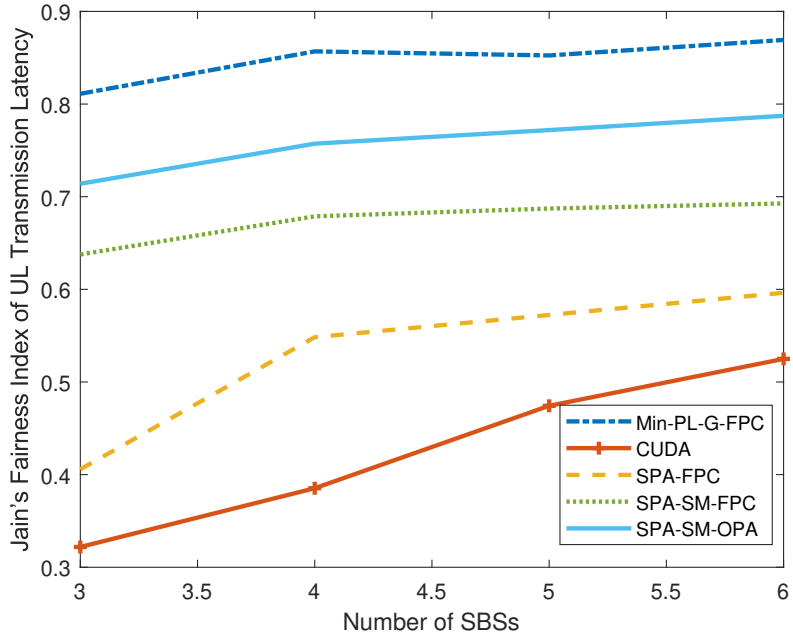

Figure 7.8: Jain's Fairness Index of UL Transmission Latency vs. number of SBSs.

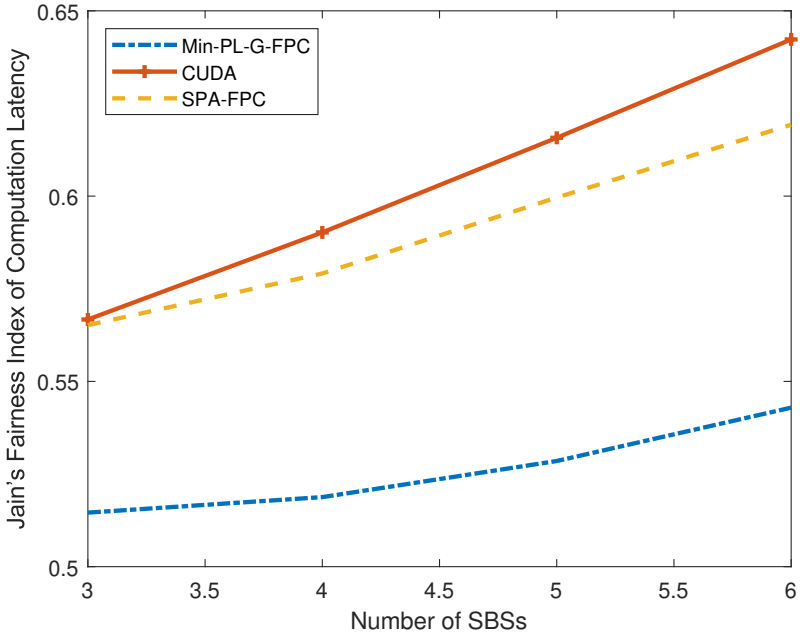

Figure 7.9: Jain's Fairness Index of Computation Latency vs. number of SBSs.

perspective of the UL path-loss can guarantee the UL transmission fairness to the most extent. The SPA scheme jointly considers the computation and transmission latency and offloads the computationally-intensive tasks to the MBS, it may cause high transmission latency to those MDs, so the fairness index is lower, but the value is still higher than the traditional coupled UL and DL access (CUDA) scheme, especially when combining SPA with swap matching, which helps reduce the inter-cell interference. As for the computation latency fairness, since the CUDA scheme associates most MDs with the MBS, and the limited SBS computation resources are allocated to the rest of the MDs, the fairness index of CUDA scheme is the highest. The SPA scheme allocates the computationally-intensive tasks to the MBSs and the others to the nearby SBSs, which can also achieve similar fairness as the CUDA scheme[10]. The Min-PL scheme does not consider the computation capabilities of different kinds of BSs, the MDs near the SBSs but have computationally-intensive tasks may suffer from high computation latency, so its fairness index is the lowest.

Fig. 7.10 depicts the UL transmission EE of the different schemes, which increases with the number of SBSs. It can be seen that the normalized EE of the Min-PL-G-FPC scheme is the highest, since it associates each MD with their nearest BS; while the

[10]SPA-FPC, SPA-SM-FPC and SPA-SM-OPA schemes have the same computation latency, as the MD-BS pairs are the same in these schemes.

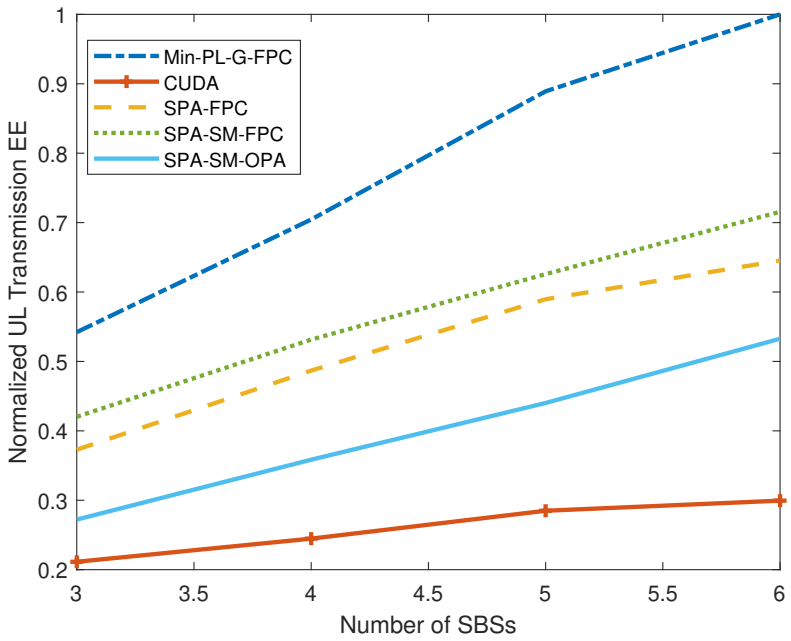

Figure 7.10: Normalized UL transmission EE vs. number of SBSs.

EE of the CUDA scheme is the lowest, which associates most MDs with the MBS. Furthermore, swap matching can improve the SINR of some MDs by swapping their subchannels, and thus improves their EE. The EE of the SPA-SM-FPC scheme is twice higher than the Min-PL-G-FPC scheme. The aim of the proposed power allocation scheme is to reduce the network sum-latency, and so the transmission powers of some MDs are increased, which reduces EE.

Fig. 7.11 depicts the 10^{th}, 20^{th}, 50^{th}, 80^{th}, and 90^{th} percentile data rates per MD. It can be seen that the CUDA scheme has the lowest data rates, especially the 10^{th} percentile data rates, because it allocates too many MDs to the MBS; and for those MDs at the MBS edge, their UL data rates are relatively low. The Min-PL scheme selects the UL serving BS by the UL path-loss, which results in a balanced MD distribution among BSs, and the data rate distribution is the most balanced (e.g. the 90^{th} percentile data rate of the Min-PL scheme is only 70% higher than it 10^{th} percentile data rate). The SPA-SM scheme has lower 10^{th}, 20^{th}, 50^{th} percentile data rates as it offloads more MDs to the MBS. However, its 80^{th} and 90^{th} percentile data rates are higher, which is due to its better inter-cell interference control. Compared with the SPA-SPA-SM-FPC scheme, the proposed optimal power allocation scheme (OPA) increases the 10^{th}, 20^{th}, 50^{th} percentile data rates at the expense of the 80^{th} and 90^{th} percentile data rates, which reduces the overall UL transmission latency, as shown in Fig. 7.4.

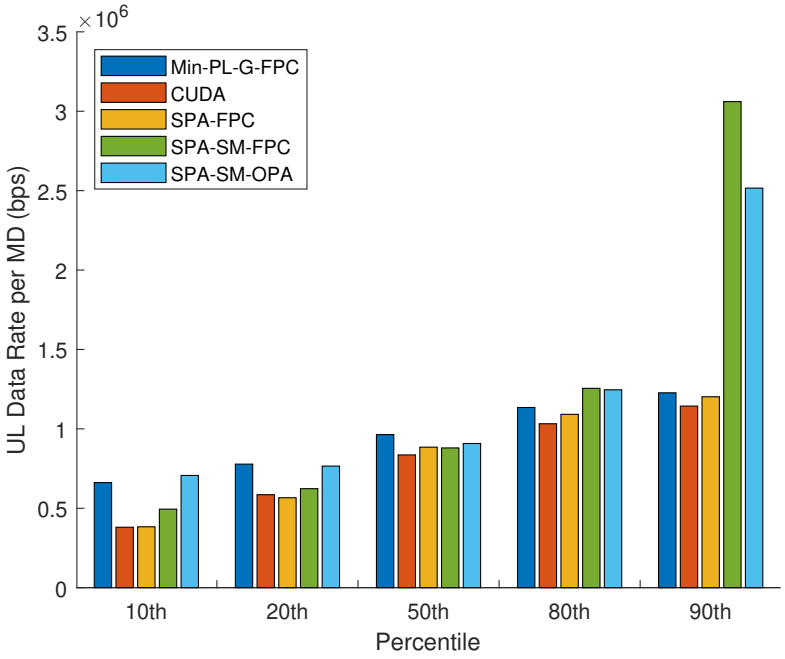

Figure 7.11: 10^{th}, 20^{th}, 50^{th}, 80^{th}, and 90^{th} percentile MD data rates based on different schemes.

7.6 Summary

This chapter has focused on exploring the utilization of DUDe in MEC networks. Existing research works considered BS association and subchannel allocation separately, and studied MEC under UL/DL coupled single BS association. In contrast, this chapter has provided a new perspective on resource allocation in MEC-enabled heterogeneous networks. Our results have successfully demonstrated that the latency of all the DUDe schemes are much lower than that of the CUDA scheme. Specifically, the network sum-latency of the SPA-SM-OPA scheme is the lowest among all the DUDe schemes, which is only 15% to 60% of the CUDA scheme, and is around 15% lower than that of the Min-PL-G-FPC scheme. The fairness of the UL transmission latency of the SPA-SM-OPA scheme is also higher than that of the CUDA scheme. The EE of the SPA-SM-FPC scheme is two times higher than the CUDA scheme. The users' data rates are increased, especially for those cell edge MDs.

Chapter 8

Conclusions and Future Research Directions

8.1 Conclusions

This thesis studies the application of the DUDe technique and explore the feasibility of exploiting its potential within other cutting-edge communication schemes. Specifically, a DUDe BS association and subchannel allocation algorithm based on capacity maximization were proposed in this thesis, and the application of DUDe on multi-connectivity, mmWave communication, D2D communication, cellular-enabled UAV communication, MEC, were investigated. It was demonstrated throughout that DUDe offers consistently improved performance under the various scenarios considered.

Specifically, in Chapter 3, an adaptive decoupling and multi-BS association scheme for the mmWave/UHF hybrid HetNets has been proposed, and its performance has been compared its performance for a wide range of metrics with benchmark single and dual connectivity alternatives. The results provide an insight into the performance of DUDe combined with mmWave and multi-connectivity techniques. It was shown that capacity-based cell association schemes (CDA, SMBA, CDA&SMBA) can achieve higher data rates than path-loss based cell association. Dual connectivity does not necessarily improve the sum-rate, especially when the density of UHF BSs is low, and the advantage of decoupled association is less effective in dual connectivity, because the UEs distribution among the BSs is more balanced in the dual connectivity scenario than in the single connectivity scenario. In mmWave/UHF hybrid HetNets, since the available mmWave bandwidth is much wider than UHF bandwidth, the network sum-rate mostly depends on the density of mmWave BSs, but UHF SBSs and MBSs are

still important to provide umbrella coverage to guarantee a consistent service.

While, in Chapter 4, a joint DL/UL decoupled cell-association, subchannel allocation and power control scheme for D2D-underlay HetNets has been proposed, and its performance has been compared with state-of-the-art alternatives. In the proposed scheme, the Min-PL based DUDe has been used for cell-association in the UL. A greedy coloring and a modified Munkres algorithm have been employed to solve the subchannel allocation problem. The D.C. programming is utilized to maximize the network sum-rate while meeting UE maximum transmission power and minimum data rate constraints. Numerical results show that the DUDe association schemes achieve higher data rates than their coupled counterparts. The proposed subchannel allocation scheme has been shown to outperform the Greedy and Random subchannel allocation schemes, and power allocation using D.C. programming dramatically improves the network sum-rate. It was also found that power optimization based on D.C. programming tends to allocate more power to UEs with higher channel quality at the expense of the UEs with lower channel quality, and it may decrease the EE if the power optimization stage continues to allocate power to the UEs when the data rate improvement is marginal.

On the other hand, in Chapter 5, a new access scheme in heterogeneous cellular networks with UAVs has been proposed. Particularly, to meet the different requirements of UAV data links and CNPC links, as well as GUE uplinks and downlinks, we separate the UAV CNPC links from the high-capacity data communication links, and separate the GUE uplinks from the downlinks. All the CNPC signals are connected to the GCSs operating in the L/C band, while the data signals are communicated to cellular BSs via the mmWave band. To further reduce interference between the UAVs and GUEs, the GUE downlinks and uplinks are also decoupled in terms of operating frequency and serving BS. Then, an optimal power allocation algorithm has been devised to optimize the EE of the DUDe access scheme. Numerical results demonstrated that the DUDe access scheme can achieve several times higher sum-rates in both UL and DL than its coupled counterparts. The proposed power allocation scheme is shown to achieve a 15% higher GUE sum-rate and twice higher GUE EE than the conventional fractional power control scheme. Furthermore, it should be noted that for noise-limited UAV communications, there is a trade-off between sum-rate and EE as simultaneously maximizing both is unattainable.

In Chapter 6, two power allocation schemes based on QL and DQL have been proposed to optimize the EE of the DUDe network, and their performances have been

compared with the fractional power control scheme (which is applied in 4G and 5G networks) and the optimal power allocation scheme we proposed in Chapter 5. The QL and DQL algorithms have shown promising results in complex wireless environments. It was shown that although reinforcement learning methods can achieve optimal results in theory, practically for some applications with predominant dynamic environment and have a limited time to execute the optimization process, QL and DQL with limited number of iterations may not achieve the optimal results. However it may achieve a near-optimal solution for EE as demonstrated in the results at Fig. 7.7 and Fig. 7.8. Nonetheless, the machine learning methods have achieved better EE performance than the baseline FPC method by around 100% and 70% for UHF band, and by around 160% and 130% for mmWave band respectively in compare to conventional fractional power control.

Finally, in Chapter 7, a joint BS association and subchannel allocation algorithm based on a student-project allocation (SPA) matching has been proposed, which takes the communication and computational disparity of SBS and MBS cloudlets into consideration and based on DUDe access. Then, an optimal power allocation algorithm is proposed to minimize the sum-latency of the network MDs. The formulated problem is a sum-of-ratios problem, which is non-convex and NP-hard. To efficiently and optimally tackle it, the proposed algorithm tightly approximates the problem as a convex optimization problem, and successively solves it until convergence to the global optimal power allocation solution. Numerical results have successfully demonstrated that the latencies of the DUDe schemes are much lower than that of the coupled scheme. Specifically, the network sum-latency of the SPA-SM-OPA scheme is the lowest among all the DUDe schemes, which is only 15% to 60% of the CUDA scheme, and is around 15% lower than that of the Min-PL-G-FPC scheme. The EE of the SPA-SM-FPC scheme is two times higher than the CUDA scheme.

8.2 Future Work

The results provide an insight into the performance of DUDe combined with mmWave, dual connectivity, and D2D, but considerably more work still needs to be done. Some possible areas of future research are list as follows.

- We applied independent Q-learning in this paper to solve the multi-agent problem, where each UE independently learns its own policy, treating other agents as part of the environment. It makes the environment become non-stationary

from the point of view of each UE, as it contains other UEs who are themselves learning, the convergence can not be guaranteed. Fortunately, substantial empirical evidence has shown that independent Q-learning often works well in practice [184]. As for DQL, we assume the states and actions of all UEs as an input. Although these methods can solve the EE optimization problem, it is necessary to investigate other multi-agent reinforcement learning methods. Interested reader may refer to [209] for a comprehensive overview in this field.

- In Chapter 7, we complete the BS association and subchannel allocation in one step by SPA algorithm. Looking still further ahead, we may consider if we can jointly solve the BS association, subchannel allocation and power control problems, for example, using 3-dimensional matching algorithms. Moreover, we assume each cloudlet's computational resources are equally shared among all tasks when two or more tasks are offloaded to the same cloudlet. More complex computational resource allocation schemes can be investigated in the future.

- We have taken cell load, computing power and communication capability into consideration when studying cell association. However, we have not taken account of the backhaul capacity of different BSs, which should be another constraint in cell association.

- Most of the proposed schemes in this thesis are centralized in nature hence require a control node. If there is no such node in the network, then distributed alternatives must be sought.

- DUDe is still far from the engineering implementation. In this report, we assumed DUDe can be achieved perfectly . However, in real networks, to achieve DUDe, BSs are supposed to communicate with each other. This will bring additional signaling overhead to the network and need new protocols to support this kind of communication.

- DUDe improves the overall network EE and fairness at the expense of some UEs with very high EE by improving the EE of the majority of UEs with lower EE. For a few special scenarios, the application of DUDe will affect the experience of those customers who require extremely high data rate or low latency, thus a compromise and correction mechanism should be introduced.

- As DUDe increases the access and handover frequency, it will offset the energy saving to some degree. Further strategies to reduce energy consumption, such

as the BS sleeping strategy, should be considered. Moreover, user mobility is a big challenge in DUDe, which further increases the switching frequency, thus should be investigated in the future.

- With the significant development of ultra-dense low Earth orbit (LEO) satellite constellations, satellite access networks have shown their potential as an expansion of terrestrial 5G and beyond cellular networks. UEs can transmit their data directly to LEO satellites via C-band with low data rates, or using a terrestrial-satellite terminal as an access point and transmit data to the satellite via Ka-band with high data rates. In both cases, the LEO satellite forwards the received data to the BS or the earth gateway station, which is connected to the core network [210]. Unlike traditional SCells (TSC) with small coverage and limited backhaul capacity connected to the core network via multihop backhaul links, the LEO-based SCelles (LSC) have vast coverage and large backhaul capacity supported by the Ka-band transmission. Explore the feasibility of DUDe for the HetNet with LSC could be interesting.

Bibliography

[1] F. Boccardi, J. Andrews, H. Elshaer, M. Dohler, S. Parkvall, P. Popovski, and S. Singh. Why to decouple the uplink and downlink in cellular networks and how to do it. *IEEE Communications Magazine*, 54(3):110–117, March 2016.

[2] H. Elshaer, F. Boccardi, M. Dohler, and R. Irmer. Downlink and uplink decoupling: A disruptive architectural design for 5G networks. In *2014 IEEE Global Communications Conference*, pages 1798–1803, Dec 2014.

[3] Jeffrey G Andrews. Seven ways that HetNets are a cellular paradigm shift. *IEEE Communications Magazine*, 51(3):136–144, 2013.

[4] Sandra Ondrusova and Dongwook Kim. Huawei's "5G implementation guidelines: NSA option 3. `https://www.gsma.com/futurenetworks/wiki/5g-implementation-guidelines/`. Accessed Nov. 27, 2020.

[5] Tim Hatt and Emanuel Kolta. 5G energy efficiencies: green is the new black. `https://data.gsmaintelligence.com/research/research/research-2020/5g-energy-efficiencies-green-is-the-new-black`. Accessed Nov. 27, 2020.

[6] Mohammed W Baidas and Emad Alsusa. Power allocation, relay selection and energy cooperation strategies in energy harvesting cooperative wireless networks. *Wireless Communications and Mobile Computing*, 16(14):2065–2082, 2016.

[7] Ritesh Madan, Jaber Borran, Ashwin Sampath, Naga Bhushan, Aamod Khandekar, and Tingfang Ji. Cell association and interference coordination in heterogeneous LTE-A cellular networks. *IEEE Journal on Selected Areas in Communications*, 28(9):1479–1489, 2010.

[8] Arman Shojaeifard, Khairi Ashour Hamdi, Emad Alsusa, Daniel KC So, Jie Tang, and Kai-Kit Wong. Design, modeling, and performance analysis of multi-antenna heterogeneous cellular networks. *IEEE Transactions on Communications*, 64(7):3104–3118, 2016.

[9] D Colombi, B Thors, and C Törnevik. Implications of EMF exposure limits on output power levels for 5G devices above 6 GHz. *IEEE Antennas and Wireless Propagation Letters*, 14:1247–1249, 2015.

[10] Zhilin Chen, Xueying Hou, and Chenyang Yang. Training resource allocation for user-centric base station cooperation networks. *IEEE Transactions on Vehicular Technology*, 65(4):2729–2735, 2015.

[11] Subramanya Chandrashekar, Andreas Maeder, Cinzia Sartori, Thomas Höhne, Benny Vejlgaard, and Devaki Chandramouli. 5g multi-rat multi-connectivity architecture. In *2016 IEEE International Conference on Communications Workshops (ICC)*, pages 180–186. IEEE, 2016.

[12] Yao Shi, Emad Alsusa, Aysha Ebrahim, and Mohammed Wael Baidas. Uplink performance enhancement through adaptive multi-association and decoupling in uhf-mmwave hybrid networks. *IEEE Transactions on Vehicular Technology*, 68(10):9735–9746, 2019.

[13] Azade Fotouhi, Haoran Qiang, Ming Ding, Mahbub Hassan, Lorenzo Galati Giordano, Adrian Garcia-Rodriguez, and Jinhong Yuan. Survey on UAV cellular communications: Practical aspects, standardization advancements, regulation, and security challenges. *IEEE Communications Surveys & Tutorials*, 2019.

[14] Y. Shi, E. Alsusa, and M. W. Baidas. An energy-efficient decoupled access scheme for cellular-enabled UAV communication systems. *IEEE Systems Journal*, 34(11):2851–2865, Nov. 2020.

[15] Imran Ashraf, Federico Boccardi, and Lester Ho. Sleep mode techniques for small cell deployments. *IEEE Communications Magazine*, 49(8):72–79, 2011.

[16] 3GPP. Evolved Universal Terrestrial Radio Access (E-UTRA) and Evolved Universal Terrestrial Radio Access Network (E-UTRAN); Overall description; Stage 2 . Technical Report (TR) 36.300, 3rd Generation Partnership Project (3GPP), 11 2011. Version 10.5.0.

[17] Mahmoud Kamel, Walaa Hamouda, and Amr Youssef. Ultra-dense networks: A survey. *IEEE Communications Surveys & Tutorials*, 18(4):2522–2545, 2016.

[18] Joseph Boccuzzi Michael. *Femtocells: design & application*. 2018.

[19] David Lopez-Perez, Ismail Guvenc, Guillaume De la Roche, Marios Kountouris, Tony QS Quek, and Jie Zhang. Enhanced inter-cell interference coordination challenges in heterogeneous networks. *arXiv preprint arXiv:1112.1597*, 2011.

[20] Assen Golaup, Mona Mustapha, and Leo Boonchin Patanapongpibul. Femtocell access control strategy in UMTS and LTE. *IEEE Communications Magazine*, 47(9):117–123, 2009.

[21] Aruna Prem Bianzino, Claude Chaudet, Dario Rossi, and Jean-Louis Rougier. A survey of green networking research. *IEEE Communications Surveys & Tutorials*, 14(1):3–20, 2010.

[22] David Lopez-Perez, Ismail Guvenc, and Xiaoli Chu. Mobility management challenges in 3GPP heterogeneous networks. *IEEE Communications Magazine*, 50(12):70–78, 2012.

[23] Holger Claussen, Florian Pivit, and Lester TW Ho. Self-optimization of femtocell coverage to minimize the increase in core network mobility signalling. *Bell Labs Technical Journal*, 14(2):155–183, 2009.

[24] Haijun Zhang, Xiangming Wen, Bo Wang, Wei Zheng, and Yong Sun. A novel handover mechanism between femtocell and macrocell for LTE based networks. In *2010 second international conference on communication software and networks*, pages 228–231. IEEE, 2010.

[25] J. Sangiamwong, Y. Saito, N. Miki, T. Abe, S. Nagata, and Y. Okumura. Investigation on cell selection methods associated with inter-cell interference coordination in heterogeneous networks for LTE-advanced downlink. In *Proc. of 17th European Wireless 2011 - Sustainable Wireless Technologies*, pages 1–6, April 2011.

[26] M. Sternad, T. Ottosson, A. Ahlen, and A. Svensson. Attaining both coverage and high spectral efficiency with adaptive OFDM downlinks. In

2003 IEEE 58th Vehicular Technology Conference. VTC 2003-Fall (IEEE Cat. No.03CH37484), volume 4, pages 2486–2490 Vol.4, Oct 2003.

[27] Ekram Hossain, Mehdi Rasti, Hina Tabassum, and Amr Abdelnasser. Evolution towards 5G multi-tier cellular wireless networks: An interference management perspective. *arXiv preprint arXiv:1401.5530*, 2014.

[28] Sundeep Rangan, Theodore S Rappaport, and Elza Erkip. Millimeter wave cellular wireless networks: Potentials and challenges. *arXiv preprint arXiv:1401.2560*, 2014.

[29] I. A. Hemadeh, K. Satyanarayana, M. El-Hajjar, and L. Hanzo. Millimeter-wave communications: Physical channel models, design considerations, antenna constructions, and link-budget. *IEEE Communications Surveys Tutorials*, 20(2):870–913, 2018.

[30] Yaniv Azar, George N Wong, Kevin Wang, Rimma Mayzus, Jocelyn K Schulz, Hang Zhao, Felix Gutierrez, DuckDong Hwang, and Theodore S Rappaport. 28 ghz propagation measurements for outdoor cellular communications using steerable beam antennas in new york city. In *2013 IEEE international conference on communications (ICC)*, pages 5143–5147. IEEE, 2013.

[31] Theodore S Rappaport, James N Murdock, and Felix Gutierrez. State of the art in 60-ghz integrated circuits and systems for wireless communications. *Proceedings of the IEEE*, 99(8):1390–1436, 2011.

[32] Stanley Chia, Max Gasparroni, and Patrick Brick. The next challenge for cellular networks: Backhaul. *IEEE Microwave Magazine*, 10(5):54–66, 2009.

[33] Eldad Perahia, Carlos Cordeiro, Minyoung Park, and L Lily Yang. IEEE 802.11 ad: Defining the next generation multi-Gbps wi-fi. In *2010 7th IEEE consumer communications and networking conference*, pages 1–5. IEEE, 2010.

[34] Steven J Vaughan-Nichols. Gigabit wi-fi is on its way. *Computer*, 43(11):11–14, 2010.

[35] Robert C Daniels, James N Murdock, Theodore S Rappaport, and Robert W Heath. 60 ghz wireless: Up close and personal. *IEEE Microwave magazine*, 11(7):44–50, 2010.

[36] Tuncer Baykas, Chin-Sean Sum, Zhou Lan, Junyi Wang, M Azizur Rahman, Hiroshi Harada, and Shuzo Kato. Ieee 802.15. 3c: the first ieee wireless standard for data rates over 1 gb/s. *IEEE Communications Magazine*, 49(7):114–121, 2011.

[37] Theodore S Rappaport, James N Murdock, and Felix Gutierrez. State of the art in 60-GHz integrated circuits and systems for wireless communications. *Proceedings of the IEEE*, 99(8):1390–1436, 2011.

[38] James N Murdock and Theodore S Rappaport. Consumption factor and power-efficiency factor: A theory for evaluating the energy efficiency of cascaded communication systems. *IEEE Journal on Selected Areas in Communications*, 32(2):221–236, 2013.

[39] Zhao Qingling and Jin Li. Rain attenuation in millimeter wave ranges. In *2006 7th International Symposium on Antennas, Propagation & EM Theory*, pages 1–4. IEEE, 2006.

[40] Theodore S Rappaport, Shu Sun, Rimma Mayzus, Hang Zhao, Yaniv Azar, Kevin Wang, George N Wong, Jocelyn K Schulz, Mathew Samimi, and Felix Gutierrez. Millimeter wave mobile communications for 5G cellular: It will work! *IEEE access*, 1:335–349, 2013.

[41] Zhouyue Pi and Farooq Khan. An introduction to millimeter-wave mobile broadband systems. *IEEE Communications Magazine*, 49(6):101–107, 2011.

[42] Hua Wang, Claudio Rosa, and Klaus I Pedersen. Dual connectivity for LTE-advanced heterogeneous networks. *Wireless Networks*, 22(4):1315–1328, 2016.

[43] Anna Zakrzewska, David López-Pérez, Stepan Kucera, and Holger Claussen. Dual connectivity in LTE HetNets with split control-and user-plane. In *2013 IEEE Globecom Workshops (GC Wkshps)*, pages 391–396. IEEE, 2013.

[44] Hisham Elshaer, Federico Boccardi, Mischa Dohler, and Ralf Irmer. Load & backhaul aware decoupled downlink/uplink access in 5G systems. In *2015 IEEE International Conference on Communications (ICC)*, pages 5380–5385. IEEE, 2015.

[45] Roha Masroor, Mohammed Burhan Abrar, and Xin Gui. Device to device (D2D) communication : Interference management perspective. 2017.

[46] D. Feng, L. Lu, Y. Yuan-Wu, G. Y. Li, S. Li, and G. Feng. Device-to-device communications in cellular networks. *IEEE Communications Magazine*, 52(4):49–55, April 2014.

[47] A. Asadi, Q. Wang, and V. Mancuso. A survey on device-to-device communication in cellular networks. *IEEE Communications Surveys Tutorials*, 16(4):1801–1819, Fourthquarter 2014.

[48] Yong Zeng, Jiangbin Lyu, and Rui Zhang. Cellular-connected UAV: Potential, challenges, and promising technologies. *IEEE Wireless Communications*, 26(1):120–127, 2018.

[49] S. Zhang, Y. Zeng, and R. Zhang. Cellular-enabled UAV communication: A connectivity-constrained trajectory optimization perspective. *IEEE Transactions on Communications*, 67(3):2580–2604, March 2019.

[50] G. Zhang, Q. Wu, M. Cui, and R. Zhang. Securing UAV communications via joint trajectory and power control. *IEEE Transactions on Wireless Communications*, 18(2):1376–1389, Feb 2019.

[51] Helin Yang and Xianzhong Xie. Energy-efficient joint scheduling and resource management for UAV-enabled multicell networks. *IEEE Systems Journal*, 14(1):363–374, 2019.

[52] Dingkun Hu, Qi Zhang, Quanzhong Li, and Jiayin Qin. Joint position, decoding order, and power allocation optimization in UAV-based NOMA downlink communications. *IEEE Systems Journal*, 14(2):2949–2960, Jun. 2019.

[53] Xiaobo Zhou, Qingqing Wu, Shihao Yan, Feng Shu, and Jun Li. UAV-enabled secure communications: Joint trajectory and transmit power optimization. *IEEE Trans. Veh. Technol.*, 68(4):4069–4073, 2019.

[54] Shuowen Zhang, Yong Zeng, and Rui Zhang. Cellular-enabled UAV communication: A connectivity-constrained trajectory optimization perspective. *IEEE Transactions on Communications*, 67(3):2580–2604, 2018.

[55] 3GPP. Enhanced LTE support for aerial vehicles. `http://www.3gpp.org/ftp//Specs/archive/36_series/36.777/`. Accessed Aug. 15, 2019.

[56] B. V. Der Bergh, A. Chiumento, and S. Pollin. LTE in the sky: Trading off propagation benefits with interference costs for aerial nodes. *IEEE Communications Magazine*, 54(5):44–50, May 2016.

[57] 3GPP. 5G; NR; base station (BS) radio transmission and reception. `http://www.3gpp.org/`. Accessed Feb. 28, 2019.

[58] C. Zhang, W. Zhang, W. Wang, L. Yang, and W. Zhang. Research challenges and opportunities of UAV millimeter-wave communications. *IEEE Wireless Communications*, 26(1):58–62, Feb. 2019.

[59] L. Zhang, H. Zhao, S. Hou, Z. Zhao, H. Xu, X. Wu, Q. Wu, and R. Zhang. A survey on 5G millimeter wave communications for UAV-assisted wireless networks. *IEEE Access*, 7:117460–117504, 2019.

[60] Ofir Nachum, Mohammad Norouzi, Kelvin Xu, and Dale Schuurmans. Bridging the gap between value and policy based reinforcement learning. In *Advances in Neural Information Processing Systems*, pages 2775–2785, 2017.

[61] China Unicom Network Technology Research Institute. China unicom edge computing technology white paper. `https://builders.intel.com/docs/networkbuilders/china-unicom-edge-computing-technology-white-paper.pdf`. Accessed Nov. 7, 2020.

[62] Pavel Mach and Zdenek Becvar. Mobile edge computing: A survey on architecture and computation offloading. *IEEE Communications Surveys & Tutorials*, 19(3):1628–1656, 2017.

[63] Yuyi Mao, Changsheng You, Jun Zhang, Kaibin Huang, and Khaled B Letaief. A survey on mobile edge computing: The communication perspective. *IEEE Communications Surveys & Tutorials*, 19(4):2322–2358, 2017.

[64] Stephen Boyd, Stephen P Boyd, and Lieven Vandenberghe. *Convex optimization*. Cambridge university press, 2004.

[65] Aylwin. 3g & 4g frequency list. `https://support.alwaysonlinewireless.com/`. Accessed Feb. 28, 2019.

[66] D Colombi, B Thors, and C Törnevik. Implications of emf exposure limits on output power levels for 5g devices above 6 ghz. *IEEE Antennas and Wireless Propagation Letters*, 14:1247–1249, 2015.

[67] Sarabjot Singh, Xinchen Zhang, and Jeffrey G Andrews. Joint rate and SINR coverage analysis for decoupled uplink-downlink biased cell associations in HetNets. *IEEE Transactions on Wireless Communications*, 14(10):5360–5373, 2015.

[68] Katerina Smiljkovikj, Petar Popovski, and Liljana Gavrilovska. Analysis of the decoupled access for downlink and uplink in wireless heterogeneous networks. *IEEE Wireless Communications Letters*, 4(2):173–176, 2015.

[69] Lan Zhang, Weili Nie, Gang Feng, Fu-Chun Zheng, and Shuang Qin. Uplink performance improvement by decoupling uplink/downlink access in HetNets. *IEEE Transactions on Vehicular Technology*, 66(8):6862–6876, 2017.

[70] H. Elshaer, M. N. Kulkarni, F. Boccardi, J. G. Andrews, and M. Dohler. Downlink and uplink cell association with traditional macrocells and millimeter wave small cells. *IEEE Transactions on Wireless Communications*, 15(9):6244–6258, Sep. 2016.

[71] Osama Waqar Bhatti, Haris Suhail, Uzair Akbar, Syed Ali Hassan, Haris Pervaiz, Leila Musavian, and Qiang Ni. Performance analysis of decoupled cell association in multi-tier hybrid networks using real blockage environments. In *2017 13th International wireless communications and mobile computing conference (IWCMC)*, pages 62–67. IEEE, 2017.

[72] M. A. Lema, E. Pardo, O. Galinina, S. Andreev, and M. Dohler. Flexible dual-connectivity spectrum aggregation for decoupled uplink and downlink access in 5G heterogeneous systems. *IEEE Journal on Selected Areas in Communications*, 34(11):2851–2865, Nov 2016.

[73] Jeffrey G Andrews, François Baccelli, and Radha Krishna Ganti. A tractable approach to coverage and rate in cellular networks. *IEEE Transactions on communications*, 59(11):3122–3134, 2011.

[74] M. K. Samimi, G. R. MacCartney, S. Sun, and T. S. Rappaport. 28 GHz millimeter-wave ultrawideband small-scale fading models in wireless channels.

In *2016 IEEE 83rd Vehicular Technology Conference (VTC Spring)*, pages 1–6, May 2016.

[75] Mathworks. Multipath fading channel. `https://www.mathworks.com`. Accessed Feb. 28, 2019.

[76] N. Kolehmainen, J. Puttonen, P. Kela, T. Ristaniemi, T. Henttonen, and M. Moisio. Channel quality indication reporting schemes for UTRAN long term evolution downlink. In *Proc. of IEEE Vehicular Technology Conference (VTC) - Spring*, pages 2522–2526, May 2008.

[77] M. Shi, K. Yang, C. Xing, and R. Fan. Decoupled heterogeneous networks with millimeter wave small cells. *IEEE Transactions on Wireless Communications*, 17(9):5871–5884, Sep. 2018.

[78] O. Arnold, F. Richter, G. Fettweis, and O. Blume. Power consumption modeling of different base station types in heterogeneous cellular networks. In *Proc. Future Network Mobile Summit*, pages 1–8, June 2010.

[79] 3GPP. Physical layer procedures. `https://www.etsi.org/`. Accessed Feb. 28, 2019.

[80] S. Berger, B. Almeroth, V. Suryaprakash, P. Zanier, I. Viering, and G. Fettweis. Dynamic range-aware uplink transmit power control in LTE networks: Establishing an operational range for LTE's open-loop transmit power control parameters(α, p_0). *IEEE Wireless Communications Letters*, 3(5):521–524, Oct 2014.

[81] A. Ebrahim, E. Alsusa, and W. Pramudito. Joint interference aware resource partitioning and cellular association for femtocell networks. In *2015 IEEE Global Communications Conference (GLOBECOM)*, pages 1–5, Dec 2015.

[82] M. Fallgren. On the complexity of maximizing the minimum shannon capacity in wireless networks by joint channel assignment and power allocation. In *2010 IEEE 18th International Workshop on Quality of Service (IWQoS)*, pages 1–7, June 2010.

[83] Martin Schlueter. Midaco software performance on interplanetary trajectory benchmarks. *Advances in Space Research*, 54:744–754, 08 2014.

[84] Campos J. Understanding the 5G NR physical layer. https://www.keysight.com/upload/cmc_upload/All/Understanding_the_5G_NR_Physical_Layer.pdf. Accessed Feb. 28, 2019.

[85] Ericsson. Designing for the future: the 5G NR physical layer. https://www.ericsson.com/en/ericsson-technology-review/archive/2017/designing-for-the-future-the-5g-nr-physical-layer. Accessed Feb. 28, 2019.

[86] Wikipedia. Percentile. https://en.wikipedia.org/wiki/Percentile. Accessed Oct. 31, 2018.

[87] Z. Kuang, G. Liu, G. Li, and X. Deng. Energy efficient resource allocation algorithm in energy harvesting-based D2D heterogeneous networks. *IEEE Internet of Things Journal*, 6(1):557–567, Feb. 2019.

[88] H. Tang and Z. Ding. Mixed mode transmission and resource allocation for D2D communication. *IEEE Transactions on Wireless Communications*, 15(1):162–175, Jan. 2016.

[89] H. Chour, E. A. Jorswieck, F. Bader, Y. Nasser, and O. Bazzi. Global optimal resource allocation for efficient FD-D2D enabled cellular network. *IEEE Access*, 7:59690–59707, 2019.

[90] Klaus Doppler, Chia-Hao Yu, Cassio B Ribeiro, and Pekka Janis. Mode selection for device-to-device communication underlaying an LTE-advanced network. In *2010 IEEE Wireless Communication and Networking Conference*, pages 1–6. IEEE, 2010.

[91] Min-Hong Han, Byung-Gook Kim, and Jang-Won Lee. Subchannel and transmission mode scheduling for D2D communication in OFDMA networks. In *2012 IEEE Vehicular Technology Conference (VTC Fall)*, pages 1–5. IEEE, 2012.

[92] Shangwen Xiang, Tao Peng, Ziyang Liu, and Wenbo Wang. A distance-dependent mode selection algorithm in heterogeneous D2D and IMT-advanced network. In *2012 IEEE Globecom Workshops*, pages 416–420. IEEE, 2012.

[93] Rui Yin, Guanding Yu, Caijun Zhong, and Zhaoyang Zhang. Distributed resource allocation for D2D communication underlaying cellular networks. In

2013 IEEE International Conference on Communications Workshops (ICC), pages 138–143. IEEE, 2013.

[94] Chen Xu, Lingyang Song, Zhu Han, Qun Zhao, Xiaoli Wang, and Bingli Jiao. Interference-aware resource allocation for device-to-device communications as an underlay using sequential second price auction. In *2012 IEEE international conference on communications (ICC)*, pages 445–449. IEEE, 2012.

[95] Chen Xu, Lingyang Song, Zhu Han, Dou Li, and Bingli Jiao. Resource allocation using a reverse iterative combinatorial auction for device-to-device underlay cellular networks. In *2012 IEEE Global Communications Conference (GLOBECOM)*, pages 4542–4547. IEEE, 2012.

[96] Lingyang Song, Dusit Niyato, Zhu Han, and Ekram Hossain. Game-theoretic resource allocation methods for device-to-device communication. *IEEE Wireless Communications*, 21(3):136–144, 2014.

[97] Mohammad Zulhasnine, Changcheng Huang, and Anand Srinivasan. Efficient resource allocation for device-to-device communication underlaying LTE network. In *2010 IEEE 6th International conference on wireless and mobile computing, networking and communications*, pages 368–375. IEEE, 2010.

[98] Pekka Janis, Visa Koivunen, Cassio Ribeiro, Juha Korhonen, Klaus Doppler, and Klaus Hugl. Interference-aware resource allocation for device-to-device radio underlaying cellular networks. In *VTC Spring 2009-IEEE 69th Vehicular Technology Conference*, pages 1–5. IEEE, 2009.

[99] Bin Wang, Li Chen, Xiaohang Chen, Xin Zhang, and Dacheng Yang. Resource allocation optimization for device-to-device communication underlaying cellular networks. In *2011 IEEE 73rd vehicular technology conference (VTC Spring)*, pages 1–6. IEEE, 2011.

[100] Chia-Hao Yu, Klaus Doppler, Cassio B Ribeiro, and Olav Tirkkonen. Resource sharing optimization for device-to-device communication underlaying cellular networks. *IEEE Transactions on Wireless communications*, 10(8):2752–2763, 2011.

[101] Anders Gjendemsjø, David Gesbert, Geir E Øien, and Saad G Kiani. Binary power control for sum rate maximization over multiple interfering links. *IEEE Transactions on Wireless Communications*, 7(8):3164–3173, 2008.

[102] C-H Yu, Olav Tirkkonen, Klaus Doppler, and Cássio Ribeiro. Power optimization of device-to-device communication underlaying cellular communication. In *2009 IEEE international conference on communications*, pages 1–5. IEEE, 2009.

[103] H Wang and X Chu. Distance-constrained resource-sharing criteria for device-to-device communications underlaying cellular networks. *Electronics letters*, 48(9):528–530, 2012.

[104] Sami Hakola, Tao Chen, Janne Lehtomaki, and Timo Koskela. Device-to-device (D2D) communication in cellular network-performance analysis of optimum and practical communication mode selection. In *2010 IEEE wireless communication and networking conference*, pages 1–6. IEEE, 2010.

[105] Hongnian Xing and Sami Hakola. The investigation of power control schemes for a device-to-device communication integrated into OFDMA cellular system. In *21st Annual IEEE International Symposium on Personal, Indoor and Mobile Radio Communications*, pages 1775–1780. IEEE, 2010.

[106] Bo Peng, Chunjing Hu, Tao Peng, and Wenbo Wang. Optimal resource allocation for multi-D2D links underlying OFDMA-based communications. In *2012 8th International conference on wireless communications, networking and mobile computing*, pages 1–4. IEEE, 2012.

[107] Namyoon Lee, Xingqin Lin, Jeffrey G Andrews, and Robert W Heath. Power control for D2D underlaid cellular networks: Modeling, algorithms, and analysis. *IEEE Journal on selected areas in communications*, 33(1):1–13, 2014.

[108] Hafiz A Mustafa, Muhammad Z Shakir, Yusuf A Sambo, Khalid A Qaraqe, Muhammad A Imran, and Erchin Serpedin. Spectral efficiency improvements in HetNets by exploiting device-to-device communications. In *2014 IEEE Globecom Workshops (GC Wkshps)*, pages 857–862. IEEE, 2014.

[109] Amal Algedir and Hazem H Refai. Adaptive D2D resources allocation underlaying (2-tier) heterogeneous cellular networks. In *2017 IEEE 28th Annual International Symposium on Personal, Indoor, and Mobile Radio Communications (PIMRC)*, pages 1–6. IEEE, 2017.

[110] Hui Gao, Min Wang, and Tiejun Lv. Energy efficiency and spectrum efficiency tradeoff in the D2D-enabled HetNet. *IEEE Transactions on Vehicular Technology*, 66(11):10583–10587, 2017.

[111] H. Dai, Y. Huang, C. Li, K. Song, and L. Yang. Resource allocation for device-to-device and small cell uplink communication networks. In *2016 IEEE Wireless Communications and Networking Conference*, pages 1–6, April 2016.

[112] Francesco Malandrino, Zana Limani, Claudio Casetti, and Carla-Fabiana Chiasserini. Interference-aware downlink and uplink resource allocation in hetnets with D2D support. *IEEE Transactions on Wireless Communications*, 14(5):2729–2741, 2015.

[113] Kai Wen, Yongli Chen, and Yunhan Hu. A resource allocation method for D2D and small cellular users in HetNet. In *2017 3rd IEEE International Conference on Computer and Communications (ICCC)*, pages 628–632. IEEE, 2017.

[114] Yifei Huang, Ali A Nasir, Salman Durrani, and Xiangyun Zhou. Mode selection, resource allocation, and power control for D2D-enabled two-tier cellular network. *IEEE Transactions on Communications*, 64(8):3534–3547, 2016.

[115] Mukesh Kumar Giluka, M Sibgath Ali Khan, Vanlin Sathya, and A Antony Franklin. Leveraging decoupling in enabling energy aware D2D communications. In *2016 IEEE International Conference on Advanced Networks and Telecommunications Systems (ANTS)*, pages 1–6. IEEE, 2016.

[116] A. Celik, R. M. Radaydeh, F. S. Al-Qahtani, and M. Alouini. Joint interference management and resource allocation for device-to-device (D2D) communications underlying downlink/uplink decoupled (DUDe) heterogeneous networks. In *Proc. of IEEE International Conference on Communications (ICC)*, pages 1–6, 2017.

[117] François Bourgeois and Jean-Claude Lassalle. An extension of the munkres algorithm for the assignment problem to rectangular matrices. *Communications of the ACM*, 14(12):802–804, 1971.

[118] Derrick Wing Kwan Ng, Ernest S Lo, and Robert Schober. Energy-efficient resource allocation in multi-cell OFDMA systems with limited backhaul capacity. *IEEE Transactions on Wireless Communications*, 11(10):3618–3631, 2012.

[119] Laurence A. Wolsey and George L. Nemhauser. *Integer and combinatorial optimization*. John Wiley & Sons, 1999.

[120] Y.-F. Liu and Y.-H. Dai. On the complexity of joint subcarrier and power allocation for multi-user OFDMA systems. *IEEE Transactions on Signal Processing*, 62(3):583–596, 2014.

[121] M. Coupechoux and J.-M. Kelif. How to set the fractional power control compensation factor in LTE ? *Proc. of 34th IEEE Sarnoff Symposium*, pages 1–5, May 2011.

[122] M. Kubale. *Graph Colorings*. Contemporary mathematics (American Mathematical Society) v. 352. American Mathematical Society, 2004.

[123] James Munkres. Algorithms for the assignment and transportation problems. *Journal of the society for industrial and applied mathematics*, 5(1):32–38, 1957.

[124] Yi. Cao. Munkres' assignment algorithm, modified for rectangular matrices. `http://csclab.murraystate.edu/~bob.pilgrim/445/munkres.html`. Accessed Feb. 28, 2019.

[125] Jin Kue Wong. A new implementation of an algorithm for the optimal assignment problem: An improved version of munkres' algorithm. *BIT Numerical Mathematics*, 19(3):418–424, 1979.

[126] Rainer E Burkard, Mauro Dell'Amico, and Silvano Martello. *Assignment problems*. Springer, 2009.

[127] Hoang Tuy, Tuy Hoang, Tuy Hoang, Viêt-nam Mathématicien, Tuy Hoang, and Vietnam Mathematician. *Convex analysis and global optimization*. Springer, 1998.

[128] Ha Hoang Kha, Hoang Duong Tuan, and Ha H Nguyen. Fast global optimal power allocation in wireless networks by local DC programming. *IEEE Transactions on Wireless Communications*, 11(2):510–515, 2011.

[129] S. Boyd and L. Vandenberghe. *Convex Optimization*. Cambridge University Press, 2003.

[130] M. Frank and P. Wolfe. An algorithm for quadratic programming. *Naval Research Logistics Quaterly*, 3(1):95–110, Mar. 1956.

[131] D. P. Palomar and Y. C.Eldar. *Convex Optimization in Signal Processing and Communications*. Cambridge University Press, New York, USA, 2010.

[132] Y. Tao, J. Sun, and S. Shao. Radio resource allocation based on greedy algorithm and successive interference cancellation in device-to-device (D2D) communication. In *IET International Conference on Information and Communications Technologies (IETICT)*, pages 452–458, Apr. 2013.

[133] MIDACO-Solver. Mixed integer distributed ant colony optimization. Online: `http://www.midaco-solver.com`.

[134] W. Mei and R. Zhang. Uplink cooperative NOMA for cellular-connected UAV. *IEEE Journal of Selected Topics in Signal Processing*, 13(3):644–656, June 2019.

[135] W. Wang, J. Tang, N. Zhao, X. Liu, X. Y. Zhang, Y. Chen, and Y. Qian. Joint precoding optimization for secure SWIPT in UAV-aided NOMA networks. *IEEE Transactions on Communications*, 68(8):5028–5040, 2020.

[136] N. Zhao, Y. Li, S. Zhang, Y. Chen, W. Lu, J. Wang, and X. Wang. Security enhancement for NOMA-UAV networks. *IEEE Transactions on Vehicular Technology*, 69(4):3994–4005, 2020.

[137] X. Liu, Y. Liu, Y. Chen, and L. Hanzo. Trajectory design and power control for multi-uav assisted wireless networks: A machine learning approach. *IEEE Transactions on Vehicular Technology*, 68(8):7957–7969, 2019.

[138] Y. Zeng and R. Zhang. Energy-efficient UAV communication with trajectory optimization. *IEEE Transactions on Wireless Communications*, 16(6):3747–3760, Jun. 2017.

[139] D. Yang, Q. Wu, Y. Zeng, and R. Zhang. Energy tradeoff in ground-to-UAV communication via trajectory design. *IEEE Transactions on Vehicular Technology*, 67(7):6721–6726, Jul. 2018.

[140] S. Zhang, Y. Zeng, and R. Zhang. Cellular-enabled UAV communication: A connectivity-constrained trajectory optimization perspective. *IEEE Transactions on Communications*, 67(3):2580–2604, Mar. 2019.

[141] S. Yin, S. Zhao, Y. Zhao, and F. R. Yu. Intelligent trajectory design in UAV-aided communications with reinforcement learning. *IEEE Transactions on Vehicular Technology*, 68(8):8227–8231, Aug. 2019.

[142] K. Venugopal, M. C. Valenti, and R. W. Heath. Device-to-device millimeter wave communications: Interference, coverage, rate, and finite topologies. *IEEE Transactions on Wireless Communications*, 15(9):6175–6188, Sep. 2016.

[143] Ruiqian Ma, Weiwei Yang, Yu Zhang, and Songqing Wang. Secure on-off transmission in UAV relay-assisted mmwave networks. *Applied Sciences*, 9(19):4138, 2019.

[144] Y. Zhu, G. Zheng, and M. Fitch. Secrecy rate analysis of UAV-enabled mmWave networks using Matérn hardcore point processes. *IEEE Journal on Selected Areas in Communications*, 36(7):1397–1409, July 2018.

[145] S. Singh, M. N. Kulkarni, A. Ghosh, and J. G. Andrews. Tractable model for rate in self-backhauled millimeter wave cellular networks. *IEEE Journal on Selected Areas in Communications*, 33(10):2196–2211, 2015.

[146] A. Al-Hourani, S. Kandeepan, and S. Lardner. Optimal LAP altitude for maximum coverage. *IEEE Wireless Communications Letters*, 3(6):569–572, Dec 2014.

[147] T. Bai and R. W. Heath. Coverage and rate analysis for millimeter-wave cellular networks. *IEEE Transactions on Wireless Communications*, 14(2):1100–1114, Feb. 2015.

[148] J. Chakareski, S. Naqvi, N. Mastronarde, J. Xu, F. Afghah, and A. Razi. An energy efficient framework for UAV-assisted millimeter wave 5G heterogeneous cellular networks. *IEEE Transactions on Green Communications and Networking*, 3(1):37–44, March 2019.

[149] David W Matolak and Ruoyu Sun. Unmanned aircraft systems: Air-ground channel characterization for future applications. *IEEE Vehicular Technology Magazine*, 10(2):79–85, 2015.

[150] D. W. Yun and W. C. Lee. LTE-TDD interference analysis in spatial, time and frequency domain. In *Proc. of Ninth International Conference on Ubiquitous and Future Networks (ICUFN)*, pages 785–787, July 2017.

[151] Hossein Shokri-Ghadikolaei, Carlo Fischione, Gabor Fodor, Petar Popovski, and Michele Zorzi. Millimeter wave cellular networks: A MAC layer perspective. *IEEE Transactions on Communications*, 63(10):3437–3458, 2015.

[152] Jeffrey G Andrews, Tianyang Bai, Mandar N Kulkarni, Ahmed Alkhateeb, Abhishek K Gupta, and Robert W Heath. Modeling and analyzing millimeter wave cellular systems. *IEEE Transactions on Communications*, 65(1):403–430, 2016.

[153] 3GPP. User equipment radio transmission and reception. `https://www.etsi.org/deliver/etsi_ts/138100_138199/13810101/15.02.00_60/ts_13810101v150200p.pdf`. Accessed Aug. 15, 2019.

[154] E Tejaswi and B Suresh. Survey of power control schemes for LTE uplink. *International Journal of Computer Science and Information Technologies (IJCSIT)*, 4(2):369–373, 2013.

[155] Alessio Zappone, Eduard Jorswieck, et al. Energy efficiency in wireless networks via fractional programming theory. *Foundations and Trends in Communications and Information Theory*, 11(3-4):185–396, 2015.

[156] J. Papandriopoulos and J. S. Evans. SCALE: a low-complexity distributed protocol for spectrum balancing in multiuser DSL networks. *IEEE Transactions on Information Theory*, 55(8):3711–3724, Aug. 2009.

[157] Stephen Boyd and Lieven Vandenberghe. *Convex optimization*. Cambridge university press, 2004.

[158] W. Dinkelbach. On nonlinear fractional programming. *Management Science*, 13(7):492–498, Mar. 1967.

[159] Jean-Pierre Crouzeix, Jacques A. Ferland, and Van Hien Nyugen. Revisting Dinkelbach-type algorithms for generalized fractional programs. *OPSEARCH*, 45(2):97–110, Jun. 2008.

[160] A. Zappone, E. Bjornson, L. Sanguinetti, and E. Jorswieck. Globally optimal energy-efficient power control and receiver design in wireless networks. *IEEE Transactions on Signal Processing*, 65(11):2844–2859, Jun. 2017.

[161] Fanzi Zeng, Zhenzhen Hu, Zhu Xiao, Hongbo Jiang, Siwang Zhou, Wenping Liu, and Daibo Liu. Resource allocation and trajectory optimization for QoE

provisioning in energy-efficient UAV-enabled wireless networks. *IEEE Transactions on Vehicular Technology*, 69(7):7634–7647, 2020.

[162] Lijun Deng, Gang Wu, Jingwei Fu, Yizhong Zhang, and Yifu Yang. Joint resource allocation and trajectory control for UAV-enabled vehicular communications. *IEEE Access*, 7:132806–132815, 2019.

[163] Zhendong Li, Ying Wang, Man Liu, Ruijin Sun, Yuanbin Chen, Jun Yuan, and Jiuchao Li. Energy efficient resource allocation for UAV-assisted space-air-ground Internet of Remote Things networks. *IEEE Access*, 7:145348–145362, 2019.

[164] Y. Azar, G. N. Wong, K. Wang, R. Mayzus, J. K. Schulz, H. Zhao, F. Gutierrez, D. Hwang, and T. S. Rappaport. 28 GHz propagation measurements for outdoor cellular communications using steerable beam antennas in New York city. In *Proc. of IEEE International Conference on Communications (ICC)*, pages 5143–5147, June 2013.

[165] Bin Li, Zesong Fei, and Yan Zhang. Uav communications for 5g and beyond: Recent advances and future trends. *IEEE Internet of Things Journal*, 6(2):2241–2263, 2018.

[166] Jingjing Cui, Yuanwei Liu, and Arumugam Nallanathan. Multi-agent reinforcement learning-based resource allocation for UAV networks. *IEEE Transactions on Wireless Communications*, 19(2):729–743, Feb. 2020.

[167] Richard S Sutton and Andrew G Barto. *Reinforcement learning: An introduction*. MIT press, 2018.

[168] C. J. C. H. Watkins and P. Dayan. Q-learning. *Machine Learning*, 8(3):279–292, May 1992.

[169] V. Mnih and et al. Human-level control through reinforcement learning. *Nature*, 518(7540):529–533, 2015.

[170] C. Zhang, P. Patras, and H. Haddadi. Deep learning in mobile and wireless networking: A survey. *IEEE Communications Surveys & Tutorials*, 21(3):2224–2287, Mar. 2019.

[171] N. C. Luong, D. T. Hoang, S. Gong, D. Niyato, P. Wang, Y.-C. Liang, and D. I. Kim. Applications of deep reinforcement learning in communications and networking: A survey. *IEEE Communications Surveys & Tutorials*, 21(4):3133–3174, May 2019.

[172] G. L. Santos, P. T. Endo, D. Sadok, and J. Klener. When 5G meets deep learning: A systematic review. *Algorithms*, 13(208):1–34, Aug. 2020.

[173] 3GPP. Enhancement for Unmanned Aerial Vehicles; Stage 1. Technical Report (TR) 22.829, 3rd Generation Partnership Project (3GPP), 09 2019. Version 17.1.0.

[174] U. Challita, W. Saad, and C. Bettstetter. Interference management for cellular-connected UAVs: A deep reinforcement learning approach. *IEEE Transactions on Wireless Communications*, 18(4):2125–2140, Apr. 2019.

[175] H. Qi, Z. Hu, H. Huang, X. Wen, and Z. Lu. Energy efficient 3-D UAV control for persistent communication service and fairness: A deep reinforcement learning approach. *IEEE Access*, 8:53172–53184, Mar. 2020.

[176] C. H. Liu, Z. Chen, J. Tang, J. Xu, and X. Piao. Energy-efficient UAV control for effective and fair communication coverage: A deep reinforcement learning approach. *IEEE Journal on Selected Areas in Communications*, 36(9):2059–2070, Sept. 2018.

[177] Hasini Viranga Abeywickrama, Ying He, Eryk Dutkiewicz, Beeshanga Abewardana Jayawickrama, and Markus Mueck. A reinforcement learning approach for fair user coverage using uav mounted base stations under energy constraints. *IEEE Open Journal of Vehicular Technology*, 1:67–81, 2020.

[178] Jin Qiu, Jiangbin Lyu, and Liqun Fu. Placement optimization of aerial base stations with deep reinforcement learning. In *ICC 2020-2020 IEEE International Conference on Communications (ICC)*, pages 1–6. IEEE, 2020.

[179] Y. S. Nasir and D. Guo. Multi-agent deep reinforcement learning for dynamic power allocation in wireless networks. *IEEE Journal on Selected Areas in Communications*, 37(10):2239–2250, Oct. 2019.

[180] R. E. Bellman. *Dynamic programming*. Princeton University Press, 1957.

[181] M. Kearns and S. Singh. Near-optimal reinforcement learning in polynomial time. *Machine Learning*, 49:209–232, Nov. 2002.

[182] Ming Tan. Multi-agent reinforcement learning: Independent vs. cooperative agents. In *Proceedings of the tenth international conference on machine learning*, pages 330–337, 1993.

[183] Singh S, T. Jaakkola, M. L. Littman, and C. Szepesvari. Convergence results for single-step on-policy reinforcement-learning algorithms. *Machine Learning*, 38:287–308, Mar. 2000.

[184] Laetitia Matignon, Guillaume J Laurent, and Nadine Le Fort-Piat. Independent reinforcement learners in cooperative markov games: a survey regarding coordination problems. *Knowledge Engineering Review*, 27(1):1–31, 2012.

[185] F Richard Yu and Ying He. *Deep Reinforcement Learning for Wireless Networks*. Springer, 2019.

[186] Fa-Long Luo. *Machine Learning for Future Wireless Communications*. John Wiley & Sons, 2020.

[187] Chi Harold Liu, Zheyu Chen, Jian Tang, Jie Xu, and Chengzhe Piao. Energy-efficient uav control for effective and fair communication coverage: A deep reinforcement learning approach. *IEEE Journal on Selected Areas in Communications*, 36(9):2059–2070, 2018.

[188] Y. LeCun, Y. Bengio, and G. Hinton. Nature. *Deep Learning*, 521:436—444, May 2015.

[189] Liang Huang, Xu Feng, Luxin Zhang, Liping Qian, and Yuan Wu. Multi-server multi-user multi-task computation offloading for mobile edge computing networks. *Sensors*, 19(6):1446, 2019.

[190] Quoc-Viet Pham, Tuan Leanh, Nguyen H Tran, Bang Ju Park, and Choong Seon Hong. Decentralized computation offloading and resource allocation for mobile-edge computing: A matching game approach. *IEEE Access*, 6:75868–75885, 2018.

[191] W. Almughalles, R. Chai, J. Lin, and A. Zubair. Task execution latency minimization-based joint computation offloading and cell selection for mec-enabled HetNets. In *2019 28th Wireless and Optical Communications Conference (WOCC)*, pages 1–5, 2019.

[192] Fagui Liu, Zhenxi Huang, and Liangming Wang. Energy-efficient collaborative task computation offloading in cloud-assisted edge computing for IoT sensors. *Sensors*, 19(5):1105, 2019.

[193] Liang Huang, Xu Feng, Anqi Feng, Yupin Huang, and Li Ping Qian. Distributed deep learning-based offloading for mobile edge computing networks. *Mobile Networks and Applications*, pages 1–8, 2018.

[194] L. Huang, S. Bi, and Y. J. Zhang. Deep reinforcement learning for online computation offloading in wireless powered mobile-edge computing networks. *IEEE Transactions on Mobile Computing*, pages 1–1, 2019.

[195] O. Muñoz, A. Pascual-Iserte, and J. Vidal. Optimization of radio and computational resources for energy efficiency in latency-constrained application offloading. *IEEE Transactions on Vehicular Technology*, 64(10):4738–4755, 2015.

[196] T. Q. Dinh, J. Tang, Q. D. La, and T. Q. S. Quek. Offloading in mobile edge computing: Task allocation and computational frequency scaling. *IEEE Transactions on Communications*, 65(8):3571–3584, 2017.

[197] Y. Wang, M. Sheng, X. Wang, L. Wang, and J. Li. Mobile-edge computing: Partial computation offloading using dynamic voltage scaling. *IEEE Transactions on Communications*, 64(10):4268–4282, 2016.

[198] Antti P Miettinen and Jukka K Nurminen. Energy efficiency of mobile clients in cloud computing. *HotCloud*, 10(4):19, 2010.

[199] Surong Xiao, Chubo Liu, Kenli Li, and Keqin Li. System delay optimization for mobile edge computing. *Future Generation Computer Systems*, 2020.

[200] Ali Al-Shuwaili and Ahmed Lawey. Achieving low-latency mobile edge computing by uplink and downlink decoupled access in HetNets. *arXiv preprint arXiv:1809.04717*, 2018.

[201] David J Abraham, Robert W Irving, and David F Manlove. Two algorithms for the student-project allocation problem. *Journal of Discrete Algorithms*, 5(1):73–90, 2007.

[202] 3GPP. Evolved Universal Terrestrial Radio Access (E-UTRA); Physical layer procedures. Technical Report (TR) 36.213, 3rd Generation Partnership Project (3GPP), 04 2017. Version 14.2.0.

[203] 3GPP. 5G; NR; Physical layer procedures for control. Technical Report (TR) 38.213, 3rd Generation Partnership Project (3GPP), 05 2019. Version 15.5.0.

[204] Elizabeth Bodine-Baron, Christina Lee, Anthony Chong, Babak Hassibi, and Adam Wierman. Peer effects and stability in matching markets. In *International Symposium on Algorithmic Game Theory*, pages 117–129. Springer, 2011.

[205] Abdulkadir Celik, Ming-Cheng Tsai, Redha M Radaydeh, Fawaz S Al-Qahtani, and Mohamed-Slim Alouini. Distributed user clustering and resource allocation for imperfect NOMA in heterogeneous networks. *IEEE Transactions on Communications*, 67(10):7211–7227, 2019.

[206] Y Jong. An efficient global optimization algorithm for nonlinear sum-of-ratios problem. *Optimization Online*, 2012.

[207] S. He, Y. Huang, L. Yang, and B. Ottersten. Coordinated multicell multiuser precoding for maximizing weighted sum energy efficiency. *IEEE Transactions on Signal Processing*, 62(3):741–751, 2014.

[208] Rajendra K Jain, Dah-Ming W Chiu, William R Hawe, et al. A quantitative measure of fairness and discrimination. *Eastern Research Laboratory, Digital Equipment Corporation, Hudson, MA*, 1984.

[209] Yaodong Yang and Jun Wang. An overview of multi-agent reinforcement learning from game theoretical perspective. *arXiv preprint arXiv:2011.00583*, 2020.

[210] Boya Di, Lingyang Song, Yonghui Li, and H Vincent Poor. Ultra-dense leo: Integration of satellite access networks into 5g and beyond. *IEEE Wireless Communications*, 26(2):62–69, 2019.

[211] L. Venturino, A. Zappone, C. Risi, and S. Buzzi. Energy-efficient scheduling and power allocation in downlink OFDMA networks with base station coordination. *IEEE Transactions on Wireless Communications*, 14(1):1–14, Jan. 2015.

Appendix A

Proof in Chapter 5

A.1 Proof of Lemma 1

Proof: The proof proceeds by noting that for fixed values of $\alpha_{i,n}$ and $\beta_{i,n}$, $\forall i \in I^G$, and $\forall n \in \mathcal{N}_{UHF}$, functions $\overline{\mathbb{R}}^G(\mathbf{Q})$ and $\overline{\mathbb{P}}^G(\mathbf{Q})$ are concave and convex, respectively. This implies that $-\overline{\mathbb{P}}^G(\mathbf{Q})$ is concave, and thus $\mathbb{F}^G\left(\lambda^{(\ell)}\right)$ is concave in $\mathbf{Q}$ for each fixed value of $\lambda^{(\ell)}$. Moreover, **Algorithm 5** successively solves a concave maximization problem with a convex constraints set, and hence is guaranteed to converge to the global optimal solution of problem **T-GUEs-EE-MAX**.

A.2 Proof of Lemma 2

Proof: The proof of **Lemma 2** is two-fold: (1) showing that **Algorithm 6** converges in a finite number of iterations, and (2) illustrating that $\mathbf{P}^\star$ is the global optimal solution that satisfies the Karush-Kuhn-Tucker (KKT) conditions for both problems, **GUEs-EE-MAX** and **T-GUEs-EE-MAX**.

Firstly, note that in the ℓ^{th} iteration, the obtained solution $\hat{\mathbf{P}}^{(\ell)} = 2^{\hat{\mathbf{Q}}^{(\ell)}}$ maximizes the objective function of problem **T-GUEs-EE-MAX** (via **Algorithm 5**), which is based on the convexified constraints of problem **GUEs-EE-MAX**, and for fixed values of $\alpha_{i,n}$ and $\beta_{i,n}$. Additionally, recall that $\hat{\mathbf{Q}}^{\ell}$ is the global optimal solution of problem **T-GUEs-EE-MAX**, as per **Lemma 1**. Furthermore, and according to (5.17), the evaluated objective function $\widehat{\mathbb{EE}}^G\left(\hat{\mathbf{P}}^{(\ell)}\right) = \mathbb{EE}^G\left(\hat{\mathbf{P}}^{(\ell)}\right)$, where the equality is due to the updated values of $\alpha_{i,n}$ and $\beta_{i,n}$, $\forall n \in \mathcal{N}_{UHF}$ and $\forall i \in I^G$. Similarly, in the $(\ell+1)^{th}$ iteration, $\hat{\mathbf{P}}^{(\ell+1)} = 2^{\hat{\mathbf{Q}}^{(\ell+1)}}$ maximizes the objective function of problem **T-GUEs-EE-MAX**,

and hence $\widehat{\mathbb{EE}}^G\left(\hat{\mathbf{P}}^{(\ell+1)}\right) \geq \widehat{\mathbb{EE}}^G\left(\hat{\mathbf{P}}^{(\ell)}\right)$. Moreover, and since $\widehat{\mathbb{EE}}^G\left(\hat{\mathbf{P}}^{(\ell+1)}\right)$ is a lower-bounded value of problem **GUEs-EE-MAX**, then $\mathbb{EE}^G\left(\hat{\mathbf{P}}^{(\ell+1)}\right) \geq \widehat{\mathbb{EE}}^G\left(\hat{\mathbf{P}}^{(\ell+1)}\right)$. By induction, one can verify that the following inequality holds [211]

$$\begin{aligned}\cdots = \mathbb{EE}^G\left(\hat{\mathbf{P}}^{(\ell+1)}\right) \geq & \widehat{\mathbb{EE}}^G\left(\hat{\mathbf{P}}^{(\ell+1)}\right) \geq \widehat{\mathbb{EE}}^G\left(\hat{\mathbf{P}}^{(\ell)}\right) \\ & = \mathbb{EE}^G\left(\hat{\mathbf{P}}^{(\ell)}\right) \geq \cdots,\end{aligned} \tag{A.1}$$

and hence $\widehat{\mathbb{EE}}^G\left(\hat{\mathbf{P}}^{(\ell)}\right)$ monotonically increases in each iteration until convergence (i.e. when $\left|\widehat{\mathbb{EE}}^G\left(\mathbf{P}^{(\ell)}\right) - \widehat{\mathbb{EE}}^G\left(\mathbf{P}^{(\ell-\mathbf{1})}\right)\right| \leq \varepsilon$).

Secondly, the KKT conditions of the reformulated problem **T-GUEs-EE-MAX** can be obtained via the Lagrange function, which is defined as

$$\begin{aligned}\mathcal{L}\left(\{Q_{i,n}\},\{\pi_i\},\{\xi_i\},\{\zeta_{i,n}\}\right) = & \overline{\mathbb{EE}}^G(\mathbf{Q}) \\ & + \sum_{i\in I^G}\pi_i\left(\overline{\mathbb{R}}_i^G(\mathbf{Q}) - R_{\min}^G\right) - \sum_{i\in I^G}\xi_i\left(\sum_{n\in\mathcal{N}_{UHF}} 2^{Q_{i,n}} - P_{\max}^G\right) \\ & + \sum_{n\in\mathcal{N}_{UHF}}\sum_{i\in I^G}\zeta_{i,n}2^{Q_{i,n}},\end{aligned} \tag{A.2}$$

with $\{\pi_i\}$, $\{\xi_i\}$, and $\{\zeta_{i,n}\}$ being the corresponding Lagrange multipliers. In turn, the KKT conditions can be obtained by differentiating $\mathcal{L}\left(\{Q_{i,n}\},\{\pi_i\},\{\xi_i\},\{\zeta_{i,n}\}\right)$ with respect to $P_{i,n}$, and setting the expression to zero. Particularly, the KKT conditions can be shown to be

$$\begin{aligned}\pi_i\left(\overline{\mathbb{R}}_i^G(\mathbf{Q}) - R_{\min}^G\right) &= 0, \forall i \in I^G, \\ \xi_i\left(\sum_{n\in\mathcal{N}_{UHF}} 2^{Q_{i,n}} - P_{\max}^G\right) &= 0, \forall i \in I^G, \\ \zeta_{i,n}2^{Q_{i,n}} &= 0, \forall i \in I^G, \forall n \in \mathcal{N}_{UHF}, \\ \overline{\mathbb{R}}_i^G(\mathbf{Q}) &\geq R_{\min}^G, \forall i \in I^G, \\ \sum_{n\in\mathcal{N}_{UHF}} 2^{Q_{i,n}} &\leq P_{\max}^G, \forall i \in I^G, \\ P_{i,n} &\geq 0, \forall i \in I^G, \forall n \in \mathcal{N}_{UHF}, \\ \pi_i, \xi_i &\geq 0, \forall i \in I^G, \\ \zeta_{i,n} &\geq 0, \forall i \in I^G, \forall n \in \mathcal{N}_{UHF},\end{aligned} \tag{A.3}$$

while

$$\frac{\partial \overline{\mathbb{EE}}^{G}(\mathbf{Q})}{\partial Q_{i,n}} = \frac{1}{\overline{\mathbb{P}}^{G}(\mathbf{Q})}\left(\frac{\partial \overline{\mathbb{R}}^{G}(\mathbf{Q})}{\partial Q_{i,n}} - \overline{\mathbb{EE}}^{G}(\mathbf{Q})\frac{\partial \overline{\mathbb{P}}^{G}(\mathbf{Q})}{\partial Q_{i,n}}\right). \tag{A.4}$$

Moreover, $\frac{\partial \overline{\mathbb{P}}^{G}(\mathbf{Q})}{\partial Q_{i,n}} = \ln(2)2^{Q_{i,n}}$, and $\frac{\partial \overline{\mathbb{R}}^{G}(\mathbf{Q})}{\partial Q_{i,n}}$ is obtained as given as

$$\frac{\partial \overline{\mathbb{R}}^{G}(\mathbf{Q})}{\partial Q_{i,n}} = B\left(\alpha_{i,n} - 2^{Q_{i,n}}|h_{i,m,n}|^2 \sum_{j\in I^G, j\neq i} \alpha_{j,n}\frac{1}{\sum\limits_{k\in I^G, k\neq j} 2^{Q_{k,n}}|h_{k,m,n}|^2 + \sigma^2}\right) \tag{A.5}$$

On the other hand, the first order optimality conditions of problem **GUEs-EE-MAX** must be verified in the $\mathbf{Q}$-space by setting $\mathbf{P} = 2^{\mathbf{Q}}$ [211]. It can be easily verified that the KKT conditions of problem **GUEs-EE-MAX** are identical to that of problem **T-GUEs-EE-MAX** but with the substitution of $\mathbf{P} = 2^{\mathbf{Q}}$. Particularly, it can be shown that

$$\frac{\partial \mathbb{EE}^{G}(\mathbf{Q})}{\partial Q_{i,n}} = \frac{1}{\mathbb{P}^{G}(\mathbf{Q})}\left(\frac{\partial \mathbb{R}^{G}(\mathbf{Q})}{\partial Q_{i,n}} - \mathbb{EE}^{G}(\mathbf{Q})\frac{\partial \mathbb{P}^{G}(\mathbf{Q})}{\partial Q_{i,n}}\right), \tag{A.6}$$

where $\frac{\partial \mathbb{P}^{G}(\mathbf{Q})}{\partial Q_{i,n}} = \ln(2)2^{Q_{i,n}}$, and $\frac{\partial \mathbb{R}^{G}(\mathbf{Q})}{\partial Q_{i,n}}$ is determined as given

$$\frac{\partial \mathbb{R}^{G}(\mathbf{Q})}{\partial Q_{i,n}} = B\left(\frac{\bar{\gamma}_{i,n}}{1+\bar{\gamma}_{i,n}} - 2^{Q_{i,n}}|h_{i,m,n}|^2 \sum_{j\in I^G, j\neq i} \frac{\bar{\gamma}_{j,n}}{1+\bar{\gamma}_{j,n}}\frac{1}{\sum\limits_{k\in I^G, k\neq j} 2^{Q_{k,n}}|h_{k,m,n}|^2 + \sigma^2}\right) \tag{A.7}$$

where

$$\bar{\gamma}_{j,n} = \frac{2^{Q_{j,n}}|h_{j,m,n}|^2}{\sum\limits_{k\in I^G, k\neq j} 2^{Q_{k,n}}|h_{k,m,n}|^2 + \sigma^2}. \tag{A.8}$$

By comparing (A.5) and (A.7), it is evident that

$$\alpha_{i,n} = \frac{\bar{\gamma}_{i,n}}{1+\bar{\gamma}_{i,n}}, \tag{A.9}$$

which is in agreement with (5.12). Moreover, $\beta_{i,n}$ can also be obtained via (5.12), $i \in I^G$, and $\forall n \in \mathcal{N}_{UHF}$. Additionally, $\frac{\partial \mathbb{P}^{G}(\mathbf{Q})}{\partial Q_{i,n}} = \frac{\partial \overline{\mathbb{P}}^{G}(\mathbf{Q})}{\partial Q_{i,n}}$, and with the update of the $\alpha_{i,n}$ and $\beta_{i,n}$ values, $\overline{\mathbb{R}}^{G}(\mathbf{Q}) \to \mathbb{R}^{G}(\mathbf{Q})$, and hence, $\overline{\mathbb{EE}}^{G}(\mathbf{Q}) \to \mathbb{EE}^{G}(\mathbf{Q})$. Lastly, since the same

KKT conditions apply to both **GUEs-EE-MAX** and **T-GUEs-EE-MAX** problems, then the obtained solution $\mathbf{P}^{\star} = 2^{\mathbf{Q}^{\star}}$ is the global optimal solution to problem **GUEs-EE-MAX**.